Dark Cosmology Centre

Genesis and evolution of dust in the early Universe

A thesis submitted for the degree of
Doctor of Philosophy (PhD)
on July 30, 2010.
Defended in Copenhagen, October 8, 2010.

Christa Gall

Supervisor: Anja C. Andersen

Co-supervisor: Jens Hjorth

Dark Cosmology Centre, Niels Bohr Institute

Faculty of Science, University of Copenhagen

Genesis and Evolution of Dust in the early Universe

Christa Gall

Dissertation
Submitted for the Degree

Philosophiæ Doctor

Dark Cosmology Centre
Niels Bohr Institute
Det Naturvidenskabelige Fakultet
Københavns Universitet

Submission: *July 30th, 2010*
Defence: *October 8th, 2010*

Supervisor: *Assoc. Prof. Anja C. Andersen*
Co-Supervisor: *Prof. Jens Hjorth*

Opponents: *Dr. Loretta Dunne*
Dr. Hiroyuki Hirashita

CONTENTS

Contents iii

Acronyms vii

List of Figures ix

List of Tables xi

Acknowledgments xiii

Abstract xv

Sammenfatning xvii

Zusammenfassung xix

1 Introduction 3
- 1.1 The first milestones . . . 4
- 1.2 Composition of dust grains . . . 5
- 1.3 Studying dust . . . 7
  - 1.3.1 From an observational point of view . . . 7
  - 1.3.2 In the laboratory . . . 10
  - 1.3.3 Theoretical approach . . . 11
  - 1.3.4 At high redshift . . . 14
- 1.4 Structure of the thesis . . . 18

2 Dust productivity of massive stars 19
- 2.1 Introduction . . . 20
- 2.2 The late stages of massive stellar evolution . . . 21
  - 2.2.1 The first stars . . . 22
  - 2.2.2 Intermediate and high-mass AGB stars . . . 23
  - 2.2.3 Core collapse supernovae . . . 24
  - 2.2.4 Stars in the critical progenitor mass range . . . 25

2.2.5 Type Ia supernovae . . . 26
2.3 Dust from massive stars . . . 26
2.3.1 Dust from AGB stars: Theory and observation . . . 26
2.3.2 Direct evidence of dust from CCSNe . . . 29
2.3.3 Dust contribution from IIn supernovae and LBVs . . . 32
2.3.4 Dust from IIb, Ic, Ib and Ia supernovae . . . 33
2.4 Supernova dust: Theory vs. observations . . . 33
2.4.1 Theory . . . 34
2.4.2 Observations . . . 38
2.5 Dust production efficiency . . . 41
2.5.1 Efficiency for AGB stars . . . 41
2.5.2 Efficiency for CCSNe . . . 42
2.5.3 Simple approximations . . . 45
2.6 Dust productivity . . . 46
2.6.1 Results . . . 48
2.6.2 Dust at high redshift . . . 51
2.7 Summary . . . 52

3 Modeling dust evolution in starburst galaxies 55
3.1 Introduction . . . 56
3.2 Modeling the evolution of dust in starburst galaxies . . . 57
3.2.1 Basic considerations . . . 58
3.2.2 Equations for AGB stars and supernovae . . . 58
3.2.3 The evolution of dust and gas in the galaxy . . . 61
3.3 Model parameters . . . 63
3.3.1 Initial conditions . . . 63
3.3.2 The initial mass function . . . 64
3.3.3 Stellar yields . . . 66
3.3.4 Dust production and destruction . . . 69
3.3.5 Dust destruction in the ISM . . . 69
3.4 Results . . . 71
3.4.1 Evolution of dust, dust-to-gas and dust-to-metal ratios . . . 72
3.4.2 Evolution of dust production rates, SFR and metallicity . . . 83
3.4.3 Evolution of gas, metals and stellar masses . . . 85
3.4.4 Comparison to other dust evolution models for high-z galaxies . . . 87
3.4.5 Results for models including a SMBH . . . 88
3.5 Discussion . . . 89
3.5.1 Caveats in our approach . . . 93
3.6 Conclusions . . . 94

4 Rapid dust evolution in QSOs at $z \gtrsim 6$ **97**
4.1 Introduction . . . 98
4.2 The model . . . 99
4.3 Results . . . 100
4.3.1 Dust and stellar mass . . . 101
4.3.2 Metallicity and SFR . . . 104
4.3.3 H_2 mass in QSOs . . . 106
4.4 Discussion . . . 109
4.4.1 Individual QSOs at $z \gtrsim 6$ . . . 109
4.4.2 SN efficiency and mass of the galaxy . . . 112
4.5 Summary and conclusions . . . 113

5 Conclusions and future prospects **117**
5.1 Conclusions . . . 118
5.2 Future prospects . . . 119
5.2.1 The near future . . . 119
5.2.2 The distant future . . . 121
5.2.3 Cosmic dust with X-shooter . . . 124

Bibliography **127**

Co-Author statements **145**

ACRONYMS

AC	Amorphous carbon
AGB	Asymptotic giant branch
AGN	Active galactic nucleus
CCSN	Core collapse supernovae
DLA	Damped Lyman Alpha system
FIR	Far-infrared
GRB	Gamma-ray Burst
HST	Hubble Space Telescope
IDPs	Interplanetary dust particles
IMF	Initial mass function
IR	Infrared
IRAM	Institut de Radioastronomie Millimétrique
IRAS	Infrared Astronomical Satellite
ISM	Interstellar medium
ISO	Infrared Space Observatory
JCMT	James Clerk Maxwell Telescope
LBV	Luminous Blue Variable (e.g. η Carinae)
LMC	Large Magellanic Cloud
LVG	Large velocity gradient
MAMBO	Max-Planck Millimeter Bolometer
MIPS	Multiband Imaging Photometer for Spitzer
NIR	Near-infrared
QSO	Quasi-stellar Object
SCUBA	Submillimeter Common-User Bolometer Array
SED	Spectral energy distribution
SFR	Star formation rate
SMBH	Super massive black hole
SMC	Small Magellanic Cloud
SMG	Sub-mm galaxy
SN	Supernova

SST	Spitzer Space Telescope
ToO	Target-of-Opportunity (proposal type/fast observation mode)
TPAGB	Thermal pulsing phase
ULIRG	Ultra Luminous Infrared Galaxy
UV	Ultra violet
VLA	ery Large Array
VLT	Very Large Telescope (Paranal/Chile)
WR	Wolf-Rayet (star)

LIST OF FIGURES

1.1 Presolar nano-diamond cluster extracted from the Allende meteorite . . 6
1.2 IR space telescopes 8
1.3 Combined SED of high-z QSOs 16

2.1 Relation between stellar mass, stellar lifetime and redshift in the early Universe 22
2.2 Inferred amount of dust from SN observations at different epochs and temperatures 30
2.3 Dust production efficiencies of AGB stars. 42
2.4 Dust production efficiencies of massive stars 43
2.5 The five IMFs considered 46
2.6 Dust yields 48
2.7 Specific dust productivity 49
2.8 Total dust productivity of AGB stars and SNe for different IMFs and SN dust production efficiencies 50

3.1 Evolution of the total dust mass and dust destruction rates for EIT08M. . 73
3.2 Evolution of the dust-to-gas and dust-to-metal mass ratios for EIT08M . 74
3.3 Evolution of the total dust mass for ET08M 75
3.4 Evolution of the total dust mass for EIT08M 76
3.5 Evolution of the dust-to-gas and dust-to-metal mass ratios for EIT08M . 77
3.6 Evolution of the total dust mass for G09M 80
3.7 Evolution of the total dust mass for WW95M and N06M 81
3.8 Evolution of the total dust mass for WW95M with constant SFR 82
3.9 Evolution of total dust injection rates for AGB stars and SNe, the AGB and SNe rates, the SFR and the metallicity 84
3.10 Evolution of the gas mass $M_{\rm G}(t)$ based on EIT08M 85
3.11 Evolution of the stellar mass, mass of metals and the CO molecular mass based on EIT08M 86
3.12 Comparison of the evolution of the dust mass between EIT08M including and without the SMBH formation 89

3.13 Relation between dust mass, stellar mass, SFR and metallicity in correlation with the total mass of the galaxy and the IMF for an epoch at 400 Myr 90

4.1 Relation between dust mass and stellar mass at an epoch of 30 Myr, for various initial gas masses and IMFs 102
4.2 Relation between dust mass and stellar mass at an epoch of 100 Myr for various initial gas masses and IMFs 103
4.3 Relation between metallicity and SFR at different epochs 105
4.4 CO conversion factor versus gas-to-H_2 ratio at different epochs 107

LIST OF TABLES

2.1 Observed and derived properties of CCSNe 31
2.2 IMF parameters 47

3.1 List of all model parameters 66
3.2 Definitions of stellar types 67
3.3 EIT08M exceeding 10^8 $M_\odot$ of dust within $\sim$ 400–500 Myr 91

4.1 Model parameters 101
4.2 Observed properties of quasars at z $\gtrsim$ 6 110
4.3 Calculated properties from the best matching models of z $\gtrsim$ 6 QSOs from our sample 110
4.4 Models which match the observed properties of z $\gtrsim$ 6 QSOs from our sample 111
4.5 Models which match the observed range of properties of $z \geq 5$ QSOs . . 114

ACKNOWLEDGMENTS

More than three years ago I had the dream to start a PhD and I owe many people my deepest thanks that my dream become reality and even more that I also managed to write this thesis.

First and foremost I would like to thank my supervisor Anja Andersen for taking me as her PhD student, for endless great support during these years and for giving me the opportunity to join many interesting conferences on even more interesting places around the world. But I most thank her for all the inspiration and motivation especially in the last not so easy months, and for always believing in me that I will complete this theses. I'd like to thank Jens Hjorth for being an incredibly great co-supervisor over the last half year, for all his help, the great discussions regarding my work, for lots of motivating words and great ideas and last but not least for teaching me that 'english is not german'. Besides my supervisors I'm deeply grateful to Johan Fynbo, Lisbeth Fogh Grove, Max Stritzinger, Søren Frandsen, Frank Grundahl, Bo Milvang-Jensen and Danka Paraficz for either sending me or taking me with to observing trips to La Palma, Teneriffe and finally to the VLT in Chile, which I just so much enjoyed. I also thank Desiree Della Monica Ferreira and Daniele Malesani for many words of encouragement whenever I really needed it. I would like to thank John Eldridge for informative discussions and for providing tabulated values of his stellar evolution models. I jointly thank all people at the DARK center for all the help I have got from you during my PhD, but also for always being helpful, friendly, organizing so many great events and creating a lively work place. I'm really happy to have met all of you.

Finally some special thanks to my family for all the support and guidance and to my husband, Michael, for all his love and assistance over all the years we know each other and for being a great father to our kids, Laura and Nico, especially over the last few Months. I particularly thank my kids, for their great understanding that I lately couldn't spend so much time with them.

I also like to acknowledge the financial support from the Faculty of Science, University of Copenhagen and the Dark Cosmology Centre.

Many thanks!

ABSTRACT

The most fascinating aspect of studying dust is the fact that small dust particles of sub-micron which we cannot see with our naked eyes are a fundamentally important component in a Universe whose dimension we hardly can imagine. Dust grains impact the evolution of the Universe in many ways. For example they are known as the main formation site of molecular hydrogen which acts as important coolant by the formation of stars similar to our Sun. Dust is essential for the formation of planets and plays an important role in the end stages of life of most stars.

Large amounts of dust have been discovered in quasars (QSOs) at high redshift where the epoch of cosmic evolution was $\sim$ 1 Gyr, but the origin and evolution of these remains elusive. Supernovae (SNe) and asymptotic giant branch (AGB) stars have been contemplated as prime dust sources due to their potential ability of generating sufficiently high amounts of dust. Though AGB stars are in fact known as the main dust source in the present Universe, their partially (too) long lifetimes questions their significance as dust contributers in the early Universe. SNe are sufficiently short-lived, but there exists a discrepancy between observationally and theoretically ascertained dust yields.

The principal aim of this thesis is to elucidate the astrophysical conditions required for generating these large amounts of dust in massive starburst galaxies and QSOs at high redshift. We first intend to identify the mass ranges of the most efficient dust producing stars at high redshift. We ascertain the dust production efficiency of stars in the mass range 3–40 $\mathrm{M}_{\odot}$ using observed and theoretical dust yields of AGB stars and SNe. Based on these efficiencies we determine the total dust productivity for different stellar sources and investigate its dependency on the initial mass function (IMF). It is found that the dust production efficiency generally decreases with increasing progenitor mass. The total dust production strongly depends on the assumed IMF. AGB stars dominate the dust production if SNe produce $\lesssim 3 \times 10^{-3}$ $\mathrm{M}_{\odot}$ of dust whereas SNe dominate if they are more efficient. The mass ranges of 8–12 $\mathrm{M}_{\odot}$ and 12–20 $\mathrm{M}_{\odot}$ for SNe are equally important and dominate the overall SN contribution regardless of the IMF.

A main part of the thesis is devoted to the development of a numerical galactic chemical evolution model. The model is constructed such that the effect of a wide range of parameters can be investigated. We ascertain the temporal progression of the

dust mass, the dust-to-gas and dust-to-metal mass ratios as well as other physical properties of a galaxy and study their dependence on the mass of the galaxy, the IMF, dust production efficiencies and the degree of dust destruction in the interstellar medium (ISM). From this study we find that the amount of dust and the physical properties of a galaxy strongly depend on the initial gas mass available. Overall, while the total amount of dust produced increases with galaxy mass, the detailed outcome depends on the SN dust production efficiency, the IMF and the strength of dust destruction in the ISM. Dust production with a dominant contribution by AGB stars is found to be insufficient to account for the dust masses in excess of 10^8 $\mathrm{M}_\odot$ within 400 Myr after starburst.

Furthermore, we investigate the influence of the star formation rate (SFR) of the starburst on the evolution of various quantities such as the amount of dust and gas, stellar masses, SFRs and the metallicity. We aim to determine the earliest epochs at which an agreement with observationally derived physical properties of QSOs at $z \gtrsim 6$ can be achieved. We apply the obtained results to individual QSOs at $z \gtrsim 6$. We find that large quantities of dust can be generated rapidly as early as 30 Myr after the onset of the starburst when the SFR of the starburst is $\gtrsim 10^3$ $\mathrm{M}_\odot$ yr^{-1}. The amount of dust and several physical quantities of individual QSOs at $z \gtrsim 6$ are satisfactorily reproduced by models at epochs 30, 70, 100 and 170 Myr and for galaxies with initial gas masses of 1–3 $\times 10^{11}$ $\mathrm{M}_\odot$. The best agreement with observations is obtained with top-heavy IMFs. A dominant dust contribution from SNe is required and a moderate dust destruction in the ISM can be accommodated, while at these epochs dust production by AGB stars is negligible.

SAMMENFATNING

Det mest fascinerende ved kosmisk støv er at disse små støvkorn, der kun er nogle mikrometer i diameter og således ikke direkte synlige for det blotte øje, har vist sig at være en vigtig astrofysisk komponent i det ufattelig store univers. Støvkorn påvirker hele universets udvikling på mange måder. Det er f.eks. på overfladen af støvkorn at meget af det molekylære brint (H_2) bliver dannet. Molekylært brint fungerer som en essentiel kølemekanisme for dannelse af stjerner som vores Sol. Støvkorn er grundlaget for dannelsen af planeter og de spiller en helt afgørende rolle i forbindelse med den sidste livsfase for flertallet af stjerner.

Overraskende store mængder af støv er blevet observeret i fjerne kvasarer (QSOs) ved en såkaldt høj rødforskydning svarende til en alder for universet på omkring 1 milliard år. Det er lidt af en gåde hvor og hvordan dette støv er blevet dannet. De oplagte kilder til dannelse af det observeret støv er supernovaer (SNe) og asymptotiske kæmpestjerner (AGB). I Mælkevejen ser AGB stjerner ud til at være den primære kilde til dannelsen af støv. Men da flertallet af AGB stjerner har en levetid på langt over 1 milliard år, er det ikke sandsynligt at de også er den primære kilde til støv i det tidlige univers. Supernovaer har en meget kort levetid og er dermed oplagte kilder til det tidlige støvs oprindelse. Teoretiske modeller for supernovaer indikerer at det i høj grad er muligt at danne store mænger af støv i en supernova rest, mens at observationer af supernova rester i det nære univers indikerer at de ikke producerer de forventet store mængder af støv.

Hovedformålet med denne afhandling er at kortlægge de nødvendige astrofysiske betingelser for at støv kan dannes under de betingelser som herskede i det tidlige univers. I første omgang har jeg undersøgt hvilke masser de relevante stjerner kan have hvis de skal kunne nå frem til deres støvproducerende livsfase inden for den korte tidsramme observationerne indikerer. Jeg har undersøgt hvor effektivt støvbidraget fra stjerner i masse intervallet 3–40 $\mathrm{M}_{\odot}$ er når der tages udgangspunkt i de teoretiske forudsigelser for støvdannelse og når der tages udgangspunkt i de observerede mængder af støv for sådanne stjerner. Baseret på disse støvbidrag har jeg bestemt den totale støvmængde som stjerner med forskellig masse kan bidrage med og sammenholdt dette med antagelser for hvordan massefordelingen (initial masse funktionen, IMF) af stjerner i en galakse kan være. Det viser sig at mængden af produceret støv generelt

falder som funktion af stjernens oprindelige masse. Det totale støvbidrag afhænger kraftigt af den antaget IMF. AGB stjerner dominerer støvproduktionen hvis SNe producerer $< 10^3 \times 10^{-3}$ $\mathrm{M}_\odot$ støv, mens at SNe dominerer for højere værdier. Masseintervallerne 8–12 $\mathrm{M}_\odot$ og 12–20 $\mathrm{M}_\odot$ for SNe er lige vigtige og dominerer helt det overordnet bidrag fra supernovaer uanset hvilken IMF der antages.

Størstedelen af denne afhandling beskriver den numeriske galakse udviklingskode som jeg har skrevet. Med koden er det muligt at undersøge en bred vifte af relevante fysiske parametre for støvdannelse i en given galakse. Jeg har brugt den til bl.a. at undersøge hvordan mængden af støv udvikler sig med tiden, hvad forholdet mellem gas og støv kan være, hvordan mængden af tungere grundstoffer forholder sig til mængden af støv, og hvordan disse ting afhænger af værts-galaksen for kvasarens masse, den antaget IMF, støvdannelsesraten og støvdestruktionsraten i det i galaksen herskende interstellare medium (ISM). Mine undersøgelser viser at mængden af støv og de fysiske egenskaber af galaksen er stærkt afhængig af den mængde af gas der er til rådighed. Overordnet er det sådan at mens den totale mængde støv der dannes stiger som funktion af galaksens masse, så vil de nærmere detaljer afhænge af supernova støvdannelsesraten, den antaget IMF og hvor effektiv støvet bliver destrueret i ISM. Den observerede støvproduktionen på $> 10^8$ $\mathrm{M}_\odot$ i galaksen efter kun 400 millioner år kan ikke forklares med AGB stjerner alene.

Koden har også været benyttet til at undersøge hvilken indflydelse stjernedannelsesraten (SFR) i en galakse har på mængden af støv og gas, stjernernes masser, SFR og mængden af tungere grundstoffer. Formålet var at bestemme det tidligste tidspunkt i universets historie hvor modellerne kunne forklare observationerne af de fjerne kvasarer ved rødforskydning $z > 6$. Det viste sig at det er muligt at forklare hvordan store mængder af støv kan dannes på så kort en tidsskala som 30 millioner år blot SFR er $> 10^3$ $\mathrm{M}_\odot$ yr-1. Mængden af støv og de deraf udledte forskellige fysiske parametre for modelgalaksen kunne fint reproducerer de observerede data for QSOs ved $z > 6$ under tidsintervaller på 30, 70, 100 og 170 millioner år hvis galaksen havde en oprindelig gasmasse på 1–3 $\times$ 10^{11} $\mathrm{M}_\odot$. Den bedste overensstemmelse mellem model og observationer opnås for en IMF der hælder mod tungere stjerner. Et anseligt støvbidrag fra supernovaer er nødvendigt, mens at bidrag fra AGB stjerner er mindre vigtigt. Der er i modellerne plads til en vis mængde støvdestruktion i det ISM.

ZUSAMMENFASSUNG

Der faszinierendste Aspekt Staub zu studieren ist die Tatsache, dass kleine Staubpartikel von wenigen Mikrometern die wir mit unserem bloßen Auge nicht sehen können, eine fundamentale und wichtige Komponente in einem Universum sind, dessen Dimension wir uns kaum vorstellen können. Staubpartikel beeinflussen die Entwicklung des Universums in vielerlei Hinsicht. Zum Beispiel gelten sie als die wichtigsten Bildungsstellen von molekularem Wasserstoff, welcher wiederum ein wichtiges Kühlmittel bei der Formation von sonnenänlichen Sternen ist. Staub ist für die Bildung von Planeten essentiell und spielt eine wichtige Rolle in den Endphasen von den meisten Sternen.

Große Mengen von Staub sind in Quasaren (QSOs) mit hoher Rotverschiebung in einer Epoche der kosmischen Entwicklung von 1 Gyr entdeckt worden. Der Ursprung und die Entwicklung dieser Staubmassen ist nur schwer fassbar. Supernovae (SN) und Sterne im asymptotischen Riesenast (AGB) sind aufgrund ihrer Fähigkeit zur Generierung ausreichend hoher Mengen an Staub als verantwortliche Quellen in Betracht gezogen worden. Obwohl AGB-Sternen in der Tat als die wichtigste Quelle von Staub im heutigen Universum bekannt sind, ist es fraglich, ob sie Aufgrund ihrer teilweise (zu) langen Lebensdauer zur Staubproduktion im frühen Universum beigetragen haben. SN sind ausreichend kurzlebig, aber es besteht eine Diskrepanz zwischen den beobachteten und theoretisch ermittelten Staubmengen.

Das Hauptziel der vorliegenden Arbeit ist es, die astrophysikalischen Bedingungen, welche für die Erzeugung dieser großen Mengen von Staub in massiven Galaxien mit bedeutendem Sternformationsausbruch und QSOs bei hoher Rotverschiebung notwendig sind, aufzuklären. Zunächst soll der Massenbereich der effizientesten staubproduzierenden Sterne bei hoher Rotverschiebung identifiziert werden. Ausgehend von den beobachteten und theoretisch ermittelten Staubmengen von AGB-Sternen und SNe wird die Staubproduktionseffizienz von Sternen im Massenbereich von 3–40 $\mathrm{M}_{\odot}$ ermittelt. Basierend auf diesen Effizienzen wird die gesamten Staubproduktivität für verschiedene stellare Quellen untersucht und ihre Abhängigkeit von der ursprünglichen Massefunktion (IMF) ermittelt. Es wurde festgestellt, dass die Effizienz der Staubproduktion in der Regel mit zunehmender Masse der Sterne abnimmt. Die gesamte Staubproduktion hängt stark von der angenommenen IMF ab. AGB-Sterne dominieren die

Staubentwicklung, wenn SNe $\lesssim 3 \times 10^{-3}$ $\mathrm{M}_{\odot}$ an Staub produzieren, während SNe die Staubproduktion dominieren wenn sie effizienter sind. Der Massenbereich von 8–12 $\mathrm{M}_{\odot}$ und 12–20 $\mathrm{M}_{\odot}$ von SNe sind gleich bedeutend und dominieren unabhängig von der IMF den gesamten Beitrag von SNe.

Ein Hauptteil der Arbeit ist der Entwicklung eines numerischen galaktischen chemischen Evolutionsmodells gewidmet. Das Modell ist so konstruiert, dass die Wirkung von einer Vielzahl von Parametern untersucht werden kann. Wir ermitteln den zeitlichen Verlauf der gesamten Staubmasse, der Staub-zu-Gas- und der Staub-zu-Metall-Massenverhältnisse sowie einiger anderer physikalischer Eigenschaften einer Galaxie, und studieren die Abhängigkeit von der Masse der Galaxie, der IMF, der Staubproduktionseffizienz und dem Grad der Staubzerstö]rung im interstellaren Medium (ISM).

Aus dieser Studie resultiert, dass die Menge an Staub und die physikalischen Eigenschaften einer Galaxie, stark von der ursprünglich zur Verfügung stehender Gasmasse abhängt. Insgesamt, während die Gesamtmenge des erzeugten Staubes mit der Masse der Galaxien steigt, hängen die detaillierten Ergebnisse von der SN Staubproduktionseffizienz, der IMF und der Stärke der Staubzerstörung im interstellaren Medium ab. Die Staubproduktion mit einer dominierenden Kontribution von AGB-Sternen wurde als nicht ausreichend befunden, um für grössere Staubmassen als 10^8 $\mathrm{M}_{\odot}$ innerhalb von 400 Millionen Jahren nach dem Sternausbruch beitragen zu können. Desweitren untersuchen wir den Einfluss der Sternbildungsrate (SFR) des Sternausbruchs an der Entwicklung der verschiedenen Grössen, wie z.B.: die Menge an Staub und Gas, Sternmassen, SFRs und die Metallizität. Als Ziel ist es die früheste Epoche, bei welcher eine Vereinbarung mit den durch Beobachtungen abgeleiteten physikalischen Eigenschaften von QSOs bei $z \gtrsim 6$ erreicht werden kann, zu bestimmen. Wir wenden die erhaltenen Ergebnisse auf einzelne QSOs bei $z \gtrsim 6$ an.

Es zeigte sich, dass große Mengen von Staub bereits 30 Millionen Jahre nach dem Beginn des Sternausbruchs schnell erzeugt werden können, wenn die SFR des Sternausbruchs $\gtrsim 10^3$ $\mathrm{M}_{\odot}$ yr $^{-1}$ ist. Die Menge von Staub und verschiedene physikalische Grössen der einzelnen QSOs bei $z \gtrsim 6$ werden von Modellen für die Epochen, 30, 70, 100 und 170 Myr und ür Galaxien mit anfänglichen Gasmassen von 1–3 $\times$ 10 ^{11} $\mathrm{M}_{\odot}$ zufriedenstellend wiedergegeben. Die beste Übereinstimmung mit den Beobachtungen wird mit einer 'top-heavy' IMF erhalten. Ein signifikanter Beitrag an Staub von SNe ist erforderlich, während die Staubproduktion von AGB-Sternen in diesen Epochen vernachlässigbar ist. Moderate Staubzerstörung im interstellaren Medium kann angewendet werden.

To the most wonderful in my life
my children Laura and Nico

Figure: *Orion Nebula; NASA, ESA, M. Robberto (Space Telescope Science Institute/ESA) and the Hubble Space Telescope Orion Treasury Project Team*

1

Introduction

By the sweat of your brow
you will eat your food
until you return to the ground,
since from it you were taken;
for dust you are
and to dust you will return.

GENESIS 3:19

1.1 THE FIRST MILESTONES

Everybody who ever glanced at the band of the Milky Way in a clear night might have noticed the dark regions where no stars seem to exist or shine.

At the end of the 18th century these regions had been described by Herschel (1785) as 'holes in the sky' and over roughly 100 years his view was prevailing. A century later Barnard (1884) still named these regions as 'holes' and terms such as 'star voids' were also used by Wolf (1904). However there were ongoing considerations about obscuring matter as an explanation for the star voids, and Wolf (1923) was certain that the matter was dust. The idea of extinction of starlight by dust particles in the interstellar space found its final acceptance and confirmation through the work by Trümpler (1930), though its effect was actually first described by Struve (1847). Around this epoch also the research of interstellar dust established itself as active field in astrophysics. Intensive investigations of the place of formation, composition, the size and shape of dust particles took place on the part of observations and theory.

The first dust models assumed 'meteoric dust' (Schalén 1929) and metallic iron grains based on mineralogical studies of meteorites. Inspired by the proposed idea by Lindblad (1935) that dust particles form and grow as a consequence of condensation of metals in the interstellar gas, a new dust model was developed by Oort & van de Hulst (1946). This so called 'dirty ice' model was based on the assumption that hydrogen-rich volatiles condense in the HI clouds of the interstellar medium. The model could also well reproduce the observed λ^{-1}-law of interstellar extinction (e.g. Stebbins et al. 1939) and some known dust properties, and was dominating the views of interstellar dust for about two decades.

The discovery of polarized light from stars by Hiltner (1947, 1949) and Hall (1949), which was found to be caused by the interaction of starlight with the dust particles in the interstellar medium, precipitated reconsiderations of the ice model. From the polarization of the light was concluded that the dust grains need to be aspherical and aligned. However, problems were encountered by forming elongated ice needles while they additionally couldn't be efficiently polarized. Besides, more arguments against the ice model arose, i.e., due to the strong deviation from the observed ultra violet (UV) extinction curves. Finally, between 1960–1970 refractory grains and minerals found their way back into consideration.

Up until then dust grains were only considered to form in cold interstellar clouds, however, the new grain models required hotter environments. Consequently, the outer layers of evolved stars or planetary systems were suggested as place of formation for refractory grains. Hoyle & Wickramasinghe (1962) and Wickramasinghe (1963) proposed a model consisting of graphite grains, which condense in the stellar atmospheres of carbon stars and are driven out by radiation pressure. Despite that the model was barely successful, it was used to explain the bump of the interstellar UV extinction curve (e.g.

Stecher & Donn 1965). The possibility of dust formation in the expanding ejecta of SNe was at the first time introduced by Cernuschi et al. (1965, 1967), and the condensation of iron grains were studied. This idea found general approval and Hoyle & Wickramasinghe (1970) extended the dust formation in SN to graphite and silicates. However, it was soon recognized that dust models based on single type grain composition formed in one environment are unable to account for all features of the observed extinction. The idea that the dust in the interstellar medium consists of a mixture of different types of grains, which was strongly favored by e.g., Friedemann & Schmidt (1967), Dorschner (1967), Friedemann (1969) and Gilra (1971), became increasingly prominent and finally also founded the current prevailing 'multi component' view of interstellar dust.

In the following decades the launch of the HELIOS space observatories in the 1970th and the first infrared (IR) satellites IRAS (Infrared Astronomical Satellite) in 1983 and ISO (Infrared Space Observatory) in 1996–1998 enhanced the identification of many different dust species on part of spectroscopy and laboratory analysis. Particularly, the observations of the vibrational bands of the SiO_4 group and the discovery of stardust bands of crystalline silicates provided ultimately evidence for the existence of silicate grains. For a thorough review about the history of the mentioned dust models and historical evolution of the diverse dust species I refer to Dorschner (e.g., 2003).

1.2 Composition of dust grains

Dust is formed by a series of chemical reactions in which atoms or molecules from the gas phase combine to clusters of increasing size. The molecular composition of the gas phase determines which atoms and molecules are available for the cluster formation and grain growth. Dust formation begins with nucleation of critical clusters followed by growth to macroscopic dust grains (e.g., Gail & Sedlmayr 1988; Gauger et al. 1990). Dust grains are significantly larger than either atoms, ions or molecules and their sizes ranges between typically a few 100–1000 $\mathring{\mathrm{A}}$.

Dust formation primarily takes place in the stellar winds of evolved stars ($< 8\ \mathrm{M}_{\odot}$) or in SN ejecta. Such dust is also often named 'Stardust'. Once such grains are released into the interstellar medium (ISM) these are subject to modification due to diverse destructive processes in for example SN shocks. However, dust grains also grow in dense molecular clouds in the ISM (e.g., Draine 2009), but these grains are significantly different from the originally ejected grains. In particular, stardust grains retain their extreme isotopic composition of the refractory elements which is typical of their nucleosynthesis source (e.g., Zinner 1998; Hoppe & Zinner 2000). The dust grains which are grown in the ISM are composed of a mixture of different elements and their final isotopic composition is therefore different. Evidence of stardust grains has been found in the fine-grained matrix of diverse primitive meteorites (e.g., Zinner 1997; Hoppe 2004; Pellin et al. 2006; Gyngard et al. 2009) originating from the Solar System. They survived the

solar collapse and bear witness of dust condensation in stellar outflows from outside the Solar System. These grains are often called 'presolar grains'. Depending on the environment where dust grains condense, different but for these environments typical dust species will result. The environments can either be oxygen rich or carbon rich and dependent on the most abundant element predominantly either silicates or carbon dust will form, respectively.

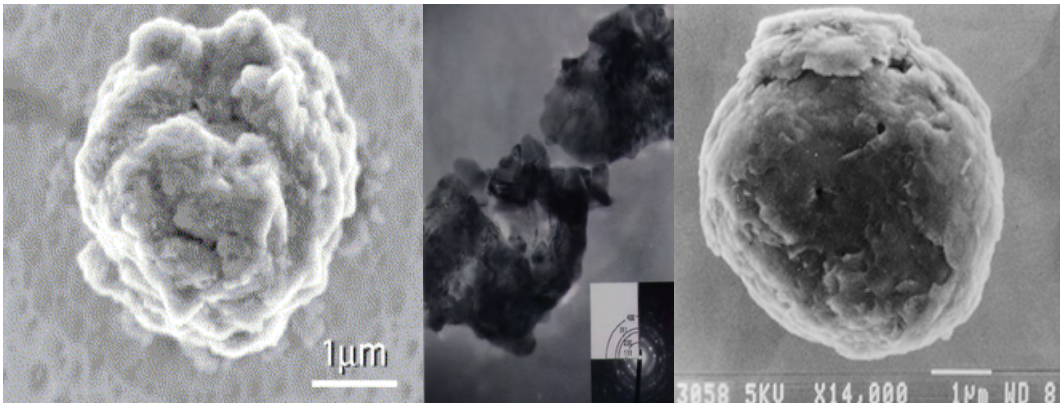

Figure 1.1: *Left panel: Presolar grain of silicon carbide (SiC) of size 3 μm. Photo by Rhonda Stroud, Naval Research Laboratory, and displayed in Nittler (2003). Middel panel: Presolar nano-diamond cluster extracted from the Allende meteorite. Each cluster consists of about 1000 nano-diamond and each diamond consists of about 1000 carbon atoms. At least part of the presolar diamond populations show isotopic anomalies consistent with an origin in core-collapse supernova (Photo from Andersen et al. 1998). Right panel: SEM micrograph of presolar graphite grain, 5 micrometers in diameter, from the Murchison meteorite. Its surface texture resembles an onion. Photo courtesy of S. Amari, Washington University, St. Louis.*

The most prominent dust species for an environment which is

- oxygen rich are:
  - Silicates: i.e., olivine ($[Mg,Fe]_2SiO_4$), forsterite (Mg_2SiO_4), pyroxene ($[Mg,Fe]_2SiO_3$), enstatite ($MgSiO_3$), magnetite (Fe_3O_4)
  - Carbonates ($[Ca,Mg,Fe,...]CO_3$), corundum (Al_2O_3), spinel ($MgAl_2O_4$), titanium oxide (TiO_2), hibonite ($CaAl_{12}O_{19}$), [Mg,Fe]O or SiO grains
- carbon rich are:
  - Carbonaceous dust (C): i.e., Amorphous carbon, graphite, nano-diamond
  - Silicon carbide (SiC), FeS or MgS grains

1.3 STUDYING DUST

During the last decades much effort has been undertaken to discover various dust species and to determine its composition, structure and size distribution. Observations and measurements of such grains shed light not only onto the processes of condensation, destruction and growth but give also insight into the physical conditions of different environments where dust is formed or modified such as in stellar outflows and the ISM. Coevally with observations and laboratory analyses much theoretical endeavor has been made to elucidate the formation of dust particles and their properties. Although improved computational resources became available, the problems turned out to be very difficult due to many unknowns of the interplay between the various chemical and physical processes. Despite the remarkable observational and theoretical progress, today's picture of the origin and evolution of dust remains unclear.

The detection of cosmic dust by observations can be accomplished directly or indirectly. The two possibilities are briefly described in the next sections.

1.3.1 FROM AN OBSERVATIONAL POINT OF VIEW

Indirect detection methods are based on the influence of dust particles on the electromagnetic radiation. Half of the non-primordial radiation is reprocessed by dust before it is observed. The radiation can be processed of three different kinds when penetrating through a medium with dust. It can be absorbed, scattered or emitted. Typically all processes will take place simultaneously. In particular, dust grains absorb UV-optical light and subsequently reemit it at infrared (IR)-millimeter wavelengths. While the interaction depends (i) on the nature of the grains, i.e. composition, size or the shape and (ii) on the wavelength of the light, ample important information about the properties of dust in for example stellar environments, SN ejecta and remnants, the ISM but also of distant galaxies and quasars can be gained. Due to the fact that most of the prominent vibrational and translational dust bands are within the IR wavelength range, IR observations but also sub-millimeter observations are a fundamental component of studying dust in the Universe. The telescopes used for studying dust are either placed in space or on Earth, a few are listed below. The following space telescopes either are, have been or will be available:

- IRAS (Infrared Astronomical Satellite), ISO (Infrared Space Observatory), MSX (Midcourse Space Experiment) in 1997, Infrared Telescope in Space in 1995
- Spitzer Space Telescope (SST): It was launched in 2003. The onboard instruments IRAC (Infrared Array Camera), IRS (Infrared Spectograph) and MIPS (Multiband Imaging Photometer for Spitzer) consist each of modules for particular wavelengths covering a total range between 3.6–160 μm. However, in 2009 the liquid helium for cooling the IR instruments was exhausted and only two modules of

IRAC continue to operate the 'Warm Mission'.

- AKARI: It was developed by the Japanese Aerospace Exploration Agency and was launched in 2006. The far-IR (FIR) and mid-IR (MIR) observations operated until August 2007, while the telescope in the near-IR (NIR) continues.

- Herschel Space Observatory (HSO): It was launched in 2009. The instruments are PACS (Photodetecting Array Camera and Spectrograph), SPIRE (Spectral and Photometric Imaging Receiver) and HIFI (Heterodyne Instrument for the Far Infrared). The detectors cover in total a wavelengths range of 55–625 μm.

- James Webb Space Telescope (JWST): The launch is planned for 2014 and it is the successor for the Hubble Space Telescope (HST). The instruments are the NIRCam (Near InfraRed Camera), NIRSpec (Near InfraRed Spectograph) and MIRI (Mid InfraRed Instrument).

- Further satellites are e.g., WISE (Wide-field Infrared Survey Explorer), SWAS (Submillimeter Wave Astronomy Satellite)

Figure 1.2: *Infrared space telescopes. The telescopes are the Spitzer Space Telescope (left), the Herschel Space Observatory (middel) and the James Webb Space Telescope (right)*

Some ground-based telescopes:

- Institut de Radioastronomie Millimétrique (IRAM), 30-m single-dish radio telescope on Pico Veleta, since 1980, Spain, six-antenna interferometer on the Plateau de Bure, France, since 1988. Instruments at the 30-m telescope are three heterodyne receiver and the Max-Planck Millimeter Bolometer array (MAMBO). The MAMBO1 camera is not used anymore but since 2001/2002 the successor MAMBO2 is operating. Both cameras work at 1.3 mm wavelength. The Plateau de Bure Interferometer (PdBI) consists of six a 15-m antenna array since 2005. Observing wavelength is at 1.3 mm and the dual polarization receivers work at 1,2 and 3 mm.

- James Clerk Maxwell Telescope (JCMT) at Mauna Kea, Hawai, since 1987. The telescope consists of a 15m primary mirror and operates in the sub-millimeter wavelength regime. Instruments are continuum detectors and spectral line detectors. For the first kind of detectors the Submillimeter Common-User Bolometer Array (SCUBA) started operating in 1997. The successor to SCUBA is SCUBA-2. Both instruments have two arrays for operations at 450 μm and 850 μ wavelengths. For spectral line observations are two heterodyne receivers, a 16 element heterodyne array receiver (HARP-B) and a digital autocorrelation spectrometer (ACSIS) available. Total frequency coverage from 1.8 – 710 GHz.

- National Radio Astronomy Observatory's (NRAO) Very Large Array (VLA), New Mexico, since about 1980. It consists of 27 independent 25-m antennas alined on three arms of a Y-shape, each of 21 km length. Eight receivers each at a different frequency bands are available, total frequency coverage of 0.074–50 GHz.

- Very Large Telescope (VLT) at Paranal, Chile. The instrument is X-shooter and it started operating in 2009. The instrument covers a total wavelength range of 300–2500 nm and is split into three arms. These arms are the UV-Blue, Visual-red and the Near-IR arm.

- Atacama Large Millimeter/submillimeter Array (ALMA) at the Altiplano de Chajnanto, Chile and will be one of the largest ground-based facilities in future. ALMA is comprised of an array of 7-m and 12-m Antennas. The completion of construction is planned for 2013.

A revolution in our understanding of the sources for the FIR to millimeter extragalactic background (high-redshift galaxies but also nearby galaxies) has been achieved with the availability of sub-millimeter observations. Submillimeter surveys undertaken with the Submillimeter Common-User Bolometer Array (SCUBA, Holland et al. 1999) mounted at the James Clerk Maxwell Telescope (JCMT) uncovered a population of dusty galaxies at $z \geq 2$ (e.g., Smail et al. 1997; Hughes et al. 1998; Eales et al. 1999; Barger et al. 1998). SCUBA, COBE and observations with the Max-Planck Millimeter Bolometer (MAMBO) at the IRAM 30-m telescope have shown that most of the energy generated in star forming galaxies at high redshift is absorbed by dust and re-emitted at FIR wavelengths (e.g., Gispert et al. 2000; Ivison et al. 2000; Bertoldi et al. 2000). For high redshift sources the peak of the thermal emission from warm dust caused by dust heated in this spectral range is red-shifted into the submillimeter and millimeter atmospheric window and therefore detectable with ground based facilities.

In the local universe the sub-millimeter waveband (100 μm $\leq \lambda \leq$ 1mm) is sensitive to thermal emission from rather cold dust (T $\geq$ 10 K). From studies at this wavelengths range (e.g., at 170 μ with ISO) evidence of a large cold dust component in various types of galaxies has been found (e.g., Stickel et al. 2000; Contursi et al. 2001; Popescu et al.

2002). Such massive cold dust was undetected by the first IRAS observations (60 and 100 μm bands) only sensitive to warmer dust (T $\geq$ 30 K). Statistical submillimeter surveys with SCUBA (bands at 450 and 850 μm) such as the Local Universe Galaxy Survey (Dunne et al. 2000; Dunne & Eales 2001; Vlahakis et al. 2005), investigated the submillimeter properties of galaxies and performed first measurements of the luminosity and dust mass function important also for interpretations of observations of high redshift sources. Using a two component dust model to fit the spectral energy distribution it has been suggested that all galaxies in their samples might have a cold dust component of similar temperature (T $\sim$ 20–21 K).

1.3.2 IN THE LABORATORY

Direct, or so called 'in-situ' detection and measurements are undertaken on dust which is collected via different methods and on different places. At Earth the main source for studying stardust are meteorites (e.g. Nittler 2003; Hoppe 2009), but also information of dust is gained from particles entering the Earths atmosphere, interplanetary dust particles (IDPs) or cometary dust (Bradley 2003; Brownlee 2008).

The most prominent meteorites for studying presolar dust grains are e.g.,

- Allende: The meteorite fell over Chihuahua, Mexico on February 8, 1969. It is the largest meteorite of the group of carbonaceous chondrites found on Earth and is most abundant of minerals which are rich on primarily calcium and aluminium.
- Murchison: The meteorite fell over Victoria, Australia on September 28, 1969. It also belongs to the group of carbonaceous chondrites and besides of calcium and aluminium rich minerals, also organic matter of various amino acids have been found.
- Further meteorites are e.g., Orgueil, Ivuna, Tieschitz, Tagish Lake

Dust is also captured in the interplanetary space via detectors on spacecrafts, or Earth orbiting satellites.

- Dust detectors are mounted of e.g., Helios, Stardust, Ulysses, Rosetta, New Horizons
- Earth orbiting satellites are e.g., Long Duration Exposure Facility (LDEF), Micro Particles Capturer (MPAC)

Measurements of interplanetary dust from dust detectors on board space crafts have shown that interplanetary dust has a fluffy and porous structure. These measurements also proved the existence of two dust components with different properties (aqueous and non-aqueous) in the inner solar system inside Earth orbit (Mann & Jessberger 2003a). Laboratory measurements on the isotopic composition of presolar grains

have shown that they are of stellar origin. The presolar grain types identified include diamond, silicon carbide, graphite, corundum, silicates and silicon nitride. Most of the silicon carbide and corundum originates from red giant and asymptotic giant branch stars (low-mass stars at the end of their evolution). They carry the isotopic signatures of H burning in the core and of the later H and He burning in thin shells. The diamond dust carries a supernova isotopic signature in Xe inclusions, which is stuck in the diamond crystal structure. Graphite, silicon nitride and a subgroup of silicon carbide, show evidence for a supernova origin in the form of extinct ^{44}Ti and large ^{28}Si excesses. Detailed studies of these different grains have provided new information on stellar evolution, nucleosynthesis, mixing in supernovae, galactic evolution, and the age of the galaxy. For a detailed overview of in-situ measurements of either dust from spacecraft or dust from meteorites we refer to e.g., Mann & Jessberger (2003b), Ott (2003), Ott & Hoppe (2007).

1.3.3 THEORETICAL APPROACH

In principle one can distinguish between models which concentrate on the condensation of dust grains out of the gas phase, and models for the temporal evolution of the dust content in galaxies.

Dust formation models

These models have been developed to investigate dust formation for example in (i) stellar outflows such as the winds of asymptotic giant branch stars (AGB), in the ejecta of SN or in luminous blue varibles (LBVs) (e.g., Ferrarotti & Gail 2001; Gail et al. 2005), but also in (ii) substellar atmospheres (e.g., Helling et al. 2008) or (iv) brown dwarfs (e.g., Burrows 2009, and references therein).

The dust formation process can be described as a two step process, i.e., the condensation of critical seed clusters out of the gas phase and the subsequent growth to macroscopic dust grains of certain size and species. The nucleation process in the majority of models is based on the so called 'classical nucleation theory' (Feder 1966) which was developed to explain the formation of water droplets in the Earths atmosphere. While the applicability of this theory to astrophysical environments has been put into question (e.g., Donn & Nuth 1985), no other theory found its breakthrough yet. It has been found that at temperatures between $\sim$700 K and $\sim$2000 K and densities in the range $\sim 10^{-13}$–10^{-15} g cm^{-3} (Feder 1966; Clayton 1979; Sedlmayr 1994) thermodynamically stable clusters can form. Dust grain formation also depends on the sticking probability, which is influenced by properties such as the material under consideration, the internal energy of the grains, the impact energy and the temperature of the gas. However, the exact sticking probability is uncertain (Draine 1979; Leitch-Devlin & Williams 1985; Gail 2003). In some models (e.g., for SN) this probability is for simplicity assumed to

be unity and means that all colliding particles stick together, leading to a maximum amount of dust to be formed under the given nucleation and growth conditions.

AGB stars and SNe are believed to be the most productive stellar sources of dust (see Sect. 2.3). The following discussion will therefore focus only on these sources.

For AGB stars numerical models solving the coupled system of equations for radiation hydrodynamics, dust formation and growth have been developed over many years (e.g., Gail & Sedlmayr 1987, 1988; Höfner et al. 1998; Andersen et al. 2003; Woitke 2006; Höfner & Andersen 2007; Höfner 2009) and proven feasible in comparison to observations (e.g., Gautschy-Loidl et al. 2004; Nowotny et al. 2005, 2010). However, in these models which are constructed to study dust formation in conjunction with mass loss mechanisms, the time dependent dynamical processes of the stellar atmospheres are treated properly, but the radiative transfer is greatly simplified. Additionally, the models are primarily constructed for low mass AGB stars of $\sim$ 1–2 $\mathrm{M}_{\odot}$ and solar metallicity. In the case of low or very high metallicity and for intermediate and high mass AGB stars ($>$ 2 $\mathrm{M}_{\odot}$) the driving mechanism for mass loss, the chemical composition of the atmospheres and hence the dust formation involved are yet poorly understood. Conversely, hydrostatic models of stellar atmospheres compass for example advanced dust chemistry and/or frequency dependent radiative transfer, but comprise simplistic dynamics (Cherchneff 2006; Ferrarotti & Gail 2006).

For SNe, dust formation models are even more in its infancy. Since the first models (e.g., Cernuschi et al. 1965; Hoyle & Wickramasinghe 1970), several approaches have been undertaken to give rise about various dust species and amounts of dust formed in SN ejecta (e.g., Kozasa et al. 1989; Clayton et al. 1999, 2001; Todini & Ferrara 2001; Nozawa et al. 2003), but the results turned out to be inconsistent with observations. Apart from the uncertainties of the dust formation theory itself, the models are hampered by many complex physical processes such as for example the SN explosion and subsequently the expansion of the ejecta which are not well understood yet. For the latter, in the majority of cases simple adiabatic expansion is assumed, and the density and temperature profiles of the ejecta, which are crucial for dust formation, are not reproduced properly. The models in general produce more dust than what is observed and the ongoing discussions are to that effect whether the inconsistency is in fact a matter of the simplistic models or the observations. However, observations of dust in SN ejecta are difficult as well and uncertain.

Dust evolution models

For studying the temporal evolution of dust in a galaxy, chemical evolution models have emerged as very useful tools.

The field of application of chemical evolution models is large, e.g. it can be used to investigate the temporal evolution of the abundance of elements and dust influenced

by formation and destruction processes, the abundance distribution of elements, stellar masses, the metallicity as well as the relative abundance of heavy elements. The models are mainly regulated by the interplay of processes such as star formation, diverse gas and dust flows and the stellar feedback, while in terms of dust additionally dust destruction and growth processes need to be considered. An additional important parameter is the IMF.

One of the earliest introductions to chemical evolution models can be traced back to Schmidt (1963) and the first dust evolution models were introduced by Dwek & Scalo (1979, 1980). The latter models were constructed to account for the observed depletion patterns in the ISM, which were under much debate. From the models was suggested that these patterns mirror the efficiency of dust destruction in the ISM. For a review see also Dwek (1998, and references therein). During the last decades, dust evolution models have been developed for many different kinds of galaxies such as spiral galaxies (e.g., Hirashita 1999), dwarf galaxies (e.g., Lisenfeld & Ferrara 1998), the Milky Way and solar neighborhood (e.g., Dwek 1998; Calura et al. 2008; Zhukovska et al. 2008), early galaxies (e.g., Edmunds 2001; Morgan & Edmunds 2003) or high-z quasars (e.g., Dwek et al. 2007; Valiante et al. 2009).

While most of the processes governing the models are uncertain, several simplifications have often been adopted. For example, the assumption of an instantaneous recycling approximation, which reflects the neglect of a lifetime dependent yield and dust injection from the stellar sources, has often been made in the earlier models. In particular, yields and dust are assumed to be released into the ISM immediately after their formation. For high mass stars (> 8 $\mathrm{M}_{\odot}$) such an assumption might be applicable due to the rather short lifetimes of these stars, but it is inappropriate for low mass stars (i.e., AGB stars) with lifetimes almost as long as the age of the Universe. Another simplification is the assumption of a so called 'closed box' model. In this case infall and outflows of material are neglected and the mass of the galaxy is constant. The applicability of such an approach is debated. For example, in the solar neighborhood evidence for an infall of gas has been given by Larson (1972) already and an infall rate of 1 $\mathrm{M}_{\odot}$ pc^{-2} Gyr^{-1} was suggested by Cox & Smith (1976). A closed box model has also been found insufficient to solve the 'G-dwarf problem' (e.g., Tinsley 1980, and references therein). However, realistic infall rates for various types of galaxies are often not known and the appropriateness of such a scenario in the course of starburst galaxies with very high SFRs will be discussed in this thesis. Outflows can be initiated by for example SN explosions which transfer with a certain efficiency energy to the ISM material. In order to generate outflows, the material needs to have an energy large enough to escape from the galactic potential well. While this is dependent on various properties of the galaxy under consideration, in most cases outflows either are or can be neglected. A common major problematic of all dust evolution models is the uncertainty of dust production by stellar sources as described above. Additionally, dust destruction and growth pro-

cesses are also only poorly understood and are often not taken into account. However, the advantage of a chemical evolution model is that it can adjusted to the need, i.e., the galaxy under consideration, and the processes entering the model can individually be improved.

1.3.4 AT HIGH REDSHIFT

Models constructed for the Milky Way and galaxies in the local Universe are guided by many observational constrains such as the abundance patterns, extinction, emission by interstellar dust, the size, mass and age of the galaxy as well as the star formation rate. These constrains are helpful in a way that models can be compared with and adjusted to these constrains.

From SCUBA, MAMBO, MAMBO-2 and VLA surveys of bright high redshift QSOs at $4 \lesssim z \leq 6.4$ (e.g., Carilli et al. 2001a; Omont et al. 2001; Isaak et al. 2002; Bertoldi & Cox 2002; Bertoldi et al. 2003a; Robson et al. 2004; Beelen et al. 2006) very high dust masses up to 10^8 $\mathrm{M}_\odot$ and star formation rates up to 10^3 $\mathrm{M}_\odot$ yr^{-1} have been inferred from the measured sub-millimeter fluxes. However, it has been proven difficult to explain the origin of these dust masses in QSOs at $z > 6$, despite some attempts (e.g., Dwek et al. 2007; Valiante et al. 2009). At this redshift the timescale available to build up such large dust masses is short, which leaves not many options for dust sources to be considered. As a consequence SNe have been strongly favored but other sources may play an important role as well. This will be investigated in this thesis.

The derived dust masses and SFRs are naturally uncertain. The basic concept and caveats of deriving the dust mass and SFRs from observations are therefore briefly discussed below.

Dust mass

Based on the method discussed by Hildebrand (1983) the dust mass is determined from the sub-millimeter flux density observed at frequency $\nu_\mathrm{o} = \nu_\mathrm{r}/(1+z)$ as follows

$$M_\mathrm{d} = \frac{S(\nu_\mathrm{o}) D_\mathrm{L}^2}{(1+z)\kappa_\mathrm{d}(\nu_\mathrm{r}) B(\nu_\mathrm{r}, T_\mathrm{d})}, \tag{1.1}$$

where ν_r is the rest-frame frequency, D_L is the luminosity distance to the object which is dependent on the cosmological model, T_d the dust temperature, $\kappa_\mathrm{d}(\nu_\mathrm{r})$ the dust absorption coefficient and $B(\nu_\mathrm{r}, T_\mathrm{d})$ is the black-body Planck function.

The Planck function is generally defined as

$$B(\nu_\mathrm{r}, T_\mathrm{d}) = \frac{2h}{c^2} \frac{\nu_\mathrm{r}^3}{exp(h\nu_\mathrm{r}/kT_\mathrm{d}) - 1} \tag{1.2}$$

where h is the Planck constant, c the speed of light and k the Boltzmann constant.

While also uncertainties are given by the cosmology which enters the dust equation, the main problems of deriving the dust mass from observations is most likely given by $\kappa_{\rm d}(\nu_{\rm r})$ and $T_{\rm d}$. According to the general formulation by Hildebrand (1983), $\kappa_{\rm d}(\nu) \equiv (3/4)Q(\nu)/a\rho$, where $Q(\nu)$ is the emissivity which varies with ν^{β}. From this formulation it is clear that $\kappa_{\rm d}(\nu)$ is significantly dependent on dust properties such as the emissivity index β, the grain radius a and the grain density ρ, while none of these properties are well known. The absorption coefficient for example has been determined by Hildebrand (1983) for a wavelength λ = 125 μm (ν_0 = 2.4 THz) which is the critical wavelength (frequency) at which a source becomes optically thin. At this wavelength $\kappa_{\rm d}(\nu_0)$ was determined to be 18.75 cm^2 g^{-1}. Usually the following expression is used to obtain $\kappa_{\rm d}(\nu)$ for any other frequency (observed or rest-frame) as

$$\kappa_{\rm d}(\nu_{\rm r}) = \kappa_{\rm d}(\nu_0) \left(\frac{\nu_{\rm r}}{\nu_0}\right)^{\beta}. \tag{1.3}$$

For other values of the absorption coefficient resulting from different approaches of deriving $\kappa_{\rm d}(\nu)$ at various wavelengths we refer to a summary of Alton et al. (2004, Table 4). While $\kappa_{\rm d}(\nu)$ increases from FIR to sub-millimeter wavelengths (Draine 1990b), it shall be noted that for similar wavelengths the inferred values for $\kappa_{\rm d}(\nu)$ often vary over an order of magnitude.

Another ambiguous parameter is the emissivity index β. It has been found that β is dependent on the wavelength (or frequency) and increases with increasing wavelength. For $\lambda \lesssim 200$ μm the emissivity index $\beta \sim 1$ and for $\lambda \gtrsim 1000$ μm $\beta \sim 2$ (e.g., Erickson et al. 1981; Schwartz 1982). However, β might also depend on the dust composition, the grain size and possibly also the temperature. For a detailed discussion we refer to Dunne & Eales (2001, and references therein). The emissivity index β as well as the dust temperature, $T_{\rm d}$, can be determined by fitting the spectral energy distribution (SED). According to Hildebrand (1983) the flux density, $S(\nu)$, is defined as

$$S(\nu) = \Omega_{\rm d} Q(\nu) B(\nu, T_{\rm d}), \tag{1.4}$$

where $\Omega_{\rm d} = N(\sigma_{\rm d}/D_{\rm L}^2)$ is the solid angle subtended by the dust source in the sky, with N the number of spherical grains each of cross section $\sigma_{\rm d}$. For high-z objects the SEDs are fitted in the rest-frame and Eq. 1.4 needs to be modified accordingly.

For a simultaneous determination of $T_{\rm d}$ and β many flux measurements at different wavelengths are necessary. This however is often not possible for high redshift objects and values for either $T_{\rm d}$ or β are simply assumed. Priddey & McMahon (2001) found that the composite SED from a sample of quasars at $z > 4$ are best fitted with a single temperature of $T_{\rm d} \sim 40$ K and an emissivity index $\beta \sim 1.95$, while Hughes et al. (1997) and Benford et al. (1999) found for high-z objects a $T_{\rm d} \sim 50$ K and $\beta \sim 1.5$. From a similar study as Priddey & McMahon (2001) but with a larger sample of high-z QSOs ($1.8 \leq z \leq 6{,}4$) Beelen et al. (2006) obtains for a combined SED of all QSOs a higher temperature $T_{\rm d} \sim 47$ K but lower $\beta \sim 1.6$. See for example Fig. 1.3.

The SED can in principle be fitted by either a single temperature model (as described above) or a two temperature component model as it is accomplished by e.g., Dunne & Eales (2001), Vlahakis et al. (2005) or Ivison et al. (2010).

For a two component model the equation for the dust mass can be expressed as

$$M_{\rm d} = \frac{S(\nu_{\rm o})D_{\rm L}^2}{(1+z)\kappa_{\rm d}(\nu_{\rm r})}\left[\frac{N_{\rm m}}{B(\nu_{\rm r},T_{\rm w})}+\frac{N_{\rm c}}{B(\nu_{\rm r},T_{\rm c})}\right] \tag{1.5}$$

where $N_{\rm w}$ and $N_{\rm c}$ represent the relative masses of the warm and cold component.

Although the uncertainties in deriving the dust mass form observations are normally large, it has been found that using a two component dust model, the derived dust masses are usually a factor of ~ 2 higher than what can be obtained from a single temperature model (e.g., Dunne & Eales 2001; Vlahakis et al. 2005) due to the larger amount of cold dust.

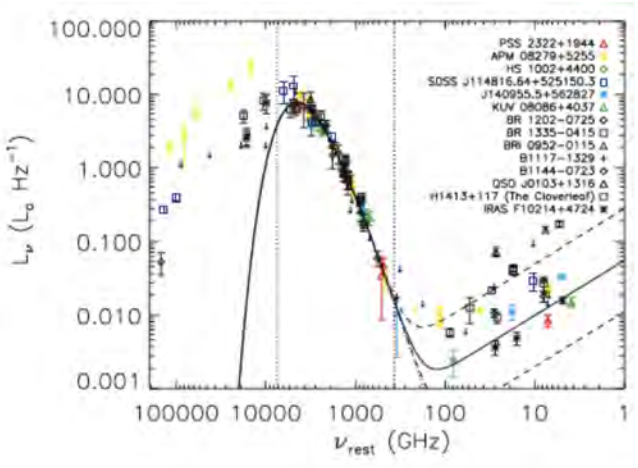

Figure 1.3: *Combined SED, in the rest frame, of high-z QSOs taken from Beelen et al. (2006). The plot comprises data from sources discussed in Benford et al. (1999), Priddey & McMahon (2001) and Beelen et al. (2006). The mean FIR data points are best fitted with a graybody of temperature $T_{\rm d} \sim 47$ K and emissivity index $\beta \sim 1.6$.*

Star formation rate

The SFR of a system can be determined using the FIR dust emission. Integrating the SED (Eq. 1.4) over the emitting area $\Omega_{\rm d}$ and over the corresponding frequency range, the FIR luminosity can be obtained (see e.g., Yun & Carilli 2002) as

$$L_{\rm FIR} = 4\pi D_{\rm L}^2 \int\int S(\nu){\rm d}\nu{\rm d}\Omega. \tag{1.6}$$

Another approach to obtain $L_{\rm FIR}$ which visualizes the relation between the FIR luminosity and the dust mass is integrating the SED using (Eq. 1.1) as

$$L_{\rm FIR} = 4\pi M_{\rm d} \int \kappa_{\rm d}(\nu)B(\nu,T_{\rm d}){\rm d}\nu. \tag{1.7}$$

For bright high-z objects FIR luminosities of the order of 10^{12-13} $\mathrm{L}_{\odot}$ are usually derived (e.g., Omont et al. 2001; Bertoldi & Cox 2002; De Breuck et al. 2003; Robson et al. 2004; Beelen et al. 2006; Wang et al. 2010; Ivison et al. 2010; Leipski et al. 2010).

The SFR of a galaxy is then directly related to its dust continuum spectrum by the FIR luminosity for example as given by Gallagher et al. (1984) and Thronson & Telesco (1986)

$$L_{\mathrm{FIR}} = \psi_{\mathrm{FIR}} t_{\mathrm{FIR}} \bar{L}/\bar{M} \tag{1.8}$$

where ψ_{FIR} is the SFR, t_{FIR} accounts for the (assumed) duration of the starburst and $\bar{L}/\bar{M}$ is the luminosity-to-mass ratio which is determined from an assumed IMF. The mean luminosity and mass are calculated as $\bar{L} = \int l(m)\phi(m)\mathrm{d}m / \int \phi(m)\mathrm{d}m$ and $\bar{M} = \int m\phi(m)\mathrm{d}m / \int \phi(m)\mathrm{d}m$, where $\phi(m)$ is the initial mass function (IMF) and $l(m)$ is the stellar luminosity function. The $l(m)$ is rather uncertain and values are taken for example from Gallagher et al. (1984).

A simplified formulation for the SFR is then often given as

$$\psi_{\mathrm{FIR}} = \delta_{\mathrm{MF}} \delta_{\mathrm{SB}} (L_{\mathrm{FIR}}/10^{10}\,\mathrm{L}_{\odot})\,\mathrm{M}_{\odot}\mathrm{yr}^{-1}, \tag{1.9}$$

where $\delta_{\mathrm{MF}} = t_{\mathrm{FIR}}\bar{L}/\bar{M}$ and δ_{SB} is the fraction of the FIR emission heated by the starburst.

Evidently, the calculated value for the SFR is sensitively dependent on the assumed IMF. In most cases simply a Salpeter IMF is used. Another critical parameter is the assumption of the duration of the starburst. Commonly for example either values of $\delta_{\mathrm{MF}} \sim$ 0.8–2.1 (Scoville & Young 1983; Thronson & Telesco 1986) or simply δ_{MF} = 1 are adopted. However, these values have been derived using a Salpeter IMF ($\phi(m) \propto m^{-\alpha}$, α = 2.35) and an assumed starburst age of for example t_{FIR} = 2 Myr (Thronson & Telesco 1986). As pointed out by Omont et al. (2001), these assumptions might in fact be inappropriate for massive starbursts in high redshift galaxies. Considering a continuous starburst of 100 Myr and a Salpeter IMF with different low mass cutoffs, Omont et al. (2001) derive $\delta_{\mathrm{MF}} \sim$ 1.2–3.8. Assuming a flat IMF (α = 1) at low masses and for t_{FIR} = 10–100 Myr results in $\delta_{\mathrm{MF}} \sim$ 0.8–2 similar to the values of Thronson & Telesco (1986). As pointed out by Dwek et al. (2007), the IMF constitutes one of the major uncertainties. So, for example, the derived SFR using a Salpeter IMF of $\sim$ 3400 $\mathrm{M}_{\odot}$ yr^{-1} for the QSO J1148+5251 (Fan et al. 2003) decreases in the case of an IMF biased towards higher masses as for a top-heavy IMF to about 380 $\mathrm{M}_{\odot}$ yr^{-1}. The range of the SFR in some high-z objects might therefore be between 10^{2-3} $\mathrm{M}_{\odot}$ yr^{-1}.

Furthermore it is controversial, whether the FIR luminosity arises solely from the starburst and if the entire stellar radiation is absorbed and re-emitted by warm dust or whether the Active galactic nucleus (AGN) heating needs to be taken into account. While this issue is often discussed, the most common view is that the heating source is the starburst and a contribution of the AGN is usually neglected, thus δ_{SB} is set to 1. Taking a contribution of the AGN into account will certainly result in a smaller amount

of dust and lower star formation rates. For more detailed discussion we refer to e.g., Omont et al. (2001) and Isaak et al. (2002).

1.4 STRUCTURE OF THE THESIS

This thesis is motivated by the discoveries of large dust masses in high-redschift QSOs and their unresolved origin and evolution.

In Chapter 2 the current stage of stellar evolution of potential dust sources is briefly reviewed and the up to date status of knowledge about dust masses produced by stellar sources on part of observations and theory is presented. Based on this information different limits of the dust production efficiencies of stars in a mass range of 3–40 $\mathrm{M}_{\odot}$ are ascertained. The dust productivity of stars in diverse mass-subranges of a single stellar population is derived and the dependency of the dust productivity on different IMFs is investigated. A simple estimate to test whether the amount of dust produced by the derived dust production efficiency limits may account for the large observed dust masses is presented.

Chapter 3 deals with the modeling of dust evolution in starburst galaxies. The equations for the chemical evolution model are described. The main input parameter and their assumed values are specified. The results of the temporal progression of dust and other physical properties for galaxies with different initial masses and variations of some model parameters are presented. In particular, the influence of diverse IMFs, dust production efficiencies and the strength of dust destruction is investigated.

In Chapter 4 the developed model is particularly applied to QSOs at $z \gtrsim 6$. The influence of variations of the SFRs on the amount of dust and some physical properties is investigated. The results are compared to individual QSOs at $z \gtrsim 6$ in order to ascertain plausible scenarios for generating large amounts of dust.

In Chapter 5 the main conclusions and some future prospects are presented.

This chapter is based on: C. Gall, A. C. Andersen and J. Hjorth – *Genesis and evolution of dust in galaxies in the early Universe – I. Dust productivity of massive stars* A&A, submitted
Figure: Cas A; NASA and Chandra Science Center

2

DUST PRODUCTIVITY OF MASSIVE STARS

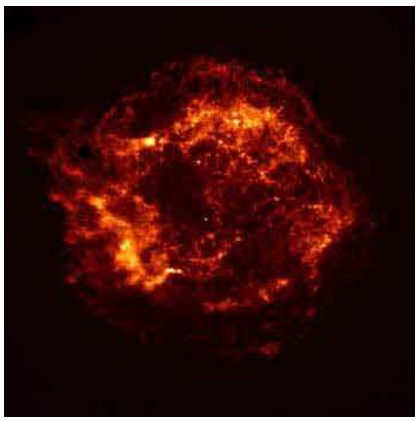

Når ifølge vane, var jeg overvejede stjernerne på en klar himmel,
jeg lagde mærke til en ny og usædvanlig stjerne,
overgår de andre stjerner i glans. . . .
Der havde aldrig før været nogen stjerne på dette sted i himlen.

TYCHO BRAHE (1572)

ABSTRACT –

Large amounts of dust appear to be present in galaxies and quasars at high redshift. At $z > 6$ only stars of relatively high mass ($> 3\,\mathrm{M}_\odot$) are sufficiently short-lived to be potential stellar sources of dust.

We aim to identify the mass ranges of the most efficient dust producing stars at high redshift and to quantify the influence of the IMF on the total dust productivity. We ascertain the dust production efficiency of stars in the mass range 3–40 $\mathrm{M}_\odot$ using observed and theoretical dust yields of AGB stars and SNe. Based on these efficiencies we determine the total dust productivity for different stellar sources and IMFs.

2.1 INTRODUCTION

The origin of the significant amounts of dust found in high-redshift galaxies and QSOs remains elusive.

Observational evidence for dust in these systems has been reported by, e.g., Pei et al. (1991); Pettini et al. (1994); Ledoux et al. (2002); Robson et al. (2004); Chary et al. (2005); Beelen et al. (2006); Hines et al. (2006). Detection of thermal dust emission from high-redshift QSOs at sub-millimeter and millimeter wavelengths (e.g., Omont et al. 2001, 2003; Carilli et al. 2001b; Bertoldi & Cox 2002) indicates far-infrared luminosities $\geq 10^{12-13}$ $\mathrm{L}_{\odot}$, implying dust masses of $\geq 10^{8}$ $\mathrm{M}_{\odot}$ and star-formation rates up to 3000 $\mathrm{M}_{\odot}$ yr^{-1} (e.g., Bertoldi et al. 2003a).

In addition, the age of the Universe at $z > 6$ was less than $\sim$1 Gyr. Early star formation is believed to have taken place at redshift 10–50 (Tegmark et al. 1997; Greif & Bromm 2006); the earliest galaxy photometrically detected so far is at $z \sim 10$ (Bouwens et al. 2009). The epoch of reionization is determined at $z = 10.4 \pm 1.2$ (Komatsu et al. 2010) ($\sim$500 Myr after the Big Bang). These facts imply that the maximum timescale to build up large dust masses is at most $\sim$400–500 Myr.

Hence, a fast and large dust production mechanism is needed. Core collapse supernovae (CCSNe) are contemplated to be the most likely sources of dust at this epoch (e.g., Dwek 1998; Tielens 1998; Edmunds 2001; Morgan & Edmunds 2003; Maiolino et al. 2004) due to their short lifetimes and large production of metals. Consequently, several theoretical models for dust formation in CCSNe have been developed and result in dust masses of up to 1 $\mathrm{M}_{\odot}$ per SN within the first $\sim$600 days after the explosion (e.g., Kozasa et al. 1989, 1991; Clayton et al. 1999, 2001; Todini & Ferrara 2001; Nozawa et al. 2003). Dwek et al. (2007) also argued that 1 $\mathrm{M}_{\odot}$ of dust per SN is necessary if SNe only are to account for the inferred amounts of dust in high-z QSOs.

However, observations of dust in the ejecta of nearby SNe a few hundred days past explosion have revealed only $\sim 10^{-4}$–10^{-2} $\mathrm{M}_{\odot}$ of hot ($\sim$400–900 K) dust (e.g., Wooden et al. 1993; Elmhamdi et al. 2003; Sugerman et al. 2006; Kotak et al. 2009). Larger amounts ($\sim 10^{-2}$ $\mathrm{M}_{\odot}$ up to $\sim$1 $\mathrm{M}_{\odot}$) of cold and warm (20–150 K) dust have been reported in SN remnants, a few 100–1000 years after explosion (e.g., Rho et al. 2008, 2009; Dunne et al. 2009; Gomez et al. 2009; Barlow et al. 2010).

The discrepancy between observationally and theoretically determined dust yields has provoked a reconsideration of the present SN dust formation theories (Cherchneff & Dwek 2010) and models including dust destruction have been developed (e.g., Bianchi & Schneider 2007; Nozawa et al. 2007; Nath et al. 2008; Silvia et al. 2010). The latter models demonstrate that dust grains can be effectively destroyed in a reverse shock from SNe on timescales up to $\sim 10^{4}$ years after their formation, but they cannot account for the observed low amounts of dust on shorter timescales of a few 100 days. Moreover, dust production in SNe seems to vary with the type of the SNe (e.g., Kozasa

et al. 2009; Nozawa et al. 2010).

In addition to SNe, intermediate and high-mass AGB stars with masses between 3–8 $\mathrm{M}_{\odot}$ have sufficiently short lifetimes of a few 10^7–10^8 years (e.g., Schaller et al. 1992; Schaerer et al. 1993; Charbonnel et al. 1993; Raiteri et al. 1996) to be potential contributors to dust production in high-redshift galaxies.

Independently of a possible influence from different types of stars on the total amount of dust in high-redshift systems, the prevailing IMF might also play an important role. In the local Universe, an IMF favoring lower mass stars is well established (e.g., Elmegreen 2009) while the IMF in the early Universe and in starburst galaxies appears to be biased towards high-mass stars (e.g., Doane & Mathews 1993; Dabringhausen et al. 2009; Habergham et al. 2010).

In this Chapter we aim to identify the most important mass ranges of stellar sources contributing to the total amount of dust in high-z galaxies. We determine the ranges of dust production efficiencies of SNe and AGB stars and investigate the influence of various IMFs on the dust productivity of stars between 3–40 $\mathrm{M}_{\odot}$. In companion papers we will incorporate these efficiency limits into a detailed galactic chemical evolution model which considers the lifetime dependent delayed dust injection from AGB stars and SNe as well as further processing of dust in the ISM.

The Chapter is arranged as follows: we first review current knowledge about stellar evolution for massive stars (Sect. 2.2) and their significance as dust producers (Sect. 2.3). We briefly summarize the complexity of determining the amount of dust theoretically and observationally in Sect. 2.4. Dust production efficiencies are quantified in Sect. 2.5 and the impact of the IMF on the total dust productivity is discussed in Sect. 2.6. Sect. 2.7 summarizes our results.

2.2 THE LATE STAGES OF MASSIVE STELLAR EVOLUTION

For the most likely dust producers, such as AGB stars and CCSNe, the majority of the dust production takes place at the end stages of their evolution. Therefore, pertaining to the observed presence of dust in galaxies and QSOs at $z \geq 6$, only stars which live short enough to die before the age of the Universe at this redshift are conceivable sources of dust.

In Fig. 2.1 we illustrate the relation between the minimum mass of stars and the redshift at which they die. We have considered three different epochs for the onset of star formation. For an onset at redshift $z = 10$ we find that the lowest mass of a star to be a possible source of dust in systems at $z = 6$ is 3 $\mathrm{M}_{\odot}$. Less massive stars can be excluded because the lifetimes are longer than the age of the Universe at this redshift. The effect of the metallicity with which a star is born is small.

Owing to this ascertainment, we are solely interested in the high-mass ($\gtrsim 3\,\mathrm{M}_{\odot}$) stellar population. The remainder of this section is devoted to a brief review of the diverse

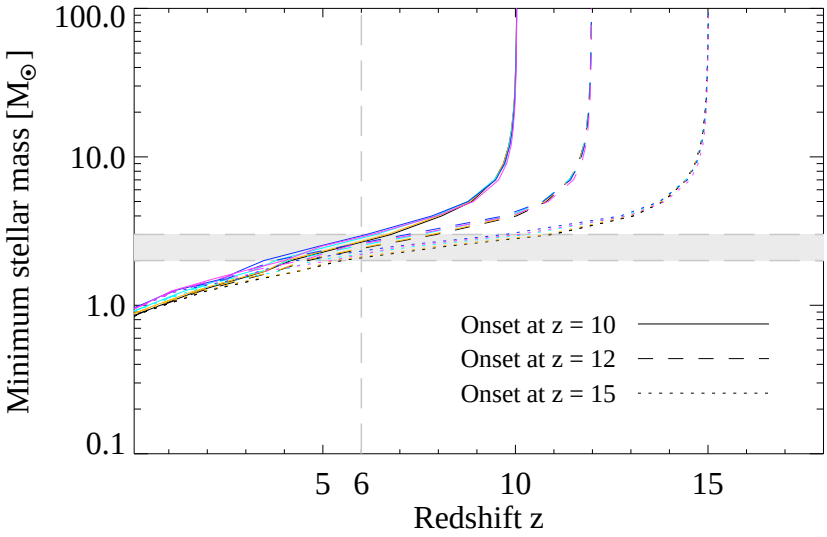

Figure 2.1: *Relation between stellar mass, stellar lifetime and redshift in the early Universe. The graphs show the minimum mass of a star dying at a given redshift for an onset of star formation at three different epochs: 260 Myr after Big Bang (dotted curves), $z = 12$ (dashed curves), $z = 10$ (solid curves). The colour coding corresponds to different metallicities: Z = 0.001 (black), Z = 0.004 (yellow), Z = 0.008 (cyan), Z = 0.020 (blue), Z = 0.040 (magenta). The vertical dashed line marks a star dying at $z = 6$, similar to the highest-redshift QSOs known. The grey shaded region indicates stars with masses between 2–3* $\mathrm{M}_\odot$*. The metallicity dependent lifetimes are taken from Schaller et al. (1992); Schaerer et al. (1993) and Charbonnel et al. (1993). The cosmological model used is a ΛCDM Universe with* $H_0 = 70$ *km* s^{-1} *Mpc*$^{-1}$, $\Omega_\Lambda = 0.7$ *and* $\Omega_m = 0.3$.

stellar evolution and end stages, which substantially influence the dust production of these stars.

2.2.1 The first stars

The first generation of stars, so-called Population III (Pop III) stars, played an important role in reionizing the Universe, and are expected to have formed at redshift $z \sim$10–50 in dark-matter mini halos of $\sim 10^6$ $\mathrm{M}_\odot$ (Tegmark et al. 1997). The very first stars (Pop III.1) are responsible for the early enrichment with metals. However, they are believed to be relatively rare, only about 10% by mass of all generations of Pop III stars (e.g., Greif & Bromm 2006; McKee & Tan 2008), but also very massive $\sim 10^{2-3}$ $\mathrm{M}_\odot$ (e.g., Bromm & Larson 2004; Schneider et al. 2006).

According to Heger et al. (2003), stars with $Z = 0$ and masses between 40–140 $\mathrm{M}_\odot$ and above 260 $\mathrm{M}_\odot$ collapse into black holes while stars in the mass range between 140–260 $\mathrm{M}_\odot$ die as pair instability SN (PISN). The explosion will entirely disrupt the star,

leaving a quite peculiar chemical signature (Heger & Woosley 2002). So far only one supernova, SN2007bi has been reported as a PISN (Gal-Yam et al. 2009).

The metal enrichment by Pop III stars leads to formation of low-mass Pop II stars, as soon as a critical metallicity of $Z_{\rm cr} \sim 10^{-6}$–10^{-4} $\rm Z_\odot$ (Bromm & Loeb 2003; Schneider et al. 2006; Tumlinson 2006) is reached. Greif et al. (2010) showed in a cosmological simulation that one single PISN (at $z \simeq 30$) can enrich the mini halo in which it forms uniformly up to $Z = 10^{-3}$ $\rm Z_\odot$ and enhance Pop II star formation (at $z \simeq 10$).

The IMF for the first stars is considered to be very top heavy with high characteristic masses $>$ 35–100 $\rm M_\odot$ (e.g., Bromm et al. 2002; Tumlinson 2006; Yoshida et al. 2008). For the second generation of Pop II stars, top heavy IMFs with somewhat lower characteristic masses or Salpeter-like IMFs are usually assumed. Tumlinson (2006) points out that metal free star formation is relatively scarce at redshift $z \sim 6$. For these reasons, PISNe and the very first stars are unlikely to be major dust sources for galaxies at $z \sim 6$.

2.2.2 Intermediate and high-mass AGB stars

Stars in the asymptotic giant branch phase are in their late stages of stellar evolution. AGB stars have initial masses in the range $\sim$ 0.85–8 $\rm M_\odot$ and have completed their helium-burning phase in their centers. They are of low surface temperature (max 3500K) but high luminosity (a few times $10^3 \rm L_\odot$) and have build up a so called helium- and hydrogen-burning shell around their degenerate cores of carbon and oxygen. The hydrogen burning shell triggers the energy needed to maintain the high luminosity. During the AGB evolution the stars develop quite strong winds with increasing mass loss rates towards their late stages whereas they lose some of their matter (e.g., Schöier & Olofsson 2001).

The late stages are characterized by intense mass loss. At the very end, stars develop a super-wind phase with mass loss rates up to 10^{-4} $\rm M_\odot$ $\rm yr^{-1}$ (e.g., Bowen & Willson 1991; Schöier & Olofsson 2001).

Low and intermediate mass stars ($<$ 8 $\rm M_\odot$) end their lives as white dwarfs. However, the final fate of stars at the upper mass end of the AGB mass range might be different (see Sect. 2.2.4). In general, stars loose up to $\sim$ 80 % of their mass during the AGB phase and form a circumstellar envelope of gas and dust.

AGB stars can be broadly divided into two distinct groups based on low-resolution spectra: The oxygen-rich M-stars whose spectra are dominated by bands of TiO molecules, and the carbon-rich C-stars whose spectra are dominated by the bands of C_2 and CN molecules (Lattanzio & Wood 2003).

The distribution of C- and M-stars is a function of stellar mass and initial metal abundance. For low initial metallicities it is easier to form C-stars as less carbon needs to be dredged up. Stellar evolutionary models by Karakas & Lattanzio (2007) predict that for LMC-like metallicities, M-stars evolve from low (1.0–1.5 $\rm M_\odot$) and high (5.0–8.0

$M_\odot$) mass stars, while C-stars originate from intermediate (1.5–5.0 $M_\odot$) mass stars. The latter has also been found by e.g., Vassiliadis & Wood (1993) and Zijlstra et al. (2006).

Generally, AGB stars with masses above 4 $M_\odot$ experience hot bottom burning (e.g., Blöcker & Schönberner 1991; D'Antona & Mazzitelli 1996) leading to a reduction of the amount of carbon which can be dredged up. At higher metallicities they appear during a main part of their AGB phase as M-stars and at lower metallicities they are C-stars (Ventura & D'Antona 2009).

2.2.3 Core collapse supernovae

CCSNe are divided into two different classes, Type II and Type I, and their subtypes (e.g., Filippenko 1997, and references therein). Type II SNe are defined by the presence of hydrogen lines in the optical spectra whereas Type I SNe are defined through their absence. The CCSNe subtypes can be aligned roughly in the order of increasing progenitor mass, starting with II-P, IIL, IIn, IIb, Ib and Ic (e.g., Anderson & James 2008), although, as we discuss below, there is no one-to-one correspondence between progenitor mass and spectral type.

The most common CCSNe are Type II-P SNe. Smartt et al. (2009) find, that the mass range of the progenitors for Type II-Ps is between 8.5–17 $M_\odot$. A lower mass limit of $\sim$8 $M_\odot$ was also found independently by Anderson & James (2008). However, theoretical predictions from stellar evolution models (e.g., Heger et al. 2003; Eldridge & Tout 2004; Poelarends et al. 2008) indicate a higher upper mass limit for II-P SNe: For solar metallicity it is $\sim$25 $M_\odot$ and increases with decreasing metallicity. It is unclear what happens with stars more massive than 17 $M_\odot$. The progenitors of II-Ps are found to be red supergiants (RSG). However, RSGs up to 25 $M_\odot$ have been found in the Local Group. One possibility is that they collapse and form a black hole (Smartt et al. 2009; Heger et al. 2003; Fryer et al. 2007). In that case, they either appear as very faint SNe or no explosion occurs at all.

Stars more massive than 25 $M_\odot$ evolve into Wolf Rayet (WR) stars and hence possibly explode as Ib or Ic supernovae (Massey & Olsen 2003; Crowther 2007). During their precursor luminous blue variable (LBV) stage before the WR phase, they loose their hydrogen envelope either in form of massive eruptions or in periods of enhanced mass loss and form a rather dense circumstellar disc (CSD). The WR phase lasts for approximately 10^5 years (e.g., Meynet & Maeder 2003; Eldridge & Vink 2006) whereupon a star finally explodes as a CCSN, leaving a black hole.

Stars above 25–30 $M_\odot$ may also explode during their LBV phase before entering the WR stage. This was the case for SN2005gj (Kotak & Vink 2006; Trundle et al. 2008) and SN2005gl (Gal-Yam et al. 2007), which both appeared as very bright CCSNe of Type IIn. The Type IIn SN2005ip (Smith et al. 2009) had a different progenitor, probably a RSG with roughly 20–40 $M_\odot$. This shows that Type IIn SNe may arise from either stars with

LBV-like mass ejection if they are very luminous, or from massive RSGs with a strong wind interaction if of moderate luminosity.

Stars more massive than roughly 17–25 $M_\odot$ will therefore not end as ordinary Type II-P supernovae, but rather explode as IIn, IIb, Ib or Ic SNe. Their final fate depends on properties such as magnetic fields, metallicity, binarity, or rotation, although the details of these dependencies are not well understood. As a consequence, there is no simple relation between type and progenitor mass: The Type II-P SN2002hh had a RSG progenitor of around 18 $M_\odot$ (Pozzo et al. 2006; Smartt et al. 2009). The progenitor of the Type IIb SN2008ax (Crockett et al. 2008; Pastorello et al. 2008) was a late-type 28 $M_\odot$ WR star with strong nitrogen emission lines in the spectra (a so-called WNL star). The mass of the progenitor of SN2003bg was estimated at 20–25 $M_\odot$ (Mazzali et al. 2009). An example of a Ic SN is SN2004gt, where the progenitor mass is estimated to be $\gtrsim 40$ $M_\odot$ (Maund et al. 2005). For the Ic SN2002ap a single star progenitor of 30–40 $M_\odot$ has been proposed, but with very high mass-loss rates (Crockett et al. 2007).

2.2.4 Stars in the critical progenitor mass range

The fate of stars in the lower mass range of 8–10 $M_\odot$ is ambiguous, since the mass border between high-mass AGBs and CCSNe is smeared out. We denote this range the critical progenitor mass range. As we discuss below, stars in this mass interval may evolve to either II-P SN directly or enter the super AGB (SAGB) phase. In the latter case, they can end as an electron capture SN (ECSN) possibly appearing as low-luminous Type IIn. Unfortunately, the decisive factors for their development are rather uncertain (e.g., Nomoto 1984, 1987).

During their final stages of evolution some stars will form an electron-degenerate oxygen, neon and magnesium core (O-Ne-Mg) and evolve to SAGB stars. These stars can either become a O-Ne-Mg white dwarf or an ECSN.

The appearance of an ECSN could be as a faint and ^{56}Ni poor II-P supernova such as SN1994N, SN1999eu and SN2005cs (Pastorello et al. 2004, 2006). However, Smartt et al. (2009) did not find any signature or convincing evidence that faint and ^{56}Ni poor II-P SN arise from ECSNe. The inferred luminosities for progenitors in this mass range rather favor normal Type II-P supernovae.

Alternatively, a ECSN could occur as a low-luminousity Type IIn SN such as SN2008S (Prieto et al. 2008). The progenitor mass of SN2008S was determined to be $\sim$10 $M_\odot$ (Prieto et al. 2008). Wesson et al. (2010) and Prieto et al. (2008) proposed that the progenitor could have been a massive AGB star triggering an ECSN, as also found by Botticella et al. (2009).

According to Wanajo et al. (2009), about 30 % of all CCSNe would appear as ECSNe, if all stars in the mass range of 8–10 $M_\odot$ end in the explosion channel. Poelarends et al. (2008, and references therein) suggest that only the most massive (9–9.25 $M_\odot$) stars will

explode as ECSNe, representing $\sim 4\%$ of all SNe. Siess (2007, 2008) showed that at very low metallicity ($Z = 10^{-6}$), the mass range for stars becoming an ECSN is much broader (7.6–9.8 $M_\odot$). Thompson et al. (2009) suggest the rate of ECSNe to be $\sim 20\%$ of all CCSNe.

2.2.5 Type Ia supernovae

Type Ia SNe are characterized by the absence of hydrogen in their spectra and are believed to be products of a thermonuclear explosion of a carbon-oxygen white dwarf (e.g., Livio 2000; Hillebrandt & Niemeyer 2000). An explosion takes place when the white dwarf reaches the Chandrasekhar mass through external mass supply. However the nature of the progenitors and explosion patterns are controversial. Two scenarios are currently prevailing; (i) a single-degenerate model where a main sequence or giant companion star transfers mass by Roche lobe overflow (Whelan & Iben 1973; Fink et al. 2007) and (ii) a double degenerate model where the companion star is also a white dwarf and the two objects merge (Iben & Tutukov 1984; Webbink 1984; Pakmor et al. 2010). The mass range of stars possibly exploding as Type Ia SN is 3–8 $M_\odot$ (e.g., Maoz 2008) which means that the stars become C-O white dwarfs after having evolved as AGB stars. This gives rise to rather long delay times between the formation of the progenitor system and the explosion due to the long lifetimes of these stars. From explosion models (e.g., Greggio & Renzini 1983; Matteucci & Recchi 2001; Greggio 2005) different delay times are predicted. Observationally, evidence of two progenitor channels resulting in SNe Ia $\lesssim 400$ Myr after progenitor formation and SNe Ia with a delay of $\gtrsim 2.4$ Gyr have been found by Brandt et al. (2010). Mannucci et al. (2006) suggest that half the SNe Ia population explode already after about 100 Myr and half of the population have longer delay times of about 3 Gyr.

2.3 Dust from massive stars

We next review the dust formation processes associated with the end-stages of massive stellar evolution.

2.3.1 Dust from AGB stars: Theory and observation

In the local Universe, AGB stars are the prime sources of dust injected into the ISM (Gehrz 1989; Sedlmayr 1994; Dorschner & Henning 1995). The dust is injected as part of the intense mass loss during their late stages (see Sect. 2.2.2). The driving mechanism of the mass loss is believed to be a combination of thermal pulsation and radiation pressure on dust grains resulting in slow dust driven winds (e.g., Höfner et al. 1998; Höfner & Andersen 2007) with typical velocities between 3–30 km s^{-1}. However, Matsuura et al. (2009) point to a 'missing dust source problem' in the Large Magellanic Cloud

(LMC) similar to the same problem found in high-z galaxies. It has been shown that AGB stars together with SNe cannot account for the existing dust mass in the ISM when taking the lifetime of dust grains (about 10^8 yr) into account. In the Milky Way, stars can only account for $\sim 10\%$ of the interstellar dust (Draine 2009) for grain lifetimes of a few 10^8 yr.

The dust composition in AGB stars depends on the C/O ratio in the photosphere of the star which is directly connected with the nucleosynthesis in the stellar interior. Newly formed elements like carbon and oxygen are mixed to the surface by a deep convective zone. The mixing processes occurs during the thermal pulsing phase (TPAGB) and involves also the external layers (Iben & Renzini 1981). The TPAGB last approximately for 10^{4-6} yr depending on the stellar mass and number of thermal pulses (Bloecker 1995). The stellar pulsations cause atmospheric shock waves propagating through the atmosphere. Subsequently gas is lifted above the stellar surface producing dense, cool layers favorable for possible solid particle formation (e.g., Höfner et al. 1998). The ongoing nuclear burning and dredge-up changes the relative abundance of carbon and oxygen as the stars evolve. A change in the C/O ratio results in a change of the spectral type and more crucial the composition of the dust. There are three different spectral types (M-, S- and C-type AGB stars) corresponding to the types of the atmospheric chemistry determined by the high bond energy of the key molecule CO.

- M-type: $\mathrm{C/O} < 1$ results in an oxygen excess since all carbon is bound in CO molecules creating an oxygen rich environment where either silicates or carbonates are formed (see Sect. 1.2)

- S-type: $\mathrm{C/O} \approx 1$ leads to an exhaustion of C and O which are almost completely bound in CO. For this type no abundant grain forming elements are available and grain species are defined by the less abundant elements.

- C-type: $\mathrm{C/O} > 1$ creates a carbon rich environment (all oxygen bound in CO) where predominantly hydrocarbon molecules and carbonaceous dust forms together with some silicon carbide.

However, deriving the dust driven mass-loss characteristics of AGB stars is difficult and the current understanding is based on numerical models. Detailed time-dependent dynamical models featuring a frequency-dependent treatment of the radiative transfer have been successfully explaining the mass loss mechanism for C-stars (e.g., Höfner et al. 2003; Höfner 2006; Winters et al. 2000). It is shown that in such stars, amorphous carbon grains form from the excess of carbon at high temperatures. Mass loss is enhanced by the radiation pressure on such grains which efficiently accelerates the dust particles away from the star dragging also the gas along. The models featuring C-rich dust driven mass loss are well tested and are consistent with observations (e.g., Gautschy-Loidl et al. 2004; Nowotny et al. 2005, 2010).

In the case of M-stars the oxygen environment leads to formation of preferentially Fe-free silicates (Woitke 2006; Höfner & Andersen 2007), in particular olivine and pyroxene type grains. Such grains are consistent with observed features of IR spectra of cool giants (Molster et al. 2002a,b,c). However small Fe-free silicates result in insufficient radiation pressure to drive a wind due to their transparency at wavelengths corresponding to the flux maximum of AGB stars. Höfner (2008) has shown that grains of sizes in a very narrow range around 1 μm can drive a wind. This mass range is also consistent with grain sizes observed in the interstellar medium.

Although processes in C- and M-stars are almost well understood, dust formation and mass loss in S-type stars pose larger problems (Höfner 2009). According to observations, S-stars show properties similar to C- and M-stars (e.g., Ramstedt et al. 2009). However, the close equality of the main abundant elements O and C inhibits the formation of known mass loss driving dust species such as amorphous carbon or micron-sized silicates in sufficient abundances. Several minor dust species have been proposed which however are either not abundant enough or of too low opacity in order to enhance mass loss (e.g., Ferrarotti & Gail 2002, 2006). Despite, that some of these species possibly play an important role, it remains uncertain which dust types or processes drive the winds.

We also need to stress that the described models for AGB stars are developed for low and intermediate mass stars. As pointed out by Höfner (2008) some insights about dust formation and outflows could be gained but uncertainties remain, i.e. the effect of metallicity. Studying the influence of metallicity on the mass loss and dust formation processes in AGB stars is important to understand their role in the early universe. Theoretical investigations by Wachter et al. (2008) on the metallicity dependency of low mass AGB stars showed that the wind velocity decreases with lowering the metallicity, but the mass loss rate remains unaffected. The latter also resulted from models by Mattsson et al. (2008) under the condition that the amount of condensible carbon in the low-metallicity AGB stars is comparable to that of the more metal-rich counterparts. Lagadec et al. (2009) performed CO observations with the JCMT of six carbon stars in the Galactic Halo and the Sagittarius stream and came to similar conclusions. The mass loss rates of C-stars are unaffected by metallicity but the expansion velocities for metal-poor C-stars are lower. Observations with the Spitzer Space Telescope of the LMC, the Small Magellanic Cloud (SMC) and the Fornax Dwarf Spheroidal are indicating that mass loss rates for M-type stars are more affected and lower at lower metallicity, while independent of metallicity for metal-poor C-stars (e.g., Zijlstra et al. 2006; Groenewegen et al. 2007; Lagadec et al. 2007b; Matsuura et al. 2007; Sloan et al. 2009). The amount of dust produced by oxygen rich stars is found to decrease with decreasing metallicities while for carbon stars it remaines unchanged (Groenewegen et al. 2007; Sloan et al. 2008). On the contrary, van Loon et al. (2008) present ESO/VLT spectra of a sample of dusty carbon stars, oxygen rich AGB stars and red supergiants

in the SMC. A comparison of the properties of molecular bands in the SMC to similar data in the LMC indicates that dust formation in C-stars and in M-stars is less efficient at lower metallicities.

Typical mass loss rates obtained observationally and theoretically are between 10^{-7}–10^{-5} $\mathrm{M}_{\odot}$ yr^{-1} (e.g., Schöier & Olofsson 2001; Willson 2007; Mattsson et al. 2008; Matsuura et al. 2009). A relation between the observed dust and the inferred mass-loss rates of AGB stars is given by the gas-to-dust mass ratio which is found to be between $\sim$ 200–400 (e.g., Ramstedt et al. 2008; Lagadec et al. 2009; Sloan et al. 2009).

A theoretical dust formation model for AGB stars in the mass range of 1–7 $\mathrm{M}_{\odot}$ has been developed by Ferrarotti & Gail (2006). Dust yields are calculated for several metallicities and result in total dust masses up to a few times 10^{-2} $\mathrm{M}_{\odot}$. The considered grain species are silicates, iron dust, SiC and carbon, which are the most abundant grain types in M-, S- and C-type AGB stars. The model combines synthetic stellar evolution models with a non-equilibrium dust formation description. However the dynamical treatment of the stellar outflows is largely simplified in a sense that stationary flows are assumed and hence the mass loss rate is an input parameter because it cannot be determined self-consistently. Nevertheless, the model by Ferrarotti & Gail (2006) is currently the only available source which provides dust yields for AGB stars covering a large range of stellar masses and metallicities and are therefor further used in this thesis.

2.3.2 Direct evidence of dust from CCSNe

Direct evidence of dust formed in SN ejecta and remnants has been reported for only a few cases so far.

- In the peculiar Type II supernova SN1987A at most about 10^{-4}–10^{-3} $\mathrm{M}_{\odot}$ of dust at epochs between 615–6067 days past explosion was found (Dwek et al. 1992; Wooden et al. 1993; Bouchet et al. 2004; Ercolano et al. 2007).

- At epochs between 214–795 days past explosion, dust masses of a few times 10^{-4} $\mathrm{M}_{\odot}$ at temperatures of a few hundred K was inferred for the Type II-P SNe SN1999em, SN2003gd, SN2004et and SN2005af (e.g., Elmhamdi et al. 2003; Sugerman et al. 2006; Meikle et al. 2007; Kotak 2008; Kotak et al. 2009).

- For SN2003gd, Sugerman et al. (2006) derived a maximum dust mass on day 499 of 1.7×10^{-3} $\mathrm{M}_{\odot}$ and 2.0×10^{-2} $\mathrm{M}_{\odot}$ on day 678 with a clumpy model. In contrast, Meikle et al. (2007) inferred only 4×10^{-5} $\mathrm{M}_{\odot}$ of hot dust and concluded that the mid-IR emission from this SN cannot support a dust mass of 2.0×10^{-2} $\mathrm{M}_{\odot}$. They also argue that the difference in the results may be due to the presence of a larger component of cold dust in the smooth model of Sugerman et al. (2006).

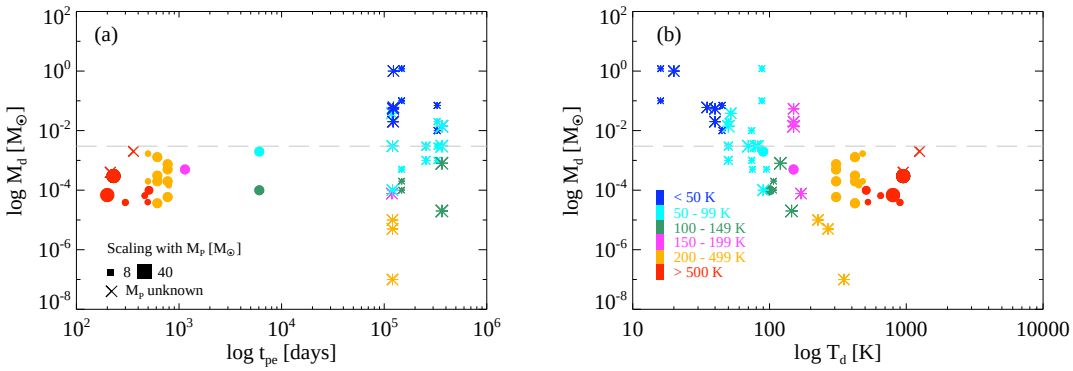

Figure 2.2: *Inferred amount of dust from SN observations at different epochs (a) and temperatures (b) given in Table 2.1. Filled circles represent observations at early epochs and stars mark observations from SNRs with an age of a few 100 yr. The colours denote the temperature (T_d) of the dust and t_pe is the time past explosion. The size of the symbols is scaled by the mass of the progenitor from the observed SN. The horizontal dashed line represents an average dust mass of* 3×10^{-3} $\mathrm{M}_\odot$ *of the SNRs.*

- A quite peculiar case is SN2006jc. Two years before explosion, a LBV-like outburst was detected and associated with the progenitor of SN2006jc (Nakano et al. 2006; Pastorello et al. 2007), which has been suggested as a very massive star (Foley et al. 2007; Pastorello et al. 2007). Evidence for ongoing dust formation in a CSD behind the forward shock at already 55 days after explosion was reported by e.g., Di Carlo et al. (2008); Smith et al. (2008b), but just a modest amount of 3×10^{-4} $\mathrm{M}_\odot$ of dust was inferred (Mattila et al. 2008). Interestingly, also larger dust masses of $\sim 8 \times 10^{-3}$ $\mathrm{M}_\odot$ (Mattila et al. 2008) or $\sim 3 \times 10^{-3}$ $\mathrm{M}_\odot$ (Sakon et al. 2009) condensed in the mass-loss wind of the progenitor prior to explosion have been observed.

In SN remnants (SNR), at an age of a few 100–1000 yr, larger masses of rather cold dust seem to be present. For example, observations of the SNR Cas A result in a few times 10^{-5} $\mathrm{M}_\odot$ of hot dust (>170 K) and a few times 10^{-2} $\mathrm{M}_\odot$ of warm and cold dust (< 150 K) for the entire SNR (e.g., Arendt et al. 1999; Douvion et al. 2001b; Hines et al. 2004; Krause et al. 2004; Rho et al. 2008). An amount of $\sim 1\mathrm{M}_\odot$ of dust at a temperature of ∼20 K was recently suggested by Dunne et al. (2009). Observations with the *Herschel Space Observatory* result in a resolved cool dust component (∼ 35 K) in the unshocked interior of Cas A with an estimated mass of 7.5×10^{-2} $\mathrm{M}_\odot$ of dust (Barlow et al. 2010). For the SNR 1E0102.2−7219 observations by Sandstrom et al. (2008) have shown that 3×10^{-3} $\mathrm{M}_\odot$ at 70 K are present as newly formed dust in the already reverse shocked ejecta. From observations in SNRs arising from Type II-P SNe such as B0540, SN1987A or the Crab nebula (Williams et al. 2008; Bouchet et al. 2004; Green et al. 2004; Temim et al. 2006) an average of about 10^{-3}–10^{-2} $\mathrm{M}_\odot$ on dust has been inferred.

Table 2.1: *Observed and derived properties of CCSNe*

SN	SN Type	Prog.	$M_{\rm P}$ [$M_\odot$][a]	$t_{\rm pe}$ [d][b]	M_d [$M_\odot$][c]	$T_{\rm d}$ [K][d]	References[e]
2006jc	pec. Ibn	LBV	~ 40	200	6.9×10^{-5}	800	1, 2
				230	3×10^{-4}	950	3
2005af	II-P	—	—	214	4×10^{-4}	—	1, 4
2004et	II-P	RSG	9	300	3.9×10^{-5}	900	1, 5
				464	6.6×10^{-5}	650	5
				795	1.5×10^{-4}	450	5
2003gd	II-P	RSG	~ 8	499	$2.0–17 \times 10^{-4}$	480	1, 6
				496	4×10^{-5}	525	7
				678	$2.7–20 \times 10^{-3}$	—	6
1999em	II-P	RSG	15	510	$\sim 10^{-4}$	510	1, 8
1998S	IIn	—	—	360	$> 2 \times 10^{-3}$	1250	1, 9
1987A	II-pec	BSG	~ 20	615	$3.7–31 \times 10^{-5}$	422	1, 10
				615	$2–13 \times 10^{-4}$	—	11
				775	$5.9–50 \times 10^{-5}$	307	10
				775	$2–7.5 \times 10^{-4}$	—	11
				1144	5×10^{-4}	150	12
				6067	$1–20 \times 10^{-4}$	90–100	13
SNR	SN Type	Prog.	$M_{\rm P}$ [$M_\odot$][a]	$t_{\rm pe}$[yr][b]	M_d [$M_\odot$][c]	$T_{\rm d}$ [K][d]	References[e]
Cas A	IIb	WR	15–30	326	7.7×10^{-5}	170	14,15
				326	3.8×10^{-2}	52	15
				330	$\sim 10^{-7}, \sim 10^{-4}$	350, 90	16
				330	$5 \times 10^{-6}, 1 \times 10^{-5}$	268, 226	17
				330	3×10^{-3}	79, 82	17
				330	< 1.5	—	18
				335	$2–5.4 \times 10^{-2}$	40–150	19
				337	~ 1	~ 20	20
				337	6×10^{-2}	~ 35	21
				337	7.5×10^{-2}	~ 35	22
Kepler	Ia / Ib	—	~ 8	405	$1–2 \times 10^{-4}$	107	23, 24, 25 ,26
				405	5×10^{-4}	75–95	23
				405	0.1–1.2	16, 88	27
B0540	II-P	—	15–25	700–1100	$1–3 \times 10^{-3}$	50–65	28, 29, 30, 29
Crab	II-P or	—	8–10	950	$1–7 \times 10^{-2}$	45	30,31, 32, 33
	ECSN	—		950	$3–20 \times 10^{-3}$	50	33
				952	$1–10 \times 10^{-3}$	74	34
1E0102	Ib/Ic or	—	~ 30	$\sim$1000	1.4×10^{-2}	50–150	35, 36, 37
	IIL/b			$\sim$1000	3×10^{-3}	70	38
				$\sim$1000	2×10^{-5}	145	38
				$\sim$1000	8×10^{-4}	120	39

References. (1) Smartt et al. (2009, and references therein); (2) Sakon et al. (2009); (3) Mattila et al. (2008); (4) Kotak (2008); (5) Kotak et al. (2009); (6) Sugerman et al. (2006); (7) Meikle et al. (2007); (8) Elmhamdi et al. (2003); (9) Pozzo et al. (2004); (10) Wooden et al. (1993); (11) Ercolano et al. (2007); (12) Dwek et al. (1992); (13) Bouchet et al. (2004); (14) Krause et al. (2008); (15) Arendt et al. (1999); (16) Douvion et al. (2001b); (17) Hines et al. (2004); (18) Wilson & Batrla (2005); (19) Rho et al. (2008); (20) Dunne et al. (2009); (21) Sibthorpe et al. (2009); (22)Barlow et al. (2010); (23) Blair et al. (2007); (24) Reynolds et al. (2007); (25) Sankrit et al. (2008); (26) Douvion et al. (2001a); (27) Gomez et al. (2009); (28) Reynolds (1985); (29) Williams et al. (2008); (30) Chevalier (2006); (31) Nomoto et al. (1982); (32) Kitaura et al. (2006); (33) Green et al. (2004); (34) Temim et al. (2006); (35) Blair et al. (2000); (36) Chevalier (2005); (37) Rho et al. (2009); (38) Sandstrom et al. (2008); (39) Stanimirović et al. (2005)

Notes. [a] $M_{\rm P}$ is the mass of the progenitor [b] $t_{\rm pe}$ is the time past explosion [c] M_d is the inferred dust mass [d] $T_{\rm d}$ is the inferred dust temperature

2.3.3 DUST CONTRIBUTION FROM IIN SUPERNOVAE AND LBVS

There is growing evidence for dust from IIn SNe and LBVs. SNe of Type IIn arise from stars at the lower mass end of CCSNe (8–10 $\mathrm{M}_{\odot}$) as well as from stars with higher masses in connection with LBVs ($> 20\ \mathrm{M}_{\odot}$). In either case they have undergone strong mass-loss and are surrounded by a dense and hydrogen-rich circumstellar disc.

In the case of ECSNe (see Sect. 2.2.4) appearing as Type IIn SNe, dust formation seems to be quite efficient. SN2008S was embedded in a dust enshrouded circumstellar shell and the progenitor was likely a SAGB star. The dust enshrouded phase lasted for $\sim 10^4$ years prior to explosion (Thompson et al. 2009) and could be associated with the super-wind phase of SAGB stars. Another example is the Type IIn SN2005ip, where dust was formed in the post-shocked shell, although actual dust masses are not reported (Fox et al. 2009; Smith et al. 2009). For the Type IIn SN1998S, Pozzo et al. (2004) inferred a dust mass of $> 2 \times 10^{-3}\ \mathrm{M}_{\odot}$.

SN2006gy was classified as the most luminous IIn event known (Ofek et al. 2007; Smith et al. 2007; Kawabata et al. 2009), but the explosion mechanism remains uncertain (Ofek et al. 2007; Smith et al. 2007, 2008a, 2010a). Near-infrared observations two years past explosion (Miller et al. 2010) showed a growing NIR excess which can be explained by a massive shell of around $10\ \mathrm{M}_{\odot}$ containing around $0.1\ \mathrm{M}_{\odot}$ of dust heated by the SN. The existence of a dusty shell has been proposed to be due to LBV eruptions lasting over ∼1500 years prior to the SN explosion (Smith et al. 2008a). The large mass of the circumstellar medium (CSM) of ∼10–20 $\mathrm{M}_{\odot}$ and the likely SN ejecta mass of 10–20 $\mathrm{M}_{\odot}$ require a progenitor mass of $\sim 100\ \mathrm{M}_{\odot}$ (Smith et al. 2010a).

Smith et al. (2003) measured the mass of a 19th century eruption from the well-known LBV η Car to be about 12–20 $\mathrm{M}_{\odot}$. A dust mass of $0.4 \pm 0.1\ \mathrm{M}_{\odot}$ surrounding η Car was estimated by Gomez et al. (2010) who also estimated that $> 40\ \mathrm{M}_{\odot}$ of gas has been ejected so far. SN1961V was classified as an η Car-like outburst with optically thick dust in a massive shell suggested based on the fading of the light curve after around 4 years (Goodrich et al. 1989). The transients UGC 2773-OT and SN2009ip (Smith et al. 2010b; Foley et al. 2010) were both LBV outbursts.

The progenitor of SN2009ip was serendipitously observed 10 yr prior to its outburst as an extremely luminous star and the mass was estimated of about 50–80 $\mathrm{M}_{\odot}$ (Smith et al. 2010b; Foley et al. 2010). UGC 2773-OT was less luminous with a mass of > 25 $\mathrm{M}_{\odot}$, but found in a very dusty environment. Finally, a dusty nebula around the object HR Car (Umana et al. 2009) consisting of amorphous silicates indicates that dust has formed during the LBV outburst.

Smith & Owocki (2006) deduced masses for the observed nebula of several LBVs and LBV candidates and concluded that a LBV giant eruption typically involves $10\ \mathrm{M}_{\odot}$ of material. The expansion velocities of such outbursts can be as high as 750 km s^{-1} as has been measured for η Car (Davidson 1971) and up to 2000–3000 km s^{-1} as for

SN1991V (Goodrich et al. 1989). Dust formed in such LBV outbursts is likely to escape before the shock from the final SN explosion catches up with the dusty shell.

2.3.4 Dust from IIb, Ic, Ib and Ia supernovae

Significant amounts of dust from Ic or Ib SNe has not been reported, and they are not currently considered as important sources of dust.

A very clear non-detection of dust for a Ic SN was obtained by Hunter et al. (2009) for the Ic SN2007gr. Besides the peculiar Ibn SN2006jc, the only proposed occurrence of dust formation for a Ib SN is for SN1990I at day ~ 250 (Elmhamdi et al. 2004).

The same seems to be the case for Type IIb SNe. However, Krause et al. (2008) has identified the supernova causing the SNR Cas A as a Type IIb. Cas A is well studied in terms of dust (see Sect. 2.3.2) and represents the only example so far for a SN of this type where dust has been reported. Kozasa et al. (2009) and Nozawa et al. (2010) theoretically investigated dust formation in SNe of this type. They found that $\sim 0.2\ \mathrm{M}_\odot$ of dust forms with a smaller average grain radius of $< 0.01\ \mu$m than for Type II-P SN. However, due to the thin H layer the reverse shock penetrates the ejecta earlier and, depending on density and geometry of the CSM and shocks, the freshly formed dust gets destroyed and only a fraction of the dust survives.

Observations of Type Ia SNe indicate that apparently only little or no dust forms in the explosions (Borkowski et al. 2006), while theoretical models on dust formation in SNe Ia are not available. The SN remnant Kepler possibly constitutes an exceptional case where dust masses ranging from a few $10^{-4}\ \mathrm{M}_\odot$ (Douvion et al. 2001a; Blair et al. 2007) up to 1–3 $\mathrm{M}_\odot$ (Morgan et al. 2003; Gomez et al. 2009) have been inferred. However, the classification of the progenitor is debated. The first claim that Kepler has its origin in a SN Ia were made by Baade (1943) which was then later also supported by Blair et al. (2007). According to suggestions by Bandiera (1987) the progenitor might have also been a runaway star with strong winds. Further possibilities are discussed by Reynolds et al. (2007), but a SN Ia event is favored. Pertaining to the meagre evidence of dust from this type of SN and its ambiguous nature and delay times, SNe Ia are likely not significant dust contributors in the early Universe and will not be further consider in this thesis.

2.4 Supernova dust: Theory vs. observations

As discussed in Sect. 2.3, dust is not efficiently formed in CCSNe on timescales of a few hundred days after explosion: On average, a few times $10^{-4}\ \mathrm{M}_\odot$ of relatively hot dust ($\sim$ 500–1000 K) has been reported. In contrast, large amounts of cold dust (< 50 K) have been claimed in SNRs which are a few 100–1000 yr old. The observational status is summarized in Table 2.1.

In Fig. 2.2 we plot the observed dust yields from Table 2.1 as a function of epoch or temperature. Regardless of SN type, only hot dust at an amount below $\sim 3 \times 10^{-3}$ $\mathrm{M}_{\odot}$ is present at early epochs. At late epochs larger amounts of cold dust appear to be produced.

On the contrary theoretical models predict that a high amount of dust in the SN ejecta can form within the first 600–1000 days (Kozasa et al. 1989, 1991; Clayton et al. 1999, 2001; Todini & Ferrara 2001; Nozawa et al. 2003; Bianchi & Schneider 2007; Cherchneff & Dwek 2010). The calculated dust masses are of order 10^{-1}–1 $\mathrm{M}_{\odot}$ for SNe in the mass range 12–40 $\mathrm{M}_{\odot}$ and for metallicities between 0–1 $\mathrm{Z}_{\odot}$.

Pertaining to this controversy, in the next sections we briefly address the difficulties of deriving the dust mass in SNe.

2.4.1 THEORY

The theoretical models which are used in the following sections to derive an upper limit for the efficiency of SNe to produce dust are briefly reviewed.

Todini & Ferrara (2001, hereafter TF01) investigated the formation of dust in Type II SN arising from progenitors with 12-35 $\mathrm{M}_{\odot}$ and different metallicities between zero, implying primordial composition of the progenitor, and solar. The nucleation of dust grains is based on the 'classical nucleation theory' (see Sect. 1.3.3), and for the formation of CO and SiO molecules chemical equilibrium is assumed. The ejecta is considered to be spherically symmetric and the chemical elements are fully mixed. The gas temperature and density are uniform throughout the considered volume. The temporal evolution of the temperature is defined by the assumption of an adiabatic expansion of the ejecta. For the kinetic energy of the explosion two different values are considered. Throughout most models, typically amorphous carbon (AC) grains are the first grains which condense out of the gas phase about 300–400 days past explosion. They form when the density is still high and the gas in the ejecta is moderately supersaturated. This results in a rapid accretion until carbon is depleted. Due to that, larger seed clusters made of N monomers are able to condense and AC grains can grow to large grain sizes of about 300 $\mathring{\mathrm{A}}$. The temperature range at which most of the AC dust is formed is very narrow, approximately 30–40 K around a gas temperature in the ejecta of about T = 1800 K. As the ejecta expands other dust species condense at lower gas temperatures, i.e., corundum at $T \sim$ 1600 K, thereafter magnetite, enstatite and forsterite at T $\sim$ 1100 K. The accretion rate is lower and comparable to the nucleation rate leading to the formation of smaller grains of about 10–20 $\mathring{\mathrm{A}}$. At zero metallicity and in the lower energy case the calculated total dust masses per SN range between about 0.08 $\mathrm{M}_{\odot} < M_{\mathrm{d}}$ < 0.3 $\mathrm{M}_{\odot}$, but are increased when a higher explosion energy is applied. By trend, the dust masses per SN increase with increasing metallicity, i.e. the amount is three times higher for $\mathrm{Z}_{\odot}$. The obtained log-normal grain size distribution is found to be rather un-

effected by metallicity changes since it significantly depends on the thermodynamics of the ejecta expansion.

The model of TF01 was revisited by Bianchi & Schneider (2007) for the purpose of investigating the evolution of the dust grains in SNe between 12–40 $\mathrm{M}_{\odot}$ from time of condensation until the passage of a reverse shock. An additional grain species, SiO_2, is added to the types already considered by TF01. Moreover only clusters with a minimum number of monomers of either $N \geq 2$ or $N \geq 10$ together with a discrete accretion of those is considered, in contrast to TF01 where no constrains on N were applied. These modifications lead to a alteration of the log-normal grain size distribution of all dust species except of AC grains. A larger mean grain size results but the grains are less numerous. With increasing N less Si-bearing grains of large grain sizes form while AC grains are not effected. It has been found that in the case of solar and sub-solar metallicity around 0.1–0.6 $\mathrm{M}_{\odot}$ of dust per SN form. However for progenitors larger than 35 $\mathrm{M}_{\odot}$ and Z = 0 no dust is produced. It is shown that the final dust masses per SN vary significantly with varying the sticking probability α. As pointed out in Sect. 1.3.3 in the case of α = 1 the maximal dust mass is obtained. Assuming α = 0.1 leads to a significant reduction of the calculated dust masses (0.001–0.1 $\mathrm{M}_{\odot}$ of dust for progenitors below 20 $\mathrm{M}_{\odot}$). Monomers stay longer in the gas phase and dust formation takes place when the supersaturation is larger, thus generally smaller grains are formed. Si-bearing grains are significantly more affected than AC grains, and in some cases the amount of dust of non-AC grains becomes negligible.

A simple semi-analytical model has been used to treat the dyamics of the reverse shock. In particular the model is based on analytical approximations provided by Truelove & McKee (1999) for the velocity and radius of the forward and reverse shocks in the non-radiative ejecta dominated and Sedov-Taylor phases of SNRs. The main critical parameters to determine the velocities and shock radii are the kinetic energy of the explosion, the mass of the ejecta and the density of the ISM. For the energy and ejecta mass similar values as for the formation model are adopted and three different values (ρ_{ISM} = 10^{-25}, 10^{-24}, 10^{-23} g cm^{-3}) for the ISM density are investigated, while a uniform ISM is considered. Furthermore, a uniform density distribution inside the spherically symmetric ejecta is assumed along with a uniform distribution of the dust grains. The grain size distribution is considered to be the same at any place. It has been found that due to erosion caused by thermal and non-thermal sputtering a shift of the size distribution function to smaller grains appears. Depending on the density of the ISM about 2–20 % of the initially formed dust mass survives (higher fraction at lower density). About 4–8 x 10^4 years after explosion the reverse shock has penetrated 95 percent of the original volume of the ejecta.

Owing to the possibility that stars more massive than a few tens to 100 $\mathrm{M}_{\odot}$ are likely to form as the first stars (see also Sect. 2.2.1), N03 studied dust formation in the ejecta of POP III stars (13–40 $\mathrm{M}_{\odot}$) taking also PISNe (with 170 and 200 $\mathrm{M}_{\odot}$) into account.

Dust nucleation is also based on the 'classical nucleation theory' (see Sect. 1.3.3), but following Gail et al. (1984) a non-steady state nucleation rate was calculated. The results of nucleosynthesis calculations of POP III SNe are taken from Umeda & Nomoto (2002). From hydrodynamic calculations followed that in less than 1 day after explosion the ejecta expansion is homologous. Thus, the time evolution of the density in the ejecta is simply calculated as $\rho(M_{\rm r}, t) = \rho(M_{\rm r}, t_0)(t/t_0)^{-3}$, where $M_{\rm r}$ is the mass coordinate and t_0 the reference time 1 day after explosion. The time evolution of the gas temperature in the ejecta is calculated by solving the multifrequency radiative transfer equations together with the energy equation including the energy deposition from the radiative elements (Iwamoto et al. 2000). Furthermore, N03 distinguish between an unmixed ejecta and a mixed ejecta. In the unmixed case the ejecta is divided into five different layers each of different elemental composition, i.e. the innermost regime is a Fe-Si-S layer followed by Si-S-Fe, O-Si-Mg, O-Mg-Si layers and outermost a He layer. The mass of each layer varies with progenitor mass. In the mixed case all elements are assumed to be uniformly distributed. For either model a formation efficiency of unity is assumed for the key molecules CO and SiO.

It has been shown that in either case the total amount of freshly formed dust increases with increasing the progenitor mass. The total amount of dust per SN for the mixed ejecta generally is found to be larger than for the unmixed ejecta. For SNe between 13–40 $\mathrm{M}_\odot$ about 2–5 % of the progenitor mass and for PISNe between 140–260 $\mathrm{M}_\odot$ approximately 15–30 % of the progenitor mass condense into dust. However, the main dust species formed are solely dependent on the model (mixed or unmixed ejecta) and are rather independent of the progenitor mass. In the mixed case the ejecta is oxygen rich due to the assumption that the formation of CO molecules is complete. Subsequently only oxide grains such as forsterite, corundum, enstatite, SiO_2 or magnetite condense, while the most abundant grain species for SNe are SiO_2 and forsterite. In the unmixed case various different grain species condense in each layer depending on the elemental composition of those. The major grain types formed are carbon, Fe, Si and forsterite. The average grain radius of each grain species depends on the elemental composition and the gas density at the formation site. Each grain type follows a log-normal size distribution at a location in the ejecta as long as the grains are larger than 0.01 μm. In the unmixed ejecta the summed-up size distribution function within the ejecta is log-normal for carbon, Fe and SiO_2 grains, while in the mixed case all grain species except corundum obey a log-normal size distribution.

Similar to the study by Bianchi & Schneider (2007) also Nozawa et al. (2007) investigate dust destruction caused by the collision with the revese shock in the SN remnant phase of POP III stars and PISNe. The ejecta is assumed to expand into a uniform ISM with primordial composition, where three different cases for the hydrogen number density are considered ($n_{\rm H,0}$ = 0.01, 1 and 10 cm^{-3}). Independently of the ISM density an ISM temperature of the order of 10^4 K is assumed, since also the ambient pressure in-

fluences the deceleration of the blast wave. For the density and velocity structure of the ejecta the hydro-dynamic models from Umeda & Nomoto (2002) together with the dust models (mixed and unmixed) from N03 are adopted. From the latter model the obtained grain size distributions are included. The ejecta is assumed to be spherical and for the time evolution of the gas the flux-splitting method (van Albada et al. 1982; Mair et al. 1988) is used. Three different radiative cooling processes are included; (i) thermal emission from collisional dust heating in the post-shock flow, (ii) inverse Compton cooling and (iii) atomic cooling. Dust destruction by sputtering and the deceleration of dust grains due to gas drag are taken into account while the effect of charge on the dust grain is neglected. Dust grains are considered to be destroyed as soon as the grain size becomes smaller than the size of the monomer.

It has been found that only initially very large grains ($a_{\rm ini} > 0.2$ μm) are expelled into the ISM through the forward shock while their size is only marginally reduced. Smaller grains are either destroyed through sputtering in the post-shock flow or are trapped and remain behind the forward shock. The critical grain size below which dust particles are fully destroyed is sensitive to the density of the ISM and is found to range between 0.01–0.2 μm for $n_{\rm H,0}$ = 0.01–10 cm^{-3}. The grain size distribution of the surviving dust is dominated by large grains, while it is deficient in small grains. The fraction of dust destroyed is found to be higher for the mixed grain model than for the unmixed, since the mixed model lacks on grains larger than $>$ 0.01–0.05 μm. Furthermore the final fate of the dust grains also dependents on the thickness of the hydrogen envelope of the progenitor star. In this study and in a more detailed study by Nozawa et al. (2010) it has been shown that in the case of a thin hydrogen envelope as expected for Type IIb SNe generally smaller grains form. Additionally the reverse shock encounters the ejecta much earlier than for SNe with a thick hydrogen envelope (as it is the case for Type IIP SNe). In the latter case the reverse shock encounters the dust $\sim 10^{3-4}$ yr after explosion, depending on the density of the ISM.

Models for dust formation in POP III stars and PISNe with progenitor masses of 20, 170 and 270 $\mathrm{M}_{\odot}$ have been accomplished by Cherchneff & Dwek (2009, 2010). For the temperature and density structure of the ejecta (described in Cherchneff & Dwek 2009) the models by N03 are adopted, while for some PISNe models simply a constant temperature and density in the inner He core is assumed. The temporal evolution of those quantities is calculated by assuming the ejecta follows an adiabatic expansion similar to the models described above. The ejecta velocity is for simplicity kept constant. The chemical compositions for a mixed ejecta model is adopted from Umeda & Nomoto (2002) while for the unmixed case those of N03 are used. It has been argued that the commonly adopted assumptions of thermodynamical and chemical equilibrium as well as the standard nucleation theory are inappropriate for describing dust formation in the dynamical flows of SN ejecta. Cherchneff & Dwek (2009, 2010) therefore use a chemical kinetic approach for the formation of molecules and dust grains. The chemical kinetic

description of the ejecta is based on (i) the initial chemical composition of the gas and (ii) a set of chemical reactions describing the chemical processes, and is applied to the physical conditions of the ejecta. For a detailed description of the included processes and the extensive chemical reaction network we refer to Cherchneff & Dwek (2009). This new approach leads to smaller dust masses by a factor of ~ 5 and to a different chemical composition of the formed dust compared to models by either TF01, N03 or Schneider et al. (2004). The main abundant grain species are pure silicon, silica and silicates, while carbon dust is negligible.

As already pointed out in Sect. 1.3.3 and evidently from the above discussed models, dust formation in SN ejecta is not an easy task and accompanied by many complex processes, which are not fully understood. The amount of dust and the variety of dust species formed in the theoretical models thus strongly depend on the assumptions made.

2.4.2 Observations

Deriving the mass of dust from observations is complex. Warm dust emits in the NIR and MIR wavelength range, whereas the emission from cold dust is shifted to FIR or submillimeter wavelengths and is often difficult to differentiate from cold foreground material. In addition, it is impossible to infer the structure of dust grains and their exact spatial distribution within the ejecta from observations. Hence, the derived dust masses rely on the models and techniques used to fit the data.

This becomes clear when looking at SNe, where various observations have been performed and dependent on the instrumentation, the methodology and the applied model, dust masses differing over orders of magnitude are derived. The methods mainly used to infer the existence of dust in SN ejecta are either (i) based on the attenuation of the red wings of spectral ejecta lines at optical/NIR wavelengths during the nebular phase or (ii) to observe the thermal emission from dust grains. Most observations of SN and SN remnants are since its launch in 2003 primarily made with the *Spitzer Space Telescope*, because ground based MIR observations are difficult. Earlier observations, e.g., of SN 1987A (Wooden et al. 1993) have been performed with the *Kuiper Airbourn Observatory*.

The attenuation of broad and intermediate spectral emission lines, i.e. the He I, Ca II IR triplet or O I line, is a relatively reliable and usually pronounced signature of the presence of dust. One reason is, because it has not been found that the attenuation arises from any other effect. Using this method direct confirmation of newly formed dust in the ejecta has been presented for some SNe, e.g., SN 1987 A (e.g., Danziger et al. 1989; Lucy et al. 1989), SN1990I (e.g., Elmhamdi et al. 2004), SN 1999em (e.g., Elmhamdi et al. 2003), SN 2004et (e.g., Sahu et al. 2006; Kotak et al. 2009). Evidence of formation of new dust not only in the ejecta but also in the post-shocked shell of IIb/IIn SNe could

be revealed for example for SN 1998S (e.g., Pozzo et al. 2004), SN 2005ip (e.g., Smith et al. 2009) and SN 2006jc (e.g., Smith et al. 2008b; Mattila et al. 2008). However with this method it is difficult to quantitatively derive the amount of dust, its composition or geometry (e.g., Kotak 2008) which therefore remains elusive.

Thermal emission from dust is typically detected in late-time IR observations of SNe as NIR or MIR 'excess'. Such an 'excess' may arise from newly formed dust in the SN ejecta or in the cool, dense shell of post-shocked gas within the forward and reverse shock. The new dust may be collisionally heated by hot gas in the reverse shocks, heated due to radioactivity or optical emission from circumstellar interaction. Alternatively, thermal emission could be caused by pre-existing dust in the circumstellar medium. In this case the dust potentially is either collisionally heated by hot, shocked gas, the flash from the SN or it is heated due to the ejecta-circumstellar matter interaction. The latter two cases result in an 'IR echo' due to light travel time effects. Evidently, it is challenging to differentiate between newly and pre-exisiting dust from observations of thermal emission. A differentiation might be possible based on the fact that an emission caused by an echo seems to appear at earlier epochs compared to dust formation which takes place a few hundred days past explosion. Also studies of the SN light curve are useful since in case of an echo the light curve shows characteristic features. However, both scenarios might as well contribute to the late-time IR flux as it has been the case of SN 2004et and SN 2006jc (e.g., Kotak et al. 2009; Mattila et al. 2008), while this is not unambiguously clear for SN 2002hh (e.g., Meikle et al. 2006).

In old SN remnants (see Sect. 2.3.2) it is possible that most of the dust is cold and has escaped detection in MIR studies. Submillimeter observations with SCUBA have been accomplished for the SN remnants Cas A (Dunne et al. 2003) and Kepler (Morgan et al. 2003). The first measurements resulted in very large derived dust masses ($\sim$ 0.3–3 $\mathrm{M}_{\odot}$) at cool temperatures of about 17–18 K. However, in particular for Cas A it has been suggested that most of the submilimeter emission likely arises from foreground molecular clouds (Krause et al. 2004; Wilson & Batrla 2005). Similar considerations and new calculations led to a revision of the dust mass for Kepler about a factor of two downwards (Gomez et al. 2009). Using submillimeter polarimetry (Dunne et al. 2009) lower dust masses were obtained for Cas A as well, although for either remnant (Cas A and Kepler) the obtained amount of dust is well above the average results of MIR-studies in SNe at early and late epochs.

Deriving the dust masses in SN ejecta and remnants is basically similar to the method used for deriving dust in galaxies as discussed in Sect. 1.3.1. The amount of dust is obtained as $M_{\mathrm{d}} = (F(\lambda)D_{\mathrm{L}}^2)/(\kappa_{\mathrm{d}}(\lambda, a)B(\lambda, T_{\mathrm{d}}))$, where λ is the wavelength of observations, F(λ) the total flux, and $\kappa_{\mathrm{d}}(\lambda, a) = (3Q(\lambda, a))/(4\rho a)$, is the dust absorption coefficient for a (spherical) grain type with $Q(\lambda, a)$ the dust emissivity, ρ the dust bulk density and a the dust particle size. The temperature T_{d} can be derived from the spectral fit. The luminosity of a single spherical grain of radius, a, and temperature T_{d} is given as

$L_{\rm d}(\lambda) = 4\pi a^2(\pi B(\lambda, T_{\rm d})Q(\lambda, a)$.

In the Rayleigh limit, when $a < \lambda$ the absorption coefficient κ is independent of the particle radius a, thus $\kappa \equiv \kappa_{\rm d}(\lambda)$, which is usually adopted since exact grain sizes and grain size distributions are not known.

The main uncertainties in deriving the dust mass are the (i) considered dust species, (ii) the assumed absorption coefficients for the considered dust species and (iii) the unknown grain size distribution. In the literature we found that for each reported dust mass estimate a rather different dust grain composition has been adopted. For similar dust species different dust absorption coefficients had been applied. Usually used grain species are for example amorphous carbon, graphite and silicate grains. While Bouchet et al. (2004) preferred silicate dust for SN 1987 A, Ercolano et al. (2007) finds for the same SN large amounts of graphite grains. For more recent SNe, Fox et al. (2010) rules out silicates and uses only graphite for SN 2005ip similar as Mattila et al. (2008) for SN 2006jc. Spectroscopic evidence for silicate dust was revealed by Kotak et al. (2009) due to a large, but declining SiO mass in SN 2004et. For the SN remnant Cas A, Hines et al. (2004) adopted a magnesium protosilicate-based grain model from Dorschner et al. (1980) and Arendt et al. (1999). Rho et al. (2008) fit the spectra with a variety of different grain species based on the theoretical models from N03 and TF01 but favors magnesium protosilicates, while Dunne et al. (2003, 2009) assumes grains which are either amorphous or have a clumpy, aggregate structure. Silicates and graphite dust has been assumed in the Crab and the SN remnant B0540 and commonly larger silicate than graphite dust masses were obtained (Green et al. 2004; Temim et al. 2006; Williams et al. 2008). Although only a few examples are listed, it is evident that the determination of the grain type composition poses some uncertainties.

Further complications in deriving the amount from SN arise from ambiguous considerations about the SN ejecta physics. In most cases it is unclear whether the ejecta is mixed or unmixed, and additionally a uniform dust and gas distribution is often assumed, while there seemingly is evidence for mixing and a clumpy ejecta. Mixing in the ejecta is likely be explained by the theoretically observed instability of the nickel bubble during explosion of the SN leading to Rayleigh-Taylor instabilities forming in the post-shocked ejecta (e.g., Chevalier & Klein 1978; Arnett 1988; Herant & Benz 1991; Herant & Woosley 1994; Kifonidis et al. 2003). This might also support suggestions for the presence of undetected larger amounts of dust at early epochs, if dust grains are assembled in optically thick clumps (e.g., Lucy et al. 1989, 1991; Elmhamdi et al. 2003; Wooden et al. 1993; Sugerman et al. 2006; Ercolano et al. 2007; Meikle et al. 2007). According to Meikle et al. (2007), generally dust in the ejecta of SNe can become optically thick in the MIR, for dust masses exceeding a few times 10^{-3} $\rm M_{\odot}$. Interestingly however, in most of the investigations using a clumpy model significantly larger dust masses than for some investigations using a smooth model could not be revealed. In particular also these models fail to explain the large dust masses predicted by theoretical models (Wooden

et al. 1993; Ercolano et al. 2007; Meikle et al. 2007).

A scenario of dust grain growth in SN remnants at longer timescales of a few 10–100 yr could also explain the difference in dust mass at early and late epochs. Nucleation of thermodynamical stable small clusters is possible at temperatures between ∼700 K and ∼2000 K and densities in the range $\sim 10^{-13}$–10^{-15} g cm^{-3} (Feder 1966; Clayton 1979; Sedlmayr 1994). Once such a stable cluster is present, further growth to macroscopic dust grains can take place. The growth regime of dust grains extends to lower temperatures and densities. However, significant growth is restricted through the available condensable material and dilution of the SN ejecta (Draine 1979; Sedlmayr 1994). The amount and timescale of grain growth might also be dependent on the type of the SN. Examples are the SNRs B0540−69.3, Cas A or the Crab nebula (see Table 2.1). For the latter, an extended dust grain growth phase could possibly explain the presence of large dust grains (Temim et al. 2006).

2.5 Dust production efficiency

Based on dust yields from observations and theory discussed in previous sections we next ascertain the efficiency limits of stellar sources to produce dust from their available metals.

We define the dust production efficiency $\epsilon(m, z)$ per stellar mass and metallicity as

$$\epsilon(m, Z) = \frac{M_{\rm d}(m, Z)}{M_{\rm Z}(m, Z)}, \tag{2.1}$$

where $M_{\rm d}(m, Z)$ is the mass of dust produced and released into the ISM, $M_{\rm Z}(m, Z)$ is the total ejected mass of heavy elements per star and $m \equiv M_*/{\rm M}_\odot$ where M_* is the zero age main sequence mass. We assume that the amount of dust is the final mass, which has formed and possibly been processed through shock interactions.

2.5.1 Efficiency for AGB stars

The dust production efficiency, $\epsilon_{\rm AGB}(m, Z)$, for AGB stars in the mass range 3–7 ${\rm M}_\odot$ is calculated from theoretical values of $M_{\rm d}(m, Z)$ and $M_{\rm Z}(m, Z)$. For the amount of dust $M_{\rm d}(m, Z)$ we use the total dust yields of Ferrarotti & Gail (2006). Stellar yields for AGB stars have been calculated by e.g., Renzini & Voli (1981), Marigo (2001), Herwig (2004), Karakas & Lattanzio (2007) and recently by Karakas (2010). However most of the models do not provide yields over the range of masses, elements or metallicities required for this work. For the sake of consistency we use for the amount of heavy elements $M_{\rm Z}(m, z)$ the yields of van den Hoek & Groenewegen (1997) covering a large grid of metallicities and stellar masses. The efficiency $\epsilon_{\rm AGB}(m, Z)$ is calculated for four different metallicities in accordance with calculations by Ferrarotti & Gail (2006).

The results are presented in Fig. 2.3. It is evident that $\epsilon_{\rm AGB}(m, Z)$ decreases quite

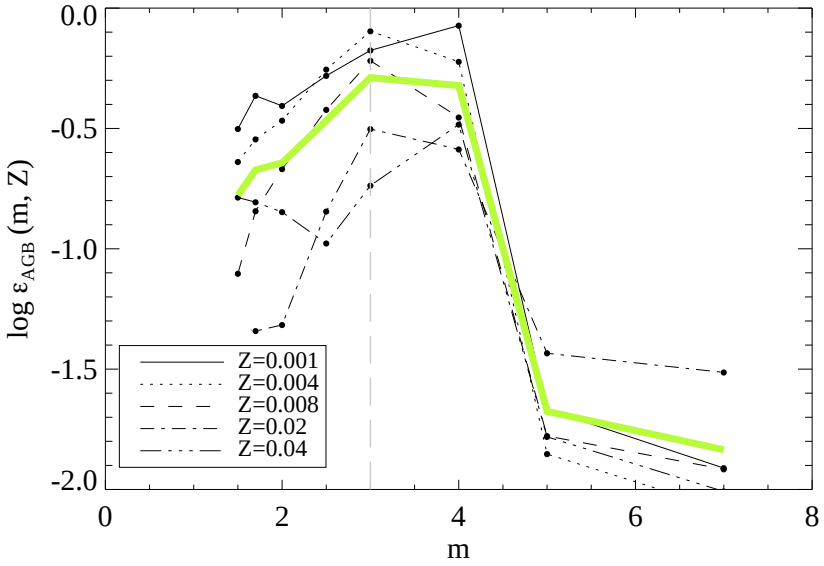

Figure 2.3: *Dust production efficiencies of AGB stars. The efficiencies are based on dust yields from Ferrarotti & Gail (2006) and yields of heavy elements from van den Hoek & Groenewegen (1997). The green line indicates the metallicity-averaged efficiency $\epsilon_{\rm AGB}(m)$. The vertical dashed line marks the boundary of 3 $\rm M_\odot$, below which AGB stars are not considered as dust contributors at high redshift. The solid, dotted, dashed, dashed-dotted and dashed-dot-dotted lines are for metallicities of Z = 0.001, Z = 0.004, Z = 0.008, Z = 0.02, and Z = 0.04, respectively.*

rapidly between 4 and 5 $\rm M_\odot$, independently of the metallicity. AGB stars between 3–4 $\rm M_\odot$ (i.e., C-stars) are apparently the most efficient dust producers. It can also be seen that at lower metallicities ($Z \leq 0.008$) these AGB stars are more efficient in condensing their available heavy elements into dust than at higher metallicities. The green thick line in Fig. 2.3 illustrates the metallicity-averaged efficiency $\epsilon_{\rm AGB}(m)$ for AGB stars.

2.5.2 Efficiency for CCSNe

There is a discrepancy between the derived SN dust yields from observations and theory. We therefore determine plausible limits for the dust production efficiency of SNe based on the dust yields obtained from either approach.

High efficiency

We first ascertain an upper limit to the SN dust production efficiency. We use the mass and metallicity dependent dust yields from TF01 to determine the mass of dust $M_{\rm d}(m, Z)$. The yields for the heavy elements $M_{\rm Z}(m, Z)$ are taken from Woosley & Weaver (1995) (hereafter WW95), since these were also used by TF01. In addition, we

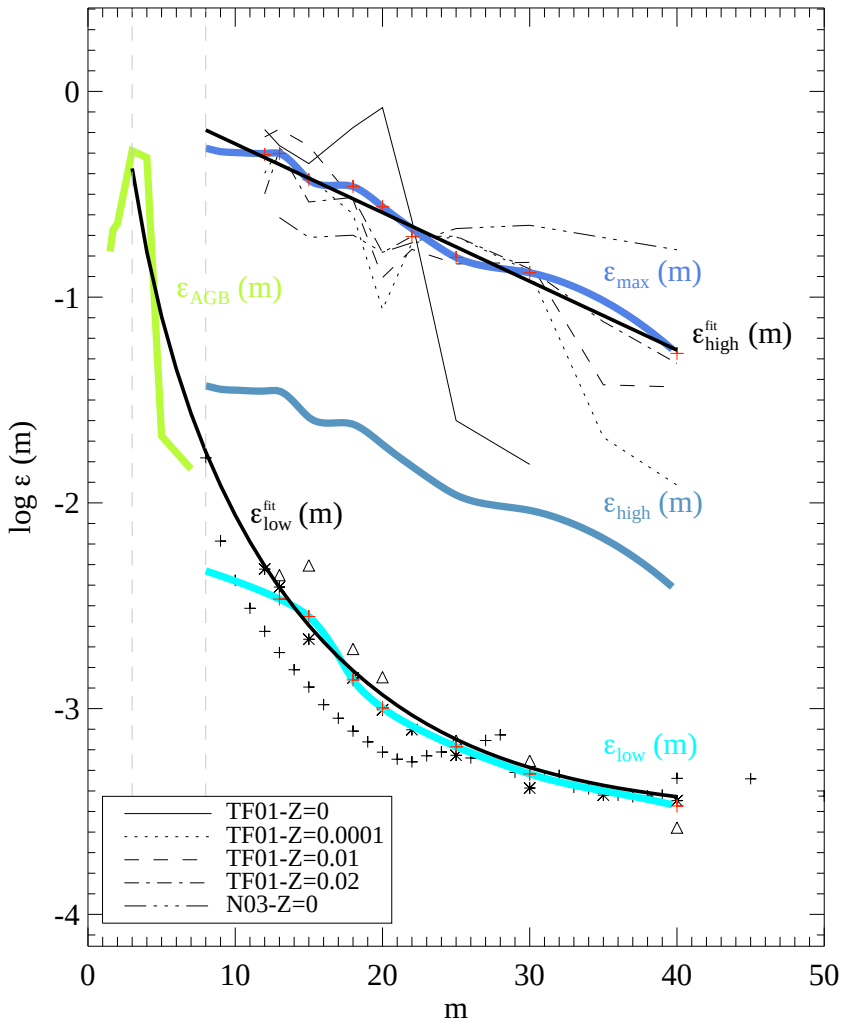

Figure 2.4: *Dust production efficiencies of massive stars. Upper curves: Efficiencies calculated from SN dust yields of TF01 and metal yields of WW95. The solid (thin), dotted, dashed and dashed-dotted lines are for metallicities of $Z = 0$, $Z = 0.0001$, $Z = 0.01$ and $Z = 0.02$, respectively. The dashed-dot-dotted line represents the efficiency at $Z = 0$ derived from dust yields of N03 and metal yields from N06. The blue thick line represents the averaged maximal efficiency $\epsilon_{\rm max}(m)$ and the black thick solid line the fitted efficiency $\epsilon^{\rm fit}_{\rm high}(m)$. The thick light blue line represents the high efficiency $\epsilon_{\rm high}(m)$. Lower symbols: Efficiencies derived from the averaged observed dust amount of 3×10^{-3} $\rm M_\odot$ of SNRs and the SN metal yields of WW95 (stars), N06 (crosses) and ET08 (triangles) for solar metallicity. The thick cyan line is the averaged low efficiency $\epsilon_{\rm low}(m)$ and the black thick solid line the fitted efficiency $\epsilon^{\rm fit}_{\rm low}(m)$. The left green line represents the averaged AGB efficiency $\epsilon_{\rm AGB}(m)$ (see also Fig. 2.3). The vertical lines mark the range of AGB stars between 3–8 $\rm M_\odot$ and SNe ≥ 8.*

derive the efficiency for Z = 0 from the dust yields of Nozawa et al. (2003) and the total amount of metals of Nomoto et al. (2006) (herafter N06) – both yields are taken from unmixed grain models. The resulting efficiencies can be seen in Fig. 2.4, where we notice a clear decline of $\epsilon(m, Z)$ with increasing progenitor mass.

The efficiencies of TF01 and N03 at $Z = 0$ differ significantly. For TF01, $\epsilon(m, Z)$ decreases quite drastically for stars between 20–25 $\mathrm{M}_{\odot}$, whereas $\epsilon(m, Z)$ from NZ03 remains more flat. To obtain a high efficiency limit we average the efficiencies obtained for each Z from these models over metallicity. This is sufficient to describe the observed tendencies and obtain an estimate of $\epsilon(m)$. The average efficiency for all stellar masses is obtained via rational spline interpolation and extrapolation in the mass regime of 8–12 $\mathrm{M}_{\odot}$ where no yields for heavy elements are available. We will refer to this as the 'maximal' SN dust production efficiency $\epsilon_{\mathrm{max}}(m)$, drawn as the dark blue line with red crosses representing the averaged data points in Fig. 2.4.

According to the predictions of Bianchi & Schneider (2007) and Nozawa et al. (2007, 2010) dust grain destruction takes place when a reverse shock penetrates the dust layer at timescales up to $\sim 10^4$ years past explosion. This leads to a significant (up to 100%) reduction of the dust formed, depending on the ISM density and grain size. For example, Nozawa et al. (2007) have shown that large grains in contrast to small grains remain relatively unaffected by the reverse shock. We account for the possibility of grain destruction by applying a reduction of 93% on $\epsilon_{\mathrm{max}}(m)$ (following Bianchi & Schneider 2007). However, the resulting reduced efficiency still represents a rather high dust production efficiency in comparison to what is derived from SN observations. Hence, this will be referred to as 'high' SN dust efficiency $\epsilon_{\mathrm{high}}(m) = 0.07\epsilon_{\mathrm{max}}(m)$.

It is noteworthy that either $\epsilon_{\mathrm{max}}(m)$ or $\epsilon_{\mathrm{high}}(m)$ might also be interpreted as the result of longer timescale dust grain growth in the SNR itself. The maximal $\epsilon_{\mathrm{max}}(m)$ presupposes that dust destruction through shock interactions is inefficient. The high $\epsilon_{\mathrm{high}}(m)$ could also be the result of smaller or no destruction, depending on how much dust would initially have formed before a possible shock interaction.

Low efficiency

The lowest feasible limit for the efficiency of SNe dust production is generated based on observed dust yields from the SNRs Cas A, B0540−69.3, Crab nebula, and 1E0102.2−7219 at temperatures between 50–100 K (see Table 2.1). The inferred amount of dust $M_{\mathrm{d}}(m, Z)$ is taken to be 3×10^{-3} $\mathrm{M}_{\odot}$ and is applied to SNe in the mass interval 8–40 $\mathrm{M}_{\odot}$.

For the mass of heavy elements $M_{\mathrm{Z}}(m, Z)$ we use the yields of WW95, N06 and Eldridge et al. (2008) (herafter ET08). The metallicity of most SN progenitors given in Table 2.1 is estimated to be between around solar (Z = 0.02) or LMC-like (Z = 0.008) (Smartt et al. 2009). We therefore assume solar metallicity for all SNe in the mass range of 8–40 $\mathrm{M}_{\odot}$ and also evaluate the metal yields $M_{\mathrm{Z}}(m, Z)$ for $\mathrm{Z}_{\odot}$. To obtain the low

efficiency limit we average the efficiencies obtained with the yields of WW95, N06 and ET08. The same interpolation and extrapolation scheme as for $\epsilon_{\rm max}(m)$ is applied and the resulting average efficiency appears as the cyan line with data points indicated as red crosses in Fig. 2.4.

Owing to this treatment we get an averaged dust production efficiency which depends only on the stellar mass. This will be referred to as low SN efficiency $\epsilon_{\rm low}(m)$ throughout the paper. Interestingly, also $\epsilon_{\rm low}(m)$ features a declining tendency with increasing stellar mass, similar to $\epsilon_{\rm max}(m)$.

There are two possible interpretations of this limit. The amount of dust produced by SNe could be similar to the low observed amount of dust at early epochs and this rather low amount of dust does not significantly grow on longer timescales. This might be the case for SN1987A (Bouchet et al. 2004) and SNR B0540−69.3 (Williams et al. 2008). Alternatively, $\epsilon_{\rm low}(m)$ may be the result of potential dust destruction of larger amounts of dust from shock interactions.

2.5.3 Simple approximations

To illustrate the general trends of different $\epsilon(m)$ we provide fits to the derived averaged efficiencies of AGB stars and SNe with simple analytical functions.

One notices from Fig. 2.4 that there might be a smooth connection of the efficiencies, $\epsilon_{\rm low}(m)$, between high-mass AGB stars and low-mass SNe. An adequate approximation covering all stars between 3–40 $\rm M_\odot$ is a power law for $\epsilon(m)$,

$$\epsilon_{\rm low}^{\rm fit}(m) = a\, m^{-\beta} + c \tag{2.2}$$

with a = 15, β = 3.25, and c = 2.8 $\times$ 10^{-4}. The negative slope reflects the decreasing efficiency of stars with increasing mass to release the produced dust grains into the ISM. It also illustrates that AGB stars in this case are more efficient, closely followed by the low-mass SNe. While $\epsilon_{\rm low}^{\rm fit}(m)$ drops by roughly three orders of magnitude in the 3–40 $\rm M_\odot$ mass range, the rather steep decline for stars between $\sim$ 3–12 $\rm M_\odot$ over approximately two orders of magnitude is noteworthy. We also note that although $\epsilon_{\rm low}^{\rm fit}(m)$ provides a fairly good approximation to $\epsilon_{\rm low}(m)$, it does not capture the strong preference for 3–4 $\rm M_\odot$ stars over 5–7 $\rm M_\odot$ stars.

The maximal SN dust formation efficiencies are better approximated by an exponential function,

$$\epsilon_{\rm high}^{\rm fit}(m) = a\, e^{-(m/m_0)}, \tag{2.3}$$

with a = 1.2 and m_0 = 13. Comparing the efficiency $\epsilon_{\rm AGB}(m)$ of AGB stars to $\epsilon_{\rm max}(m)$, we find no possibility for a smooth connection. In this case, stars between 8–12 $\rm M_\odot$ are the most efficient dust producers. The general decline of $\epsilon_{\rm high}^{\rm fit}(m)$ for stars between 8–40 $\rm M_\odot$ is about an order of magnitude, comparable to the drop of $\epsilon_{\rm AGB}(m)$ from a 4 $\rm M_\odot$ to a 6 $\rm M_\odot$ AGB star.

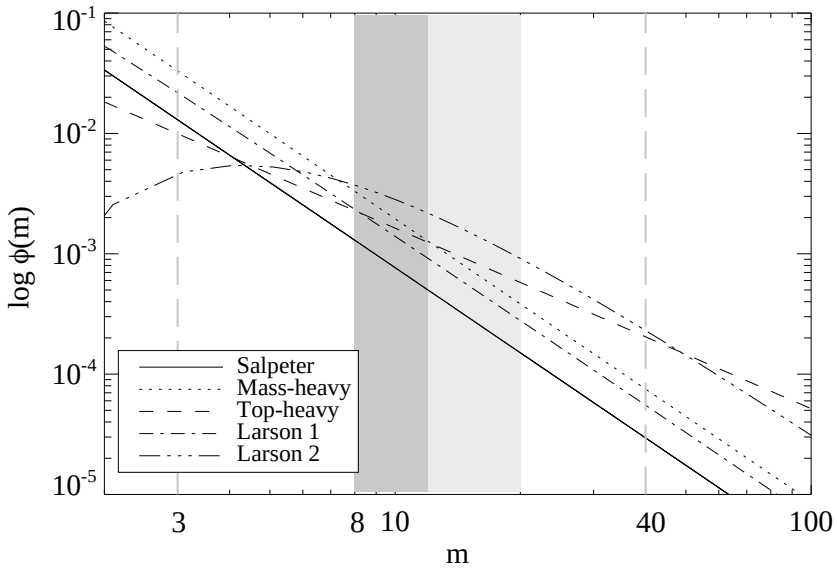

Figure 2.5: *The five IMFs considered. The solid, dotted, dashed, dashed-dotted, and dashed-dot-dotted lines represent the Salpeter, mass-heavy, top-heavy, Larson 1 and Larson 2 IMF, respectively. The dark grey area signifies the critical mass range of 8–12* $\mathrm{M}_{\odot}$ *and the light grey area signifies SNe between 12–20* $\mathrm{M}_{\odot}$*. The vertical dashed lines mark the limits of the range in stellar mass considered (between 3* $\mathrm{M}_{\odot}$ *and 40* $\mathrm{M}_{\odot}$*).*

The resulting fits for both cases are shown in Fig. 2.4 as black solid curves.

2.6 DUST PRODUCTIVITY

Besides the dust production efficiency, the total amount of dust produced in a galaxy depends on the SFR, $\psi(t)$ and the IMF, $\phi(m)$.

In models of dust evolution in galaxies and high-z quasars (e.g., Morgan & Edmunds 2003; Dwek et al. 2007) a Salpeter IMF is often used. However there is also observational indication for a top-heavy IMF in these systems (for a detailed overview we refer to Sect. 3.3.2). In view of this we consider five different IMFs (Table 2.2). The power law IMFs (Salpeter, mass heavy and top heavy) have the form $\phi(m) \propto m^{-\alpha}$ while the lognormal Larson IMFs (Larson 1998) are given as $\phi(m) \propto m^{-(\alpha+1)} \exp(-m_{\mathrm{ch}}/m)$, where m_{ch} is the characteristic mass. The 'top-heavy' IMF is characterized by a flatter slope than the Salpeter IMF. The 'mass-heavy' IMF has a similar slope as the Salpeter IMF but the formation of stars with stellar masses below 1 $\mathrm{M}_{\odot}$ is suppressed leading to the formation of more stars in the mass intervall [m_1, m_2] compared to the Salpeter IMF. The log normal IMFs have the same slope as the Salpeter IMF in the high mass tail of the IMF, but flatten or decline for masses below the characteristic mass. The 'Larson 1' is closest to a Salpeter IMF while the 'Larson 2' IMF is biased towards higher stel-

Table 2.2: *IMF parameters*

IMF	α	m_1	m_2	$m_{\rm ch}$
Salpeter	2.35	0.1	100	—
Mass-heavy	2.35	1.0	100	—
Top-heavy	1.5	0.1	100	—
Larson 1	1.35	0.1	100	0.35
Larson 2	1.35	0.1	100	10.0

lar masses and can be referred to as 'top-heavy' IMF (see also Sect. 3.3.2). The IMF is normalized in the mass interval [m_1, m_2] so that

$$\int_{m_1}^{m_2} m\,\phi(m)\,{\rm d}m = 1 \tag{2.4}$$

where m_1 and m_2 are the lower and upper limits of the IMF given in Table 2.2.

In Fig. 2.5 we plot the IMFs considered. From the shape of the curves for $\phi(m)$ it is evident that the majority of the stars are formed in the mass range of 3–8 $\rm M_\odot$ for all IMFs, followed by stars between 8–12 $\rm M_\odot$. Note that this includes the critical mass range of 8–10 $\rm M_\odot$ (see Sect. 2.2.4). For SNe between 10–12 $\rm M_\odot$ dust yields or metal yields are uncertain or unavailable, leading to uncertainties in the dust production efficiency. We therefore extend the previously defined critical mass range up to 12 $\rm M_\odot$.

The amount of dust produced per star, $M_{\rm d}(m)$, is calculated from the dust formation efficiencies as $M_{\rm d}(m) = M_{\rm Z}(m)\,\epsilon(m)$.

The yields of heavy elements $M_{\rm Z}(m)$ are taken from WW95 (for SNe) and van den Hoek & Groenewegen (1997) (for AGBs). We study two cases, $Z = {\rm Z_\odot}$ and $Z = 0.01{\rm Z_\odot}$.

To quantify the effect of the various IMFs and the dust production efficiencies on the total dust contribution from AGBs and SNe we define the total dust productivity of all stars in the mass interval [m_L, m_U] as

$$\mu_{\rm D} = \int_{m_L}^{m_U} \phi(m)\,M_{\rm Z}(m)\,\epsilon(m)\,{\rm d}m. \tag{2.5}$$

The lower and upper mass limits, m_L and m_U, delimitate the interval 3–40 $\rm M_\odot$, which will be further divided into the AGB star range 3–8 $\rm M_\odot$, and the SN ranges 8–12 $\rm M_\odot$, 12–20 $\rm M_\odot$ and 20–40 $\rm M_\odot$. The total dust productivity $\mu_{\rm D}$ depends on the IMF, the efficiency and the metal yields through the integrand $\xi_{\rm d}(m) = \phi(m)\,M_{\rm Z}(m)\,\epsilon(m)$, which is the specific dust productivity.

To calculate $M_{\rm d}(m)$, $\xi_{\rm d}(m)$ and $\mu_{\rm D}$ we consider for AGB stars $\epsilon(m) = \epsilon_{\rm AGB}(m)$, $\epsilon^{\rm fit}_{\rm low}(m)$. For SNe we take $\epsilon(m) = \epsilon_{\rm max}(m)$, $\epsilon_{\rm high}(m)$, $\epsilon_{\rm low}(m)$, $\epsilon^{\rm fit}_{\rm high}(m)$, $\epsilon^{\rm fit}_{\rm low}(m)$.

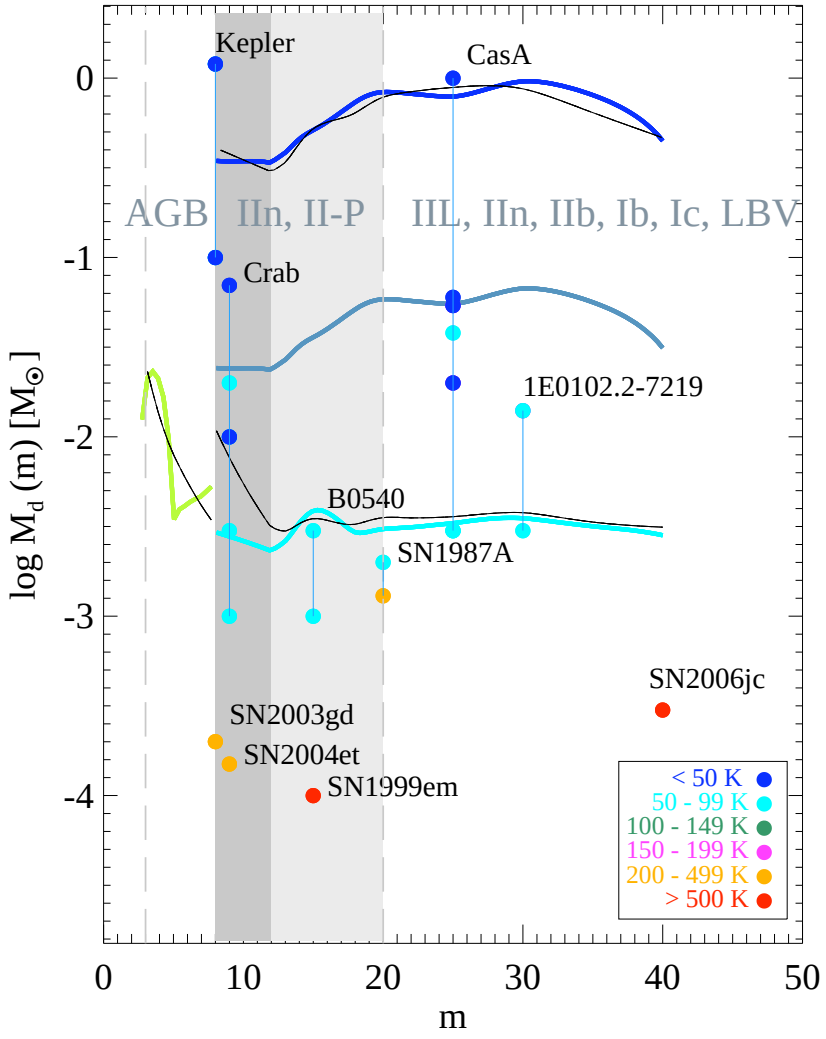

Figure 2.6: *Dust yields for AGB stars and SNe calculated for $\epsilon_{\mathrm{max}}(m)$ (dark blue line), $\epsilon_{\mathrm{high}}(m)$ (light blue line), $\epsilon_{\mathrm{low}}(m)$ (cyan line), $\epsilon^{\mathrm{fit}}_{\mathrm{high}}(m)$ and $\epsilon^{\mathrm{fit}}_{\mathrm{low}}(m)$ (black lines) as well as for AGB stars (green line). Filled circles represent observed dust yields for different SNe at different temperatures. The dark grey zone corresponds to the critical mass range (8–12 $\mathrm{M}_{\odot}$) and the light grey region corresponds to the approximate mass range for Type II-P SNe.*

2.6.1 Results

The calculated amount of dust $M_{\mathrm{d}}(m)$ for each efficiency limit is presented in Fig. 2.6. The amount of dust produced by AGB stars per stellar mass is between the values of $M_{\mathrm{d}}(m)$ for SNe with $\epsilon_{\mathrm{low}}(m)$ and $\epsilon_{\mathrm{high}}(m)$. Using $\epsilon^{\mathrm{fit}}_{\mathrm{low}}(m)$ for all stars in the range 3–40 $\mathrm{M}_{\odot}$ results in lower dust yields for stars between 6–7 $\mathrm{M}_{\odot}$ and a significant increase of $M_{\mathrm{d}}(m)$ for stars in the critical mass range 8–10 $\mathrm{M}_{\odot}$. Using $\epsilon^{\mathrm{fit}}_{\mathrm{high}}(m)$ for the maximal

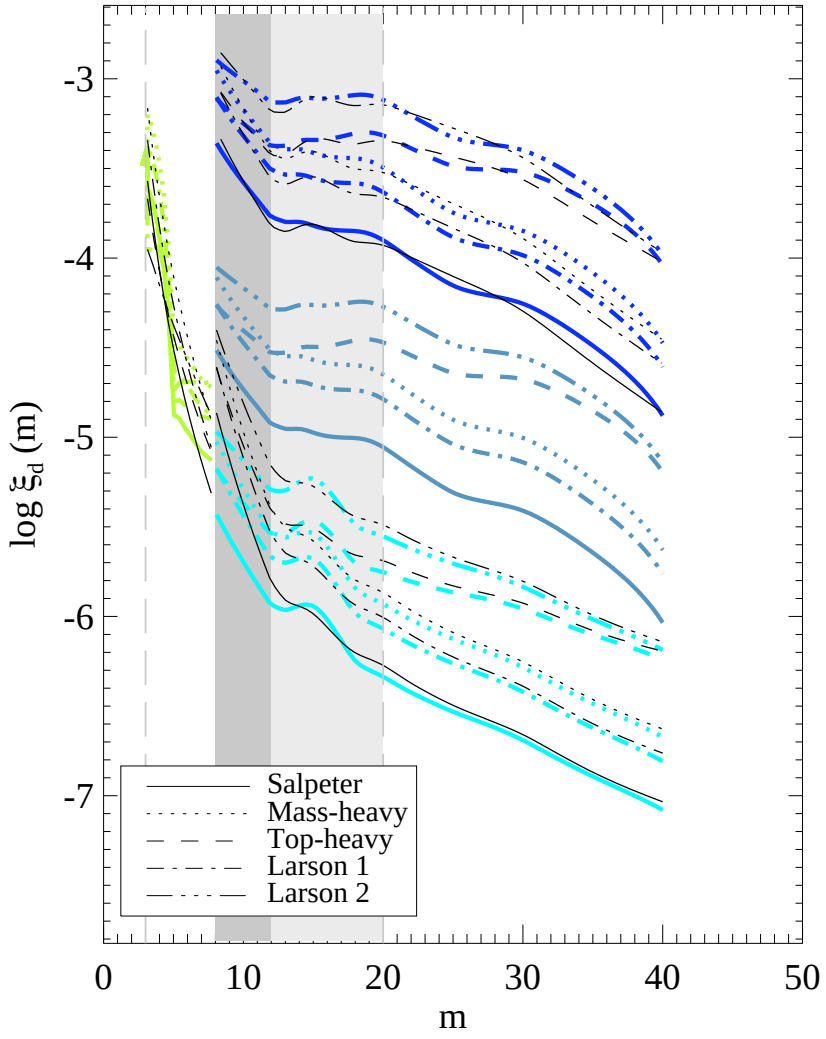

Figure 2.7: *Specific dust productivity. (a) Specific dust productivity $\xi_{\rm d}(m)$ of stellar masses calculated for $\epsilon_{\rm max}(m)$ (dark blue line), $\epsilon_{\rm high}(m)$ (light blue line), $\epsilon_{\rm low}(m)$ (cyan line), $\epsilon^{\rm fit}_{\rm high}(m)$ and $\epsilon^{\rm fit}_{\rm low}(m)$ (black lines) as well as for AGB stars (green line). The dark grey zone corresponds to the critical mass range (8–12 $\rm M_{\odot}$) and the light grey region corresponds to the approximate mass range for Type II-P SNe. The solid, dotted, dashed, dashed-dotted, and dashed-dot-dotted curves represent the Salpeter, mass-heavy, top-heavy, Larson 1 and Larson 2 IMFs, respectively.*

efficiency is consistent with using $\epsilon_{\rm max}(m)$. For comparison we plot the highest inferred dust yields from the observed SNe listed in Table 2.1. The two upper values for Cas A (Rho et al. 2008; Dunne et al. 2009) at low temperature match the dust yields calculated using $\epsilon_{\rm max}(m)$ or $\epsilon_{\rm high}(m)$. Dust masses for SNe calculated using $\epsilon_{\rm low}(m)$ are also in good agreement with the observed dust yields from several SNRs.

We also plot the observationally derived upper dust yields for the Kepler remnant

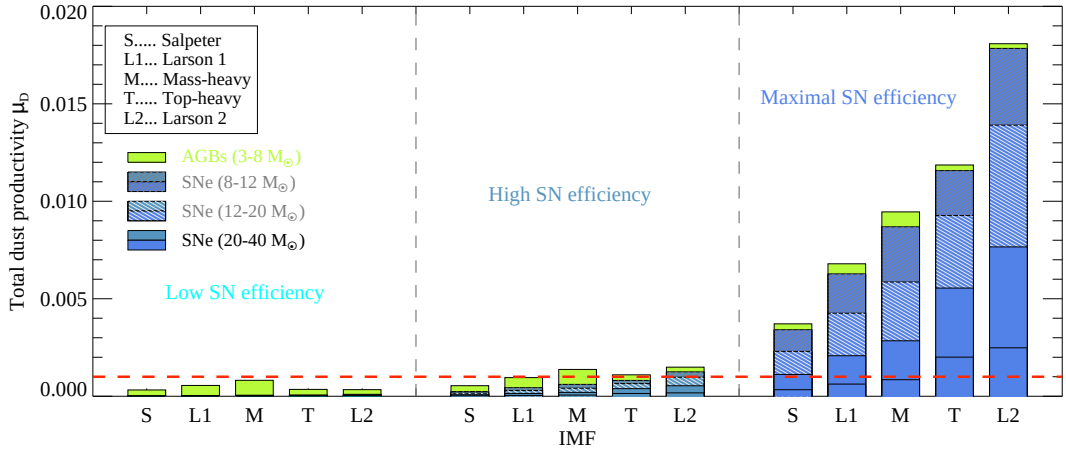

Figure 2.8: *Total dust productivity of AGB stars and SNe for different IMFs and SN dust production efficiencies. The height of the bars represents the total dust productivity of stars in the mass range 3–40* $\mathrm{M}_\odot$*. The contribution from AGB stars is marked in green, the SN mass ranges of 8–12* $\mathrm{M}_\odot$*, 12–20* $\mathrm{M}_\odot$ *and 20–40* $\mathrm{M}_\odot$ *are the dark grey shaded, light grey shaded and solid blue areas. The contribution from stars in the mass range of 30–40* $\mathrm{M}_\odot$ *is the area from the bottom to the black solid line in the bar. The letters S, L1, M, T, L2 stand for the Salpeter, Larson 1, mass-heavy, top-heavy and Larson 2 IMFs, respectively. The red dashed line marks the minimum estimated dust productivity of* $\mu_\mathrm{D} = 10^{-3}$ *to account for high dust masses in QSOs at* $z \geq 6$*.*

(Gomez et al. 2009). This SNR most likely arises from a Type Ia SN. (e.g. Blair et al. 2007; Reynolds et al. 2007; Sankrit et al. 2008). The inferred dust yields from this SNR therefore are not representative for dust from CCSNe. However, in view of the general uncertainty about dust from stars with such a progenitor mass, this SNR provides an interesting comparison with CCSN.

In Fig. 2.7 we present the results for the specific dust productivity $\xi_\mathrm{d}(m)$ for all $\epsilon(m)$ and the various considered IMFs. The slopes of $\xi_\mathrm{d}(m)$ exhibit a declining trend with increasing stellar masses regardless of the choice of $\epsilon(m)$. SNe between 30–40 $\mathrm{M}_\odot$ are thus found to be ~ 10 times less productive than SNe between 8–12 $\mathrm{M}_\odot$. For AGB stars $\xi_\mathrm{d}(m)$ decreases steeply between 3–7 $\mathrm{M}_\odot$ stars resulting in about an order of magnitude lower value for the higher mass AGB stars. The most productive AGB stars therefore are 3–4 $\mathrm{M}_\odot$ stars due to also higher dust production efficiencies $\epsilon_\mathrm{AGB}(m)$ (see Fig. 2.4 and Fig. 2.6).

The highest dust productivity for SNe between 8–40 $\mathrm{M}_\odot$ is obtained for a Larson 2 IMF, independently of the dust production efficiency. The lowest productivity is obtained for a Salpeter IMF. The difference in $\xi_\mathrm{d}(m)$ between either a Larson 2 or a top-heavy IMF and the Salpeter IMF is larger for the most massive stars ($\sim$ 30–40 $\mathrm{M}_\odot$). This sensitivity to the IMFs decreases towards lower mass SNe; the top-heavy IMF gives a higher specific dust productivity than a mass-heavy IMF for SNe in the mass range

of 8–12 $\mathrm{M}_\odot$. For AGB stars, the largest sensitivity to the IMF occurs for 3–4 $\mathrm{M}_\odot$ stars which exhibits the largest difference in $\xi_\mathrm{d}(m)$ for a mass-heavy IMF (highest value) vs. a Larson 2 IMF (lowest value).

The total dust productivity μ_D of AGB stars and SNe, subdivided into 3 mass ranges, is presented in Fig. 2.8. For a low SN efficiency $\epsilon_\mathrm{low}(m)$ the total amount of dust produced from all stars between 3–40 $\mathrm{M}_\odot$ is almost exclusively manufactured by AGB stars. Dust production by SNe in this case is negligible for all considered IMFs.

For stars between 3–40 $\mathrm{M}_\odot$ the total dust productivity is increased as soon as SNe are assumed to produce dust with the high efficiency $\epsilon_\mathrm{high}(m)$. For a Salpeter, Larson 1 and mass-heavy IMF, AGB stars still dominate the dust production whereas for a top-heavy or Larson 2 IMF, SNe are the prime dust producers.

In case of the maximal SN efficiency $\epsilon_\mathrm{max}(m)$, dust is primarily manufactured by SNe and the dust supply from AGB stars is negligible. For this efficiency the amount of dust produced by SNe is roughly 5–10 times higher than for $\epsilon_\mathrm{low}(m)$ and $\epsilon_\mathrm{high}(m)$, depending on the IMF. We find that for the IMFs favouring lower mass stars, the three SN mass ranges (8–12 $\mathrm{M}_\odot$, 12–20 $\mathrm{M}_\odot$, 20–40 $\mathrm{M}_\odot$) are nearly equally important. While it is uncertain to assume that all stars between 30–40 $\mathrm{M}_\odot$ are able to form dust, this mass range is found to be the least significant range of all SNe. Hence, SNe dust production is in general dominated by stars in the mass range of 8–20 $\mathrm{M}_\odot$ with an almost equal contribution from stars between 8–12 $\mathrm{M}_\odot$ and 12–20 $\mathrm{M}_\odot$. These relations also apply to the case of the high SNe $\epsilon_\mathrm{high}(m)$.

For the calculations with yields for heavy elements at a metallicity of Z = 0.01$\mathrm{Z}_\odot$ we find the same tendencies. This shows that these relations most likely also apply to high-z galaxies.

2.6.2 Dust at high redshift

This work is partly motivated by the unresolved origin of large dust masses in QSOs at high-redshift. In the following we therefore roughly estimate whether our derived dust productivities may be sufficient to account for the 2–7 $\times$ 10^8 $\mathrm{M}_\odot$ inferred in QSOs at $z \geq 6$ (e.g. Bertoldi et al. 2003a; Robson et al. 2004; Beelen et al. 2006).

We assume a minimum required dust mass of M_D = 2 $\times$ 10^8 $\mathrm{M}_\odot$ and a maximum available time span of Δt = 400 Myr for building up this amount of dust. The minimum required average amount of dust produced per unit time is expressed as the dust production rate in this period, R_D = $M_\mathrm{D}/\Delta t = 0.5\,\mathrm{M}_\odot$ yr^{-1} = $\mu_\mathrm{D}\,\psi(t)$. We assume a high constant average SFR $\psi(t)$ = 500 $\mathrm{M}_\odot$ yr^{-1}, based on derived SFRs from observed high-z QSOs ranging from 100–3000 $\mathrm{M}_\odot$ yr^{-1} (e.g. Bertoldi et al. 2003a; Dwek et al. 2007; Riechers et al. 2009; Wang et al. 2010). With these assumptions, all cases for which $\mu_\mathrm{D} \leq 10^{-3}$ can be excluded (see Fig. 2.8).

For the low SN dust production efficiency $\epsilon_\mathrm{low}(m)$ none of the IMFs give a suffi-

ciently high dust productivity. Only a mass-heavy IMF is close to the limit. Moreover, the long lifetimes of 3–4 $\mathrm{M}_\odot$ AGB stars (see Fig. 2.1), which dominate the AGB dust production (see Sec. 2.6 and Fig. 2.6), is problematic. These stars will start contributing with a delay of more than $\sim$ 200 Myr so will produce dust for only approximately half the time of our assumed maximal time span of 400 Myr. Thus, a low SN dust production efficiency is insufficient to account for the dust at high-redshift.

In case of a high SN efficiency, $\epsilon_{\mathrm{high}}(m)$, the majority of the IMFs might lead to a sufficiently high dust productivity. Due to their short lifetimes, SNe can be assumed to release dust immediately after formation. Thus, SNe dominate the dust production for a Larson 2 or top heavy IMF. Taking into account the reduction of the AGB dust contribution due to the long lifetimes of these stars, the Salpeter or Larson 1 IMFs most likely do not lead to sufficiently large amounts of dust at high-z.

For a maximal SN efficiency $\epsilon_{\mathrm{high}}(m)$ the total dust production rates R_{D} of 3–18 $\mathrm{M}_\odot$ yr^{-1} are achieved primarily by SN dust production. This leads to possible dust masses in excess of 10^9 $\mathrm{M}_\odot$ produced in high-z systems, even for significantly lower star formation rates than assumed in our scenario.

We note that it is unclear if a high SFR can be sustained over 400 Myr. In fact, the very high derived SFRs ($\geq$ 1000 $\mathrm{M}_\odot$ yr^{-1}) are attributed to shorter ($\leq 10^8$ yr) durations of the starburst (e.g. Bertoldi et al. 2003a; Dwek et al. 2007; Riechers et al. 2009). Assuming a SFR $\psi(t)$ = 1000 $\mathrm{M}_\odot$ yr^{-1} and a Δt = 200 Myr leads to the same dust productivity $\mu_{\mathrm{D}} = 10^{-3}$ as discussed above, although the AGB stars contribution is overestimated due to too long lifetimes.

We stress, however, that these estimates are based on a simple scenario, which does not take further processing of dust grains in the ISM into account. A more careful investigation will be presented in the next Chapter.

2.7 SUMMARY

In this work we have investigated the dust productivity of AGB stars and SNe as well as their contribution to the total amount of dust in high-z galaxies. Based on inferred dust yields from SN dust observations and theoretically calculated dust masses we have ascertained a low, high and maximal limit for the dust production efficiency of SNe. Using these efficiencies we have evaluated the total dust productivity of AGB stars and SNe in the mass interval 3–40 $\mathrm{M}_\odot$ for five different IMFs. The main results can be summarized as follows:

1. The minimum mass of a stellar source able to contribute to the total amount of dust in galaxies at redshift $z \sim 6$ is $\sim$3 $\mathrm{M}_\odot$ (see Fig. 2.1). Therefore AGB stars between 3–8 $\mathrm{M}_\odot$ are considered as potential sources for dust in high-z galaxies.

2. The dust production efficiency for AGB stars and SNe exhibit a decreasing ten-

dency with increasing progenitor mass (see Fig. 2.4)

3. The dust productivity of stars between 3–40 $\mathrm{M}_{\odot}$ is in general significantly dependent on the IMF. This is more pronounced when stars between 8–40 $\mathrm{M}_{\odot}$ form dust with maximal SN efficiency.

4. The contribution from AGB stars to the total dust productivity of stars between 3–40 $\mathrm{M}_{\odot}$ prevails when SNe are assumed to produce dust with the low SN efficiency $\epsilon_{\mathrm{low}}(m)$. The contribution from AGB stars becomes insignificant for high to maximal SN dust production efficiency and for IMFs biased towards high stellar masses.

5. The SNe mass ranges of 8–12 $\mathrm{M}_{\odot}$ and 12–20 $\mathrm{M}_{\odot}$ are equally important and together dominate the dust production from all SNe between 8–40 $\mathrm{M}_{\odot}$. Dust produced by stars between 20–40 $\mathrm{M}_{\odot}$ is influenced by the fractions of the various types of CCSNe.

6. The total dust production rate from AGB stars and SNe with a high dust production efficiency and a high SFR $\psi(t) \geq 500\ \mathrm{M}_{\odot}\ \mathrm{yr}^{-1}$ can account for the high dust masses inferred in $z > 6$ QSOs provided the IMF is weighted towards higher stellar masses.

This chapter is based on: C. Gall, A. C. Andersen and J. Hjorth – *Genesis and evolution of dust in galaxies in the early Universe – II. Modeling dust evolution in starburst galaxies* A&A, submitted
Figure: Active galaxy M82; NASA, ESA, and the Hubble Heritage Team (STScI/AURA), Hubble Space Telescope ACS/WFC, STScI-PRC06-14a

3

MODELING DUST EVOLUTION IN STARBURST GALAXIES

Vi er alle enige om,
at din teori er vanvittig,
men er den vanvittig nok?

NIELS BOHR (1885-1962)

ABSTRACT –

The aim is to elucidate the astrophysical conditions required for generating large amounts of dust in massive starburst galaxies at high redshift. We have developed a numerical galactic chemical evolution model. The model is constructed such that the effect of a wide range of parameters can be investigated. It takes into account results from stellar evolution models, a differentiation between diverse types of CCSN and the contribution of AGB stars in the mass range 3–8 $\mathrm{M}_{\odot}$*. We consider the lifetime-dependent yield injection into the ISM by all sources as well as dust destruction due to SN shocks in the ISM. We ascertain the temporal progression of the dust mass, the dust-to-gas and dust-to-metal mass ratios as well as other physical properties of a galaxy and study their dependence on the mass of the galaxy, the IMF, dust production efficiencies and dust destruction in the ISM.*

3.1 INTRODUCTION

Modeling the evolution of dust in galaxies is a key ingredient towards understanding the origin of large observed dust masses in high-redshift galaxies and QSOs.

Dust masses $\geq 10^8$ $\mathrm{M}_\odot$ have been derived from observations in QSOs at redshift $z \gtrsim 6$ (e.g., Bertoldi et al. 2003a; Robson et al. 2004; Beelen et al. 2006; Hines et al. 2006; Michałowski et al. 2010b) along with high SFR up to a few times 10^{2-3} $\mathrm{M}_\odot$ yr^{-1} (e.g., Walter et al. 2004; Wang et al. 2010). Additionally, QSOs at $z > 6$ harbour supermassive black holes (SMBHs) with masses $> 10^9$ $\mathrm{M}_\odot$ (e.g., Willott et al. 2003; Vestergaard 2004; Jiang et al. 2006). Kawakatu & Wada (2008, 2009) showed that in order to form a SMBH $> 10^9$ $\mathrm{M}_\odot$, a large mass supply of $> 10^{10-11}$ $\mathrm{M}_\odot$ is needed. These requirements together with derived molecular gas masses from CO line emission measurements in excess of 10^{10} $\mathrm{M}_\odot$ (e.g., Cox et al. 2002; Carilli et al. 2002; Bertoldi et al. 2003b; Walter et al. 2003; Riechers et al. 2009; Wang et al. 2010) set significant constrains on the physical properties of the host galaxies. These in turn have implications on the origin and evolution of dust. Furthermore, a tendency of increased dust attenuation with higher galaxy masses for systems at $z \sim 6$–8 has been found by Schaerer & de Barros (2010).

Analytical and numerical models for dust evolution have been developed. Dwek et al. (2007) propose 1 $\mathrm{M}_\odot$ of dust per SN to be necessary to account for dust masses in high-z QSOs, while contemplating SNe as the only source. Such high dust masses for SNe are in contradiction with derived dust masses from nearby SNe and SN remnants, which reveal on average a few times 10^{-4}–10^{-2} $\mathrm{M}_\odot$ of dust (e.g., Wooden et al. 1993; Elmhamdi et al. 2003; Temim et al. 2006; Meikle et al. 2007; Rho et al. 2008; Kotak et al. 2009; Sibthorpe et al. 2009; Barlow et al. 2010). A review of observationally and theoretically derived dust from stellar sources is provided in Chapter 2.

The issue of whether SNe produce large amounts of dust is unclear. Other sources of dust such as AGB stars have been taken into account (Morgan & Edmunds 2003; Valiante et al. 2009) in chemical evolution models of high-redshift galaxies. Valiante et al. (2009) claimed that with the contribution of AGB stars, 10^8 $\mathrm{M}_\odot$ of dust can be reached, with AGB stars dominating the dust production. AGB stars (0.85–8 $\mathrm{M}_\odot$) are the main source of dust in the present universe, but only stars with masses $\gtrsim 3$ $\mathrm{M}_\odot$ are likely to contribute at $z > 6$ (e.g., Marchenko 2006, Sect. 2.2). Evidence that metal deficient AGB stars also undergo strong mass loss and are able to efficiently produce dust is supported observationally (e.g., Zijlstra et al. 2006; Groenewegen et al. 2007; Lagadec et al. 2007a; Matsuura et al. 2007; Sloan et al. 2009) and theoretically (e.g., Wachter et al. 2008; Mattsson et al. 2008). However, the theoretical models (Dwek et al. 2007; Morgan & Edmunds 2003; Valiante et al. 2009) greatly differ with respect to the assumptions made for the mass of the galaxy, dust contribution from stellar sources as well as the treatment of the star formation. Thus the origin of dust and its evolution remain unclear.

In Chapter 2 we derived plausible dust production efficiency limits for stellar sources between 3–40 $\mathrm{M}_{\odot}$, and determined the dust productivity of these sources for a single stellar population. In this Chapter we investigate the evolution of dust in high-z galaxies. We develop a numerical chemical evolution model, which allows exploration of the physical parameter space for galaxies at $z > 5$–6. Different types of core collapse supernovae are specified and the contribution from AGB stars and the impact of SMBHs are taken into account. We furthermore follow the evolution of some physical properties of these galaxies. The main parameters varied in the model are the IMF, the mass of the galaxy, yields for SNe, the strength of dust destruction in the ISM as well as the dust production efficiency limits. Models with or without the SMBH formation are considered.

This Chapter is arranged as follows: In Sect. 3.2 the equations used to construct the model are developed. We discuss the model parameters and their possible values in Sect. 3.3. A detailed analysis of the results is presented in Sect. 3.4, which is followed by a discussion in Sect. 4.4 and our conclusions of this work in Sect. 3.6.

3.2 Modeling the evolution of dust in starburst galaxies

In this section we formulate the equations necessary to follow a galaxy's time dependent evolution in a self-consistent numerical model.

The main basic logic is adopted from Tinsley (1980, and references therein) which has also been used in other chemical evolution models to study dust in galaxies (e.g., Morgan & Edmunds 2003; Dwek et al. 2007). We focus on an elaborate treatment of dust from different types of CCSNe and AGB stars. To calculate the amount of dust from these sources we use the dust production efficiencies derived in Chapter 2. In particular, the lifetime dependent delayed dust and gas injection from AGB stars and SNe is taken into account. The metallicity dependent lifetimes of all stars are taken from Schaller et al. (1992), Schaerer et al. (1993) and Charbonnel et al. (1993). In Chapter 2 we showed that the variation of the lifetime with metallicity is minimal. We therefore calculate and use a metallicity-averaged lifetime for all stars. The recycled gaseous material is defined as the remaining ejected stellar yields from all massive stars in the mass range 3–100 $\mathrm{M}_{\odot}$ which has not been incorporated into dust grains. This also includes the stellar feedback from very massive stars ($\gtrsim$ 30–40 $\mathrm{M}_{\odot}$) in the form of stellar winds. Dust and gas is assumed to be released instantaneously after the death of the stars.

We strictly treat the elements in the gas and solid phases separately while taking care of their interplay. Thus, we define $M_{\mathrm{g}}(t)$ as the total mass of elements in the ISM which are in the gas phase and $M_{\mathrm{d}}(t)$ as the total amount of elements in the solid dust phase. The mass of the ISM is defined as $M_{\mathrm{ISM}}(t) \equiv M_{\mathrm{g}}(t) + M_{\mathrm{d}}(t)$, which in the

literature is often referred to as the 'gas' mass. The total amount of dust in our models is solely calculated from the dust contributions from SNe and AGB stars. Thus, no further growth in the ISM is contemplated. However, dust destruction in the ISM through SN shocks is taken into account. The formation of the SMBH is considered as a simple sink for dust, gas and metals.

We assume a so-called 'closed box' model, i.e., the effect of infalling and outflowing gas in the galactic system is neglected. Although galaxies may not evolve in such a simple manner this assumption is plausible since massive starburst galaxies are assumed to have SFRs $\psi(t) \gtrsim 10^3$ $\mathrm{M}_\odot$ yr^{-1}. Infall of neutral gas would only affect the system when the infall rate is comparable to the SFR. In this case a large gas reservoir needs to be present in the vicinity of the galaxy already. Besides, infall-rates for high-z galaxies are not known. We further assume the ISM to be homogeneously mixed and we evolve our model only up to the first Gyr. Examples of 'closed box' models being sufficiently accurate include the works of Frayer et al. (1999) and Tecza et al. (2004) for the luminous and massive submillimeter galaxy SMMJ14011+0252 at z = 2.565.

3.2.1 Basic considerations

The initial mass functions (IMF) $\phi(m)$ is normalized to unity in the mass interval [m_1, m_2] as

$$\int_{m_1}^{m_2} m\,\phi(m)\,\mathrm{d}m = 1, \tag{3.1}$$

where m_1 and m_2 are the lower and upper limits of the IMF (see Sect. 3.3.2).

The relation between the total mass $M_{\mathrm{ISM}}(t)$ and the SFR $\psi(t)$ is given by the Kennicutt law (Kennicutt 1998), where $\psi(t) \propto M_{\mathrm{ISM}}(t)^k$. Analogously to Dwek et al. (2007) we apply the following notation to calculate the SFR

$$\psi(t) = \psi_{\mathrm{ini}} \left[\frac{M_{\mathrm{ISM}}(t)}{M_{\mathrm{ini}}}\right]^k, \tag{3.2}$$

where ψ_{ini} is the initial SFR, M_{ini} the initial gas mass of the galaxy and $M_{\mathrm{ISM}}(t)$ the mass of the ISM. The value of k is between 1 and 2, so we set k = 1.5. This value has also often been assumed in other models (e.g., Dwek 1998; Dwek et al. 2007; Calura et al. 2008).

3.2.2 Equations for AGB stars and supernovae

The amount of dust from all stellar sources released into the ISM per unit time is simply calculated as the amount of dust produced by the stellar sources times the source rate. The considered dust producing stellar sources are AGB stars and CCSNe. We account for a potential diverse dust contribution by different SNe subtypes and distinguish between Type IIP SNe and the remaining Type II subtypes (see Chapter 2). Type Ib and Ic

SNe, collectively referred to as Ib/c, are not considered as dust producing SNe. However they inject their stellar yields into the ISM. A specification of these sources and their lower and upper stellar mass limits $m_{\mathrm{L(i)}}$ and $m_{\mathrm{U(i)}}$, respectively, are discussed in Sect. 3.3.3. In the following equations these sources are indicated by the subscript i = AGB, IIP, II, Ib/c.

The AGB and SN rate $R_{\mathrm{i}}(t)$ calculates as

$$R_{\mathrm{i}}(t) = \int_{m_{\mathrm{L(i)}}}^{m_{\mathrm{U(i)}}} \psi(t-\tau)\,\phi(m)\,\mathrm{d}m, \tag{3.3}$$

where $\tau = \tau(m)$ is the lifetime of a star with a zero age main sequence (ZAMS) mass m, i.e., the star was born at time $(t-\tau)$ when it dies at time t. It is evident that stars only contribute when the condition $t - \tau \geq 0$ is fulfilled.

For SNe the time of releasing the total produced elements is assumed to take place right after explosion. The main sequence lifetime for AGB stars is defined as the time until the end of the early asymptotic giant branch phase, which can take up to several 100 Myr. However, the most efficient mass loss phase itself is less than 1 Myr at the very end of the AGB phase and is relatively short compared to the total lifetime of AGB stars. Thus, we make the same approximation as for SNe: All produced elements and dust are released instantaneously after the main sequence lifetime.

For each kind of source the total produced dust per unit time is calculated as

$$E_{\mathrm{d,i}}^{\mathrm{prod}}(t) = \int_{m_{\mathrm{L(i)}}}^{m_{\mathrm{U(i)}}} \left(Y_{\mathrm{Z}} + Y_{\mathrm{WIND}}\, Z(t-\tau)\right) \epsilon_{\mathrm{i}}(m,Z)\,\psi(t-\tau)\,\phi(m)\,\mathrm{d}m, \tag{3.4}$$

where $Y_{\mathrm{Z}} = Y_{\mathrm{Z}}(m,Z)$ with $Z = Z(t-\tau)$ is the mass (m) and metallicity (Z) dependent amount of ejected heavy elements per star. The metallicity Z is defined as the metallicity with which the star was born at a time $(t-\tau)$. The parameter $\epsilon_{\mathrm{i}}(m,Z)$ is defined as the dust production efficiency. The assumed efficiencies are further described in Sect. 3.3.4. For Type Ib/c SNe $E_{\mathrm{d,Ib/c}}^{\mathrm{prod}}(t) = 0$.

The total amount of mass lost in stellar winds prior to explosion, Y_{WIND}, caused by mass loss during stellar evolution of SNe, is calculated as

$$Y_{\mathrm{WIND}} = m - M_{\mathrm{fin}}, \tag{3.5}$$

where $Y_{\mathrm{WIND}} = Y_{\mathrm{WIND}}(m,Z)$ and $M_{\mathrm{fin}} = M_{\mathrm{fin}}(m,Z)$. The latter is the final mass of a SN before explosion. Type II SN suffer strong mass loss leading to the formation of dense circumstellar disks. Dust in these disks has been found for some SNe (see Chapter 2). However, the actual amount of metals in these disks is not known and data are not available, thus we cannot account for them. In the case of AGB stars and for SN models where no mass loss prescription is available $Y_{\mathrm{WIND}} = 0$.

Beside elements bound in dust grains elements in the gas phase are also released

into the ISM. The produced amount of elements in gaseous form is calculated as

$$E_{\mathrm{g,i}}(t) = \int_{m_{\mathrm{L(i)}}}^{m_{\mathrm{U(i)}}} (Y_{\mathrm{E}} + Y_{\mathrm{WIND}} - (Y_{\mathrm{Z}} + Y_{\mathrm{WIND}}\, Z(t-\tau))\, \epsilon_{\mathrm{i}}(m,Z))\, \psi(t-\tau)\, \phi(m)\, \mathrm{d}m, \quad (3.6)$$

where $Y_{\mathrm{E}} = Y_{\mathrm{E}}(m,Z)$ is the amount of all ejected elements per star. For SNe of Type Ib/c $\epsilon_{\mathrm{i}}(m,Z) = 0$.

The total mass of heavy elements released into the ISM per unit time is calculated as

$$E_{\mathrm{Z,i}}(t) = \int_{m_{\mathrm{L(i)}}}^{m_{\mathrm{U(i)}}} (Y_{\mathrm{Z}} + Y_{\mathrm{WIND}}\, Z(t-\tau))\, \psi(t-\tau)\, \phi(m)\, \mathrm{d}m. \quad (3.7)$$

We include the possibility of dust destruction in the SN remnant (SNR) due to reverse shock interaction. Dust destruction time scales up to 10^4 yr have been predicted by Bianchi & Schneider (2007) and Nozawa et al. (2007, 2010). However, this timescale is relatively short in comparison to the lifetime of a star, and we make the approximation that dust is destroyed immediately after formation.

We define the parameter ξ_{SN} as the SN dust destruction factor, i.e., the destroyed mass of dust per unit time of all SNe is

$$E_{\mathrm{d,i}}^{\mathrm{dest}}(t) = E_{\mathrm{d,i}}^{\mathrm{prod}}(t)\, \xi_{\mathrm{SN}}. \quad (3.8)$$

This term applies only to Type IIP and Type II SNe, thus i = IIP, II.

The final SN dust injection rate per unit time is calculated as

$$E_{\mathrm{d,SN}}(t) = \sum_{\mathrm{i=IIP,II}} E_{\mathrm{d,i}}^{\mathrm{prod}}(t) - E_{\mathrm{d,i}}^{\mathrm{dest}}(t), \quad (3.9)$$

while the final AGB dust injection rate is

$$E_{\mathrm{d,AGB}}(t) = E_{\mathrm{d,AGB}}^{\mathrm{prod}}(t). \quad (3.10)$$

Recycled gaseous material

The recycled material from SNe and AGB stars consists of all the mass of the elements not being incorporated into dust grains and hence in the gas phase. Very massive stars ending as BHs may contribute with their stellar winds to the recycled material. We will refer to stars which directly form a BH as the 'remaining stars'. Pertaining to the short lifetime of very massive stars and the resultant short duration of the wind phase we assume that all the elements lost in the wind phase are released after the death of the star. The total mass of the released elements per unit time of the remaining stars is

$$E_{\mathrm{g,R}}(t) = \int_{m_{\mathrm{L(R)}}}^{m_{\mathrm{U(R)}}} X_{\mathrm{g,R}}\, \psi(t-\tau)\, \phi(m)\, \mathrm{d}m, \quad (3.11)$$

where $X_{\rm g,R} = X_{\rm g,R}(m, Z)$ is the mass of elements released into the ISM per star, while the subscript 'R' stands for 'remaining stars'.

For these remaining stars the following two scenarios are possible: (1) a supernova without display (Eldridge & Tout 2004) occurs even if a BH is formed and elements are ejected or (2) no SN occurs because no SN shock is launched. For the first case, the term $X_{\rm g,R}$ can either be substituted with $(Y_{\rm E} + Y_{\rm WIND})$, or if $Y_{\rm E}$ and $Y_{\rm WIND}$ are not known, the common approximation of $X_{\rm g,R} = m - M_{\rm rem}$ can be made. The mass $M_{\rm rem} = M_{\rm rem}(m, Z)$ is the remnant mass of a star. In the second case we assume that no nucleosynthesis products will be ejected. A contribution to the gas household in the ISM comes solely from the stellar winds, thus $X_{\rm g,R} = Y_{\rm WIND}$.

The mass of released metals from these stars per unit time is given by

$$E_{\rm Z,R}(t) = \int_{m_{\rm L(R)}}^{m_{\rm U(R)}} X_{\rm Z,R}\, \psi(t-\tau)\, \phi(m)\, {\rm d}m, \tag{3.12}$$

where $X_{\rm Z,R} = X_{\rm Z,R}(m, Z)$ is the mass of the ejected heavy elements per star. For the first case $X_{\rm Z,R} = Y_{\rm Z} + Y_{\rm WIND}\, Z(t-\tau)$. For the second case $X_{\rm Z,R} = Y_{\rm WIND}\, Z(t-\tau)$.

Extending the subscript i to i = AGB, IIP, II, Ib/c, R the total returned mass of gaseous material to the ISM per unit time calculates as

$$E_{\rm g}(t) = \sum_{\rm i} E_{\rm g,i}(t) + \sum_{\rm i=IIP,II} E_{\rm d,i}^{\rm dest}(t). \tag{3.13}$$

It is important to note that elements locked up in dust grains will return into the gas phase when dust destruction takes place. Hence, the amount of destroyed dust in SNRs must be added to the total amount of gas in the ISM (second term in Eq. 3.13).

3.2.3 The evolution of dust and gas in the galaxy

The chemical evolution of a galaxy is mainly determined by the equations balancing the net amount of gas, dust, and heavy elements.

Effect of a super massive black hole

We take the effect of a SMBH into account as an additional sink for the gas, dust and metals. We base our assumptions for the treatment of the BH on the theoretical work of Kawakatu & Wada (2008, 2009). In order to form a SMBH, super Eddington growth is required. This necessitates a large mass supply of $\sim 10^{10-11}$ $\rm M_\odot$ on a short supply timescale of $t_{\rm SMBHsup} \sim 10^8$ yr from the host galaxy to a massive circumnuclear disk. Kawakatu & Wada (2009) found that the final SMBH mass is around 1–10 % of the supply mass $M_{\rm BHsup}$.

We will not treat the formation of the disk in detail, but assume that the supply mass needed is equal to the initial mass $M_{\rm ini}$ of our considered systems. We therefore only

take the overall mass of the ISM needed for the formation of the SMBH into account. A simple constant growth rate is calculated as

$$\Psi_{\rm SMBH} = \frac{M_{\rm SMBH}}{t_{\rm SMBH}}, \tag{3.14}$$

where $M_{\rm SMBH}$ is the mass of the final SMBH, and $\Psi_{\rm SMBH}$ = const. for $t \leq t_{\rm SMBH}$, whereas $\Psi_{\rm SMBH}$ = 0 for $t > t_{\rm SMBH}$. The growth timescale to build up the SMBH is equal to the supply timescale $t_{\rm SMBH}$ = $t_{\rm SMBHsup}$. The onset of the SMBH formation coincides with the onset of starburst of the whole galaxy. In case the SMBH is not taken into account the growth rate is set to zero ($\Psi_{\rm SMBH} = 0$).

The amount of dust in the ISM

The evolution of the amount of dust $M_{\rm d}(t)$ in the galaxy is

$$\frac{{\rm d}M_{\rm d}(t)}{{\rm d}t} = E_{\rm d,SN}(t) + E_{\rm d,AGB}(t) - E_{\rm D}(t). \tag{3.15}$$

The first and second terms are the dust injection rates from supernovae and AGB stars contributing to the increase of the dust household in the ISM. The third term $E_{\rm D}(t)$ is defined as the total dust destruction rate. It determines the dust reduction through astration as well as the SMBH formation and destruction in the ISM caused by SN shocks, if considered. The total dust destruction rate is calculated as

$$E_{\rm D}(t) = \eta_{\rm d}(t)\,(\psi(t) + \Psi_{\rm\ SMBH} + M_{\rm cl}\,R_{\rm SN}(t)). \tag{3.16}$$

The variable $\eta_{\rm d}(t) = M_{\rm d}(t)/M_{\rm ISM}(t)$ is the fraction of dust in the ISM and will be referred to as the 'dust-to-gas mass ratio'. For simplicity we make the assumption that the produced dust will be immediately mixed with the material in the ISM. The dust destruction in the ISM through SN shocks will be discussed in more detail in Sect. 3.3.5.

The amount of gas in the ISM

The temporal evolution of the gas content in the galaxy is calculated as

$$\begin{aligned}\frac{{\rm d}M_{\rm g}(t)}{{\rm d}t} &= E_{\rm g}(t) + \eta_{\rm d}(t)\,M_{\rm cl}\,R_{\rm SN}(t) \\ &\quad - (1-\eta_{\rm d}(t))\,(\psi(t) + \Psi_{\rm\ SMBH}).\end{aligned} \tag{3.17}$$

$E_{\rm g}(t)$ is the recycled gaseous material (see Eq. 3.13). The second term is the amount of destroyed dust in gaseous form (see Sect. 3.2.3). The third term accounts for the depletion of the gas in the ISM through incorporation into stars and the loss to the SMBH. The fraction of gas in the ISM is expressed as $(1 - \eta_{\rm d}(t))$.

Metallicity

Owing to the separation of the ISM mass into the material locked in dust and gas, respectively, it is necessary to formally take care of the transition of elements from the dust phase to the gas phase (due to destruction). For the evolution of heavy elements we do not distinguish between their chemical states.

The equation for the evolution of the total amount of heavy elements is formulated as

$$\frac{\mathrm{d}M_{\mathrm{Z}}(t)}{\mathrm{d}t} = E_{\mathrm{Z}}(t) - \eta_{\mathrm{Z}}(t)\,(\psi(t) + \Psi_{\,\mathrm{SMBH}}), \tag{3.18}$$

where

$$E_{\mathrm{Z}}(t) = \sum_{\mathrm{i}} E_{\mathrm{Z,i}}(t), \tag{3.19}$$

is the total ejected mass of heavy elements per unit time from all considered sources. The last term in Eq. 3.18 determines the reduction of heavy elements due to astration and the loss to the SMBH.

The total metallicity of the system is defined as $Z(t) = \eta_{\mathrm{Z}}(t) = M_{\mathrm{Z}}(t)/M_{\mathrm{ISM}}(t)$. The fraction of metals in the ISM which are bound in dust grains is calculated as $\eta_{\mathrm{Zd}}(t) = M_{\mathrm{d}}(t)/M_{\mathrm{Z}}(t)$.

The amount of metals in the gas phase is

$$M_{\mathrm{Z,g}}(t) = (1 - \eta_{\mathrm{zd}}(t))\, M_{\mathrm{Z}}(t). \tag{3.20}$$

The gas phase metallicity is given as $\eta_{\mathrm{Zg}}(t) = M_{\mathrm{Z,g}}(t)/M_{\mathrm{g}}(t)$.

3.3 MODEL PARAMETERS

In this section we describe the prime model parameters as well as the values used in this study. In particular, we consider the initial conditions of the galaxy, the IMF, stellar yields and the destruction rates of dust in the ISM. These characterize the system and significantly influence the evolution of gas, dust, and metals. In addition we define some switches, which specify various possibilities for some model parameters. All parameters and their considered values as well as the possibilities for the switches are listed in Table 3.1.

3.3.1 INITIAL CONDITIONS

The model is defined by the initial values of the parameters. It does not depend on or is influenced by additional input from other models, i.e., it does not depend on a cosmological model. Therefore it can be applied to any galaxy within the accuracy

limit of a 'closed-box' treatment. We are mainly interested in massive high-redshift galaxies in which large dust masses, stellar masses and H_2 masses have been inferred from observations. The parameters of our computed models are therefore tuned to such galaxies.

One of the main parameters is the baryonic initial gas mass $M_{\rm ini}$ which is equal to the total mass of the galaxy in baryons. A relation between $M_{\rm ini}$ and the mass of the dark matter halo $M_{\rm DM}$ hosting such systems is given through $M_{\rm ini} = \Omega_b/\Omega_m\, M_{\rm DM}$. In this work we consider five different massive galaxies with $M_{\rm ini}$ = 1.3 $\times$ 10^{12} $\mathrm{M}_\odot$, $M_{\rm ini}$ = 5 $\times$ 10^{11} $\mathrm{M}_\odot$, $M_{\rm ini}$ = 3 $\times$ 10^{11} $\mathrm{M}_\odot$, $M_{\rm ini}$ = 1 $\times$ 10^{11} $\mathrm{M}_\odot$, and $M_{\rm ini}$ = 5 $\times$ 10^{10} $\mathrm{M}_\odot$.

In Sect. 2.2.1 we argued that the very first population of stars (so called Pop III stars) are not likely to be the main sources of large dust masses at high redshift. Thus we consider only the next generations of stars (Pop II or Pop I). The formation of these stars takes place as soon as a critical metallicity of $Z_{\rm cr} \sim 10^{-6}$–10^{-4} $\mathrm{Z}_\odot$ (Bromm & Loeb 2003; Schneider et al. 2006; Tumlinson 2006) in the star forming region is reached. In this regard we assume an initial metallicity in accordance with the critical metallicity of $Z_{\rm ini} = Z_{\rm cr} = 10^{-6}$ $\mathrm{Z}_\odot$.

Pertaining to the rather high derived star formation rates from observations of some high-z massive galaxies and QSOs (e.g. Frayer et al. 1999; Bertoldi et al. 2003a; Riechers et al. 2007), we consider an initial SFR of $\psi_{\rm ini}$ = 1 $\times$ 10^3 $\mathrm{M}_\odot$ yr^{-1}. The evolution is determined using the Kennicutt law as described in Sect. 3.2.1, Eq. 3.2. We also consider a case of constant SFR where $\psi(t) = \psi_{\rm ini}$ = 1 $\times$ 10^3 $\mathrm{M}_\odot$ yr^{-1}.

In our model the onset of starburst is not directly connected to redshift. Hence, the age of the galaxy is identical to the evolutionary time after starburst. For dusty galaxies seen at redshift 5–6 the earliest onset of starburst with very high SFRs can be considered to have taken place at $z \backsimeq 10$. For a ΛCDM universe with H_0 = 70 km s^{-1} Mpc^{-1}, Ω_Λ = 0.73 and Ω_m = 0.27 and Ω_b = 0.04 (Spergel et al. 2003), the evolutionary time of interest for building up large dust masses possibly lies then within 400–500 Myr. We compute all models presented in this Chapter up to an age of the galaxy of $t_{\rm max}$ = 1 Gyr.

3.3.2 THE INITIAL MASS FUNCTION

The initial mass function is an important parameter influencing the evolution of dust, gas and metals in a galaxy. It determines the mass distribution of a population of stars with a certain ZAMS mass. The IMF was first proposed by Salpeter (1955) and had been derived for Galactic field stars. Original, the IMF was not a power law but composed of a logarithmic slope of about -1.7 for stars below 1 $\mathrm{M}_\odot$ and -1.2 for stars between 1–10 $\mathrm{M}_\odot$. It was suggested that a power law with slope -1.35 applied to the whole function is appropriate, but strictly speaking it is only valid for stars between 0.4–10 $\mathrm{M}_\odot$. Nevertheless, the Salpeter IMF is still often applied to more extended mass ranges (e.g., 0.1–100 $\mathrm{M}_\odot$) (see for detailed reviews e.g., Scalo 2005; Chabrier 2005). Later studies

have shown that the IMF flattens for stars below 0.5 $\mathrm{M}_{\odot}$ and significantly declines in the mass regime < 0.1 $\mathrm{M}_{\odot}$ (e.g., Kroupa 2002; Chabrier 2003a,b). A steeper decline for intermediate mass stars has also been suggested (Scalo 1986, 1998). A characteristic mass has been defined such that half the initial mass goes into stars with masses lower than the characteristic mass and half into stars more massive. The characteristic mass describes the mass at which stars are preferentially formed. From the field star IMFs described above such mass results of about 1 $\mathrm{M}_{\odot}$ (e.g., Larson 2006).

One fundamental debate regarding the IMF is whether there is a systematic variation of the IMF with some physical conditions of star formation or whether it is universal. A variability of the IMF results from several theoretical approaches. Systematic changes of the IMF leading to a shift of the characteristic mass towards higher stellar masses are found in star-forming environments with increased ambient temperatures (e.g., Larson 1998) or high-densities (Murray & Lin 1996; Krumholz et al. 2010). The absence of a variation of the characteristic mass due to a change of the equation of state as a result of dust processes is suggested by Bonnell et al. (2007). Usually any IMF with a characteristic mass shifted towards high stellar masses resulting in an overabundance of high mass stars is referred to as 'top-heavy' IMF. The likelihood of a top-heavy IMF in low metallicity environments and in particular in the early Universe has been suggested already many years ago Schwarzschild & Spitzer (1953) and plausible evidence is extensively discussed in e.g., Larson (1998) and Tumlinson (2006). Further indirect and direct evidence for a top-heavy IMF has been found in various systems such as e.g., starburst galaxies (ee.g., Rieke et al. 1993; Doane & Mathews 1993; Dabringhausen et al. 2009), disturbed galaxies (Habergham et al. 2010), elliptical galaxies (e.g., Gibson & Matteucci 1997) and SMGs (e.g., Baugh et al. 2005; Nagashima et al. 2005; Michałowski et al. 2010c). Increasing evidence for IMF variations towards higher stellar masses arise also from observations of the Galactic Center region and Galactic globular clusters (e.g., D'Antona & Caloi 2004; Ballero et al. 2007; Maness et al. 2007; Bartko et al. 2010).

However, it shall be emphasized that any reference to a top-heavy IMF needs to be assessed critical. Usually the degree to which the IMF is 'top-heavy' varies significantly among different studies. Differences can be due to extreme assumptions of the exponent for the power law IMFs (i.e., x = 0) or due to different characteristic masses in lognormal IMFs, but also due to the assumed mass interval of the IMF. This often leads to uncertainties in the results challenging also its validity.

Pertaining to the controversy of the IMF and significant evidence for an IMF different from the commonly adopted Salpeter IMF in starburst galaxies, we will further investigate the IMFs already introduced in Chapter 2. There, the strong influence of these IMFs on the dust production rates from stellar sources was demonstrated, while the impact on various other properties will be ascertained in following Chapters. Similar IMFs were used in chemical evolution models by Dwek et al. (2007) and Valiante et al. (2009) for high-z OSOs. Our models are therefor comparable with those. The

Table 3.1: *List of all model parameters*

Parameters	Value	Unit	Description
$M_{\rm ini}$	5×10^{10}, 1×10^{11}, 3×10^{11}, 5×10^{11}, 1.3×10^{12}	$\mathrm{M}_\odot$	Initial mass of the galaxy
$\psi_{\rm ini}$	1×10^3	$\mathrm{M}_\odot\ \mathrm{yr}^{-1}$	Star formation rate
$Z_{\rm ini}$	10^{-6}	$\mathrm{Z}_\odot$	Initial metallicity
k	1.5		Power for the relation $\psi(t) \propto M_{\rm ISM}(t)^k$
$M_{\rm cl}$	800, 100, 0	$\mathrm{M}_\odot$	Swept up ISM mass per SN
$M_{\rm core}^{\rm crit}$	15	$\mathrm{M}_\odot$	Critical He core mass
$\xi_{\rm SN}$	0.93		SN dust destruction factor
$M_{\rm SMBH}$	3×10^9, 5×10^9	$\mathrm{M}_\odot$	Mass of the SMBH
$t_{\rm SMBH}$	4×10^8	yr	Growth timscale for the SMBH
$t_{\rm max}$	10^9	yr	Maximum computed age of the galaxy

Parameters	Switch	Description
$Y_{\rm Z}$, $Y_{\rm E}$, $Y_{\rm Q}$ (SN)	EIT08, WW95, Nomoto et al. (2006), Georgy et al. (2009)	Possibilities for the SN yields
$Y_{\rm Z}$, $Y_{\rm E}$, $Y_{\rm Q}$ (AGB)	van den Hoek & Groenewegen (1997)	Possibilities for the AGB yields
$\phi(m)$	Salpeter, mass-heavy, top-heavy, Larson 1, Larson 2	Initial mass function
SFR	evolving / constant	Additional switch for the SFR
$\epsilon_{\rm AGB}(m, Z)$	only one case considered	Dust formation efficiency, AGB
$\epsilon_{\rm SN}(m)$	max / low	SN dust formation efficiency
$\xi_{\rm SN}$	considered / not considered	SN dust destruction
BH / SN	SN when BH / no SN when BH	Possibility, if a SN occurs even a BH is formed or not
SMBH	considered / not considered	Growth of SMBH

parameters are given in Table 2.2. The power law IMFs (Salpeter, mass heavy and top-heavy) have the form $\phi(m) \propto m^{-\alpha}$. The lognormal Larson IMFs (Larson 1998) are given as $\phi(m) \propto m^{-(\alpha+1)} \exp(-m_{\rm ch}/m)$, where $m_{\rm ch}$ is the characteristic mass.

3.3.3 STELLAR YIELDS

The model is adapted to published results from stellar evolution models. Using these models the metallicity dependent upper and lower mass limits of the mass range of diverse SNe subtypes can be determined. For comparison to the usually adopted treatment of SNe we calculate simplified models with a fixed mass range for CCSNe between 8–40 $\mathrm{M}_\odot$ and use stellar yields from nucleosynthesis calculations for SNe. For SNe we therefore distinguish between three different structural models.

Table 3.2: *Definitions of stellar types*

Type	$M_{\rm H}(m,Z)$ [$\rm M_\odot$]	$M_{\rm core}(m,Z)/M_{\rm core}^{\rm crit}$
Type II-P	≥ 2	≤ 1
Remaining Type II	≥ 0.1 and < 2	≤ 1
Type Ib/c	< 0.1	≤ 1
Remaining stars	—	> 1

SN yields from stellar evolution models

We adopt the stellar yields for the hydrogen mass $M_{\rm H}(m,Z)$ in the envelope, the He core mass $M_{\rm core}(m,Z)$ and the final mass $M_{\rm fin}(m,Z)$ of the progenitors as well as $Y_{\rm E}(m,Z)$ and $Y_{\rm Z}(m,Z)$ from the single stellar evolution models by Eldridge et al. (2008, herafter EIT08). These yields are based on previous works (Eldridge & Tout 2004, 2005). EIT08 adopt a mass loss prescription using the rates of de Jager et al. (1988) with the rates of Vink et al. (2001) for pre-Wolf-Rayet (WR) and from Nugis & Lamers (2000) for WR evolution including overshooting. In their study, this model is closest to a set of SN progenitor observations.

Eldridge & Tout (2004, 2005) also show that at metallicities roughly below $Z = 10^{-4}$ all stars end up as II-P SN, while with increasing metallicity the upper mass limit for II-Ps decreases, i.e., at solar metallicity it is at roughly 28 $\rm M_\odot$. Type II-P SNe are per definition all stars which have retained at least 2 $\rm M_\odot$ of hydrogen in their envelopes at their pre SN stage (Heger et al. 2003). Since mass loss is more efficient at higher metallicities, the upper mass limit for II-P supernovae decreases.

With increasing metallicity further types of CCSNe such as IIL, Ib, and Ic SNe arise. The upper limit for IILs is defined by the small hydrogen fraction of ~ 0.1 $\rm M_\odot$ in the envelope. In case little or no hydrogen in the envelope of the progenitor is present SNe appear as Type Ib or Ic. SNe arising from the higher mass end of all Type IIs are the subtypes IIb or IIn. These types are difficult to fit into a quiescent mass loss prescription and are not specified by EIT08. Thus we simply assume that these subtypes may be part of the fraction of supernovae which is determined as IIL in the models of Eldridge & Tout (2004). These SNe will be collectively referred to as the remaining Type II supernovae.

We define the conditions for determining the lower $m_{\rm SL,(i)}$ and upper $m_{\rm SU,(i)}$ boundaries of the different SN subtypes analogous to Eldridge & Tout (2004) as given in Table 3.2.

The masses $M_{\rm H}(m,Z)$, $M_{\rm core}(m,Z)$ are dependent on metallicity. Therefore the lower and upper mass limits for these SN types are $m_{\rm SL,(i)} = m_{\rm SL,(i)}(Z)$ and $m_{\rm SU,(i)} = m_{\rm SU,(i)}(Z)$. The lower mass limit for Type II-P SNe is fixed at $m_{\rm SL,IIP}(Z) \equiv m_{\rm SL,IIP} = 8$ $\rm M_\odot$. The absolute upper mass limit for the most massive stars is the cutoff mass

defined by the IMF, thus $m_{\mathrm{SU,(i)}}(Z) \equiv m_{\mathrm{SU,(i)}} = m_2$.

The criterion for direct BH formation is based on the system used by Heger et al. (2003) and Eldridge & Tout (2004). A direct BH forms when the final He core mass $M_{\mathrm{core}}(m, Z)$ exceeds the critical He core mass, $M_{\mathrm{core}}^{\mathrm{crit}} = 15\ \mathrm{M}_{\odot}$.

Models using yields from EIT08 will be referred to as 'EIT08M'.

SN yields from rotating stellar models

We take the yields for $M_{\mathrm{H}}(m, Z)$, $M_{\mathrm{fin}}(m, Z)$, $Y_{\mathrm{E}}(m, Z)$ and $Y_{\mathrm{Z}}(m, Z)$ from Georgy et al. (2009). Rotationally enhanced mass loss becomes very efficient with increasing metallicity. The mass loss description used in their models are from Meynet & Maeder (2003, 2005) with a rotational velocity of 300 km/s. Provided that a SN occurs even if a BH is formed, the resulting range for Type II SN (without further subdivision) is between 8–54 $\mathrm{M}_{\odot}$ at a metallicity $Z = 0.004\ \mathrm{Z}_{\odot}$. However, only stars between 8–25 $\mathrm{M}_{\odot}$ form neutron stars. At $\mathrm{Z}_{\odot}$ the Type II mass range becomes narrower (8–25 $\mathrm{M}_{\odot}$) and stars above the upper limit will become WR stars and explode as Ib/c SNe. The range for neutron stars at this metallicity extends up to 35 $\mathrm{M}_{\odot}$.

To determine the lower $m_{\mathrm{SL,(i)}}(Z)$ and upper $m_{\mathrm{SU,(i)}}(Z)$ mass limits for the considered SNe types and remaining stars (i = IIP, II, Ib/c, R) we apply the same definitions as described for the EIT08M models. However, the direct BH cut is constrained by the mass of the remnant star $M_{\mathrm{rem}}(m, Z)$ instead of $M_{\mathrm{core}}(m, Z)$. We follow the notation for the BH formation by Georgy et al. (2009), where a BH forms when $M_{\mathrm{rem}}(m, Z) > 2.7$ $\mathrm{M}_{\odot}$. Models where these yields and the above SN type division and BH formation are applied, will be referred to as 'G09M'.

Models with fixed SN mass range

A treatment, in which the boundaries of the mass range for all considered dust forming supernovae and remaining stars are fixed throughout the evolution, is quite common and has been used in previous models (e.g. Dwek 1998; Morgan & Edmunds 2003; Dwek et al. 2007; Valiante et al. 2009).

We use the stellar yields for $Y_{\mathrm{E}}(m, Z)$, $Y_{\mathrm{Z}}(m, Z)$ and certain elements $Y_{\mathrm{Q}}(m, Z)$ with Q = C,O from nucleosynthesis models of either Woosley & Weaver (1995, hereafter WW95) or Nomoto et al. (2006). All SNe are of Type II and considered to be within the mass intervall $m_{\mathrm{L,(II)}} = 8\ \mathrm{M}_{\odot}$ and $m_{\mathrm{U,(II)}} = 40$. Yields for the final mass prior to explosion are not available, thus in all equations $Y_{\mathrm{WIND}} = 0$.

The remaining very massive stars between $m_{\mathrm{L,(R)}} = m_{\mathrm{U,(II)}} = 40$ and the upper limit $m_{\mathrm{U,(R)}} = m_2$ are assumed to turn into BHs. We apply the yields from EIT08 to these remaining stars in order to account for the gas return into the ISM from their mass loss phase according to Eq. 3.11 and 3.12. Thus, the option of whether a SN explosion occurs or not is retained.

The models with stellar yields from WW95 will be referred to as 'WW95M' and the models with yields from Nomoto et al. (2006) will be referred to as 'N06M'.

AGB stars

For high mass AGB stars we use the stellar yields for the total ejected mass $Y_{\rm E}(m,Z)$, the metals $Y_{\rm Z}(m,Z)$ and certain elements $Y_{\rm Q}(m,Z)$ with Q = C,O from van den Hoek & Groenewegen (1997). The mass interval is set to a fixed mass range of $m_{\rm L,(i)}$ = 3 $\rm M_{\odot}$ and $m_{\rm U,(i)}$ = 8 $\rm M_{\odot}$, i = AGB. AGB stars with masses below 3 $\rm M_{\odot}$ are not considered.

3.3.4 DUST PRODUCTION AND DESTRUCTION

The values for the AGB and SN dust production efficiencies $\epsilon_{\rm i}(m,Z)$ are taken from those derived in Chapter 2 The efficiencies for AGB stars, $\epsilon_{\rm AGB}(m,Z)$ are mass and metallicity dependent and based on calculated dust yields from Ferrarotti & Gail (2006).

The maximal SN efficiency, $\epsilon_{\rm max}(m)$, is motivated by theoretical SN dust formation models while the low SN efficiency $\epsilon_{\rm low}(m)$ is based on observationally inferred SN dust yields. In Chapter 2 we also defined a high SN dust production efficiency $\epsilon_{\rm high}(m)$ obtained by applying a SN dust destruction factor, $\xi_{\rm SN}$ = 0.93, to $\epsilon_{\rm max}(m)$ due to dust destruction by SN reverse shock interaction. The SN efficiencies from Chapter 2 had been averaged over metallicity and are therefore solely dependent on the stellar mass.

3.3.5 DUST DESTRUCTION IN THE ISM

Once a dust grain is injected into the interstellar medium, it is subject to either growth, disruptive or destructive processes. We here focus on the destructive and disruptive ones due to supernova shocks.

Disruptive processes are those which lead to fragmentation of large dust grains (radius > 1000 $\rm \mathring{A}$) into smaller dust grains (radius < 500 $\rm \mathring{A}$). Jones et al. (1996) found that shattering due to grain-grain collisions dominates over vaporization and therefore also determines the grain size redistribution, which is shifted towards smaller grains.

Destructive processes return dust grains back into the gas phase. The main destruction of dust grains in the ISM is due to sputtering caused by interstellar shock waves with shock velocities $\geq$ 100 km $\rm s^{-1}$ (Seab 1987; Jones et al. 1996). The destruction takes place because of high-velocity gas-grain impacts of smaller projectiles (radius < 100 $\rm \mathring{A}$), such as energetic $\rm He^{+}$ ions, onto dust grains. This results in the removal of dust species at or near the surface of the grains.

A dust grain is exposed to thermal and nonthermal sputtering as well as vaporization during the passage of the shock. Jones et al. (1996) also found that graphite grains are mainly destroyed due to thermal sputtering. Silicates are equally affected by thermal and non thermal sputtering in high velocity shocks with velocities $\rm v_{\it s}$ >150 km $\rm s^{-1}$,

while vaporization is negligible. These processes determine the lifetime of dust grains in the ISM. The timescale $\tau_{\rm dl}(t)$ of the dust grains against destruction, or simply the lifetime of the dust grains, and the dust destruction rate in the ISM $E_{\rm D,ISM}(t)$ are given (McKee 1989; Dwek 1998; Dwek et al. 2007) through

$$\begin{aligned} \tau_{\rm dl}(t) &= \frac{M_{\rm ISM}(t)}{M_{\rm cl}\, R_{\rm SN}(t)}; \\ E_{\rm D,ISM}(t) &= \frac{M_{\rm d}(t)}{\tau_{\rm dl}(t)}, \end{aligned} \tag{3.21}$$

where $M_{\rm ISM}(t)$ is the mass of the ISM and $R_{\rm SN}(t)$ is the supernova rate of all supernovae causing the destruction. The mass $M_{\rm cl}$ is the mass of the ISM, which is completely cleared of dust through one single supernova remnant. These two equations combined lead to an expression for $E_{\rm D,ISM}(t)$ in the form

$$E_{\rm D,ISM}(t) = \eta_{\rm d}(t)\, M_{\rm cl}\, R_{\rm SN}(t). \tag{3.22}$$

which shows that besides $R_{\rm SN}(t)$ and $M_{\rm cl}$, the dust destruction rate in the ISM also depends on the dust-to-gas ratio $\eta_{\rm d}(t)$.

An expression for $M_{\rm cl}$ which is dependent on the shock velocity is given by Dwek et al. (2007). For a homogenous ISM and under the assumption that silicon and carbon grains are equally mixed, Dwek et al. (2007) obtained $M_{\rm cl}$ = 1100–1300 $\rm M_\odot$. However the ISM is inhomogeneous, characterized by cold, warm and hot phases with different densities (e.g., McKee 1989, and references therein). The density contrast between the cold and warm phase and the hot phase can be relatively large. Shocks traveling through these phases are found not to be very efficient in destroying dust (Jones 2004). The destruction process is solely effective in the warm (T $>$ 100K) phase of the interstellar medium while SN shocks propagating through a hot ISM with low density are not efficiently destructive (McKee 1989; Nomoto et al. 2006).

Another important parameter is the injection timescale of stellar yields and dust into the ISM. Following McKee (1989), we estimate the injection timescale of the dust from stellar sources as

$$\tau_{\rm in}(t) \simeq \frac{M_{\rm d}(t)}{E_{\rm d,SN}(t) + E_{\rm d,AGB}(t)}. \tag{3.23}$$

In Chapter 2 we made a rough estimate of the minimum averaged dust injection rate from SNe and AGBs of 0.5 $\rm M_\odot\ yr^{-1}$ based on data for high-z QSOs. Using this dust injection rate we obtain an average injection time $\tau_{\rm in}(t) = 4 \times 10^8$ yr.

For comparison we estimate the lifetime $\tau_{\rm dl}(t)$ of the dust grains. The mass of the ISM is assumed to be $M_{\rm ISM} = 2 \times 10^{10}$ $\rm M_\odot$. SN rates are calculated for a constant SFR of 500 $\rm M_\odot\ yr^{-1}$ and for a Larson 2 IMF. This results in a timescale of $\tau_{\rm dl}(t) \sim 1.3 \times 10^7$ yr for $M_{\rm cl} = 100$ $\rm M_\odot$. A shorter timescale $\tau_{\rm dl}(t) \sim 1.6 \times 10^6$ yr is obtained for $M_{\rm cl} = 800$ $\rm M_\odot$.

When using a Salpeter IMF for the SN rates, the timescales are usually longer ($\tau_{\rm dl}(t) \sim 6.6 \times 10^7$ yr, for $M_{\rm cl}$ = 100 $\rm M_\odot$).

We note that this is a rather rough estimate. Typically $\tau_{\rm in}(t)$ and $\tau_{\rm dl}(t)$ are strongly dependent on the IMF, $M_{\rm ISM}(t)$ and the SNe dust production efficiency $\epsilon_{\rm i}(m, Z)$. Hence, the values will deviate from the above estimated average during evolution.

However, this example demonstrates that the dust injection timescale can be longer than the lifetimes of the dust grains. The difference between these timescales is influenced by the value of $M_{\rm cl}$. Pertaining to the formation of large dust masses in galaxies this has significant consequences. An injection timescale $\tau_{\rm in}(t)$ longer than the destruction timescale $\tau_{\rm dl}(t)$ does not allow the build up of large dust masses in the galaxy. This implies that the dust injection rate must be higher than the dust destruction rate. A lowering of the dust destruction rate could be achieved if dust grains are shielded from destruction. Alternatively a rapid dust grain growth in the ISM might be an option, if SNe and AGBs cannot generate the necessary high dust injection rate. Grain growth however is not incorporated into our model and remains to be investigated.

Furthermore we assume that the starburst occurs in an initially dust free galaxy. Consequently dust produced by the first generations of SNe might be ejected into the ISM unhindered. The epoch at which the first SN shocks are able to sweep up ISM gas mixed with dust remains elusive.

In view of these considerations, we stress that dust destruction in the ISM is uncertain, particularly when considering galaxies with conditions as described in Sect. 3.3.1 and 3.3.2.

Despite our simple assumption of dust being immediately homogeneously mixed with the gas in the ISM, we will account for the uncertainty of the lifetime of dust grains against destruction by using $M_{\rm cl}$ as a parameter. This was also done by Dwek et al. (2007). The considered cases are for $M_{\rm cl}$ = 800 $\rm M_\odot$ as the highest destruction, $M_{\rm cl}$ = 100 $\rm M_\odot$ for modest destruction and $M_{\rm cl}$ = 0 for no dust destruction.

3.4 RESULTS

In this section we present the results of several models calculated within the first Gyr after starburst. We will focus on the total dust mass in a galaxy. At redshift $z > 6$, the time to build up large dust masses of $> 10^8$ $\rm M_\odot$ is limited to 400–500 Myr. Models able to exceed an amount of 10^8 $\rm M_\odot$ of dust within this time are therefore of particular interest. General evolutionary tendencies of certain quantities such as dust injection rates, SFR, metallicity, or the amount of gas are also discussed.

3.4.1 EVOLUTION OF DUST, DUST-TO-GAS AND DUST-TO-METAL RATIOS

We study models with all considered initial gas masses $M_{\rm ini}$. We assume the same value for the initial SFR in all models as given in Table 3.1. The models discussed are calculated for the case that no SN occurs when a BH is formed (see Sect. 3.2.2). Models including SMBH formation are deferred to Sect. 3.4.5.

Models with SN type differentiation

EIT08M with $M_{\rm ini}$ = 5 $\times$ 10^{11} $\rm M_\odot$: In Fig. 3.1 the results are presented for the mass of dust $M_{\rm d}(t)$ in a galaxy with $M_{\rm ini}$ = 5 $\times$ 10^{11} $\rm M_\odot$. Calculations are performed for a maximal (top row), a high (middle row) and a low (bottom row) SN dust production efficiency $\epsilon_{\rm i}(m)$. Dust destruction in the ISM is included for three values of $M_{\rm cl}$ (see Sect. 3.3.5). This model is considered as a reference model. We therefore describe it in detail.

Dust masses $M_{\rm d}(t)$ obtained with the maximal SN dust production efficiency $\epsilon_{\rm max}(m)$ exceed 10^8 $\rm M_\odot$ of dust in all cases of $M_{\rm cl}$ and for all IMFs. In fact, 10^8 $\rm M_\odot$ of $M_{\rm d}(t)$ is reached within the first few Myr. This is insensitive to the IMF as well as to the amount of $M_{\rm cl}$. The latter however determines the suppression of $M_{\rm d}(t)$ as the system evolves. For $M_{\rm cl}$ = 800 $\rm M_\odot$ (top left), a maximum amount of $\sim 4 \times 10^8$ $\rm M_\odot$ is reached for a Larson 2 IMF and sustained until the end of the computation. Only the IMFs favouring lower masses exhibit a shallow decline of $M_{\rm d}(t)$. Dust destruction with $M_{\rm cl}$ = 100 $\rm M_\odot$ (top middle) leads to nearly constant dust masses retainable over 1 Gyr of evolution. The amount of dust for most IMFs is a few times 10^9 $\rm M_\odot$. Assuming no dust destruction (top right) a broader spread of the dust masses for the different IMFs develops. The amount of dust increases with time regardless of the IMF and yields up to 10^{9-10} $\rm M_\odot$ are reached.

In the case of a high SN dust production efficiency, $\epsilon_{\rm high}(m)$, similar trends are featured. However the amount of dust is lower. Without dust destruction ($M_{\rm cl}$ = 0) dust masses up to a few times 10^8 $\rm M_\odot$ are attained for all IMFs (Fig. 3.1 middle right). The timescale to exceed 10^8 $\rm M_\odot$ of dust ranges from 80 Myr (Larson 2 IMF) up to 400 Myr (Salpeter IMF). Taking dust destruction with only a modest amount of $M_{\rm cl}$ = 100 $\rm M_\odot$ into account decreases $M_{\rm d}(t)$ substantially (Fig. 3.1 middle middle). The IMFs favouring high masses are most affected, while the reduction of $M_{\rm d}(t)$ for a Salpeter IMF is small. Except for the Salpeter IMF, all remaining IMFs lead to more than 10^8 $\rm M_\odot$ of dust. The highest amount of dust is reached with either a Larson 2 or a mass-heavy IMF and is $\sim 2 \times 10^8$ $\rm M_\odot$ at an epoch of $\sim$ 400 Myr. Considering a very high destruction with $M_{\rm cl}$ = 800 $\rm M_\odot$ results in a strong reduction of $M_{\rm d}(t)$ and only $\sim$ 2–3 $\times$ 10^7 $\rm M_\odot$ of dust remains throughout the evolution (Fig. 3.1 middle left).

The results for $M_{\rm d}(t)$ with a low SN dust production efficiency $\epsilon_{\rm low}(m)$ are dominated by AGB dust production (see also Sect. 2.2). Without dust destruction dust

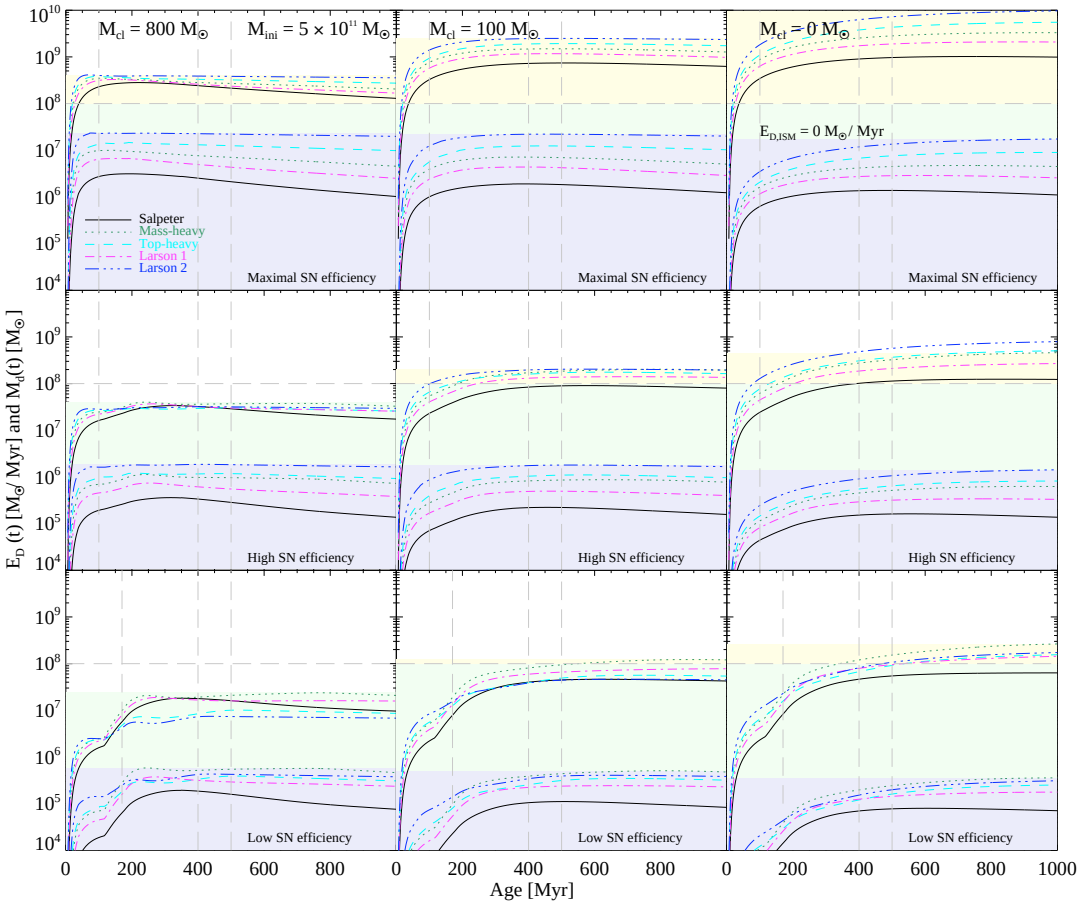

Figure 3.1: *Evolution of the total dust mass and dust destruction rates for EIT08M. The initial gas mass of the galaxy $M_{\rm ini}$ = 5 × 10^{11} $\mathrm{M}_\odot$. Calculations are performed for a maximal (top row), a high (middle row) and a low (bottom row) SN dust production efficiency $\epsilon_{\rm i}(m)$. Dust destruction is taken into account for a $M_{\rm cl}$ = 800 $\mathrm{M}_\odot$ (left column), 100 $\mathrm{M}_\odot$ (middle column) and 0 $\mathrm{M}_\odot$ (right column). The bottom group of curves in the bluish area represents the total dust destruction rate $E_{\rm D}(t)$. The upper group of curves in the green or yellow zones displays the evolution of the total amount of dust $M_{\rm d}(t)$ in the galaxy. The yellow area marks dust masses exceeding 10^8 $\mathrm{M}_\odot$ of dust. The grey horizontal dashed line marks the limit of 10^8 $\mathrm{M}_\odot$ of dust. The grey vertical dashed lines indicate epochs at 100, 170, 400 and 500 Myr after the onset of starburst. The black solid, green dotted, cyan dashed, magenta dashed-dotted and blue dashed-dot-dotted lines represent the Salpeter, mass-heavy, top-heavy, Larson 1 and Larson 2 IMF, respectively.*

masses up to 1–2 × 10^8 $\mathrm{M}_\odot$ is reached after ∼ 300–500 Myr for most of the IMFs. Applying a modest dust destruction of $M_{\rm cl}$ = 100 $\mathrm{M}_\odot$ reduces $M_{\rm d}(t)$ analogously to the higher SN efficiencies $\epsilon_{\rm max}(m)$ or $\epsilon_{\rm high}(m)$. Dust masses for either the top-heavy or the Larson 2 IMF are efficiently decreased and comparable to $M_{\rm d}(t)$ for a Salpeter IMF. Increasing

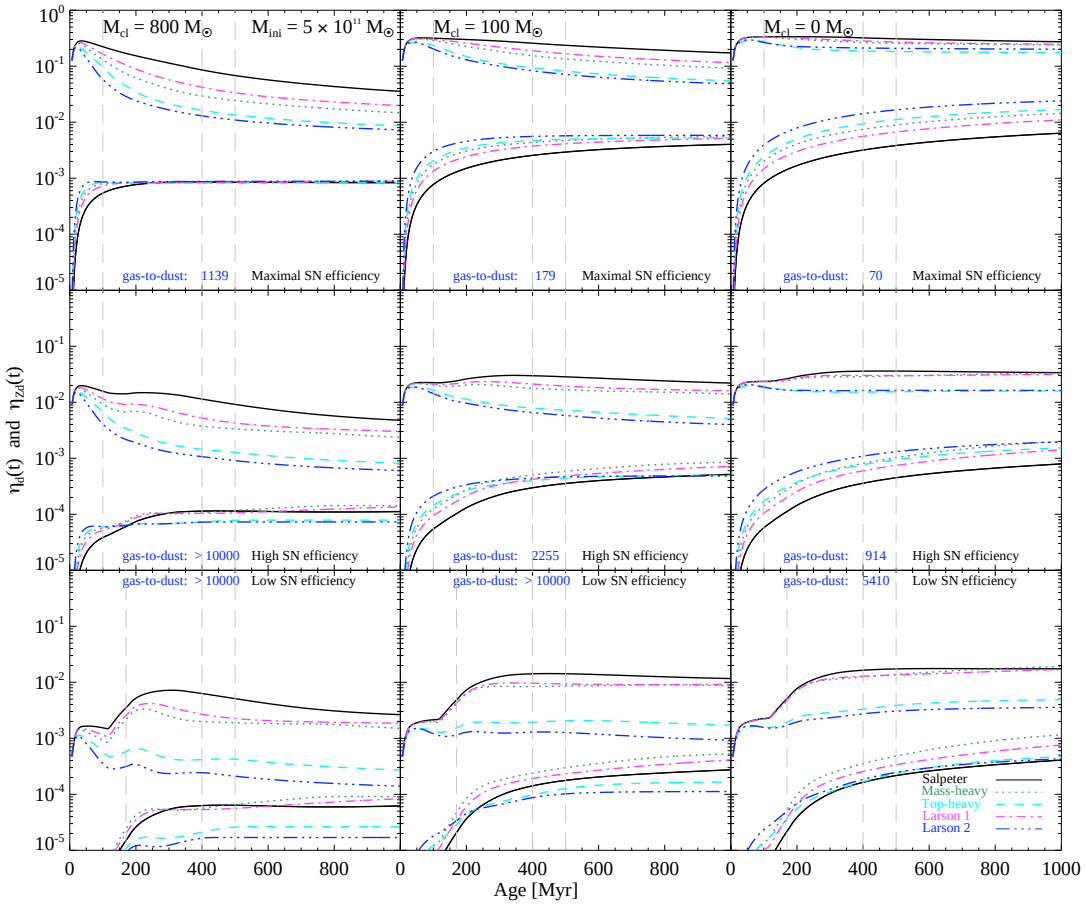

Figure 3.2: *Evolution of the dust-to-gas and dust-to-metal mass ratios for EIT08M. The initial gas mass of the galaxy $M_{\rm ini}$ = 5 × 10^{11} $\mathrm{M}_\odot$. Calculations are performed for a maximal (top row), a high (middle row) and a low (bottom row) SN dust production efficiency $\epsilon_{\rm i}(m)$. Dust destruction is taken into account for a $M_{\rm cl}$ = 800 $\mathrm{M}_\odot$ (left column), 100 $\mathrm{M}_\odot$ (middle column) and 0 $\mathrm{M}_\odot$ (right column). The upper group of curves signifies the dust-to-metal mass ratio $\eta_{\rm Zd}(t)$. The lower group of curves represents the dust-to-gas mass ratio $\eta_{\rm d}(t)$. The gas-to-dust ratio displayed in the figures is calculated for a Larson 2 IMF at an epoch of 400 Myr. The grey vertical dashed lines indicate epochs at 100, 400 and 500 Myr after the onset of starburst. The black solid, green dotted, cyan dashed, magenta dashed-dotted and blue dashed-dot-dotted lines represent the Salpeter, mass-heavy, top-heavy, Larson 1 and Larson 2 IMF, respectively.*

$M_{\rm cl}$ to 800 $\mathrm{M}_\odot$ leads to a stronger reduction of $M_{\rm d}(t)$ for these IMFs, resulting in lower dust masses than for a Salpeter IMF.

A considerable difference in the progression of $M_{\rm d}(t)$ for the low SN efficiency $\epsilon_{\rm low}(m)$ compared to the higher SN efficiencies is encountered during the first $\sim$ 200 Myr. While for either $\epsilon_{\rm max}(m)$ or $\epsilon_{\rm high}(m)$ a fast rise of $M_{\rm d}(t)$ is identifiable, for $\epsilon_{\rm low}(m)$

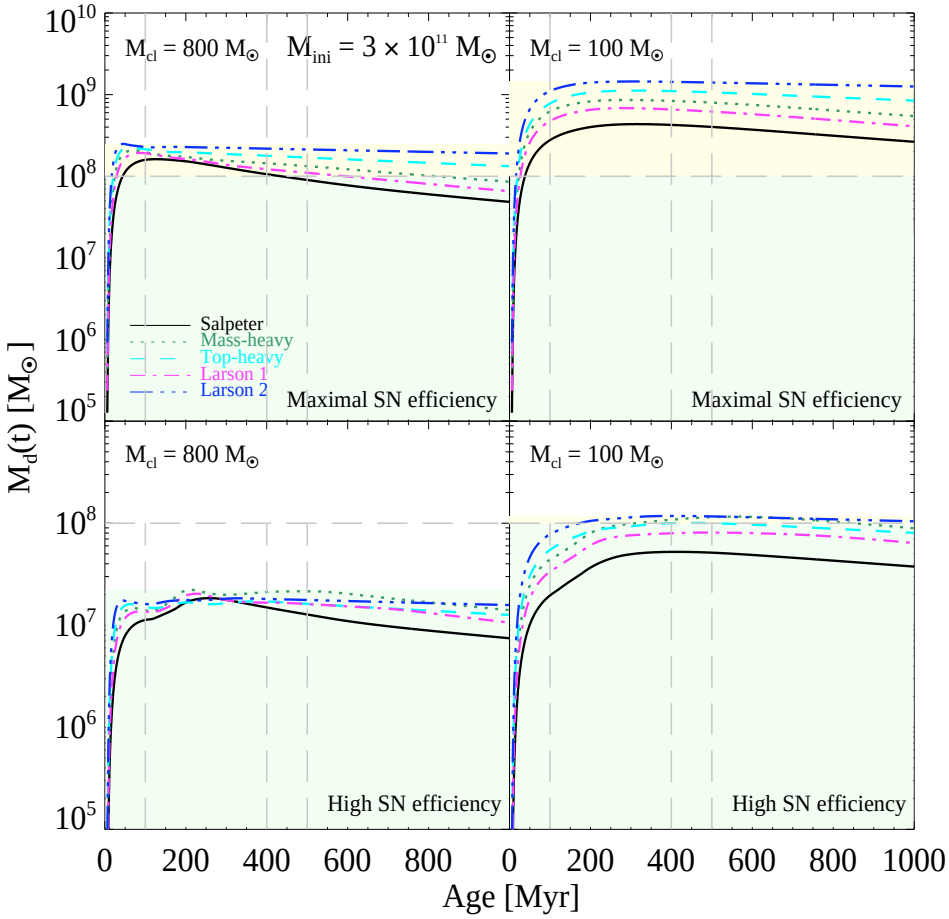

Figure 3.3: *Evolution of the total dust mass for ET08M. ET08M is presented for a galaxy with* $M_{\rm ini}$ *=* 3×10^{11} $\mathrm{M}_{\odot}$*. Total dust masses* $M_{\rm d}(t)$ *are shown for a maximal (top row) and a high (bottom row) SN dust production efficiency* $\epsilon_{\rm i}(m)$*. Dust destruction is taken into account for a* $M_{\rm cl}$ *= 800* $\mathrm{M}_{\odot}$ *(left column) and 100* $\mathrm{M}_{\odot}$ *(right column). Maximum dust masses below* 10^8 $\mathrm{M}_{\odot}$ *are indicated as green shaded zones and as yellow shaded zones when exceeding* 10^8 $\mathrm{M}_{\odot}$*. The grey horizontal dashed line marks the limit of* 10^8 $\mathrm{M}_{\odot}$ *of dust. The grey vertical dashed lines indicate epochs at 100, 400 and 500 Myr after the onset of starburst. The black solid, green dotted, cyan dashed, magenta dashed-dotted and blue dashed-dot-dotted lines represent the Salpeter, mass-heavy, top-heavy, Larson 1 and Larson 2 IMF, respectively.*

the dust mass remains between 10^{6-7} $\mathrm{M}_{\odot}$ during this epoch. This is caused primarily by high mass AGB stars with short lifetimes ($>$ 4–5 $\mathrm{M}_{\odot}$). A further increase of the dust mass due to the delayed AGB dust injection from the less massive but more efficient AGB stars results in a second dust bump at an epoch of $\sim$ 200–300 Myr. Large dust masses at early epochs (100–200 Myr) are not possible with $\epsilon_{\rm low}(m)$.

The curves at the bottom in the bluish area in Fig. 3.1 represent the dust destruction rate $E_{\rm D}(t)$. For $M_{\rm cl}$ = 0 and independent of $\epsilon_{\rm i}(m)$ the dust destruction rate reflects the amount of dust incorporated into stars per unit time and is calculated as

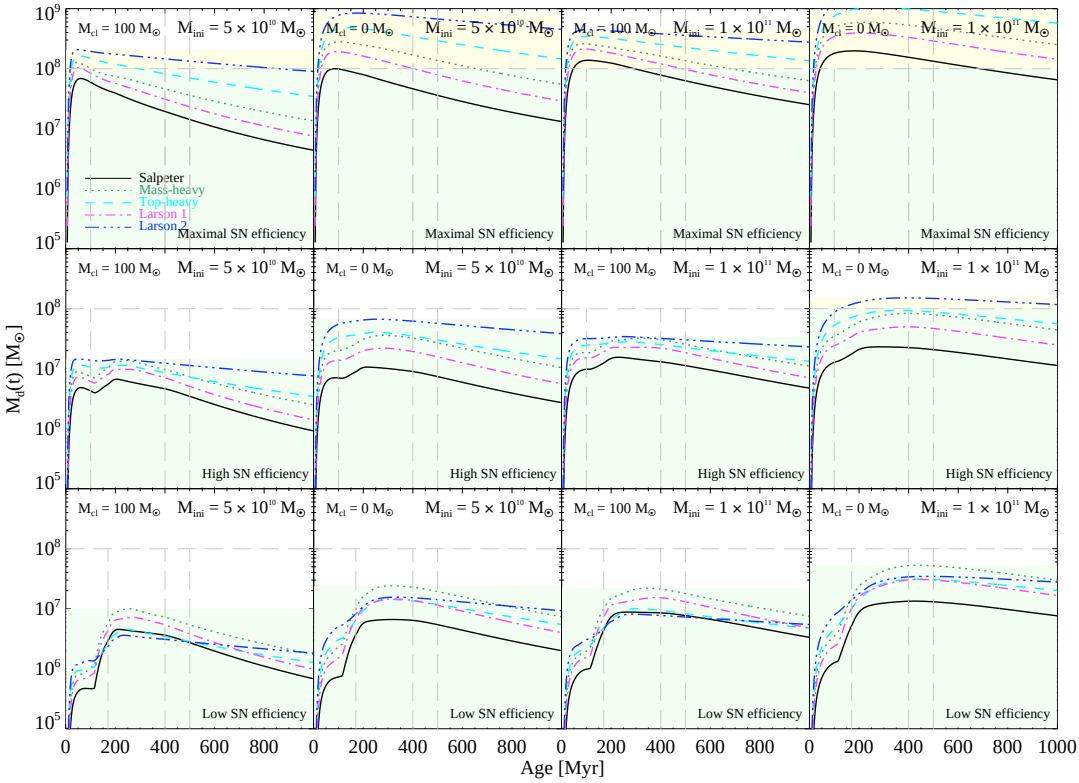

Figure 3.4: *Evolution of the total dust mass for EIT08M. Calculations for galaxies with initial gas masses of $M_{\rm ini}$ = 5 × 10^{10} $\mathrm{M}_\odot$ are presented in the two left columns and for $M_{\rm ini}$ = 1 × 10^{11} $\mathrm{M}_\odot$ in the two right columns. Total dust masses $M_{\rm d}(t)$ are shown for a maximal (top row), a high (middle row) and a low (bottom row) SN dust production efficiency $\epsilon_{\rm I}(m)$. Dust destruction is taken into account for a $M_{\rm cl}$ = 100 $\mathrm{M}_\odot$ (left-left and left-right columns) and 0 $\mathrm{M}_\odot$ (right-left and right-right columns). Maximum dust masses below 10^8 $\mathrm{M}_\odot$ are indicated as green shaded zones and as yellow shaded zones when exceeding 10^8 $\mathrm{M}_\odot$. The grey horizontal dashed line marks the limit of 10^8 $\mathrm{M}_\odot$ of dust. The grey vertical dashed lines indicate epochs at 100, 170, 400 and 500 Myr after the onset of starburst. The black solid, green dotted, cyan dashed, magenta dashed-dotted and blue dashed-dot-dotted lines represent the Salpeter, mass-heavy, top-heavy, Larson 1 and Larson 2 IMF, respectively.*

$E_{\rm D}(t) = \eta_{\rm d}(t)\,\psi(t)$. For $M_{\rm cl} > 0$ $E_{\rm D}(t)$ is given by Eq. 3.16 and consists additionally of the destroyed dust in the ISM, $E_{\rm D,ISM}(t)$.

We find that $E_{\rm D}(t)$ increases faster and earlier with increasing $M_{\rm cl}$. Consequently, dust destruction rates comparable to SN injection rates are reached at earlier epochs. Given Eq. 3.22 for the amount of dust destroyed through SN shocks, the high SN rates $R_{\rm SN}(t)$ at the beginning of evolution in conjunction with $M_{\rm cl}$ lead to a high base value of $E_{\rm D,ISM}(t)$. This suppresses the rise of the amount of dust at early epochs. Additionally, SN rates are higher for the IMFs biased towards more massive stars affecting these IMFs

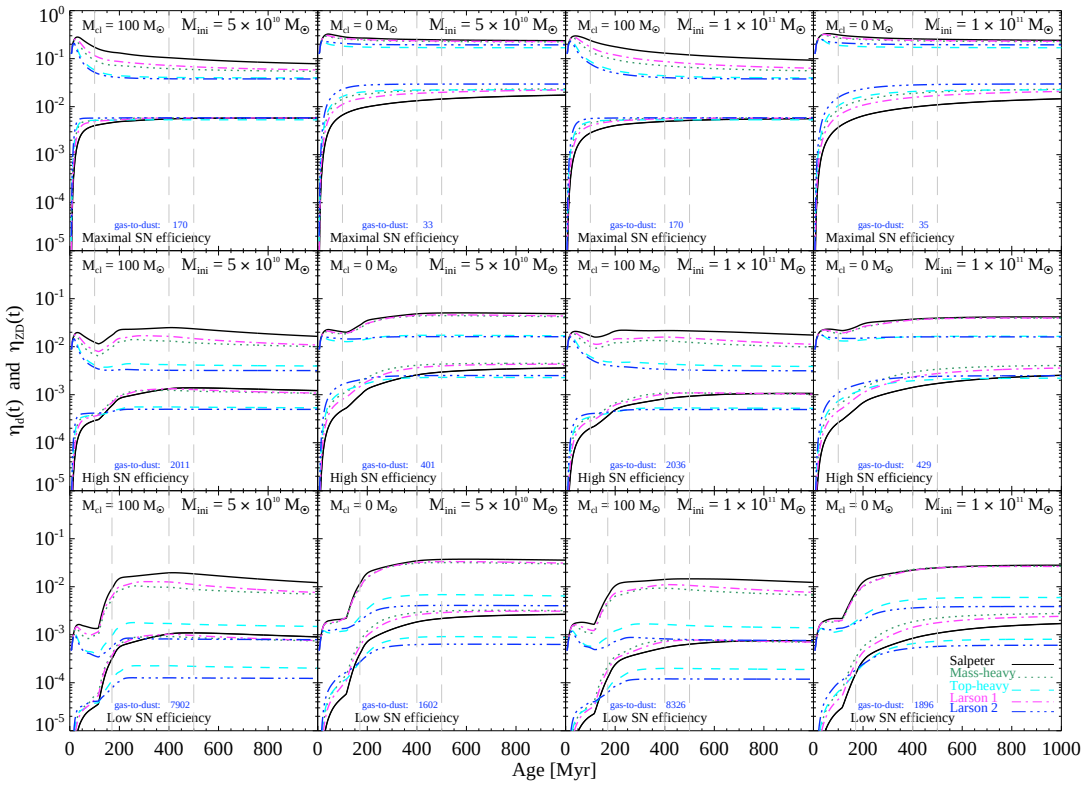

Figure 3.5: *Evolution of the dust-to-gas and dust-to-metal mass ratios for EIT08M. Calculations for galaxies with initial gas masses of $M_{\rm ini}$ = 5 × 10^{10} $\rm M_\odot$ are presented in the two left columns and for $M_{\rm ini}$ = 1 × 10^{11} $\rm M_\odot$ in the two right columns. Results are presented for a maximal (top row), a high (middle row) and a low (bottom row) SN dust production efficiency $\epsilon_{\rm i}(m)$. Dust destruction is taken into account for a $M_{\rm cl}$ = 100 $\rm M_\odot$ (left-left and left-right columns) and 0 $\rm M_\odot$ (right-left and right-right columns). The upper group of curves signifies the dust-to-metal mass ratio $\eta_{\rm Zd}(t)$. The lower group of curves represents the dust-to-gas mass ratio $\eta_{\rm d}(t)$. The gas-to-dust ratio displayed in the figures is calculated for a Larson 2 IMF at an epoch of 400 Myr. The grey vertical dashed lines indicate epochs at 100, 170, 400 and 500 Myr after the onset of starburst. The black solid, green dotted, cyan dashed, magenta dashed-dotted and blue dashed-dot-dotted lines represent the Salpeter, mass-heavy, top-heavy, Larson 1 and Larson 2 IMF, respectively.*

most. Later in the evolution, the dust destruction rates remain almost constant in most cases, with a marginal increase for $M_{\rm cl}$ = 0 or decline for $M_{\rm cl} > 0$. Dust destruction and injection appear to be balanced, resulting in the flat development of $M_{\rm d}(t)$.

In Fig. 3.2 we present the results for the evolution of the dust-to-gas mass ratio $\eta_{\rm d}(t)$ and the dust-to-metal mass ratio $\eta_{\rm Zd}(t)$. Commonly the curves for $\eta_{\rm d}(t)$ for all IMFs are slowly increasing with time except for $M_{\rm cl}$ = 800 $\rm M_\odot$ for which they remain approximately constant. Interestingly, in this case and for $\epsilon_{\rm max}(m)$ the dust-to-gas ratio

for all IMFs sustains a constant value of $\sim 10^{-3}$ over the whole evolution. Without dust destruction (top right) $\eta_{\rm d}(t)$ increases up to values above $\sim 10^{-2}$ for most of the IMFs. For either a high or low SN efficiency the values are below $\sim 10^{-3}$. Only for $\epsilon_{\rm high}(m)$ and $M_{\rm cl}$ = 0 (middle right) $\eta_{\rm d}(t)$ is further increased. These overall trends show that for massive galaxies $\eta_{\rm d}(t)$ can be very low even if the galaxy appears dusty.

The dust-to-metal mass ratio $\eta_{\rm Zd}(t)$ is significantly lower for the Larson 2 and top-heavy IMF than for the other IMFs. This feature is exhibited in all calculated models. The degree of this separation between different IMFs depends primarily on the SN dust production efficiency and secondly on the destruction rate in the ISM, and is larger for $\epsilon_{\rm low}(m)$. This reflects the decrease of the SN dust production efficiency towards the higher mass end of the SN mass interval. Additionally, Type Ib/c SNe produce no dust, but they do inject metals into the ISM at higher rates for the top-heavy IMFs. In case of $M_{\rm cl}$ = 0 and $\epsilon_{\rm high}(m)$ the amount of metals bound in dust grains is between $\sim$ 1.5–3 %. For $M_{\rm cl}$ = 100 $\rm M_\odot$ the fraction of metals bound in dust grains for the two IMFs favouring high masses is below 1 % and decreases further with increasing $M_{\rm cl}$. Generally, for a low SN efficiency, $\eta_{\rm Zd}(t)$ remains below 10^{-2} for all IMFs. For the maximal SN efficiency $\epsilon_{\rm max}(m)$ the dust-to-metal ratio $\eta_{\rm Zd}(t)$ is about a factor of 10 higher than for $\epsilon_{\rm high}(m)$.

EIT08M with $M_{\rm ini}$ = 3 $\times$ 10^{11} $\rm M_\odot$: Fig. 3.3 shows the temporal evolution of $M_{\rm d}(t)$ for $M_{\rm ini}$ = 3 $\times$ 10^{11} $\rm M_\odot$.

Large dust masses of a few times 10^{8-9} $\rm M_\odot$ are attained with the maximal SN efficiency for modest or no dust destruction in the ISM. With a high destruction of $M_{\rm cl}$ = 800 $\rm M_\odot$ maximally $\sim$ 3 $\times$ 10^8 $\rm M_\odot$ of dust is possible for the top-heavy IMFs. For the IMFs biased towards lower masses $M_{\rm d}(t)$ declines after $\sim$ 100 Myr.

An amount of 10^8 $\rm M_\odot$ of dust is also exceeded with a high SN efficiency $\epsilon_{\rm high}(m)$ and without destruction in the ISM for most IMFs. Dust masses up to 5 $\times$ 10^8 $\rm M_\odot$ are attained with the top-heavy IMFs. With a modest destruction ($M_{\rm cl}$ = 100 $\rm M_\odot$) and either a Larson 2, a top-heavy or a mass-heavy IMF 10^8 $\rm M_\odot$ of dust is reached after $\sim$ 200–400 Myr and sustained until an age of 1Gyr. A high destruction of $M_{\rm cl}$ = 800 $\rm M_\odot$ results in roughly 10^7 $\rm M_\odot$ of dust. With a mass-heavy IMF and in case of $\epsilon_{\rm low}(m)$, a dust mass of 10^8 $\rm M_\odot$ can roughly be reached after $\sim$ 400 Myr when $M_{\rm cl}$ = 0.

The dust-to-gas mass ratio $\eta_{\rm d}(t)$ and the dust-to-metal mass ratio $\eta_{\rm Zd}(t)$ are comparable to the system with $M_{\rm ini}$ = 5 $\times$ 10^{11} $\rm M_\odot$.

EIT08M with $M_{\rm ini}$ = 1 $\times$ 10^{11} $\rm M_\odot$: In Fig. 3.4 (two right columns) the results are presented for $M_{\rm d}(t)$ in cases of either no or a modest destruction and all three SN dust formation efficiencies $\epsilon_{\rm max}(m)$, $\epsilon_{\rm high}(m)$, $\epsilon_{\rm low}(m)$.

The top row of Fig. 3.4 depicts the evolution of the amount of dust $M_{\rm d}(t)$ for $\epsilon_{\rm max}(m)$. It is evident that large dust masses beyond 10^8 $\rm M_\odot$ are obtained for both cases of $M_{\rm cl}$. The maximal value for $M_{\rm d}(t)$ is already reached shortly after the onset of the starburst.

Thereafter $M_{\rm d}(t)$ follows a negative slope which is steepest for the IMFs biased towards low mass stars. This decline is globally observable in all cases of $M_{\rm cl}$ and $\epsilon_{\rm i}(m)$. The cause of this is that dust is incorporated into stars on higher rates than is replenished by stellar sources. This dust decrease is amplified by dust destruction in the ISM as is demonstrated for $M_{\rm cl} = 100$ M$_\odot$. For $\epsilon_{\rm high}(m)$ and $M_{\rm cl}$ = 0 a high total dust mass $\geq 10^8$ M$_\odot$ can be achieved with a Larson 2 IMF after $\sim$ 200 Myrs (Fig. 3.4 middle row, right column). For all remaining cases of either $M_{\rm cl}$ or for $\epsilon_{\rm low}(m)$ and regardless of the IMF, $M_{\rm d}(t)$ stays below 10^8 M$_\odot$. The tendencies for the various IMFs resemble those identified for $M_{\rm ini} = 5 \times 10^{11}$ M$_\odot$.

The curves of the dust-to-gas ratio $\eta_{\rm d}(t)$ the dust-to-metal ratio $\eta_{\rm ZD}(t)$ are also similar to the system with $M_{\rm ini} = 5 \times 10^{11}$ M$_\odot$, although the amount is higher (see Fig. 3.5 two left columns). For $M_{\rm cl}$ = 0 and maximal SN efficiency, $\eta_{\rm d}(t)$ is roughly independent of the IMF, while exhibiting a wider range for $\epsilon_{\rm low}(m)$.

The fraction of metals bound in dust grains is $\lesssim$ 4 % ($M_{\rm cl}$ = 0) for IMFs favoring low mass stars and $\epsilon_{\rm high}(m)$; for $\epsilon_{\rm max}(m)$ it is roughly 20–30 %.

EIT08M with $M_{\rm ini}$ = 5 $\times$ 10^{10} M$_\odot$: The evolution of $M_{\rm d}(t)$ within the first Gyr exhibits similar, but more strongly pronounced, tendencies for the various IMFs as the galaxy system with $M_{\rm ini} = 1 \times 10^{11}$ M$_\odot$. Results are presented in Fig. 3.4 (two left columns).

Even with a maximal SN efficiency $\epsilon_{\rm max}(m)$, large dust masses of a few times 10^8 M$_\odot$ cannot be reached or sustained when dust destruction in the ISM is considered.

In Fig. 3.5 (two left columns) it is evident that the dust-to-gas ratios $\eta_{\rm d}(t)$ and the dust-to-metal ratios $\eta_{\rm ZD}(t)$ result in higher values in comparison to the higher mass galaxy systems (see Fig. 3.2, 3.5 two right columns). The tendencies are in general the same.

G09M: In Fig. 3.6 the results are shown for models with a rotationally enhanced mass loss prescription. The galaxy under consideration has $M_{\rm ini} = 5 \times 10^{11}$ M$_\odot$. The outcome is similar to the reference EIT08M (Fig. 3.1), although the obtained dust yields are increased for the IMFs favouring higher masses. For a Larson 2 IMF, $M_{\rm d}(t)$ exceeds 10^9 M$_\odot$ after $\sim$ 650 Myr. Interestingly, even though the dust yields are high for no dust destruction in the ISM, for $M_{\rm cl}$ = 800 M$_\odot$ the dust mass also stays below 10^8 M$_\odot$. In case of a low SN dust production efficiency 10^8 M$_\odot$ cannot be reached within the first 400 Myr. However, for the IMFs biased towards high masses an amount of dust $> 10^8$ M$_\odot$ is attained later in the evolution.

Models with fixed SNe mass range

In Fig. 3.7 the results of $M_{\rm d}(t)$ are shown for WW95M (top row) and N06M (bottom row) for a galaxy with $M_{\rm ini} = 5 \times 10^{11}$ M$_\odot$ and a high SN efficiency $\epsilon_{\rm high}(m)$. The

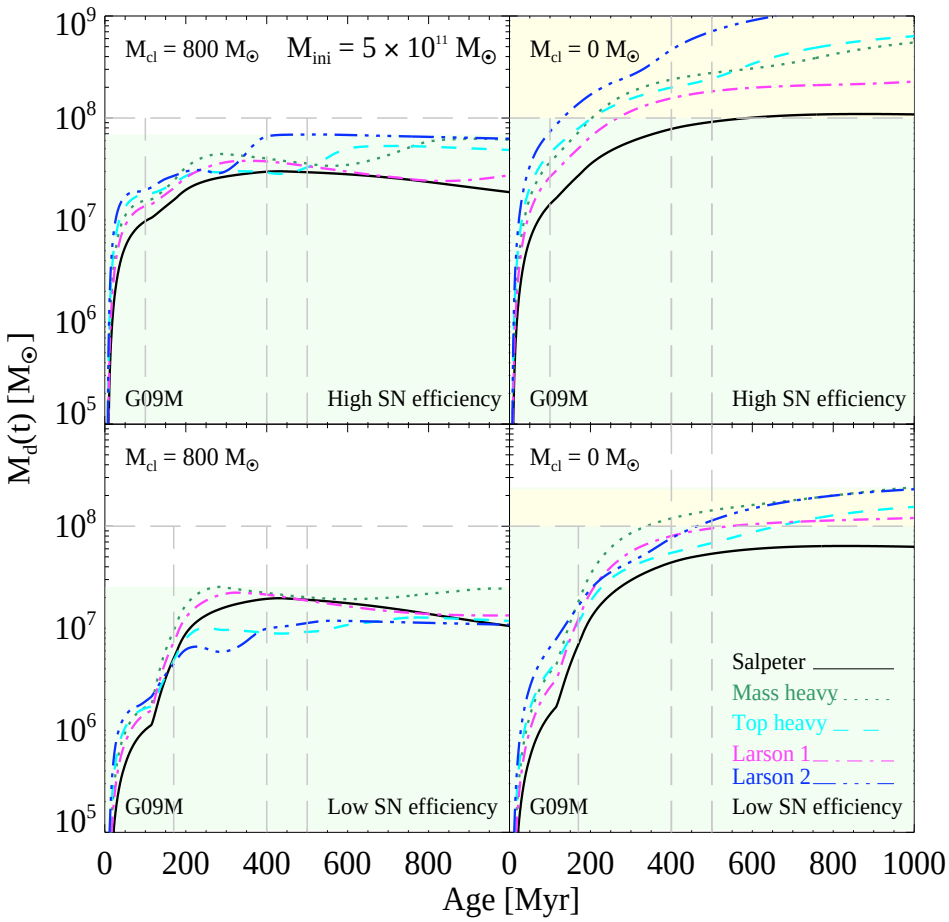

Figure 3.6: *Evolution of the total dust mass for G09M. G09M is presented for a galaxy with* $M_{\rm ini}$ = 5 × 10^{11} $\mathrm{M}_{\odot}$. *Total dust masses* $M_{\rm d}(t)$ *are shown for a high (top row) and a low (bottom row) SN dust production efficiency* $\epsilon_{\rm i}(m)$. *Dust destruction is taken into account for a* $M_{\rm cl}$ = *800* $\mathrm{M}_{\odot}$ *(left column) and 0* $\mathrm{M}_{\odot}$ *(right column). Maximum dust masses below* 10^8 $\mathrm{M}_{\odot}$ *are indicated as green shaded zones and as yellow shaded zones when exceeding* 10^8 $\mathrm{M}_{\odot}$. *The grey horizontal dashed line marks the limit of* 10^8 $\mathrm{M}_{\odot}$ *of dust. The grey vertical dashed lines indicate epochs at 100, 170, 400 and 500 Myr after the onset of starburst. The black solid, green dotted, cyan dashed, magenta dashed-dotted and blue dashed-dot-dotted lines represent the Salpeter, mass-heavy, top-heavy, Larson 1 and Larson 2 IMF, respectively.*

amount of dust in N06M early in the evolution is larger than for WW95M for the IMFs favouring massive stars, but flattens later, leading to slightly lower dust masses than achieved with WW95M. The dust masses achieved with either the maximal or the low SN dust production efficiencies are nearly identical to EIT08M and are therefore not shown. Generally, the evolution of these models is similar to EIT08M.

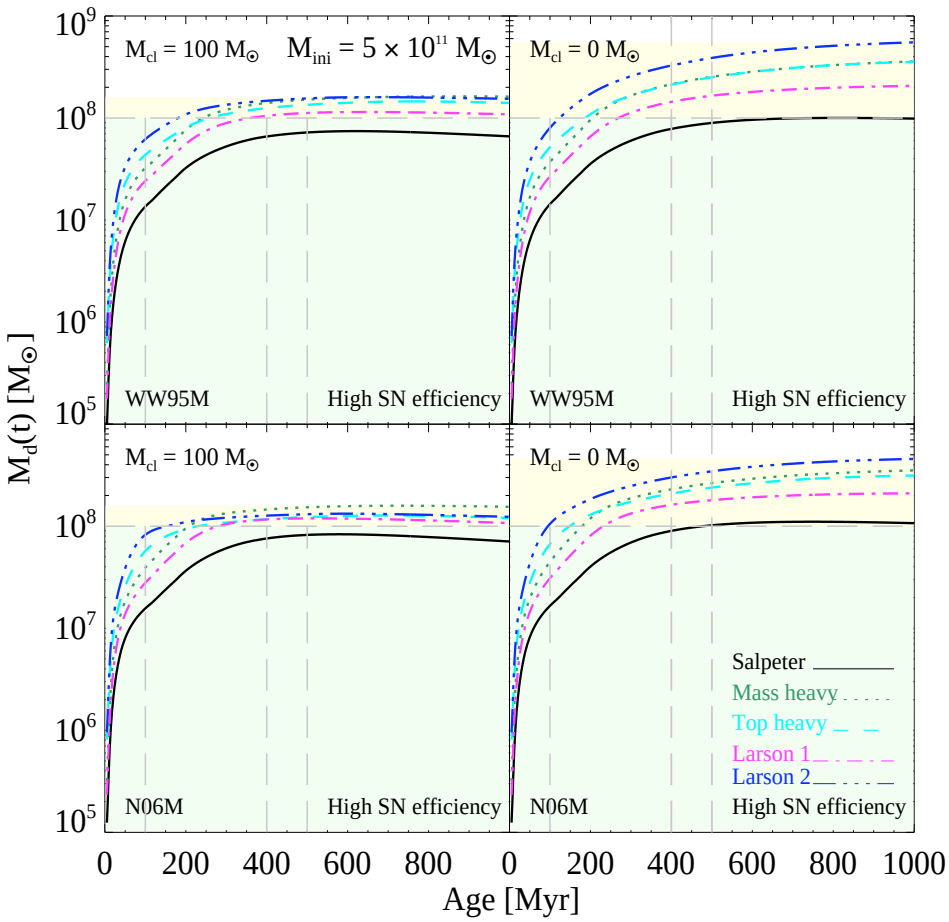

Figure 3.7: *Evolution of the total dust mass for WW95M (top row) and N06M (bottom row). Both models are presented for a galaxy with* $M_{\rm ini} = 5 \times 10^{11}$ $\mathrm{M}_\odot$. *Total dust masses* $M_{\rm d}(t)$ *are shown for a high SN dust production efficiency* $\epsilon_{\rm high}(m)$. *Dust destruction is taken into account for a* $M_{\rm cl} = 100$ $\mathrm{M}_\odot$ *(left column) and 0* $\mathrm{M}_\odot$ *(right column). Maximum dust masses below* 10^8 $\mathrm{M}_\odot$ *are indicated as green shaded zones and as yellow shaded zones when exceeding* 10^8 $\mathrm{M}_\odot$. *The grey horizontal dashed line marks the limit of* 10^8 $\mathrm{M}_\odot$ *of dust. The grey vertical dashed lines indicate epochs at 100, 170, 400 and 500 Myr after the onset of starburst. The black solid, green dotted, cyan dashed, magenta dashed-dotted and blue dashed-dot-dotted lines represent the Salpeter, mass-heavy, top-heavy, Larson 1 and Larson 2 IMF, respectively.*

Very high $M_{\rm ini}$ and the case of constant SFR

Fig. 3.8 displays the results for a case with constant SFR $\psi(t) = 1 \times 10^3$ $\mathrm{M}_\odot$ yr^{-1} and a galaxy with a high initial gas mass of $M_{\rm ini} = 1.3 \times 10^{12}$ $\mathrm{M}_\odot$. Such a high $M_{\rm ini}$ is necessary when assuming a constant SFR, since in the lower mass galaxies the available mass for star formation gets exhausted before an age of 1 Gyr is reached.

We find that with a high amount of destruction a build up of large dust masses also

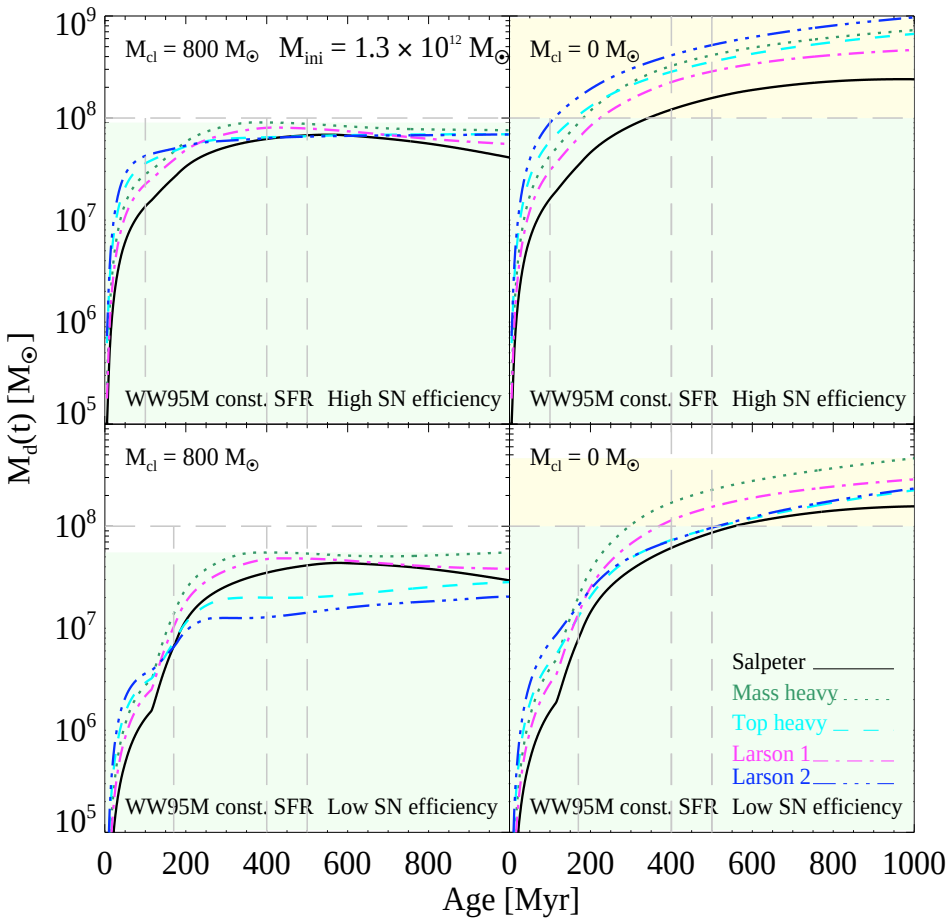

Figure 3.8: *Evolution of the total dust mass for WW95M with constant SFR. WW95M is presented for a galaxy with $M_{\rm ini} = 1.3 \times 10^{12}$ $\rm M_\odot$. Total dust masses $M_{\rm d}(t)$ are shown for a high (top row) and a low (bottom row) SN dust production efficiency $\epsilon_{\rm i}(m)$. Dust destruction is taken into account for a $M_{\rm cl}$ = 800 $\rm M_\odot$ (left column) and 0 $\rm M_\odot$ (right column). Maximum dust masses below 10^8 $\rm M_\odot$ are indicated as green shaded zones and as yellow shaded zones when exceeding 10^8 $\rm M_\odot$. The grey horizontal dashed line marks the limit of 10^8 $\rm M_\odot$ of dust. The grey vertical dashed lines indicate epochs at 100, 170, 400 and 500 Myr after the onset of starburst. The black solid, green dotted, cyan dashed, magenta dashed-dotted and blue dashed-dot-dotted lines represent the Salpeter, mass-heavy, top-heavy, Larson 1 and Larson 2 IMF, respectively.*

for such massive galaxies is greatly suppressed. With none of the IMFs 10^8 $\rm M_\odot$ of dust is attained, apart from the models with $\epsilon_{\rm max}$. Large dust masses with either $\epsilon_{\rm high}$ or $\epsilon_{\rm low}$ are only possible in case of modest or no dust destruction. For the latter the results are shown in the right column of Fig. 3.8. Interestingly, also for a low SN dust production efficiency dust masses $> 10^8$ $\rm M_\odot$ are possible after $\sim$ 300–400 Myr.

The results are very similar to a EIT08M with such high $M_{\rm ini}$ and an evolving SFR. A slight difference appears for $M_{\rm d}(t)$ and IMFs favouring low mass stars. These models

remain close to constant after 500–600 Myr, while the models for constant SFR slowly decline. The similarity between these models can be explained by the very high mass of the galaxy. In neither models the ISM mass gets significantly reduced.

3.4.2 Evolution of dust production rates, SFR and metallicity

In Fig. 3.9 we present the evolution of quantities such as the total dust injection rates $E_{\rm d,SN}(t)$, $E_{\rm d,AGB}(t)$, the AGB and SNe rates $R_{\rm AGB}(t)$, $R_{\rm SN}(t)$, the SFR and the metallicity $Z(t)$ for a range of initial galaxy gas masses.

The rates and the metallicities are independent of the assumed dust formation efficiency and can be globally discussed for each initial mass $M_{\rm ini}$. The results for these quantities originating from EIT08M, WW95M and N06M with identical parameter setting are very similar. Consequently these quantities are discussed based on EIT08M.

Fig. 3.9 (upper row) shows the dust injection rates of AGB stars $E_{\rm d,AGB}(t)$ and SNe $E_{\rm d,SN}(t)$. For supernovae $E_{\rm d,SN}(t)$ is highest for a Larson 2 IMF and lowest for a Salpeter IMF. The SN dust production rates are approximately one order of magnitude lower for $\epsilon_{\rm low}(m)$ (black lines) than for $\epsilon_{\rm high}(m)$ (blue lines). In all cases a clear separation of the values of $E_{\rm d,SN}(t)$ amongst the various IMFs is visible throughout the evolution.

The dust injection rates for AGB stars, $E_{\rm d,AGB}(t)$, are considerably influenced by the long lifetimes. After $\sim$ 200 Myr the AGB dust production rates $M_{\rm d,AGB}(t)$ are comparable to the dust injection rates for SNe with $\epsilon_{\rm high}(m)$. This is caused by the higher dust production efficiency for AGB stars between $\sim$ 3–4 $\rm M_\odot$ than for AGB stars in the mass range of 4–8 $\rm M_\odot$ see (Chapter 2). The small variations of $E_{\rm d,AGB}(t)$ are mainly due to alteration of the stellar yields and dust formation efficiencies at different metallicities.

The SNe and AGB dust injection rates decline as a consequence of decreasing SNe and AGB rates, as shown in Fig. 3.9 (second row). Both rates exhibit a faster decline for the lower massive galaxies and for IMFs biased towards the intermediate and low mass stars.

This behaviour is determined by the slope of the SFR which is dependent on the initial mass of the galaxy (see Fig. 3.9 third row). The decline of the SFR for systems with $M_{\rm ini} \geq 3 \times 10^{11}$ $\rm M_\odot$ is more shallow. For these galaxies a high SFR of a few hundred $\rm M_\odot\ yr^{-1}$ can be sustained over at least 1Gyr of evolution. For the lower mass galaxies the SFR declines faster and exhibits a strong dependency on the IMFs. At a time of 400 Myr the SFR for a galaxy with $M_{\rm ini}$ = 1 $\times$ 10^{11} $\rm M_\odot$ is between 60 (Salpeter) to 500 (Larson 2) $\rm M_\odot\ yr^{-1}$. In case of $M_{\rm ini}$ = 5 $\times$ 10^{10} $\rm M_\odot$, $\psi(t)$ = 20–400 $\rm M_\odot\ yr^{-1}$. After $\sim$ 1 Gyr the difference between the SFRs obtained with a Larson 2 IMF and a Salpeter IMF is more than an order of magnitude.

In Fig. 3.9 (bottom row) it is seen that the metallicity $Z(t)$ in the two lower mass galaxies rises quickly within the first 100–200 Myr up to values of more than 5 $\rm Z_\odot$ for either a top-heavy or Larson 2 IMF. Thereafter it remains rather constant. For the system

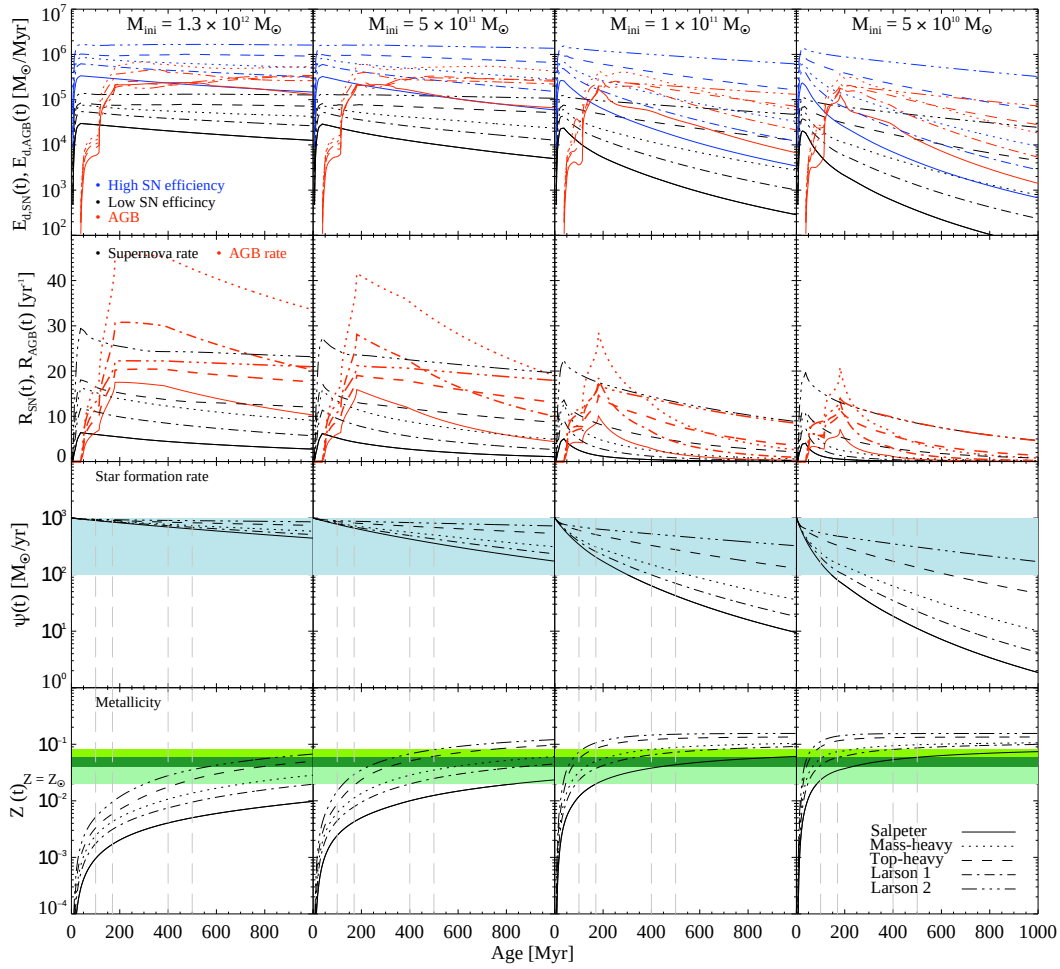

Figure 3.9: *Evolution of total dust injection rates for AGB stars and SNe, the AGB and SNe rates, the SFR and the metallicity. Results are shown for* $M_{\rm ini} = 1.3 \times 10^{12}$ $\rm M_\odot$ *(first column),* 5×10^{11} $\rm M_\odot$ *(second column),* 1×10^{11} $\rm M_\odot$ *(third column) and* 5×10^{10} $\rm M_\odot$ *(fourth column). First row: Total SN dust injection rates* $E_{\rm d,SN}(t)$ *for a low (black lines) and high (blue lines) SN efficiency* $\epsilon_{\rm i}(m)$*, and AGB dust injection rates* $E_{\rm d,AGB}(t)$ *(red lines). Second row: SNe rates* $R_{\rm SN}(t)$ *(black lines) and AGB rates* $R_{\rm AGB}(t)$ *(red lines). Third row: Evolution of the SFR. The blue area marks the region between a SFR of 100–1000* $\rm M_\odot$ yr^{-1}*. Fourth row: Evolution of the metallicity* $Z(t)$*. The green regions mark a metallicity between 1–2* $\rm Z_\odot$ *(light green), 2–3* $\rm Z_\odot$ *(dark green), 3–4* $\rm Z_\odot$ *(grass green). The grey vertical dashed lines indicate epochs at 100, 170, 400 and 500 Myr after the onset of starburst. The solid, dotted, dashed, dashed-dotted and dashed-dot-dotted lines represent the Salpeter, mass-heavy, top-heavy, Larson 1 and Larson 2 IMF, respectively.*

with $M_{\rm ini} = 5 \times 10^{11}$ $\rm M_\odot$ the metallicity increases slower than in the lower mass galaxies. At an epoch of 400 Myr a metallicity of 2-3 $\rm Z_\odot$ can be observed for the top-heavy and Larson 2 IMFs, while the Salpeter IMF achieves only a bit less than half solar. In the

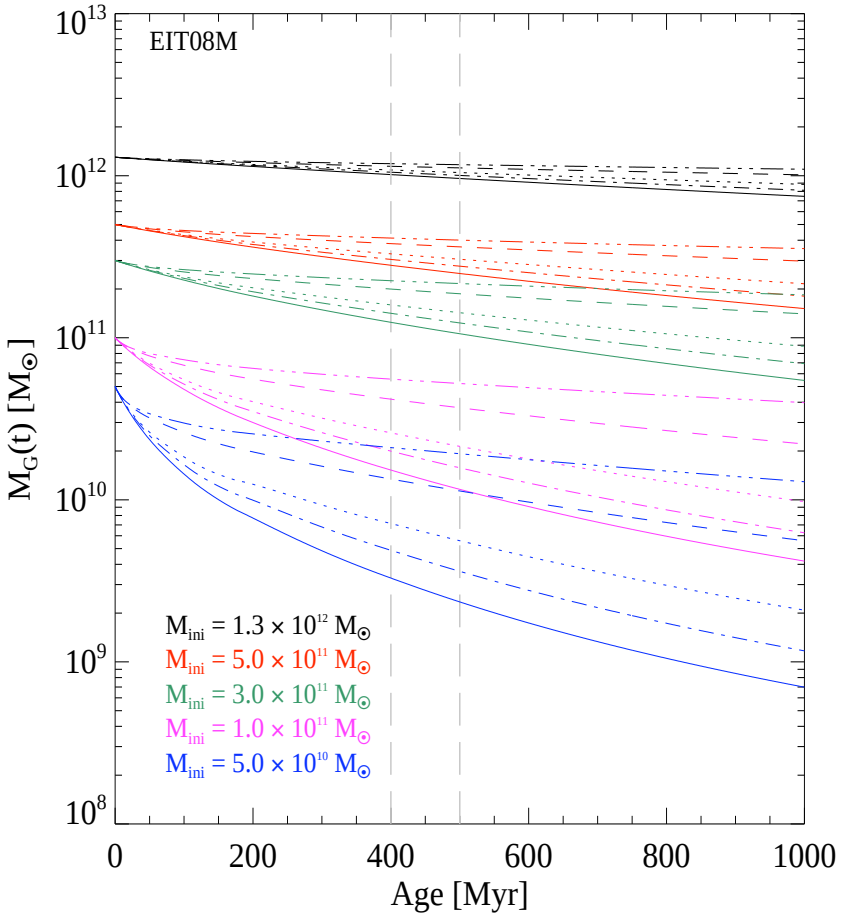

Figure 3.10: *Evolution of the gas mass $M_{\rm G}(t)$ based on EIT08M. Results are shown for $M_{\rm ini}$ = 1.3 × 10^{12} $\rm M_\odot$ (black lines), 5 × 10^{11} $\rm M_\odot$ (red lines), 3 × 10^{11} $\rm M_\odot$ (green lines), 1 × 10^{11} $\rm M_\odot$ (magenta lines) and 5 × 10^{10} $\rm M_\odot$ (blue lines). The grey vertical dashed lines indicate epochs at 400 and 500 Myr after the onset of starburst. The solid, dotted, dashed, dashed-dotted and dashed-dot-dotted lines represent the Salpeter, mass-heavy, top-heavy, Larson 1 and Larson 2 IMF, respectively.*

most massive galaxies the metallicity exceeds $\rm Z_\odot$ only in case of the top-heavy IMFs before an age of 400–500 Myr but remains below $\rm Z_\odot$ for the IMFs favouring lower mass stars.

3.4.3 Evolution of gas, metals and stellar masses

The evolution of quantities such as the gas mass, mass of metals and stellar masses is discussed based on EIT08M.

Fig. 3.10 illustrates the evolution of the H + He gas mass $M_{\rm G}(t)$. As a consequence of the scaling of the SFR with the mass of the ISM, $M_{\rm ISM}(t) \equiv M_{\rm G}(t) + M_{\rm Z}(t)$, the

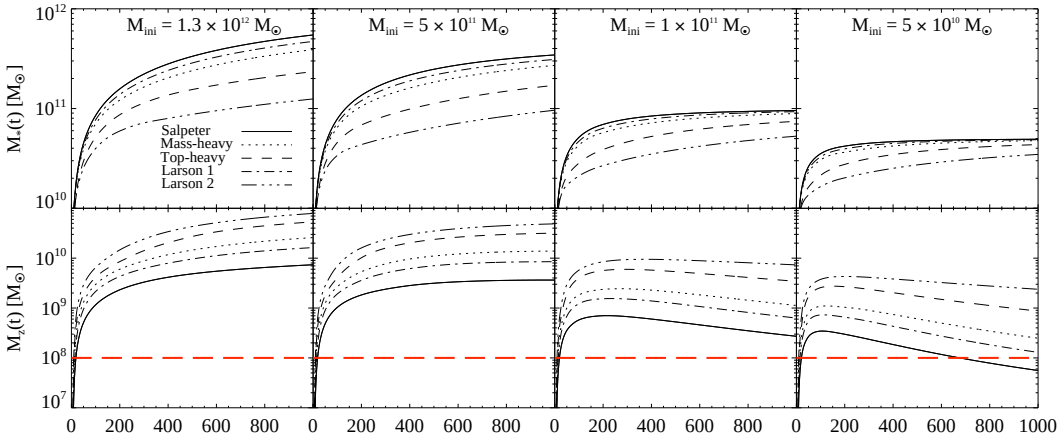

Figure 3.11: *Evolution of the stellar mass, mass of metals and the CO molecular mass based on EIT08M. Results are shown for $M_{\rm ini}$ = 1.3 × 10^{12} M$_\odot$ (first column), 5 × 10^{11} M$_\odot$ (second column), 1 × 10^{11} M$_\odot$ (third column) and 5 × 10^{10} M$_\odot$ (fourth column). Top row: Stellar mass $M_*(t)$. Bottom row: Mass of metals $M_{\rm Z}(t)$. The red lines mark a metal mass of 10^8 M$_\odot$. The solid, dotted, dashed, dashed-dotted and dashed-dot-dotted lines represent the Salpeter, mass-heavy, top-heavy, Larson 1 and Larson 2 IMF, respectively.*

progression of $M_{\rm G}(t)$ is identical to the SFR described in Sect. 3.4.2.

The most massive galaxy with $M_{\rm ini}$ = 1.3 × 10^{12} M$_\odot$ has a residual gas mass $M_{\rm G}(t)$ of ∼ 10^{12} M$_\odot$ after 1 Gyr. This explains the very low dust-to-gas ratio for such a system even though very high dust masses can be reached. The galaxy with $M_{\rm ini}$ = 5 × 10^{11} M$_\odot$ gets more exhausted, but also retains a gas mass $M_{\rm G}(t)$ of 3–4 × 10^{11} M$_\odot$ after ∼ 400–500 Myr.

In analogy with the curves of the SFR, the curves of the gas mass for the system with $M_{\rm ini}$ = 1 × 10^{11} M$_\odot$ feature a pronounced separation between the IMFs. A Larson 2 IMF shows a flat evolution leading to a slower depletion of the gas than for the Salpeter IMF and after 400–500 Myr ∼ 5 × 10^{10} M$_\odot$ of gas is still present. The lowest mass system ($M_{\rm ini}$ = 5 × 10^{10} M$_\odot$) exhibits the strongest dependence on the IMF. After 400 Myr $M_{\rm G}(t)$ is ∼ 2 × 10^{10} M$_\odot$ for a Larson 2 IMF. The difference between a Salpeter IMF and a Larson 2 IMF after one Gyr is an order of magnitude. The residual gas mass with a Salpeter IMF is a few times 10^8 M$_\odot$ at this time.

The steepness of the decline in the progression of $M_{\rm G}(t)$ is influenced by the stellar feedback. For either a Larson 2 or top-heavy IMF more massive stars are formed. Such stars are short-lived and release most of their mass back into the ISM, through either stellar winds or in explosive events. The IMFs favouring lower masses however lock most of the gas used for star formation into intermediate to low mass stars. These stars are formed at higher rates than massive stars. The latter ones live long and additionally

do not inject much material back into the ISM during our considered time span of 1 Gyr. As a consequence, the material available for star formation gets more rapidly depleted for the IMFs favouring low mass stars than for the top-heavy IMFs. Hence, the evolution of the gas mass and the SFR results in a steeper decline.

This is contrary to the stellar masses $M_*(t)$ (Fig. 3.11 top row) obtained from the relation $M_*(t) = M_{\rm ini} - M_{\rm ISM}(t)$. For the IMFs favouring lower mass stars $M_*(t)$ rises steeply and approaches the initial mass of this galaxy in case of the lower massive galaxy systems. The slope of $M_*(t)$ for the top-heavy IMFs is shallower and lower stellar masses $M_*(t)$ are achieved.

Fig. 3.11 (bottom row) depicts the mass of the ejected heavy elements $M_{\rm Z}(t)$. For systems with $M_{\rm ini} \geq$ 3–5 $\times$ 10^{11} $\mathrm{M}_\odot$ the metal enrichment in the ISM is considerable. The mass of the heavy elements increases up to a few times 10^{10} $\mathrm{M}_\odot$.

In the lower mass galaxies $M_{\rm ini} \leq 1 \times 10^{11}$ $\mathrm{M}_\odot$, the amount of metals $M_{\rm Z}(t)$ attained reaches a maximum within the first 200 Myr whereafter $M_{\rm Z}(t)$ declines. This is caused by astration. The maximum mass of metals obtained with a Salpeter IMF is only a few times 10^8 $\mathrm{M}_\odot$. In case of the lowest mass galaxy the amount of metals after $\sim$ 600 Myr for a Salpeter IMF is less than 10^8 $\mathrm{M}_\odot$. This implies that dust masses $M_{\rm d}(t)$ in excess of 10^8 $\mathrm{M}_\odot$ for this IMF are unfeasible, even if dust grain growth in the ISM were invoked.

3.4.4 Comparison to other dust evolution models for high-z galaxies

The models with a maximal SN dust production efficiency for a system with $M_{\rm ini}$ of 5 $\times$ 10^{10} $\mathrm{M}_\odot$ (Fig. 3.4 two left columns, first row) can be compared to models of Dwek et al. (2007). For this efficiency the AGB dust production is negligible and the SN dust yields are similar to the dust yields used by Dwek et al. (2007). The assumed initial SFR and the treatment of the evolution of the SFR are consistent with our models (see Sect. 3.2.1). Our results for a top-heavy IMF and $M_{\rm cl}$ = 0 at an epoch of 400 Myr are in agreement with their results, while they disagree for a Salpeter IMF and for cases with $M_{\rm cl}$ = 100 $\mathrm{M}_\odot$.

The origin of this disagreement can be traced to the neglect of the lifetime dependent mass injection of stars and a different treatment of the mass recycled into the ISM in the models of Dwek et al. (2007). The latter is approximated as $0.5\psi(t)$ in their models, which leads to an IMF independent evolution of the ISM mass. In case of a Salpeter IMF this simple approximation has consequences for the evolution of all physical properties. It implicitly presupposes that also stars, which are formed between the lower mass limit of the IMF and the lower SN mass limit, immediately return half of their stellar mass back into the ISM. However, stars between 3–8 $\mathrm{M}_\odot$ eject their elements up to a few 100 Myr delayed and stars $\lesssim$ 3 $\mathrm{M}_\odot$ do not eject a significant amount of elements within the first Gyr. For a Salpeter IMF, where more low mass stars than high mass stars are

formed, we have shown that the mass of the ISM gets faster exhausted than for the IMFs favouring higher masses (see Sect. 3.4.3). This results in a steeper decline of the SFR, the SN rates and the SN dust injection rates. Thus, our models lead to lower dust masses than the models by Dwek et al. (2007) for a Salpeter IMF.

The model for a system with $M_{\rm ini}$ = 1.3 $\times$ 10^{12} $\mathrm{M}_{\odot}$, $M_{\rm cl}$ = 800 $\mathrm{M}_{\odot}$ (Fig. 3.8 top left), a Larson 1 IMF and the high SN efficiency is directly comparable to the model by Valiante et al. (2009) with constant SFR of 1000 $\mathrm{M}_{\odot}$ yr^{-1}. Our results are in good agreement with their results, although our model does not quite reach 10^8 $\mathrm{M}_{\odot}$. This discrepancy may be due to differences in the SN dust yields used. Additionally, the treatment of the feedback,i.e., the amount of the recycled material, from stars between 40–100 $\mathrm{M}_{\odot}$ by Valiante et al. (2009) is not unambiguously traceable.

3.4.5 Results for models including a SMBH

We have investigated, whether the inclusion of the formation of the SMBH leads to differences in the evolution of either the total amount of dust or the physical properties of a galaxy.

Based on the observed SMBH masses $\geq 10^9$ $\mathrm{M}_{\odot}$ for high redshift QSOs (e.g., Willott et al. 2003; Vestergaard 2004; Jiang et al. 2006; Wang et al. 2010) we study two cases for the SMBH mass, $M_{\rm SMBH}$ = 3 $\times$ 10^9 $\mathrm{M}_{\odot}$ and $M_{\rm SMBH}$ = 5 $\times$ 10^9 $\mathrm{M}_{\odot}$. According to Kawakatu & Wada (2009) the final SMBH mass takes up approximately 1–10 % of the supply mass $M_{\rm SMBHsup}$. This implies that in order to grow a SMBH of 3(5) $\times$ 10^9 $\mathrm{M}_{\odot}$ the minimum required supply mass ranges between 3(5) $\times$ 10^{10} to 3(5) $\times$ 10^{11} $\mathrm{M}_{\odot}$. In view of our assumption that $M_{\rm SMBHsup} \equiv M_{\rm ini}$ we included the SMBH formation in galaxies with $M_{\rm ini}$ = 5 $\times$ 10^{10} $\mathrm{M}_{\odot}$, $M_{\rm ini}$ = 1 $\times$ 10^{11} $\mathrm{M}_{\odot}$, and $M_{\rm ini}$ = 3 $\times$ 10^{11} $\mathrm{M}_{\odot}$.

In Fig. 3.12 we show the results of $M_{\rm d}(t)$ for a Salpeter and Larson 1 IMF for a EIT08M and $M_{\rm ini}$ = 5 $\times$ 10^{10} $\mathrm{M}_{\odot}$ where the SMBH formation has been included. These results are compared to those of a model with the same $M_{\rm ini}$, but without a SMBH.

Taking the SMBH into account leads to a steeper decline of $M_{\rm d}(t)$ and therefore to a lower amount of dust than for the model without a SMBH after $\sim$ 100 Myr. All models are similar within the first $\sim$ 100 Myr. For $M_{\rm SMBH}$ = 5 $\times$ 10^9 $\mathrm{M}_{\odot}$ the difference is at most $\sim$ 50 % for a Salpeter IMF and $\sim$ 30 % for a Larson 1 IMF at an epoch of 400 Myr. At the same epoch but for a $M_{\rm SMBH}$ = 3 $\times$ 10^9 $\mathrm{M}_{\odot}$ the dust mass for a Salpeter IMF is reduced by only about 30 %, and 20 % for the Larson 1 IMF. In cases of IMFs biased towards higher masses and in the more massive galaxy systems the formation of the SMBH, as introduced here, does not noticeably effect the progression of $M_{\rm d}(t)$ and the physical properties of a galaxy.

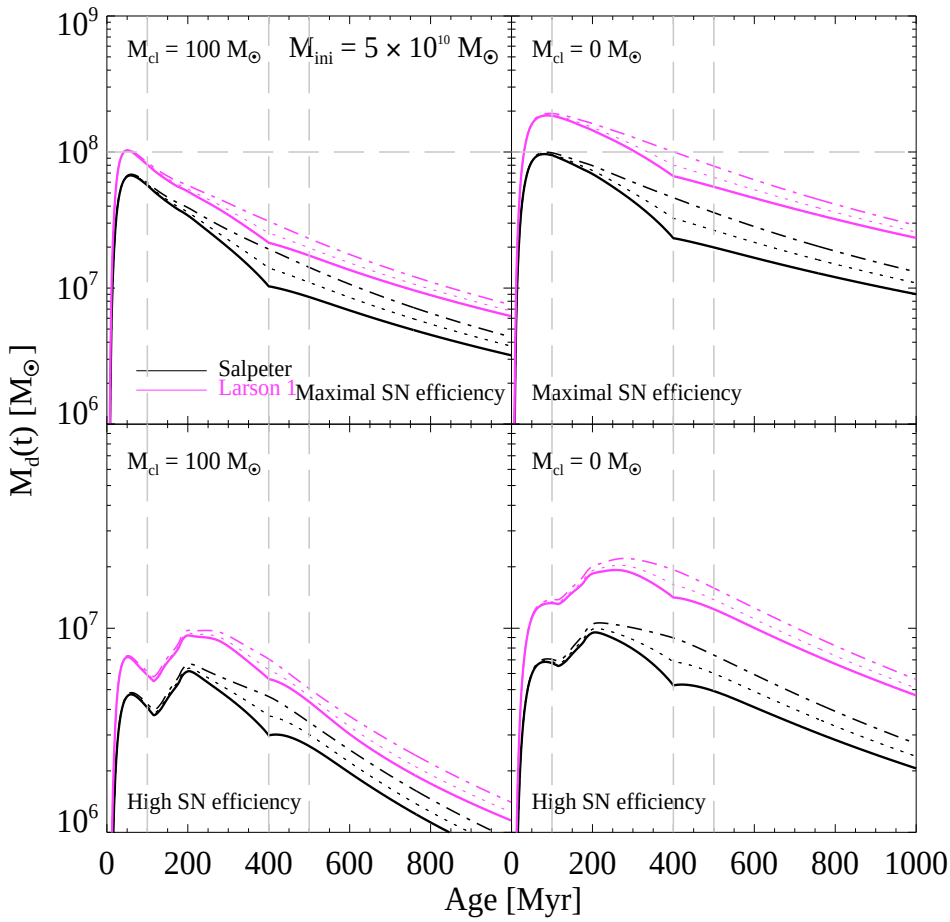

Figure 3.12: *Comparison of the evolution of the dust mass between EIT08M including and without the SMBH formation. The initial gas mass of the galaxy $M_{\rm ini}$ = 5 × 10^{10} $\rm M_\odot$. Calculations are shown for a maximal (top row) and a high (bottom row) SN dust production efficiency $\epsilon_{\rm i}(m)$. Dust destruction is taken into account for $M_{\rm cl}$ = 100 $\rm M_\odot$ (left column) and 0 $\rm M_\odot$ (right column). Calculations including the SMBH are performed for a SMBH mass $M_{\rm SMBH}$ = 5 × 10^9 $\rm M_\odot$ (solid curves) and for a $M_{\rm SMBH}$ = 3 × 10^9 $\rm M_\odot$ (dotted curves). The calculations without the SMBH are illustrated as dot-dashed curves. The black lines represent the Salpeter IMF and the magenta lines the Larson 1 IMF. The grey horizontal dashed line marks the limit of 10^8 $\rm M_\odot$ of dust. The grey vertical dashed lines indicate epochs at 100, 400 and 500 Myr after the onset of starburst.*

3.5 Discussion

We have shown that, depending on the assumptions for certain model parameters, dust masses in excess of 10^8 $\rm M_\odot$ can be obtained in our model. All models leading to dust masses $\geq 10^8$ $\rm M_\odot$ within the first 400 Myr are listed in Table 3.3.

In Fig. 3.13 we show the resulting relations between the dust mass and stellar mass, SFR and metallicity at 400 Myr.

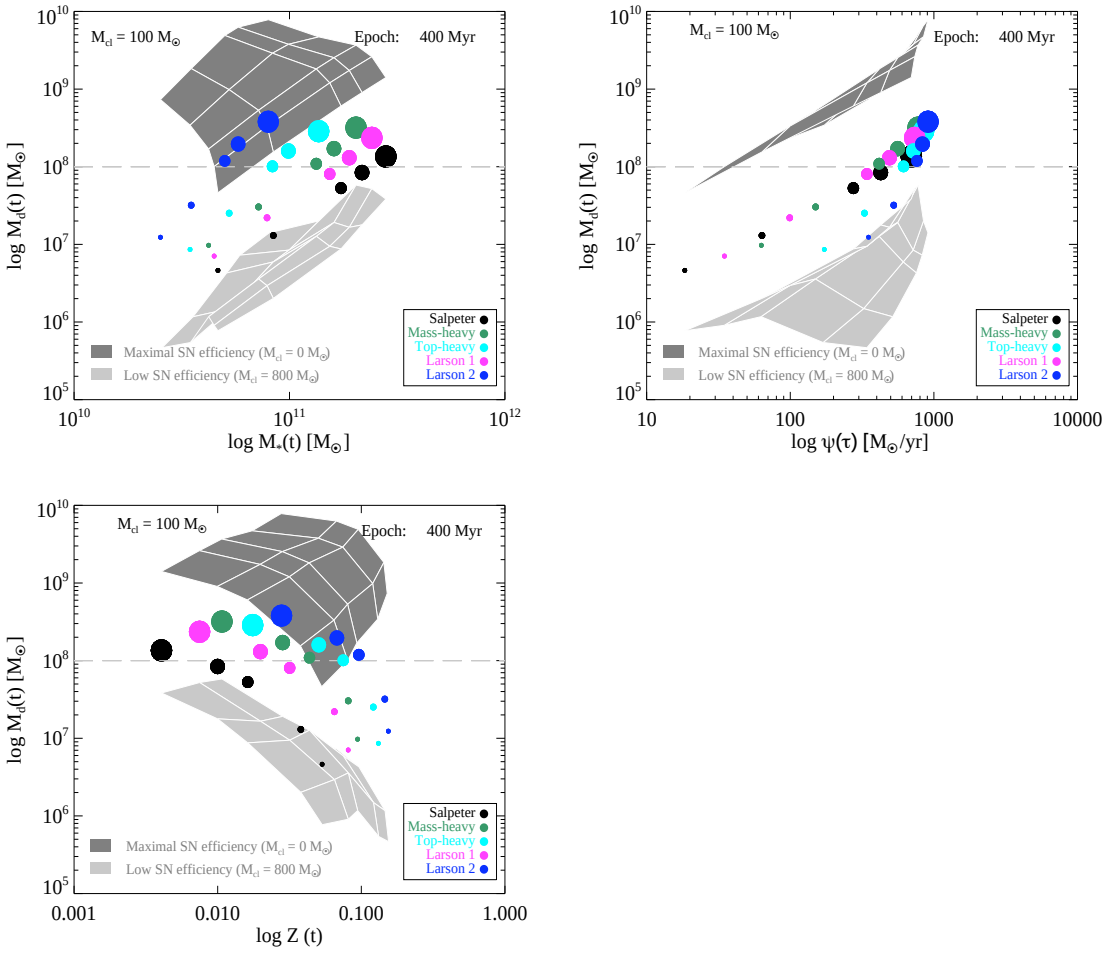

Figure 3.13: *Relation between dust mass, stellar mass, SFR and metallicity in correlation with the total mass of the galaxy and the IMF for an epoch at 400 Myr. Top-left panel: Dust mass $M_{\rm d}(t)$ versus stellar mass $M_*(t)$. Top-right panel: Dust mass $M_{\rm d}(t)$ versus SFR $\psi(t)$. Bottom-left panel: Dust mass $M_{\rm d}(t)$ versus metallicity $Z(t)$. The dark grey shaded area marks the dust masses $M_{\rm d}(t)$ obtained with a maximal SN dust production efficiency $\epsilon_{\rm max}(m)$ and no dust destruction in the ISM ($M_{\rm cl}$ = 0 $\rm M_\odot$). The light grey shaded area marks dust masses $M_{\rm d}(t)$ for the low SN dust production efficiency $\epsilon_{\rm low}(m)$ with dust destruction in the ISM ($M_{\rm cl}$ = 800 $\rm M_\odot$). Cross points of the thin white lines indicate the data points for each IMF and mass $M_{\rm ini}$ of the galaxy. The colored filled circles signify the dust masses obtained for a high SN efficiency $\epsilon_{\rm high}(m)$ and a dust destruction in the ISM with $M_{\rm cl}$ = 100 $\rm M_\odot$. The size of the circles is scaled by the initial mass $M_{\rm ini}$ of the galaxy. The black, green, cyan, magenta and blue colors denote the Salpeter, mass-heavy, top-heavy, Larson 1 and Larson 2 IMF, respectively.*

It is evident that the dust yields are related to the mass of the galaxy. For a given combination of IMF, SN dust production efficiency and $M_{\rm cl}$ higher dust yields are obtained with increasing $M_{\rm ini}$. In the discussion below we consider $\epsilon_{\rm high}$ with $M_{\rm cl}$ = 100 $\rm M_\odot$ as the reference case.

Table 3.3: *EIT08M exceeding* 10^8 $\mathrm{M}_\odot$ *of dust within* $\sim$ *400–500 Myr*

$M_{\rm ini}$	$\epsilon_{\rm SN}$	$M_{\rm cl}$	IMF
1.3×10^{12} $\mathrm{M}_\odot$	max	0	all
	max	100	all
	max	800	all
	high	0	all
	high	100	all
	low	0	mass-heavy, Larson 1
	low	100	mass-heavy, Larson 1
5×10^{11} $\mathrm{M}_\odot$	max	0	all
	max	100	all
	max	800	all
	high	0	all
	high	100	top-heavy, Larson 1, 2, mass-heavy
	low	0	mass-heavy
3×10^{11} $\mathrm{M}_\odot$	max	0	all
	max	100	all
	max	800	all
	high	0	top-heavy, Larson 1, 2, mass-heavy
	high	100	top-heavy, Larson 2, mass-heavy
	low	0	mass-heavy
1×10^{11} $\mathrm{M}_\odot$	max	0	all
	max	100	top-heavy, Larson 1, 2, mass-heavy
	high	0	Larson 2
5×10^{10} $\mathrm{M}_\odot$	max	0	top-heavy, Larson 1, 2, mass-heavy
	max	100	Larson 2
	max[a]	100	top-heavy, Larson 1, mass-heavy

Notes. [a]Top-heavy IMF: only within the first $\sim$ 300 Myr, Larson 1 and mass-heavy IMF only within the first $\sim$ 100 Myr

The left panel in Fig. 3.13 visualizes the dust mass versus the stellar mass. For a given IMF the stellar masses increase with $M_{\rm ini}$. However for a given $M_{\rm ini}$ a large spread of the stellar mass is found with varying IMF. We find that for the reference case, galaxies with $M_{\rm ini} > 3 \times 10^{11}$ $\mathrm{M}_\odot$ and an IMF biased towards higher masses reproduce dust masses $> 10^8$ $\mathrm{M}_\odot$, while, with a Salpeter IMF, this is only possible in the most massive system. The stellar masses for these galaxies and with the more top-heavy IMFs are in good agreement with observations of galaxies at high-z. Santini et al. (2010)

and Michałowski et al. (2010a) showed that out of a sample of high-z sub-millimeter galaxies and local ULIRGs most of these are assembled at stellar masses around 10^{11} $\mathrm{M}_{\odot}$ and have dust masses between 10^{8-10} $\mathrm{M}_{\odot}$.

Alternatively a maximal SN dust production efficiency can account for the required dust mass. For this SN efficiency, even a higher dust destruction in the ISM of M_{cl} = 800 $\mathrm{M}_{\odot}$ can be accomodated. However, both assumptions of either ϵ_{max} or M_{cl} = 800 $\mathrm{M}_{\odot}$ are controversial. So far only in the SN remnants Cas A (Wilson & Batrla 2005; Dunne et al. 2009) and Kepler (Gomez et al. 2009) dust masses have been claimed which are consistent with a maximal SN efficiency ϵ_{max}. Most SN dust observations reveal dust masses implying efficiencies in the range of ϵ_{low}–ϵ_{high} (see Chapter 2). Additionally, theoretical models (Nozawa et al. 2010) predict that depending on density and geometry of the CSM and shocks, only a part of the dust may survive the destructive reverse shock.

The uncertainty of dust destruction through SN shocks has been discussed in Sect.-3.3.5. The results obtained in this work strengthen the concerns of a high value for M_{cl}. Apart from the maximal SN efficiency, for a high value of M_{cl} = 800 $\mathrm{M}_{\odot}$ only the combination of a high SN efficiency ϵ_{high} with M_{ini} = 1.3 $\times$ 10^{12} $\mathrm{M}_{\odot}$ leads to dust masses close to 10^{8} $\mathrm{M}_{\odot}$, regardless of the IMF. However the remaining gas mass $M_{\mathrm{G}}(t)$ is $> 10^{12}$ $\mathrm{M}_{\odot}$, implying dust-to-gas mass ratios $\eta_{\mathrm{d}}(t) < 10^{-4}$, is not supported by observations. For example, Santini et al. (2010) compare dust-to-gas ratios of high-z SMGs, ULIRGs, local spirals and local dwarf galaxies and show that SMGs and ULIRGs have higher dust-to-gas ratios ($\sim 10^{-2}$) than spiral galaxies which also have dust-to-gas ratios $> 10^{-4}$. Further evidence comes also from galaxies in the local Universe (e.g., Dunne et al. 2000; Dunne & Eales 2001; da Cunha et al. 2010) where inferred dust-to-gas ratios are also $> 10^{-4}$. In high-z QSOs the typical dust-to-H_2 ratios are $\sim 10^{-2}$ (e.g., Cox et al. 2002; Bertoldi et al. 2003b; Michałowski et al. 2010b). The low dust-to-gass mass ratio is also the reason, why dust destruction in the ISM is less efficient than in the lower mass galaxy systems.

In principle, the fairly sensitive interplay between dust-to-gas ratio $\eta_{\mathrm{d}}(t)$ and SN rates might be important when contemplating additional dust source in less massive galaxies. As long as SN rates are high, any increase of the dust mass, and thereby $\eta_{\mathrm{d}}(t)$, leads to higher destruction rates. This shows that for M_{cl} = 800 $\mathrm{M}_{\odot}$ it is difficult to reach high amounts of dust, unless a rapid enrichment with large dust masses from either stellar sources or grain growth in the ISM takes place. In the latter case, grain growth rates must be comparable to SN dust injection rates for ϵ_{max}. Alternatively, a lowering of the dust-to-gas ratio $\eta_{\mathrm{d}}(t)$ due to for example infalling gas might be an option. However this alternative results in an increased total mass of the galaxy anyway.

Given these uncertainties we find that the reference case constitutes the most likely scenario. In Fig. 3.13 (middle panel) we have plotted the dust mass versus SFR. The highest SFRs can be sustained for the high mass weighted IMFs in the more massive

galaxies. For the less massive systems, also with top-heavy IMFs, the SFR declines rather fast. In comparison to observations of galaxies containing large dust masses at $z > 6$ we find that all systems more massive than 1×10^{11} $\mathrm{M}_{\odot}$ are in good agreement with the observed SFRs (e.g., Bertoldi et al. 2003a; Wang et al. 2010).

Fig. 3.13 (right panel) shows that the metallicity decreases with increasing dust mass. IMFs favouring low masses lead to lower metallicities than the more top-heavy IMFs. The IMFs favouring low masses lock most material used for star formation in low mass stars. These stars however do not recycle material back into the ISM, which therefore gets rapidly exhausted. In turn this leads to a high stellar mass $M_*(t)$. The more top-heavy IMFs form more short living massive stars at higher rates. These stars recycle a copious amount of their mass back into the ISM. Therefore these IMFs lead to lower stellar masses $M_*(t)$, since the remnant mass of SNe is small. In addition, massive stars enrich the ISM with metals, while low mass stars, due to their longer lifetimes, do not eject a significant amount, if any at all, of heavy elements back into ISM within 1 Gyr. This leads to a lower metallicity for the lower mass star weighted IMFs, and a higher metallicity for the top-heavy IMFs.

Metallicities $> \mathrm{Z}_{\odot}$ have been found in strong star forming galaxies such as ULIRGs or sub-millimeter galaxies as well as in high-z QSOs (e.g., Fan et al. 2003; Freudling et al. 2003; Kawara et al. 2010). In comparison to our calculated models, such metallicities can only be reached with the IMFs biased towards higher masses. In the lowest mass systems with these IMFs the metallicity reaches values of $\sim 5 \times \mathrm{Z}_{\odot}$.

3.5.1 Caveats in our approach

The presented models are based on rather simple assumptions such as a closed box environment, a common constant initial SFR of the starburst, and a very simple treatment of the SMBH growth. With these assumptions the models are comparable with similar works (e.g., Dwek et al. 2007; Valiante et al. 2009) and diverse evolutionary trends could be investigated in more detail, as discussed in previous sections.

However, such models usually do not capture possible impacts on the evolution of the galaxy arising from galaxy mergers or gas flows powered by for example SNe or the SMBH. Different evolutionary paths likely caused by these effects and the mass of the galaxy possibly result in starburst intensities different from our assumption, leading to a different temporal progression of various quantities. Furthermore, the growth of the SMBH is linked to several physical processes, e.g., the energy feedback of SNe, and realistically may not take place on a constant growth rate. Despite the neglect of these effects in our model, some general remarks about their influence can be made based on our results.

For example, infall rates which could effect the systems might have to be unrealistically high due to the very high SFRs. However, merging of galaxies might have an

effect. The same applies to outflows in the host galaxy or the feedback from the SMBH into the ISM. In our models the loss of material to fuel the SMBH can in principle be interpreted as some constant 'outflow' of the host galaxy. Although we introduced a rough treatment for the SMBH growth, we could show that 'outflow' rates of the host galaxy of about 7.5–12.5 $\mathrm{M}_{\odot}$ yr^{-1} over a timescale of 400 Myr only effect the amount of dust in the least massive systems (and IMFs biased towards low mass stars), but are negligible in the larger galaxies. In this regard it remains to be investigated, whether the energy deposition by SNe/AGNs in the ISM could be large enough to initiate sufficiently higher outflow rates impacting the total amount of dust in a galaxy.

A change in the evolution of the dust mass and other properties may also result from quasar winds, in which dust formation has been suggested in addition (Elvis et al. 2002). According to Elvis et al. (2002) the estimated mass-loss rates of about > 10 $\mathrm{M}_{\odot}$ yr^{-1} in the most luminous quasars with luminosities $> 10^{47}$ ergs s^{-1} (e.g., Omont et al. 2001, 2003; Carilli et al. 2001b; Bertoldi & Cox 2002) imply an amount of $\sim 10^{7}$ $\mathrm{M}_{\odot}$ of dust produced over 10^{8} yr. Comparing these rates to our model results we find that neither the mass-loss rates nor the dust mass seem to be large enough to be of relevance for the evolution of dust and other properties.

We find that a strong impact on the evolution of dust is caused by the dust sources. Despite the included detailed treatment of the dust contribution from stellar sources in the developed model, the poorly understood dust production by SNe, but also dust destruction by SN shock interactions, likely constitute the largest uncertainties in the evolution of dust. Although not included in the model, alternative dust sources such as dust grain growth in the ISM might be of relevance (e.g., Dwek et al. 2007; Draine 2009; Michałowski et al. 2010b).

3.6 Conclusions

In this Chapter we have developed a chemical evolution model for starburst galaxies at high redshift. The main purpose is to investigate the evolution of the dust content arising from SNe and AGB stars on timescales less than 1 Gyr. In addition, we have elaborated on the evolution of several physical properties of galaxies. The model allows the exploration of a wide range of parameters. The main parameters which had been varied are the mass of the galaxy, the IMF, SN dust production efficiencies, and dust destruction in the ISM through SN shocks and stellar yields. The main results can be summarized as follows:

1. The total amount of dust and the physical properties of a galaxy are strongly dependent on the IMF and correlate with the mass of the galaxy. For many properties we find an increasing disparity between the IMFs with decreasing mass of the galaxy. Higher dust masses are obtained with increasing mass of the galaxy.

2. The maximum dust masses can be obtained with IMFs biased towards higher mass stars and a maximal SN dust production efficiency in galaxies with masses between 5×10^{10} $\mathrm{M}_\odot$ and 1.3×10^{12} $\mathrm{M}_\odot$. This is found independently of the strength of dust destruction in the ISM. The case of maximal SN efficiency and no destruction constitute the maximum possible dust masses attainable with SNe and AGB dust production. The case with low SN efficiency and a high dust destruction ($\mathrm{M_{cl}}$ = 800 $\mathrm{M}_\odot$) gives the lowest possible dust masses.

3. The contribution by AGB stars is best visible in cases where a low SN dust formation efficiency is considered. In this case the mass-heavy IMF dominates throughout all considered initial masses $\mathrm{M_{ini}}$, and leads to the highest dust masses. However, dust production with this efficiency is found to be insufficient to fully account for dust masses in excess of 10^8 $\mathrm{M}_\odot$ within 400 Myr. In the galaxies with $M_{\mathrm{ini}} \geq 3 \times 10^{11}$ $\mathrm{M}_\odot$ this limit can be reached at epochs $\gtrsim$ 400 Myr if there is no dust destruction in the ISM.

4. The total dust mass is considerably reduced when destruction due to SN shock waves is taken into account. The strength of destruction in the ISM is given in terms of the mass M_{cl}, which is the mass of the ISM that is swept up and cleared of the containing dust through one SN remnant. Top heavy IMFs are sensitive to dust destruction, while IMFs favouring lower masses are more resistent to destruction due to lower SN rates. This leads to a significantly larger reduction and in some cases to a lower amount of dust with the top-heavy IMFs.

5. At early epochs ($<$ 200 Myr) SNe are primarily responsible for a significant enrichment with dust. For a high SN dust production efficiency SNe can generate 10^8 $\mathrm{M}_\odot$ within the first 100 Myr. In comparison, for a low SN dust production efficiency SNe are only able to increase the dust mass up to a few times 10^6 $\mathrm{M}_\odot$ in the first 100–150 Myr.

6. Taking the growth of the SMBH into account leads to a reduction of the amount of dust of at most $\sim$ 50 %. This is achieved for a SMBH mass $M_{\mathrm{SMBH}} = 5 \times 10^9$ $\mathrm{M}_\odot$ in a galaxy with $M_{\mathrm{ini}} = 5 \times 10^{10}$ $\mathrm{M}_\odot$ and only for IMFs favoring low mass stars. In more massive systems and for top-heavy IMFs no variation of the dust mass and properties of the galaxy are encountered.

7. To account for dust masses $> 10^8$ $\mathrm{M}_\odot$ we find that galaxies with an initial gas mass of M_{ini} = 1–5 $\times 10^{11}$ $\mathrm{M}_\odot$ in connection with top-heavy IMFs, a high SN dust production efficiency ϵ_{high} and a dust destruction in the ISM of $\mathrm{M_{cl}}$ = 100 $\mathrm{M}_\odot$ are favored. Models with the highest amount of $M_{\mathrm{ini}} = 1.3 \times 10^{12}$ $\mathrm{M}_\odot$ and lowest of $M_{\mathrm{ini}} = 5 \times 10^{10}$ $\mathrm{M}_\odot$ are disfavored.

This chapter is based on: C. Gall, A. C. Andersen and J. Hjorth – *Genesis and evolution of dust in galaxies in the early Universe – III. Rapid dust evolution in quasars at $z \gtrsim 6$* A&A, submitted
Figure: QSO PG 0052+251; John Bahcall (Institute for Advanced Study, Princeton) Mike Disney (University of Wales) and NASA/ESA

4

RAPID DUST EVOLUTION IN QSOS AT $z \gtrsim 6$

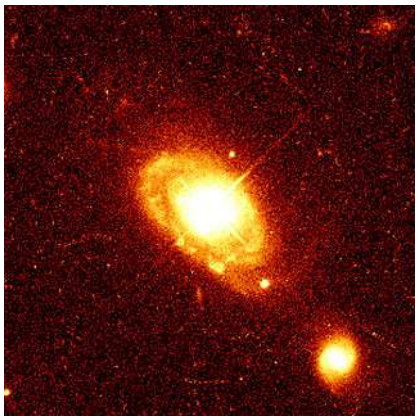

Unser Bildner hat zu den Sinnen den Geist gefügt, nicht bloß,
damit der Mensch seinen Lebensunterhalt erwerbe
- das können viele Arten von Lebewesen mit ihrer vernunftlosen Seele viel geschickter -,
sondern auch dazu, daß wir vom Sein der Dinge, die wir mit Augen betrachten,
zu den Ursachen ihres Seins und Werdens vordringen,
wenn auch später kein Nutzen damit verbunden ist.

JOHANNES KEPLER (1596)

ABSTRACT –

We intend to assess the most plausible scenarios for generating large amounts of dust in high-z QSOs on the basis of observationally derived physical properties of QSOs at $z \gtrsim 6$ We use a chemical evolution model to compute the temporal progression of quantities such as the amount of dust and gas, stellar masses, SFRs and the metallicity for various combinations of the IMF, the mass of the galaxy, dust production efficiencies and the degree of dust destruction in the ISM. We investigate the influence of the SFR on the evolution of these quantities and determine the earliest epochs at which an agreement with observations can be achieved. We apply the obtained results to individual QSOs at $z \gtrsim 6$.

4.1 INTRODUCTION

Studying QSOs at high redshift ($z > 6$) is important to gain deeper insights into the formation and evolution of galaxies, the origin of dust production and the build up of stellar bulge masses in coevolution with a supermassive black hole (SMBH).

While the most distant known QSO, J114816.64+525150.3 (Fan et al. 2003, herafter J1148+5251), is at z = 6.4, several tens of QSOs have been discovered at $z \sim 6$ (e.g., Fan et al. 2004, 2006; Willott et al. 2007; Jiang et al. 2010). Most of the observed QSOs at this redshift, where the epoch of cosmic evolution is $\sim$ 1 Gyr, exhibit extreme physical properties such as very high far-infrared (FIR) luminosities which imply large dust masses (e.g., Omont et al. 2001, 2003; Carilli et al. 2001b; Bertoldi & Cox 2002) and SMBHs with masses $> 10^9$ $\mathrm{M}_\odot$ (e.g., Barth et al. 2003; Willott et al. 2003; Vestergaard 2004).

Observations of QSOs have shown that dust emission at near-infrared (NIR) wavelengths arise from warm and hot dust ($T \sim 1000$ K) assembled within a few parsec (e.g., Hines et al. 2006; Jiang et al. 2006). The NIR emission is believed to be powered by the active galactic nucleus and related to the QSO activity (e.g., Polletta et al. 2000). However, two QSOs without detectable emission from hot dust have been found (Jiang et al. 2006, 2010). It has been proposed that these QSOs are at a too early evolutionary stage to have built up a significant amounts of hot dust.

The FIR luminosity of $L_{\mathrm{FIR}} \sim 10^{12-13}$ $\mathrm{L}_\odot$ is attributed to cold dust ($T \sim$ 30–60 K) (e.g., Wang et al. 2008) which is probably distributed over kpc scales throughout the host galaxy (Leipski et al. 2010). The amount of cold dust inferred is about a few times 10^8 $\mathrm{M}_\odot$ (e.g., Bertoldi et al. 2003a; Robson et al. 2004; Beelen et al. 2006; Michałowski et al. 2010b). The dominant source of the high FIR luminosity is believed to be dust heated by intense star formation in the circumnuclear region (e.g., Carilli et al. 2004; Riechers et al. 2007; Wang et al. 2008). Detection of [C II] line emission at 158μm (Maiolino et al. 2005) within a central region with radius $\sim$ 750 pc of the host galaxy of J1148+5251 also implies a high star formation rate surface density of 1000 $\mathrm{M}_\odot$ yr^{-1} kpc^{-2} (Walter et al. 2009). Wang et al. (2010) derived SFRs between 530–2300 $\mathrm{M}_\odot$ yr^{-1} from observations of a sample of QSOs at redshift $z > 5$. Observations of strong metal emission of high-z QSOs (e.g., Barth et al. 2003; Dietrich et al. 2003; Maiolino et al. 2003; Becker et al. 2006) indicate strong star forming activity in the QSO hosts and signify solar or supersolar metallicity (e.g., Fan et al. 2003; Freudling et al. 2003; Juarez et al. 2009). The latter has also been found theoretically (e.g., Di Matteo et al. 2004).

The high inferred SFRs imply short timescales ($\leq$ 10^8 yr) of the starburst (e.g. Bertoldi et al. 2003a; Walter et al. 2004; Dwek et al. 2007; Riechers et al. 2009) and consequently a young age of the QSOs. An early evolutionary stage of $z > 4$ QSOs has also been suggested from studies of extinction curves of broad absorption line QSOs (e.g., Gallerani et al. 2010) which turned out to be best fitted with extinction curves for

SN-like dust (e.g., Maiolino et al. 2004, 2006; Gallerani et al. 2010). This suggests SNe as the preferential source of dust at early epochs (e.g., Dwek 1998; Morgan & Edmunds 2003; Hirashita et al. 2005; Dwek et al. 2007), even though the dust productivity of SNe is poorly constrained (see also Chapter 2). The dust in high-z QSOs could also be predominantly grown in the ISM (e.g., Draine 2009; Michałowski et al. 2010b). Finally, a dominant dust production by asymptotic giant branch stars has been claimed (Valiante et al. 2009).

Molecular gas masses of the order of $\sim$ 1–2.5 $\times$ 10^{10} $\mathrm{M}_{\odot}$ have been inferred from detections of high excitation CO line emission in QSOs at $z > 5$ within a $\sim$ 2.5 kpc radius region (e.g., Bertoldi et al. 2003b; Walter et al. 2003, 2004; Wang et al. 2010). The dynamical masses inferred from these CO observations are a few times $\sim 10^{10-11}$ $\mathrm{M}_{\odot}$ which sets an upper limit on stellar bulge masses. These however are roughly two orders of magnitude lower than required from the present day black hole-bulge relation (e.g., Marconi & Hunt 2003). It therefore has been proposed that the formation of the SMBH occurs prior to the formation of the stellar bulge. QSOs will then have to accrete additional material to build up the required bulge mass (e.g., Walter et al. 2004; Riechers et al. 2009; Wang et al. 2010). Kawakatu & Wada (2009) showed that super-Eddington growth on timescales shorter than $\sim$$10^8$ yr is required to form a SMBH $> 10^9$ $\mathrm{M}_{\odot}$ at $z >$ 6. It has also been predicted that QSOs at $z \sim 6$ likely have formed in dark matter halos of 10^{12-13} $\mathrm{M}_{\odot}$ (e.g., Li et al. 2007; Kawakatu & Wada 2009).

In Chapter 3 we developed a chemical evolution model to elucidate the conditions required for generating large dust masses in high-z starburst galaxies. We showed that galaxies with masses of 1–5 $\times$ 10^{11} $\mathrm{M}_{\odot}$ are suitable for enabling the production of large amounts of dust within $\sim$ 400 Myr. In the present Chapter we apply this model to QSOs at $z \gtrsim 6$. We perform more detailed comparison between model results and values inferred from observations of $z \gtrsim 6$ QSOs to identify the most likely scenario. Furthermore, we consult additional parameters such as the H_2 mass and the CO conversion factor for more refined evaluations. In particular, calculations with higher SFRs than in Chapter 3 are considered. We aim to determine the earliest epochs at which the model results are in agreement with those from observations.

The structure of this Chapter is as follows: In Sec. 4.2 we briefly describe the model and the parameter which are different from those in Chapter 3. A detailed analysis of the results is presented in Sec. 4.3 followed by a discussion in Sec. 4.4 and our conclusions in Sec. 4.5.

4.2 THE MODEL

The galactic chemical evolution model described in Chapter 3 is self-consistent, numerically solved and has been developed to ascertain the temporal progression of dust, gas, metals and diverse physical properties of starburst galaxies. The incorporated stellar

sources are AGB stars in the mass range 3–8 $\mathrm{M}_{\odot}$ and SNe. A differentiation between diverse SN subtypes has been implemented. Their roles as sources of dust production, dust destruction or suppliers of gas and heavy elements are taken into account. The lifetime dependent yield injection by the stellar sources as well as dust destruction in the ISM due to SN shocks are also taken into account. Moreover, the formation of a SMBH is considered. We use a 'closed-box' scenario. The validity and limitations of such a treatment are addressed in Chapter 3 . The prime parameters are summarized in the following.

- Three different possible prescriptions for the stellar yields of SNe are implemented. For calculations in this Chapter we only use the models adapted to stellar evolution models by Eldridge et al. (2008) (referred to 'EIT08M'). The stellar yields for AGB stars are taken from van den Hoek & Groenewegen (1997).

- The amount of dust produced by SNe and AGB stars is calculated using the dust formation efficiencies derived in Chapter 2. For SNe three different efficiency limits are determined, i.e. a 'maximal' SN efficiency, a 'high' SN efficiency and a 'low' SN efficiency. The 'maximal' SN efficiency originates from theoretical SN dust formation models. Dust destruction in reverse shock interaction has been applied to the 'maximal' SN efficiency to obtain the 'high' SN efficiency. The low SN efficiency is based on SN dust yields inferred from observations.

- We differentiate between five different IMFs. These are a Salpeter (1955) IMF, a top-heavy and a mass-heavy IMF as well as IMFs (Larson 1998) with characteristic masses of either m_{ch} = 0.35 (Larson 1) or m_{ch} = 10 (Larson 2).

- Dust destruction in the ISM is implemented in terms of the mass of ISM material, M_{cl}, swept up by a single SN shock and cleared of the containing dust.

For calculations in this Chapter most parameters have the same settings as defined in Chapter 3 . The SMBH growth is considered with a shorter growth timescale and calculations are performed with higher initial SFRs. For the SN yields we only consider the case of EIT08M. The parameters which differ from those used in Chapter 3 are listed in Table 4.1.

4.3 RESULTS

In this section we present the results of models calculated within short timescales after the starburst.

A short enrichment timescale of a few times 10^7 yr for an intense starburst with a SFR of $\sim 3 \times 10^3$ $\mathrm{M}_{\odot}$ yr^{-1} has been proposed by e.g., Bertoldi et al. (2003a), Walter et al. (2004), Dwek et al. (2007), Riechers et al. (2009). Owing to this suggestion we are interested in whether the observed large dust masses in excess of 10^8 $\mathrm{M}_{\odot}$ can be

Table 4.1: *Model parameters*

Parameters	Value	Unit	Description
$\psi_{\rm ini}$	$3 \times 10^3, 1 \times 10^4$	$\mathrm{M}_\odot\ \mathrm{yr}^{-1}$	Star formation rate
$M_{\rm SMBH}$	3×10^9	$\mathrm{M}_\odot$	Mass of the SMBH
$t_{\rm SMBH}$	1×10^8	yr	Growth timscale for the SMBH

reached within 100 Myr. Consequently we performed calculations with an initial SFR for the starburst with $\psi_{\rm ini} = 3 \times 10^3\ \mathrm{M}_\odot\ \mathrm{yr}^{-1}$ for galaxies with initial gas masses $M_{\rm ini} = 5 \times 10^{10}\ \mathrm{M}_\odot$, $M_{\rm ini} = 1 \times 10^{11}\ \mathrm{M}_\odot$, $M_{\rm ini} = 3 \times 10^{11}\ \mathrm{M}_\odot$ and $M_{\rm ini} = 5 \times 10^{11}\ \mathrm{M}_\odot$. For the most massive system with $M_{\rm ini} = 1.3 \times 10^{12}\ \mathrm{M}_\odot$ an initial SFR $\psi_{\rm ini} = 1 \times 10^4\ \mathrm{M}_\odot\ \mathrm{yr}^{-1}$ is adopted. We included the results with a lower initial SFR of $10^3\ \mathrm{M}_\odot\ \mathrm{yr}^{-1}$ of those models computed in Chapter 3 for comparison.

In Chapter 3 we analyzed the evolution of the amount of dust and various physical properties and found that these are strongly dependent on the mass of the galaxy. Moreover, for a given initial SFR all quantities evolve faster in less massive galaxies. We identified the shortest epoch, where some model results are in accordance with observations as 30 Myr. We perform detailed comparison between model results and observed values of the total dust mass, $M_{\rm d}$, the stellar mass, M_*, the SFR, ψ, and the metallicity, Z. We also discuss the possible amount of molecular hydrogen.

4.3.1 Dust and stellar mass

In Fig. 4.1 we present the results for the mass of dust versus the stellar mass for galaxies with different initial gas masses and initial SFRs at an epoch of 30 Myr. The displayed models are computed for a 'maximal' SN efficiency (top row) and a high SN efficiency (bottom row). Dust destruction in the ISM is considered for values of $M_{\rm cl} = 800\ \mathrm{M}_\odot$ (left column), $M_{\rm cl} = 100\ \mathrm{M}_\odot$ (middel panel) and $M_{\rm cl} = 0$ (right panel).

The dark grey region represents the mass ranges of the stellar mass and dust mass derived from observations of QSOs at $z > 6$. The lower and upper limits of the stellar mass are estimated by subtracting the molecular gas masses, $M_{\rm H_2}$ from the total dynamical masses, $M_{\rm dyn}$. Values for $M_{\rm dyn}$ and $M_{\rm H_2}$ are based on data from Wang et al. (2010, and references therein) for three QSOs at $z > 6$. For an estimation of $M_{\rm dyn}$ an inclination angle $i = 65^\circ$ of the gas disk is taken for QSO J1148+5251 (Walter et al. 2004), while $i = 40^\circ$ similar to Wang et al. (2010) is applied to the remaining two QSOs. We adopt the lower and upper limits for the dust masses from Beelen et al. (2006) and Michałowski et al. (2010b). The light grey region covers the range of derived stellar masses and dust masses from observations of QSOs > 5 (Wang et al. 2010; Michałowski

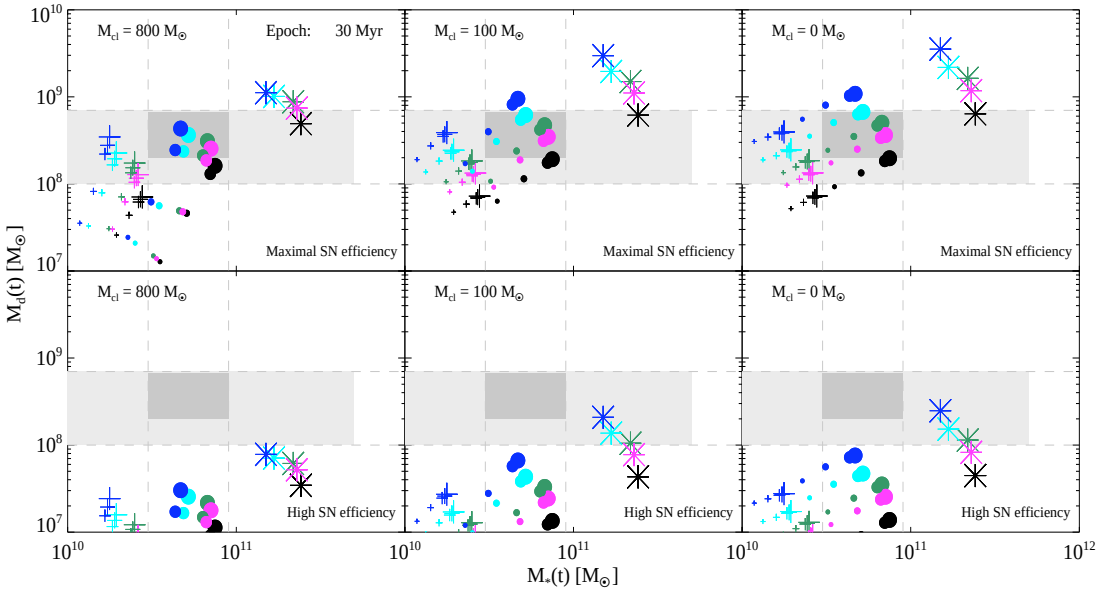

Figure 4.1: *Relation between dust mass and stellar mass at an epoch of 30 Myr for various initial gas masses and IMFs. Calculations are performed for a 'maximal' SN dust production efficiency (top row) and a high SN dust production efficiency (bottom row). Dust destruction in the ISM is considered for a $M_{\rm cl}$ = 800 $\rm M_\odot$ (left column), $M_{\rm cl}$ = 100 $\rm M_\odot$ (middle column) and $M_{\rm cl}$ = 0 (right column). The colored symbols are obtained for different initial gas masses, $M_{\rm ini}$, SFRs and IMFs. The size of the symbols is scaled by $M_{\rm ini}$. The crosses correspond to calculations for a initial SFR $\psi_{\rm ini}$ = 10^3 $\rm M_\odot$ yr^{-1}, the filled circles to $\psi_{\rm ini}$ = 3 × 10^3 $\rm M_\odot$ yr^{-1} and the stars to $\psi_{\rm ini}$ = 10^4 $\rm M_\odot$ yr^{-1}. The black, green, cyan, magenta and blue colors denote the Salpeter, mass-heavy, top-heavy, Larson 1 and Larson 2 IMF, respectively. The dark grey region indicates the mass range of stellar masses and dust masses derived from observations of QSOs at $z > 6$. The vertical dashed lines represent the lower and upper limits of the observed stellar masses. The light grey area illustrates the whole mass ranges derived from observations of QSOs > 5 and accounts for uncertainties of the derived quantities. The horizontal dashed lines mark the lower and upper mass limit of the derived dust masses.*

et al. 2010b). The boundaries for the stellar masses are estimated similar to the QSOs at $z > 6$ (with $i = 40°$ for deriving $M_{\rm dyn}$). We set the lower dust limit to 10^8 $\rm M_\odot$ to account for the uncertainties of derived dust masses from observations.

Despite the short time span of 30 Myr, it is evident that most models are within the plausible mass ranges illustrated by the light and dark grey regions. This signifies a rapid build-up of a large amount of dust, provided SNe are highly efficient dust producers. For galaxies with $M_{\rm ini}$ = 1–5 × 10^{11} $\rm M_\odot$ all models with an initial SFR of 3 × 10^3 $\rm M_\odot$ $\rm yr^{-1}$ are in agreement with the observed values for the stellar masses for QSOs at $z > 6$. The requirements for $M_{\rm d}$ are best accomplished with either a top-heavy, mass-heavy or Larson 1 IMF for both values of $M_{\rm cl}$. In a galaxy with $M_{\rm ini}$ = 1 × 10^{11} $\rm M_\odot$ the amount of dust reached with a Larson 2 IMF and $M_{\rm cl}$ = 100 $\rm M_\odot$ also matches with the

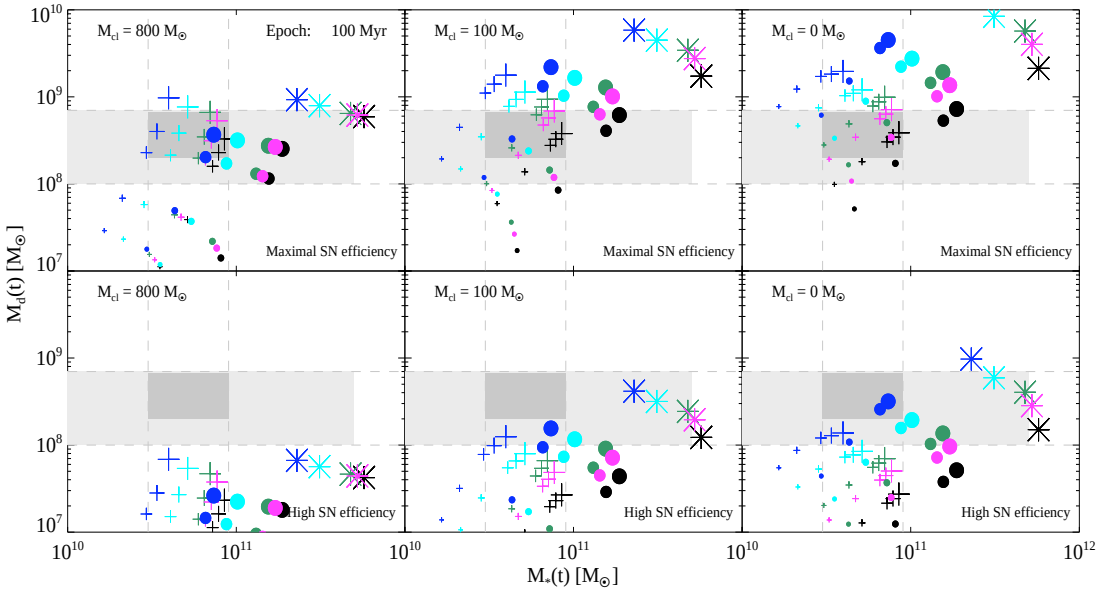

Figure 4.2: *Relation between dust mass and stellar mass at an epoch of 100 Myr for various initial gas masses and IMFs. Calculations are performed for a 'maximal' SN dust production efficiency (top row) and a high SN dust production efficiency (bottom row). Dust destruction in the ISM is considered for a $M_{\rm cl}$ = 800 $\rm M_\odot$ (left column), $M_{\rm cl}$ = 100 $\rm M_\odot$ (middle column) and $M_{\rm cl}$ = 0 (right column). The colored symbols are obtained for different initial gas masses, $M_{\rm ini}$, SFRs and IMFs. The size of the symbols is scaled by $M_{\rm ini}$. The crosses correspond to calculations for a initial SFR $\psi_{\rm ini}$ = 10^3 $\rm M_\odot$ yr^{-1}, the filled circles to $\psi_{\rm ini}$ = 3 × 10^3 $\rm M_\odot$ yr^{-1} and the stars to $\psi_{\rm ini}$ = 10^4 $\rm M_\odot$ yr^{-1}. The black, green, cyan, magenta and blue colors denote the Salpeter, mass-heavy, top-heavy, Larson 1 and Larson 2 IMF, respectively. The dark grey region indicates the mass range of stellar masses and dust masses derived from observations of QSOs at $z > 6$. The vertical dashed lines represent the lower and upper limits of the observed stellar masses. The light grey area illustrates the whole mass ranges derived from observations of QSOs > 5 and accounts for uncertainties of the derived quantities. The horizontal dashed lines mark the lower and upper mass limit of the derived dust masses.*

dark grey region. Models for either a high or low SN efficiency did not quite reach 10^8 $\rm M_\odot$ of dust. Only in the most massive galaxy ($M_{\rm ini}$ = 1.3 × 10^{12} $\rm M_\odot$) and for top-heavy IMFs with a high SN efficiency an amount of dust $> 10^8$ $\rm M_\odot$ is obtained.

In Fig. 4.2 we illustrate the results for dust and stellar masses at an epoch of 100 Myr. We present models for a maximal SN efficiency (top row) and a high SN efficiency (bottom row), while dust destruction in the ISM is considered for a $M_{\rm cl}$ = 800 $\rm M_\odot$ (left column), $M_{\rm cl}$ = 100 $\rm M_\odot$ (middle column) and $M_{\rm cl}$ = 0 (right column). We carried out calculations for a low SN efficiency, but the obtained dust masses of these models remained below 10^8 $\rm M_\odot$.

Independent of the IMF it is evident that M_* is consistently shifted towards higher masses for models with an initially higher SFR. It is interesting to note that in the less

massive galaxies (0.5–1 $\times$ 10^{11} $M_\odot$) dust masses obtained for the higher initial SFR ($\psi_{\rm ini}$ = 3 $\times$ 10^3 $M_\odot$ yr^{-1}) are lower than dust masses obtained for the lower SFR ($\psi_{\rm ini}$ = 10^3 $M_\odot$ yr^{-1}). Moreover, in these galaxies the amount of dust reached at an epoch of 30 Myr (see Fig. 4.1) and for $M_{\rm cl}$ = 100–800 $M_\odot$ is also higher than that seen at the epoch of 100 Myr for same $M_{\rm cl}$.

We find that the stellar masses for models with an initial SFR $\psi_{\rm ini}$ = 1–3 $\times$ 10^3 $M_\odot$ yr^{-1} are within the observed region for $z > 5$ QSOs. For some models with $\psi_{\rm ini}$ = 3 $\times$ 10^3 $M_\odot$ yr^{-1}, stellar masses are identified within the mass range for $z > 6$ QSOs. The systems involved are with either $M_{\rm ini}$ = 0.5–1 $\times$ 10^{11} $M_\odot$ (all IMFs) or with $M_{\rm ini}$ = 3–5 $\times$ 10^{11} $M_\odot$ and top heavy IMFs. Stellar masses within the dark grey area are also found with $\psi_{\rm ini}$ = 10^3 $M_\odot$ yr^{-1} for galaxies with either $M_{\rm ini}$ = 3–13 $\times$ 10^{11} $M_\odot$ and top heavy IMFs or for the less massive galaxies in combination with the IMFs favoring low mass stars.

In the case of $M_{\rm cl}$ = 800 $M_\odot$ and for a 'maximal' SN efficiency most models with $M_{\rm ini}$ = 3–13 $\times$ 10^{11} $M_\odot$ and $\psi_{\rm ini}$ = 10^3 $M_\odot$ yr^{-1} fit within the dark grey region. However for the higher initial SFR $M_{\rm d}$ is within or close to this zone only for galaxies with $M_{\rm ini}$ = 3–5 $\times$ 10^{11} $M_\odot$ and top-heavy IMFs. For $M_{\rm cl}$ = 100 $M_\odot$ and a maximal SN efficiency the dust mass obtained in a galaxy with $M_{\rm ini}$ = 1 $\times$ 10^{11} $M_\odot$, $\psi_{\rm ini}$ = 3 $\times$ 10^3 $M_\odot$ yr^{-1} and for top-heavy IMFs is in agreement with observations, while the dust masses in the more massive galaxies for some IMFs and SFRs are higher than required. In the case of no dust destruction the dust masses reached for some IMFs and SFRs are able to match within the dark grey area also in the least massive galaxy.

We find that in case of a 'high' SN efficiency and for $\psi_{\rm ini}$ = 3 $\times$ 10^3 $M_\odot$ yr^{-1} in galaxies with initial masses 3–5 $\times$ 10^{11} $M_\odot$ and top-heavy IMFs high dust masses are possible, even if dust destruction is included (i.e., $M_{\rm cl}$ = 0–100 $M_\odot$).

4.3.2 METALLICITY AND SFR

We next present the obtained metallicities and SFRs which correspond to the models previously discussed.

Fig. 4.3 depicts the metallicity versus SFR at epochs of 30 Myr (left panel) and 100 Myr (right panel). With respect to observations of QSOs $>$ (5) 6 we marked the range of derived values as a dark grey zone. The lower and upper limits of the SFR are based on observations by Bertoldi et al. (2003a) and Wang et al. (2010). Despite the fact that the metallicity is not precisely determined, we set the lower limit at solar metallicity and the upper limit at 5 $Z_\odot$. This is based on the inferred solar or supersolar metallicities in high-z QSOs (e.g., Barth et al. 2003; Dietrich et al. 2003; Fan et al. 2003; Freudling et al. 2003; Maiolino et al. 2003; Di Matteo et al. 2004; Becker et al. 2006; Juarez et al. 2009). We note that there are no strong constraints on the upper limit and therefore the zone above 5 $Z_\odot$ is marked as light grey shaded region to account for the uncertainty.

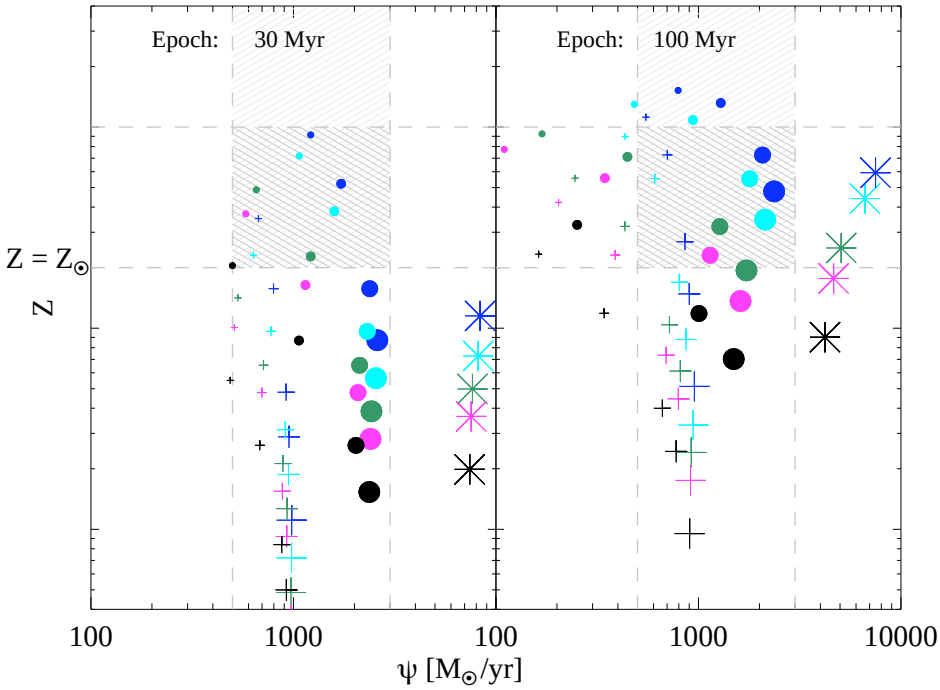

Figure 4.3: *Relation between metallicity and SFR at epochs of 30 Myr (left panel) and 100 Myr (right panel). The colored symbols are obtained for different initial gas masses, $M_{\rm ini}$, SFRs and IMFs. The size of the symbols is scaled by $M_{\rm ini}$. The crosses correspond to calculations for a initial SFR $\psi_{\rm ini}$ = 10^3 $\rm M_\odot$ yr^{-1}, the filled circles to $\psi_{\rm ini}$ = 3 $\times$ 10^3 $\rm M_\odot$ yr^{-1} and the stars to $\psi_{\rm ini}$ = 10^4 $\rm M_\odot$ yr^{-1}. The black, green, cyan, magenta and blue colors denote the Salpeter, mass-heavy, top-heavy, Larson 1 and Larson 2 IMF, respectively. The dark grey shaded region indicates the range of the metallicity and SFR based on observations of QSOs at $z > 6$. The vertical dashed lines represent the lower and upper limits of the observationally derived SFRs. The light grey shaded area accounts for the uncertainty of the upper limit of the metallicity. The horizontal dashed lines mark the lower and possibly upper limit of the metallicity.*

We find that at an epoch of 30 Myr high metallicities in the less massive galaxies are already reached. The best result is attained by a system with $M_{\rm ini}$ = 1 $\times$ 10^{11} $\rm M_\odot$, $\psi_{\rm ini}$ = 3 $\times$ 10^3 $\rm M_\odot$ $\rm yr^{-1}$ and IMFs biased towards higher masses. In a galaxy with $M_{\rm ini}$ = 5 $\times$ 10^{10} $\rm M_\odot$ and for either all models with the same initial SFR or models with the lower SFR and top-heavy IMFs are within the dark grey shaded region as well.

At an epoch of 100 Myr the metallicity has increased in all models, while the SFR in the less massive galaxies has significantly decreased. The models for $M_{\rm ini}$ = 3–5 $\times$ 10^{11} $\rm M_\odot$, $\psi_{\rm ini}$ = 3 $\times$ 10^3 $\rm M_\odot$ $\rm yr^{-1}$ and top heavy IMFs constitute the best results. In galaxies with $M_{\rm ini}$ = 3 $\times$ 10^{11} $\rm M_\odot$, the same initial SFR and either a mass-heavy or Larson 1 IMF the obtained values for Z and $\psi(t)$ are also in agreement with the observed values. The metallicities in the low mass galaxies which give the best match at 30 Myr are now shifted above the upper limit, while the SFRs remain in the observed range. The models for a galaxy with $M_{\rm ini}$ = 1 $\times$ 10^{11} $\rm M_\odot$, a lower initial SFR of 10^3 $\rm M_\odot$ $\rm yr^{-1}$ and top-heavy

IMFs at this epoch (100 Myr) reach sufficiently high metallicities, while high enough SFRs are sustained.

4.3.3 H_2 MASS IN QSOs

The molecular gas mass in a galaxy is another quantity which we consult to evaluate the calculated models in order to ascertain the most likely scenario for dust production and evolution in high-z galaxies.

Observational status

Detections of high excitation CO line emission in QSOs at $z >$ (5) 6 indicate the presence of 0.7–2.5 $\times$ 10^{10} $M_\odot$ of molecular hydrogen (e.g., Bertoldi et al. 2003b; Walter et al. 2003, 2004; Riechers et al. 2009; Wang et al. 2010). This molecular gas mass is derived from the relation $M_{H_2} = \alpha \times L'_{CO(1-0)}$, where α is the conversion factor between the low excitation CO J = 1–0 line luminosity $L'_{CO(1-0)}$ and M_{H_2}.

For spiral galaxies the conversion factor α is typically $\sim$ 4.6 $M_\odot$ (K km s^{-1} pc^2)$^{-1}$ (e.g., Solomon & Barrett 1991), while for the center of nearby ultra luminous starburst galaxies a conversion factor of α = 0.8-1 $M_\odot$ (K km s^{-1} pc^2)$^{-1}$ is found to be appropriate (e.g., Downes & Solomon 1998). This latter value of α is usually used to infer M_{H_2} i.e., in high-z QSOs (e.g., Bertoldi et al. 2003b; Walter et al. 2003; Wang et al. 2010), high-z ($z > 6.5$) Lyman-α emitters (Wagg et al. 2009), Ultra Luminous Infrared Galaxies (ULIRGs) (Yan et al. 2010) or for high-z SMGs (Tecza et al. 2004; Greve et al. 2005).

Due to the fact that the CO (1→0) line flux at very high-z is unobservable with ground based observational methods, the line flux of the higher transitions, e.g., CO (3→2), CO (5→4), CO (6→5) or CO (7→6) have been observed instead (e.g., Bertoldi et al. 2003b; Walter et al. 2003; Carilli et al. 2007; Wang et al. 2010). From the measured line flux at any of these transitions the line luminosity is calculated according to Solomon et al. (e.g., 1992) as $L'_{CO} = (c^2/2k) S_{CO} \Delta v \nu_{obs}^{-2} D_L^2 (1+z)^{-3}$ K km s^{-1} pc^2)$^{-1}$, where D_L is the luminosity distance (dependent on the used cosmological model, see also Sect. 1.3.1) and $S_{CO}\Delta v$ is the velocity-integrated CO line flux for a given transition.

However α is not well known in the case of such very high excitations and $L'_{CO(1-0)}$ needs to be inferred from the luminosities of the higher transitions. This for example is accomplished by extrapolating L'_{CO} to the $L'_{CO(1-0)}$ (e.g., Bertoldi et al. 2003b) assuming a constant line brightness temperature from J = 1 to the highest stage. Another possibility is to apply line ratios between the higher excitation and the CO (1→0) transition which have been determined from CO transition large velocity gradient (LVG) modeling (e.g., Scoville & Solomon 1974; Papadopoulos et al. 2000; Weiß et al. 2007; Riechers et al. 2009; Wang et al. 2010). From the LVG modeling predictions about the kinetic gas temperature T_{kin} and gas density $n(H_2)$ are obtained. The main parameters entering LVG models are the CO abundance per velocity gradient with a typically as-

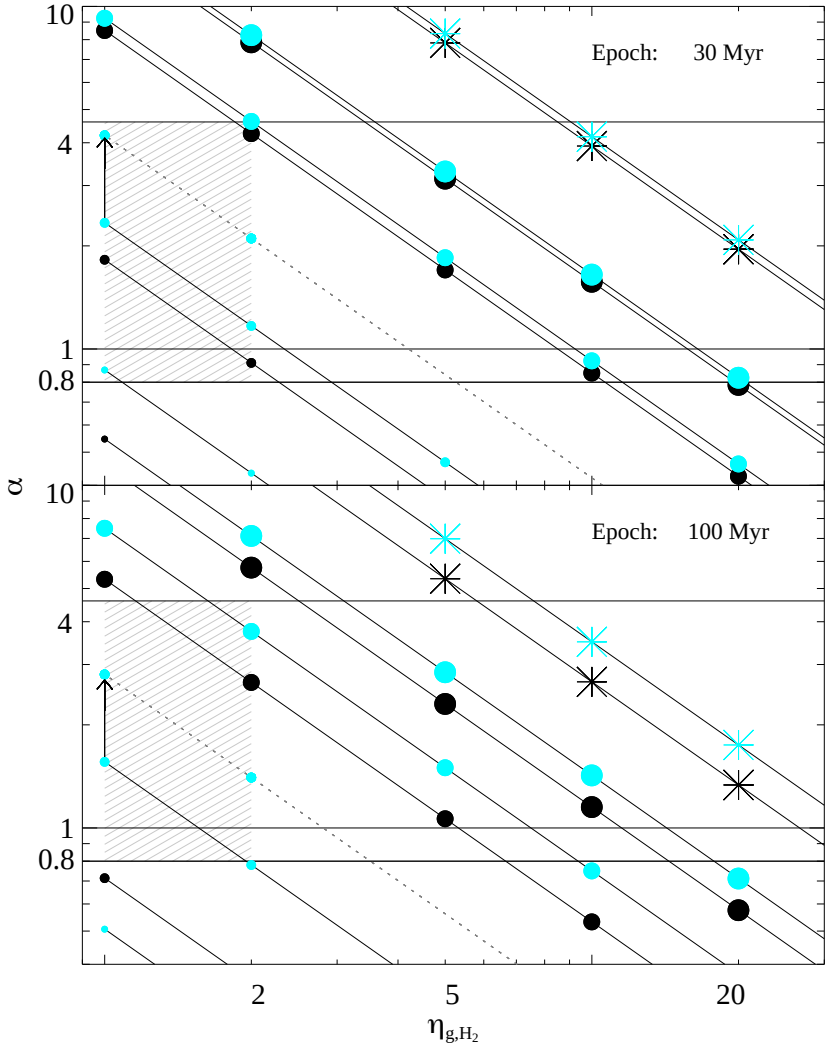

Figure 4.4: *CO conversion factor versus gas-to-H_2 ratio at epochs 30 Myr (top panel) and 100 Myr (bottom panel). The lines with colored symbols signify the values for the CO conversion factor α as a function of the gas-to-H_2 ratio $\eta_{\mathrm{g,H_2}}$ obtained for different initial gas masses, M_{ini}, and different IMFs. The solid lines with symbols correspond to calculations of α for a CO line luminosity of $L'_{\mathrm{CO(1-0)}}$ = 2.7 $\times$ 10^{10} K km s^{-1} pc^2. The dotted line with filled circles represents a calculation of α for a galaxy with M_{ini} = 1 $\times$ 10^{11} $\mathrm{M}_\odot$ and a lower CO line luminosity of $L'_{\mathrm{CO(1-0)}}$ = 1.5 $\times$ 10^{10} K km s^{-1} pc^2. The arrow visualizes the difference of α between the higher and lower value of $L'_{\mathrm{CO(1-0)}}$ for the same model. The size of the symbols is scaled by M_{ini}. The filled circles correspond to a ψ_{ini} = 3 $\times$ 10^3 $\mathrm{M}_\odot$ yr^{-1} and the stars to a ψ_{ini} = 10^4 $\mathrm{M}_\odot$ yr^{-1}. The black and cyan colors denote the Salpeter and top-heavy IMF, respectively. The grey shaded region signifies the possible range of α and $\eta_{\mathrm{g,H_2}}$. The horizontal black solid lines mark the values of α = 0.8 $\mathrm{M}_\odot$ (K km s^{-1} pc^2)$^{-1}$ and α = 1 $\mathrm{M}_\odot$ (K km s^{-1} pc^2)$^{-1}$.*

sumed value of [CO]/Δv = 1 $\times$ 10^{-5} pc (km s^{-1})$^{-1}$ (e.g., Weiß et al. 2005, 2007; Riechers et al. 2006), the CO collision rates (usually taken from Flower 2001) and a used ortho-to-para ratio of 3. Apart from the choice of either a spherical single component model or a two component gas model (including a lower and higher excitation gas component), possible uncertainties are given by the CO disk radius which can be obtained from observations. Typical values derived or applied are for example $L'_{\rm CO(6-5)}/L'_{\rm CO(1-0)} \sim$ 0.78, $L'_{\rm CO(5-4)}/L'_{\rm CO(1-0)} \sim 0.88$ (e.g., Riechers et al. 2009) and $L'_{\rm CO(3-2)}/L'_{\rm CO(1-0)} \sim 0.65$ (e.g., Devereux et al. 1994).

CO conversion factor versus gas-to-H_2 ratio

In our models we cannot calculate $M_{\rm H_2}$ directly. However, we have computed the total (H + He) gas mass $M_{\rm G}$ which is remaining in the galaxies at a given epoch. The molecular gas mass constitutes a certain fraction of the total gas mass, $M_{\rm G}$. Hence we introduce the gas-to-H_2 mass ratio as $\eta_{\rm g,H_2} = M_{\rm G}/M_{\rm H_2}$. The CO conversion factor can thereby be expressed as a function of $\eta_{\rm g,H_2}$ as

$$\alpha = \frac{M_{\rm G}}{\eta_{\rm g,H_2}\, L'_{\rm CO(1-0)}}. \tag{4.1}$$

while $\eta_{\rm g,H_2} \geq 1$. In ULIRGs and SMGs a major fraction of the gas is believed to exist in form of molecular hydrogen (e.g., Sanders & Mirabel 1996). A value for $\eta_{\rm g,H_2}$ of ~ 1 for example has also been found for the z = 3 radio galaxy B3 J2330+3927 (De Breuck et al. 2003). This might also be the case for QSOs and would imply a gas-to-H_2 ratio between 1 and 2.

In Fig. 4.4 we show the results for α as a function of $\eta_{\rm g,H_2}$ for an initial SFR $\psi_{\rm ini}$ = 3 $\times$ 10^3 M$_\odot$ yr^{-1} and two different epochs; 30 Myr (top panel) and 100 Myr (bottom panel). The IMFs involved are the top-heavy IMF and the Salpeter IMF. We adopt a CO line luminosity $L'_{\rm CO(1-0)}$ = 2.7 $\times$ 10^{10} K km s^{-1} pc^2, which is based on the derived values of J1148+5251 (Bertoldi et al. 2003b; Walter et al. 2003; Wang et al. 2010). In two of the three QSOs in the sample of Wang et al. (2010) a lower $L'_{\rm CO(1-0)}$ = 1.5 $\times$ 10^{10} K km s^{-1} pc^2 has been derived. Calculations for this $L'_{\rm CO(1-0)}$ are performed to investigate the effect of a lower $L'_{\rm CO(1-0)}$ on the resulting α and $\eta_{\rm g,H_2}$. Results are visualized as dashed line for a galaxy with $M_{\rm ini}$ = 1 $\times$ 10^{11} M$_\odot$. The grey shaded area signifies a possible range for α and $\eta_{\rm g,H_2}$ as discussed above.

It is evident that regardless of the epoch and for a fixed value of α the gas-to-H_2 ratio increases with increasing mass of the galaxy. Conversely, for a fixed $\eta_{\rm g,H_2}$, α increases with increasing $M_{\rm ini}$. The maximum value of α is obtained for $\eta_{\rm g,H_2}$ = 1 i.e., $M_{\rm G} \equiv M_{\rm H_2}$. We find that at both epochs, the maximum value of α for the less massive galaxies is lower than $\sim$ 4.6 M$_\odot$ (K km s^{-1} pc^2)$^{-1}$. It is also evident that either α or $\eta_{\rm g,H_2}$ for a given $M_{\rm ini}$ are lower at later epochs, but also for higher $L'_{\rm CO(1-0)}$.

At an epoch of 30 Myr the values for α and $\eta_{\mathrm{g,H_2}}$ are similar for all IMFs and galaxies with $M_{\mathrm{ini}} > 1 \times 10^{11}$ $\mathrm{M}_\odot$, while the difference becomes larger with decreasing M_{ini}. Feasible values of α and $\eta_{\mathrm{g,H_2}}$ are possible for galaxies with $M_{\mathrm{ini}} = 1 \times 10^{11}$ $\mathrm{M}_\odot$ and the higher value of $L'_{\mathrm{CO}(1-0)}$. For top-heavy IMFs $\eta_{\mathrm{g,H_2}} = 1$ results in a maximum α of ~ 2.3 $\mathrm{M}_\odot$ (K km s^{-1} pc^2)$^{-1}$, while for $\alpha = 0.8$ $\mathrm{M}_\odot$ (K km s^{-1} pc^2)$^{-1}$, the fraction of molecular hydrogen is about one third of the total gas mass. The least massive system with $M_{\mathrm{ini}} = 5 \times 10^{10}$ $\mathrm{M}_\odot$ is at this epoch already significantly exhausted. For a top-heavy IMF $\alpha \approx 0.8$ $\mathrm{M}_\odot$ (K km s^{-1} pc^2)$^{-1}$ presupposes that all the gas in the system is in the form of molecular hydrogen. In any other case of $\eta_{\mathrm{g,H_2}}$ a lower value for α is obtained, implying also lower $M_{\mathrm{H_2}}$. In more massive systems with $M_{\mathrm{ini}} = 1$–3×10^{11} $\mathrm{M}_\odot$, $\alpha \approx 0.8$–1 $\mathrm{M}_\odot$ (K km s^{-1} pc^2)$^{-1}$ presumes that the molecular hydrogen constitutes only a small fraction of about 1/10–1/20 of the total gas mass.

Applying the lower CO line luminosity $L'_{\mathrm{CO}(1-0)} = 1.5 \times 10^{10}$ K km s^{-1} pc^2 leads to a shift of α to higher values for a given $\eta_{\mathrm{g,H_2}}$, but also corresponds to a lower $\mathrm{H_2}$ mass. This is demonstrated for the system with $M_{\mathrm{ini}} = 1 \times 10^{11}$ $\mathrm{M}_\odot$ and top-heavy IMF (dashed line), where the arrow signifies the amount of the increase of α.

At an epoch of 100 Myr a clear separation between the IMFs is noticeable. For a Salpeter IMF the galaxies underwent a stronger gas exhaustion than for a top-heavy IMF, which is more significant for the less massive galaxies. Similar to the epoch at 30 Myr the system with $M_{\mathrm{ini}} = 1 \times 10^{11}$ $\mathrm{M}_\odot$ and top-heavy IMF is plausible, i.e., for $\alpha \sim 0.8$ $\mathrm{M}_\odot$ (K km s^{-1} pc^2)$^{-1}$ the gas-to-$\mathrm{H_2}$ ratio $\eta_{\mathrm{g,H_2}} = 2$. For the galaxies with $M_{\mathrm{ini}} = 3$–5×10^{11} $\mathrm{M}_\odot$ and top-heavy IMF we obtain $\alpha = 1.4$–1.5 for a corresponding gas-to-$\mathrm{H_2}$ ratio $\eta_{\mathrm{g,H_2}} = 5$–$10$, resulting in a molecular mass of $M_{\mathrm{H_2}} \sim 3.7 \times 10^{10}$ $\mathrm{M}_\odot$. Alternatively, a higher value for α up to 4.6 results in a lower $\eta_{\mathrm{g,H_2}} = 2$–$4$. It is noteworthy that for the assumed CO line luminosity $L'_{\mathrm{CO}(1-0)} = 2.7 \times 10^{10}$ K km s^{-1} pc^2, $\alpha = 4.6$ $\mathrm{M}_\odot$ (K km s^{-1} pc^2)$^{-1}$ implies $M_{\mathrm{H_2}} = 1.2 \times 10^{11}$ $\mathrm{M}_\odot$. The presence of large amounts of cold and low-excited molecular gas has been suggested by Papadopoulos et al. (2001) for the QSO APM 08279+5255 at $z = 3.91$. The likelihood that such a high $M_{\mathrm{H_2}}$ could have been built up within a short timescale of 30–100 Myr however remains unclear.

4.4 Discussion

4.4.1 Individual QSOs at $z \gtrsim 6$

We ascertain plausible scenarios by comparing the model results discussed in Sect. 4.3 with the derived values from observations for certain quantities of individual QSOs listed in Table 4.2. The calculated values for diverse properties such as M_{d}, M_*, $M_{\mathrm{H_2}}$, metallicity and SFR from the models discussed below, which best match the QSOs, are listed in Table 4.3. The corresponding model parameters are presented in Table 4.4.

We find that at an epoch of 30 Myr the models with an initial mass of the galaxy of

Table 4.2: *Observed properties of quasars at $z \gtrsim 6$*

Object	z	$L'_{\rm CO(1-0)}$ 10^{10} K km s^{-1} pc^2	SFR $M_\odot$ yr^{-1}	$M_{\rm d}$ 10^8 $M_\odot$	$M_{\rm H_2}$ 10^{10} $M_\odot$	$M_{\rm dyn}\sin^2 i$ 10^{10} $M_\odot$	Ref.
J1148+5251	6.42	3.0 ± 0.3	2380	5.9 ± 0.7	2.4 / 3.7[a]	4.5	1,2,3,4
J1048+4637	6.23	1.2 ± 0.2	650	4.3 ± 0.6	1.0	4.5	1,2,3
J2054-0005	6.06	1.5 ± 0.3	1180	3.4 ± 0.8	1.2	4.2	5,2,3
J0840+5624	5.85	3.2 ± 0.4	1460	4.7 ± 0.9	2.5	24.2	6,2,3

References. (1) Fan et al. (2003); (2) Wang et al. (2010); (3) Michałowski et al. (2010b); (4) Walter et al. (2004); (5) Jiang et al. (2008); (6) Fan et al. (2006)

Notes. [a] $M_{\rm H_2} = 3.7 \times 10^{10}$ $M_\odot$ deduced from [C I] line detections by Riechers et al. (2009)

Table 4.3: *Calculated properties from the best matching models of $z \gtrsim 6$ QSOs from our sample*

Object[a,b]	SFR $M_\odot$ yr^{-1}	$M_{\rm d}$ 10^8 $M_\odot$	M_* 10^{10} $M_\odot$	Z $Z_\odot$	$\eta_{\rm g,H_2}$	α	$M_{\rm H_2}$ 10^{10} $M_\odot$
J1148+5251(A)	1600	3.1–5.1	3.5	2	3.0–1.0 / 1.7	0.8–2.3 / 1.4	2.16–6.2 / 3.7
J1148+5251(B)	1000	2.4–8.9	5.4	5	2.0–1.0	0.78–1.55	2.10–4.1
J1048+4637(A)	1000	2.4–8.9	5.4	5	3.4–1.0 / 2.0	0.8–2.8 / 1.4	1.2– 4.2 / 2.1
J1048+4637(B)	610	3.5	2.8	3.4	5.8–1.0 / 2.0	0.8–4.5 / 2.2	1.2–6.7 / 3.3
J2054-0005	1150	2.7	4.7	4.4	3.0–1.0 / 2.0	0.8–3.2 / 1.6	1.2– 4.8 / 2.4
J0840+5624(A)	1500	2.1	11.0	4	7.0–1.2 / 2.0	0.8–4.6 / 2.7	2.5–14.7 / 8.6
J0840+5624(B)	1400	4.8	20.0	5	10–1.8 / 2.0	0.8–4.6 / 4.2	2.5–14.7 / 13.4

Notes. [a]All models are calculated for a top-heavy IMF. [b]Capital letters in brackets (A,B) signify that different models (see corresponding models in Table 4.4) are applied for the same object

$M_{\rm ini} = 1 \times 10^{11}$ $M_\odot$, an initial SFR of $\psi_{\rm ini} = 3 \times 10^3$ $M_\odot$ yr^{-1} and either a Larson 2 IMF, a top-heavy or a mass-heavy IMF reproduce the observed quantities of some QSOs at $z > 6$ in the case for a 'maximal' SN efficiency.

In particular, the model with a top-heavy IMF is best applicable to the QSO J1148+5251. The amount of dust reached is between 3.1–5.1 $\times 10^8$ $M_\odot$ for dust destruction in the ISM with $M_{\rm cl}$ = 100–0 $M_\odot$, while a 'maximal' SN efficiency is required. A stellar mass of $M_* \sim 3.5 \times 10^{10}$ $M_\odot$ is obtained. The metallicity in the system is ~ 2 $Z_\odot$ and a SFR of ~ 1600 $M_\odot$ yr^{-1} could be sustained. This model is also favored given its values of α and $\eta_{\rm g,H_2}$. The higher H_2 mass of $M_{\rm H_2} = 3.7 \times 10^{10}$ $M_\odot$ derived by Riechers et al. (2009) leads to $\eta_{\rm g,H_2} < 2$ and $\alpha \sim 1.4$ $M_\odot$ (K km s^{-1} pc^2)$^{-1}$. However, such a galaxy with $M_{\rm ini} = 1 \times 10^{11}$ $M_\odot$ implies that the dynamical mass is larger than the derived $M_{\rm dyn}$ of $\sim 5.5 \times 10^{10}$ $M_\odot$ (for a $i = 65°$) by Walter et al. (2004). While none of the models for $M_{\rm ini} = 5 \times 10^{10}$ $M_\odot$, which was used by Dwek et al. (2007), can be applied, a lower inclination angle similar to what has been adopted for the other QSOs might be considered.

Table 4.4: *Models which match the observed properties of $z \gtrsim 6$ QSOs from our sample*

Object[a,b]	Epoch Myr	$M_{\rm ini}$ 10^{11} $M_\odot$	$\psi_{\rm ini}$ 10^3 $M_\odot$ yr^{-1}	SN efficiency	$M_{\rm cl}$ $M_\odot$
J1148+5251(A)	30	1	3	max	100–0
J1148+5251(B)	100	1	3	max	100–0
J1048+4637(A)	100	1	3	max	100–0
J1048+4637(B)	100	1	1	max	100–0
J2054-0005	70	1	3	max	100
J0840+5624(A)	170	3	3	high	100–0
J0840+5624(B)	400	5	3	high	100–0

Notes. [a]All models are calculated with a top-heavy IMF. [b]Capital letters in brackets signify that different models (A,B) are applicable for the same object

Another possible fit to the properties of J1148+5251 is achieved by the same constellation of $M_{\rm ini}$, $\psi_{\rm ini}$ and IMF at an epoch of 100 Myr. The calculated stellar mass is within the estimated range from observations and the dust mass is $\sim$ 2.4–8.9 $\times$ 10^8 $M_\odot$, depending on $M_{\rm cl}$. However, the SFR dropped to $\sim$ 1000 $M_\odot$ yr^{-1}, while the metallicity increased to $\sim$ 5 $Z_\odot$. In view of the lower SFR reached by these models at both epochs than suggested by observations, a higher initial SFR than the 3 $\times$ 10^3 $M_\odot$ yr^{-1} might be conceivable. In Fig. 4.3 one notices that a longer evolution with the same (or lower) initial SFR as used here does not lead to a better agreement with observations, since this denotes an even lower SFR and higher metallicity.

In view of this we find that this scenario at an epoch of 100 Myr is more appropriate for the QSOs J1048+4637 (Fan et al. 2003) at z = 6.23 and J2054-0005 (Jiang et al. 2008) at z = 6.06. For the latter QSO a fine tuning of the epoch to 70 Myr results in a better fit. At this epoch we obtain a SFR of 1150 $M_\odot$ yr^{-1} and a metallicity of $\sim$ 4.4 $Z_\odot$. The amount of dust is $M_{\rm d} \sim 2.7 \times 10^8$ $M_\odot$ (for $M_{\rm cl}$ = 100 $M_\odot$), while the stellar mass is of $M_* \sim 4.7 \times 10^{10}$ $M_\odot$. The lower derived $L'_{\rm CO(1-0)}$ leads to $\eta_{\rm g,H_2} \sim$ 3–4 in case α = 0.8–1 $M_\odot$ (K km s^{-1} pc^2)$^{-1}$ is applied, while for $\eta_{\rm g,H_2} \sim 2$ a value for α of $\sim$ 1.6 would be required. For the QSO J1048+4637 the model for a lower initial SFR of $\psi_{\rm ini}$ = 10^3 $M_\odot$ yr^{-1} might be an option. The SFR is $\sim$ 610 $M_\odot$ yr^{-1} and the metallicity is $\sim$ 3.4 $Z_\odot$. While the stellar mass remains low, $M_* \sim 2.8 \times 10^{10}$ $M_\odot$, a dust mass of $M_{\rm d} \sim 3.5 \times 10^8$ $M_\odot$ is obtained for a 'maximal' SN efficiency and moderate dust destruction in the ISM. However, for α = 0.8–1 $M_\odot$ (K km s^{-1} pc^2)$^{-1}$ the gas-to-H_2 ratio is $\sim$ 5–6, since for the lower initial SFR the system at this epoch is less exhausted. At either the same or later epoch the more massive galaxies with $M_{\rm ini}$ = 3–5 $\times$ 10^{11} $M_\odot$, an initial SFR of $\psi_{\rm ini}$ = 3 $\times$ 10^3 $M_\odot$ yr^{-1} and IMFs biased towards higher stellar masses are applicable to some $z \sim 6$ QSOs. The stellar mass, metallicity and SFR of these systems are in agreement with observations, while either top-heavy IMFs or a mass-heavy IMF lead to the best results. The amount

of dust can be produced by SNe with a high SN efficiency and $M_{\rm cl} \leq 100$ M$_\odot$, although the dust masses reached are at the lower limit.

At an epoch of 170 Myr the system with $M_{\rm ini} = 3 \times 10^{11}$ M$_\odot$ is plausible for the QSO J0840+5624 (Fan et al. 2006) at $z = 5.85$, if an inclination angle higher than the assumed 40° is assumed. The SFR is ~ 1500 M$_\odot$ yr^{-1} and the metallicity is ~ 4 Z$_\odot$. The stellar mass is around 1.1×10^{11} M$_\odot$. The amount of dust obtained with a high SN efficiency is 2.1×10^8 M$_\odot$, while with the 'maximal' SN efficiency the dust mass exceeds a few times 10^9 M$_\odot$ (as already at an epoch of 100 Myr). However, for a $L'_{\rm CO(1-0)} = 3.2 \times 10^{10}$ K km s^{-1} pc^2 as derived for this QSO the gas-to-H$_2$ ratio of $\eta_{\rm g,H_2} \sim$ 5–7 for $\alpha = 0.8$–1 M$_\odot$ (K km s^{-1} pc^2)$^{-1}$ is higher than for the less massive galaxies. In case of a lower $\eta_{\rm g,H_2}$ of $\sim$ 2, $\alpha \sim 2.7$ M$_\odot$ (K km s^{-1} pc^2)$^{-1}$ is required. The larger galaxy with $M_{\rm ini} = 5 \times 10^{11}$ M$_\odot$, $\psi_{\rm ini} = 3 \times 10^3$ M$_\odot$ yr^{-1} and top heavy IMF can account for the observed quantities at an epoch of 400 Myr. The amount of dust reached with a 'high' SN efficiency is $\sim 4.8 \times 10^8$ M$_\odot$ and the SFR is ~ 1400 M$_\odot$ yr^{-1}. The metallicity and stellar mass are in agreement, but the fraction of $M_{\rm H_2}$ is around 1/10 for $\alpha = 0.8$ M$_\odot$ (K km s^{-1} pc^2)$^{-1}$, while $\alpha \sim 4$ M$_\odot$ (K km s^{-1} pc^2)$^{-1}$ is needed for $\eta_{\rm g,H_2}$ of ~ 2. A higher amount of $M_{\rm H_2}$ as denoted by the higher value of α in these massive galaxies might be possible. For example, the presence of large amounts of cold and low-excited molecular gas have been suggested by Papadopoulos et al. (2001) for the QSO APM 08279+5255 at $z = 3.91$.

4.4.2 SN EFFICIENCY AND MASS OF THE GALAXY

We find that with increasing mass of the galaxy lower SN dust production efficiencies or a higher destruction in the ISM can be accommodated, while large dust masses are still produced. This is best demonstrated by models for the most massive galaxies with $M_{\rm ini} = 3$–13×10^{11} M$_\odot$ in which in case of moderate to no dust destruction a 'high' SN efficiency is sufficient.

However, the largest system with $M_{\rm ini} = 1.3 \times 10^{12}$ M$_\odot$ exceeds the plausible dynamical masses derived from observations of QSOs at $z \gtrsim$ (5) 6 by more than an order of magnitude. Moreover, our computed models show that at least one of the properties of either SFR, Z or M_* are not in agreement with observations at any epoch for any assumption of either the initial SFR or the IMF (see also **(alias?)**). Additionally the values for $\eta_{\rm g,H_2}$ remain very high even for $\alpha = 4.6$ M$_\odot$ (K km s^{-1} pc^2)$^{-1}$. We therefore conclude that such a massive system as advocated by Valiante et al. (2009), cannot be applied to QSOs at $z >$ (5) 6. Although systems with $M_{\rm ini} = 3$–5×10^{11} M$_\odot$ are appropriate for some QSOs at $z < 6$, such massive systems can only be applied to QSOs > 6 when the inclination angle is lower than the assumed average angle.

The models which best reproduce the observed properties of QSOs > 6 are for a galaxy with $M_{\rm ini} = 1 \times 10^{11}$ M$_\odot$, but necessitate a 'maximal' SN efficiency and/or a moderate amount of dust destruction. The overall rapid evolution of dust and some

properties in these models indicates that such QSOs could possibly be present at a higher redshift than $z > 6.4$. An interesting example at a lower redshift of z = 1.135 is the ULIRG SST J1604+4304, which shows properties similar to the considered high-z QSOs. Kawara et al. (2010) reported a dust mass in this ULIRG of 1–2 $\times$ 10^8 $\mathrm{M}_\odot$, a metallicity of around 2.5 $\mathrm{Z}_\odot$ and estimated the age of the stellar population to be 40–200 Myr.

The possibility of moderate dust destruction in the ISM was already discussed in Chapter 3 . We found that the amount of dust for some models fit better with observations for $M_{\rm cl} \leq$100 $\mathrm{M}_\odot$, which would be in agreement with the values of $M_{\rm cl}$ of 50–70 $\mathrm{M}_\odot$ derived for a multiphase ISM (e.g., McKee 1989; Dwek et al. 2007).

The 'maximal' SN efficiency might be problematic. There is only little observational evidence that SN can be very efficient (e.g., Wilson & Batrla 2005; Douvion et al. 2001a; Dunne et al. 2009), and theoretical models predict significant dust destruction in reverse shocks of SNe (e.g., Bianchi & Schneider 2007; Nozawa et al. 2007, 2010). On the other hand, these models also show that the effectiveness of dust destruction depends on various properties such as the geometry of the shocks, the density of the ejecta and the ISM, the size and shape of the grains, clumping in the SNe ejecta and different SN types. In addition there is some observational evidence that Type IIn SNe and sources such as luminous blue variables are possibly efficient dust producers (Fox et al. 2009; Smith et al. 2009; Gomez et al. 2010). While dust production and destruction in SNe is yet unresolved, a 'maximal' SN efficiency cannot be ruled out (see also Chapter 2). Alternatively, either dust formation in the outflowing winds of QSOs (Elvis et al. 2002) or grain growth in the ISM might be an option (e.g., Dwek et al. 2007; Draine 2009; Michałowski et al. 2010b) as supplementary or primary dust sources. However it remains to be investigated, if dust grain growth can be as efficient as required under the prevailing conditions of 'high' star formation activity and a short time span. Typical grain growth timescales in molecular clouds (MCs) are of order 10^7 yr, but depending on the density and metallicity these can possibly be shorter (e.g., Hirashita 2000; Zhukovska et al. 2008; Draine 2009). The fact that the starburst is assumed to occur in an initially dust free galaxy implies that heavy elements first need to be ejected into the ISM before grain growth can take place.

4.5 Summary and conclusions

In this work we applied the chemical evolution model developed in Chapter 3 to QSOs at $z \gtrsim 6$. We have investigated, whether large amounts of dust in QSOs can be generated rapidly within 100 Myr for a high initial SFR of 3 $\times$ 10^3 $\mathrm{M}_\odot$ yr^{-1}. We evaluated the models by comparing the results of various properties to the derived values from observations of QSOs at $z \gtrsim 6$ and discussed the most favorable scenarios. All models which match the discussed properties within the range defined by observations are

Table 4.5: *Models which match the observed range of properties of $z \geq 5$ QSOs*

$M_{\rm ini}$	$\psi_{\rm ini}$	SN efficiency	$M_{\rm cl}$	IMF
$M_\odot$	10^3 $M_\odot$ yr^{-1}		$M_\odot$	
Epoch: 30 Myr				
5×10^{10}	3	max	100	top-heavy, Larson 1, 2, mass-heavy
	3	max	0	top-heavy, Larson 1, 2
	3	**max**	**0**	**mass-heavy**
	1	max	0,100	top-heavy, Larson 2
1×10^{11}	**3**	**max**	**100**	**top-heavy, Larson 2, mass-heavy**
	3	**max**	**0**	**top-heavy, mass-heavy**
	3	high	0	Larson 2
Epoch: 100 Myr				
5×10^{10}	3	max	100	Larson 2
	3	**max**	**0**	**top-heavy, Larson 2**
	1	max	100	Larson 2
1×10^{11}	**3**	**max**	**100**	**top-heavy, Larson 2**
	3	high	0	Larson 2
	1	max	100	top-heavy, Larson 2
	1	max	0	top-heavy
3×10^{11}	3	max	800	Larson 1, mass-heavy
	3	**max**	**800**	**top-heavy, Larson 2**
	3	max	100	Larson 1, mass-heavy
	3	high	0	mass-heavy
	3	**high**	**0**	**top-heavy, Larson 2**
	1	**max**	**800**	**Larson 2**
	1	high	0	Larson 2
5×10^{11}	3	max	800	mass-heavy
	3	**max**	**800**	**top-heavy, Larson 2**
	3	high	100	top-heavy, mass-heavy
	3	**high**	**100**	**Larson 2**
	3	high	0	mass-heavy
	3	**high**	**0**	**top-heavy, Larson 2**

Notes. All models which also match the observed range of all properties of **$z \geq 6$ QSOs** are marked with bold letters.

summarized in Table 4.5.

We find that large dust masses can be generated within short timescales after starburst. The shortest plausible epoch at which some models reproduce the properties of QSOs at $z > 6$ is determined to be 30 Myr. For a lower initial SFR of 10^3 $M_\odot$ yr^{-1} one model at an epoch of 100 Myr is found to be suitable. Individual QSOs are adapted to models at 30, 70, 100 and 170 Myr. The most favorable environments are galaxies with initial gas masses of $M_{\rm ini}$ = 1–3 $\times$ 10^{11} $M_\odot$, while top-heavy IMFs are preferred. The observed amount of dust can solely be manufactured by SNe, while at these epochs the dust contribution from AGB stars is not essential.

At early epochs ($\leq$ 100 Myr) and for galaxies with $M_{\rm ini}$ = 1 $\times$ 10^{11} $\mathrm{M}_{\odot}$ a substantial dust contribution from SNe (i.e. a 'maximal' SN efficiency) is needed. For galaxies with $M_{\rm ini}$ = 3–5 $\times$ 10^{11} $\mathrm{M}_{\odot}$ and at later epochs (i.e., 170 or 400 Myr) a SN dust production with a 'high' SN efficiency is found to be sufficient. Overall, a moderate dust destruction in the ISM is preferred. Galaxies with masses of $M_{\rm ini}$ = 1.3 $\times$ 10^{12} $\mathrm{M}_{\odot}$ are found not to be appropriate for QSOs at $z \gtrsim 6$.

Figure: *Galaxies of all shapes host black holes; NASA/JPL-Caltech/T. Pyle (SSC)*

5

Conclusions and future prospects

What we know is a drop,
what we do not know is an ocean.

ISAAC NEWTON (1642 - 1727)

Abstract –

The most significant findings of the accomplished investigations about the evolution of dust in starburst galaxies and QSOs are briefly summarized and discussed. Several interesting ideas devoted to further improvements of the model developed in this thesis and future projects are presented.

5.1 Conclusions

In this thesis we have performed studies about the origin and evolution of dust in starburst galaxies in the early Universe.

The principal objectives have been to

- identify the mass ranges of the most efficient dust producing stars at high-redshift
- quantify the influence of the IMF on the total dust productivity of stars between 3–40 $\mathrm{M}_{\odot}$
- ascertain the astrophysical conditions required for generating large amounts of dust
- investigate the temporal evolution of the total dust content manufactured by SNe and AGB stars on timescales less than 1 Gyr
- investigate how rapidly the observed amount of dust in QSOs at $z \gtrsim 6$ can be generated and to determine the epoch when the physical properties are in agreement with those observed.

Pertaining to most of these aims we have developed a simple chemical evolution model adjusted to starburst galaxies and QSOs.

We have shown that the amount of dust reached in galaxies is not only dependent on the sources which generate the dust, but also on the environment in which dust further evolves. This in particular refers to the mass of the galaxy. We have disclosed that under the same preconditions of IMF, SFR, SN dust production efficiency and the degree of dust destruction in the ISM, larger dust masses can be reached with increasing mass of the galaxy. This results due to the faster evolution in the less massive galaxies than in the more massive galaxies where higher SFRs can be sustained over longer time spans.

However, we have also shown that not all systems where large dust masses could be reached are applicable to QSOs at high redshift. Thus, it results that the least massive (5×10^{10} $\mathrm{M}_{\odot}$) and highest (1.3×10^{12} $\mathrm{M}_{\odot}$) considered galaxies most likely can be excluded, since the theoretical obtained properties of these QSOs cannot be brought into agreement with those observed.

A significant finding is that large dust masses can be generated rapidly ($\lesssim$ 100–170 Myr) when the SFR of the starburst is very high, but similar to the SFRs observed in high-z QSOs. Under such a condition, several calculated models are in agreement with not only the amount of dust but also other observed properties such as the metallicity, the SFR at time of observation, the stellar and H_2 masses. Our results therefore point to a rapid evolution and hence are suggestive for a young age of the QSOs at high-z.

From these results some (speculative) conclusions can be drawn. For example the rapid evolution in the less massive galaxies is indicative for a short SFR history prior of

reaching the SFR of the starburst. The SFR of the starburst must also be generated fast, because any significant star formation on longer timescales will lead to a fast exhaustion of the system. Also the metallicity and stellar mass will increase, but may remain in the observed range.

In the more massive systems the SFR history prior to the maximal SFR of the starburst most likely plays an important role. However the effect will be the same. Any SFR history with significant SFR will increase the stellar mass and metallicity. This in fact might be an advantage and the time of generating the large dust masses in conjunction with metallicity, SFR at time of observation and the stellar and H_2 mass being in agreement with observations might be shorter. The overall age of the system however will be higher and dependent on how fast the SFR of the starburst is reached.

While with the model developed in this thesis this can only be concluded on a speculative level, further development including diverse gas flow scenarios will be required to reach final confirmation.

5.2 FUTURE PROSPECTS

The model developed in this thesis is constructed as a closed box model and can be called a 'simple model'. The use of it is debated but as has been argued in the thesis this approach is sufficient to investigate divers trends of different properties for the galaxies and QSOs under consideration. However, many interesting questions and ideas emerged during the work, which could not be investigated with the current model. In the following I will propose several projects for improvements to further shed light onto the evolution of dust in these QSOs.

5.2.1 THE NEAR FUTURE

Infall scenarios

The first steps of advancement will be the investigation of diverse infall scenarios. Although realistic infall rates may not be large enough to affect the evolution of such QSOs as have been discussed, it would still be an interesting investigation.

The idea is to test different infall timescales for a given system of dynamical mass and SFR at a given time of observation, while also different combinations of dynamical masses and epochs of observation might be considered. As shown in Chapter 2, an agreement of the model results with observations for the total dust mass and several physical properties can be reached rather quickly after strong starburst. It would be interesting, how fast and massive an infall of matter needs to be in order to reach the observed conditions of QSOs and whether in such a system large dust masses can be built up, depending on diverse IMFs and the strength of dust destruction through SN shocks.

Two infall scenarios will be considered:

- Constant infall:
  In this case the infall rate is given by the total mass, also the dynamical mass, $M_{\rm dyn}$, at time of observation, divided through the infall timescale, $\tau_{\rm inf}$, which can be varied.
  $$\Psi_{\rm g}^{\rm inf} = \frac{M_{\rm dyn}}{\tau_{\rm inf}} \tag{5.1}$$
- Exponential infall:
  In this case the infall rate decreases exponentially with time.
  $$\Psi_{\rm g}^{\rm inf}(t) = \frac{M_{\rm dyn}}{\tau_{\rm inf}} \left[1 - \exp\left(-\frac{t_0}{\tau_{\rm inf}}\right)\right]^{-1} \exp\left(-\frac{t}{\tau_{\rm inf}}\right), \tag{5.2}$$
  where t_0 is the epoch of observation.

SMBH formation

In the presented model a simple case for investigating the effect of the formation of a SMBH on the amount of dust is introduced. We estimated a constant growth rate over a given growth timescale for the SMBH formation. The onset of the formation of the SMBH was assumed to coincide with the starburst, while it coevally grows with the evolution of the system. The estimated growth rate for the SMBH can principally also be seen as some kind of outflow of the system. However, the results have shown that the effect is marginal. This simple approach implies that any outflows lower than the estimated growth rate will certainly also have no effect on the evolution of the system, but it remains to be investigated how large outflow rates for example initiated by SN explosions indeed will be especially in the case of very high SFRs.

A self-consistent evolution model for a SMBH growth and the circumnuclear disk similar to what has been proposed by Kawakatu & Wada (2008, 2009) combined with chemical evolution will provide an accurate basis for studying dust evolution in QSOs and is therefore a primary future project.

Galaxy formation

Hierarchical galaxy evolution models form a framework which possibly provides an interesting way to test the applicability of our models. Such models, i.e., the semi-analytical model GALFORM (Cole et al. 2000), have been developed to study the physical processes of the formation of galaxies in hierarchical clustering cosmologies. The models provide a detailed treatment of the astrophysical processes participating in the beginning of the formation of galaxies out of primordial Gaussian density fluctuations generated during inflation, over processes significantly influencing the evolution such as the cooling of gas in halos, feedback effects on interstellar gas, chemical evolution

and merging of galaxies. The field of application of these models is large. For example modified versions of GALFORM have been used to reproduce the number counts of SMGs (Baugh et al. 2005), to study the K-band luminosity and galaxy stellar mass functions including the feedback from AGNs (Bower et al. 2006) or to investigate the properties of SMGs (Swinbank et al. 2008).

Despite the fact that sophisticated treatment for diverse processes are implemented, the chemical evolution contains simple assumptions. For example in the model described by Cole et al. (2000) no lifetime or metallicity dependent treatment for the chemical evolution is employed. Additionally the feedback from stars i.e., the recycled material, is calculated using a constant mass return fraction for stars below 8 $\mathrm{M}_{\odot}$ and one for stars more massive. The constant mass return fractions are estimated from diverse stellar evolution calculations and are based on either a Kennicutt or a Salpeter IMF. In our models it is evident that the lifetime and metallicity dependent mass return from stars has an impact on the evolution of properties of a galaxy, for instance on the stellar mass or star formation rate. Using a lifetime independent treatment of the recycled material with constant return fractions possibly leads to an underestimation of the stellar masses, since low mass stars do not immediately recycle mass back into the ISM. Furthermore, the amount of dust in the GALFORM model is estimated using the local ISM dust-to-gas ratio, but no explicit dust mass calculations are implemented. However, Santini et al. (2010) showed that the dust-to-gas ratio for SMGs or ULIRGs can be higher than for local spiral galaxies. The problem of partially poorly constrained parameters and parameters, adjusted for the local universe but applied to investigations of the high-z Universe in the GALFORM model, has amongst other issues been pointed out by Bower et al. (2010).

It would be interesting to see, whether a more detailed chemical evolution as developed in this thesis combined with the GALFORM model could further elucidate the evolution of dust in high-z objects such as QSOs. On the other hand it might be interesting whether such a combination matters for studies of e.g., the K-band luminosity function or the stellar mass problem of SMGs in comparison to the work by Baugh et al. (2005).

5.2.2 The distant future

Once the overall environment has been settled and a rough picture of dust evolution in QSOs emerged, more detailed investigation of the dust formation of different sources, if until then not already available, definitely need to be undertaken. According to the outcome from the presented work, the main source for dust supply are most likely SNe, since in any case of a rapid evolution AGB stars are too long-lived for a significant contribution. This is demonstrated in Chapter 2, where it clearly can be seen that the high mass AGB stars which have shorter lifetimes are less efficient dust producers than

the lower massive stars. The latter stars however have already longer lifetimes than the timescales of interest (max. 400–500 Myr) are. On the other hand it also turned out that some models require a SN dust production efficiency which is somewhat in contradiction with the majority of observational evidence from dust observations of SN ejecta and remnants.

The most obvious investigations are therefore the inclusion of additional sources and developments towards more self-consistent SN dust formation models. The following projects would be interesting to undertake.

Grain growth

The inclusion of dust grain growth in the ISM is definitely a necessary extension of the model. It will not only give clarity to the existing speculations about the possibility of grain growth but certainly elucidate the importance of it.

In dense MCs in the ISM dust grain growth by accretion of condensible material onto preexisting refractory grains (e.g., Dwek 1998; Zhukovska et al. 2008) has been proven feasible. Apart from the accretion process, grains also grow via collisions with other grains provided the collisions are gently enough so that the individual particles can stick together instead of being destroyed or shattered (e.g., Blum 2004). The sticking probability and the grain growth timescale are mainly determined by the density of the environment (e.g., Draine 1990a). For example, in MCs the gas density ranges between 10^{2-5} cm^{-3}. As mentioned in Sect. 4.4.2 the derived grain growth timescales in MCs with such densities are approximately of order 10^{7-8} yr (e.g., Hirashita 2000; Draine 2009). However, whether elements/grains are able to stick on surfaces of interest is also dependent on the grain temperature, the binding energy and the relative velocities of the particles. These properties are difficult to determine and can vary with different types of either elements or grains (e.g., Draine 2009; Hirashita & Yan 2009). For example the binding energies of the most abundant dust forming elements such as e.g., C, Mg, Si or Fe to grain surfaces of silicates or carbonaceous dust particles are not known.

Although large masses of molecular hydrogen seem to be present in high-z QSOs, it is unclear whether the prevailing conditions, in particular the gas density, temperature or the abundance of elements are appropriate to invoke sufficient grain growth. In addition, for objects at $z \gtrsim 6$ in which we are interested, the timescales for possible grain growth are very limited. Pertaining also to the high SN rates in case of high star formation it remains to be investigated if grain growth could take place and whether it could be efficient enough to either balance or prevail over the associated dust destruction through SN shocks.

Owing to the rather complicated processes involved in grain growth, details about a possible approach can yet not be given. The advanced models by e.g., Dwek (1998) or Zhukovska et al. (2008) combined with works by e.g., Hirashita (2000) or Hirashita

& Yan (2009) might form the basis of such elaboration.

Dust formation in SN ejecta

In the course of the PhD I started out on the development of a SN dust formation model based on radiation hydrodynamics. The complexity of this project unfortunately did not allow to finish it in the given time and further development is required. The concept is similar to the models for AGB stars (e.g., Gail & Sedlmayr 1987; Höfner & Andersen 2007; Höfner 2009) where the coupled system of radiation hydrodynamics, dust formation and grain growth is solved simultaneously.

The proposed model is an implicit model, i.e., the solution at the subsequent time level cannot be calculated by some sort of extrapolation from the physical values given at the old time levels. The method used is based on a finite volume discretization ensuring the conservation properties of the hyperbolic equations. Shock fronts are treated by an artificial viscosity and the individual grid points are freely moving within the computational domain, while their locations are determined by a grid-equation. The grid equation is simultaneously solved together with the physical equations (e.g., Dorfi 1998). The compression at the shock front possibly cause variations in the equation of state by opening new degree of freedom in a non-perfect gas or by triggering chemical reactions which might lead to dust formation. It is therefore necessary to simultaneously solve the full set of discrete radiation hydrodynamic equations together with equations of time-dependent dust formation (Gail & Sedlmayr 1988; Gauger et al. 1990). The solution provides the complex interaction between dust, radiation and matter.

An advantage of this model is that the reverse shock develops out of the flow structure. The adaptive grid on which the code is structured is able to trace the contact discontinuity, which separates the stellar ejecta from the interstellar medium removed by the blast wave. At the sweep-up time the reverse shock moves inward and heats up the interior, which can effect dust destruction. The output from the model provides information of the dust size distribution and dust mass, from the time of formation in the ejecta (a few hundred days after explosion) to its survival in the SN remnant (thousands of years later). This leads to estimates of the total dust production efficiency.

Dust destruction and grain growth in SN remnants

The main idea is to investigate whether dust formation or dust grain growth can be enhanced by SN shocks. In Chapter 2 we have shown that more dust seem to be present in the older remnants than what can be formed at short epochs after explosion. We also suggested the possibility of grain growth in the remnant over longer timescales as explanation for this difference. It would therefor be interesting, if the total amount of dust is different in the remnants from SNe exploding in either a low metallicity or more metal rich environment.

It is well known that SN shocks which overrun a certain fraction of the interstellar medium will either destroy or shatter the dust (e.g., McKee 1989; Jones et al. 1996) within the shocked medium. The amount of dust either destroyed or shattered is amongst other properties such as the explosion energy and the shock velocity also dependent on the dust-to-gas ratio in this medium. While shattering will lead to a grain size redistribution towards smaller grains, the elements which had been locked up in grains are returned back into the gas phase after destruction. These elements might therefore possibly be available for further dust grain growth on for example the dust grains formed in the ejecta behind the shock, but also on the remaining grains from the shattering process. In any case the material which gets overrun is already more metal rich, further elements are available. Hence, in total eventually a higher amount of dust and possibly larger grains can be grown in the SN remnants over longer timescales. Larger grains will certainly also more likely survive any kind of reverse shocks.

While somewhat speculative, dust observations of SN remnants in different environments might be of interest. Also self-consisten models for dust destruction or shattering in conjunction with grain growth or dust formation in SN remnants in different environments are therefore interesting future projects.

5.2.3 Cosmic dust with X-shooter

The below suggested observation of the formation of dust in SNe is part of an X-shooter program, which also comprises the extinction curves of dust surrounding QSOs, extinction properties of DLAs, and the evolution of dust properties to high redshift. The spectral resolution of X-shooter combined with its very broad wavelength coverage and sensitivity makes it well-suited for these studies.

Early and late-time observation of Core Collapse Supernovae to study dust formation

Evidence for dust formation in a SN during the first 100 days after explosion was presented by Smith et al. (2008b). Based on spectra of the peculiar type Ib SN 2006jc features of hot dust grains have been found. The formation of dust was supported (i) by the appearance of a strong continuum at red/NIR wavelengths and (ii) by the fading of the redshifted sides of the narrow He I emission lines. However, the origin of the formation is quite unclear since the onset of dust formation for Type II SNe is believed to occur later than 300 to 600 days after the explosion. It has been speculated that the dust grains were formed by prior LBV-like eruptions creating a dense CSM medium around the progenitor star. The possibility of formation of Carbon dust grains after 50 days in Ib SNe (in contrast to Type II SN) has been theoretically explained by Nozawa et al. 2008. Further examples and investigation of dust production by SN are necessary to understand this process.

We therefore intend to observe the effect of dust formation in a core-collapse SN similar to SN 2006jc. To detect these effects requires a series of observations of a single SN (we aim for approximately six observations between 10 and 100 days past explosion) showing the development of the dust signature in line asymmetry and hot dust emission. The latest time we intend to observe is approximately 100 days after maximum, but dependent on the brightness of the SN. In order to be able to observe a core collapse supernova with $S/N \sim 5$ per resolution element in the optical in less than about 45 minutes, requires a source brighter than $R \sim 15$ mag at peak brightness. Therefore any core-collapse supernova brighter than $R \sim 15$ mag at peak brightness observable less than a few weeks after peak and observable for at least a month thereafter are suitable candidates. The observation is requested in ToO mode, since it can only be examined if a SN appears, which fulfills these requirements.

From the first spectra the abundance of the CSM can be derived. The following individual spectra will prove the abundance of elements produced by the SN and distinguish between dust formed out of the SN elements and during the interaction with the CSM. Comparison of the subtracted and individual spectra will lead to information about properties of the dust and the ambient gas. This investigation will also be complemented by other MIR studies.

BIBLIOGRAPHY

Alton, P. B., Xilouris, E. M., Misiriotis, A., Dasyra, K. M., & Dumke, M. 2004, A&A, 425, 109

Andersen, A. C., Höfner, S., & Gautschy-Loidl, R. 2003, A&A, 400, 981

Andersen, A. C., Jorgensen, U. G., Nicolaisen, F. M., Sorensen, P. G., & Glejbol, K. 1998, A&A, 330, 1080

Anderson, J. P. & James, P. A. 2008, MNRAS, 390, 1527

Arendt, R. G., Dwek, E., & Moseley, S. H. 1999, ApJ, 521, 234

Arnett, W. D. 1988, ApJ, 331, 377

Baade, W. 1943, ApJ, 97, 119

Ballero, S. K., Kroupa, P., & Matteucci, F. 2007, A&A, 467, 117

Bandiera, R. 1987, ApJ, 319, 885

Barger, A. J., Cowie, L. L., Sanders, D. B., et al. 1998, Nature, 394, 248

Barlow, M. J., Krause, O., Swinyard, B. M., et al. 2010, ArXiv e-prints

Barnard, E. E. 1884, Astronomische Nachrichten, 108, 369

Barth, A. J., Martini, P., Nelson, C. H., & Ho, L. C. 2003, ApJ, 594, L95

Bartko, H., Martins, F., Trippe, S., et al. 2010, ApJ, 708, 834

Baugh, C. M., Lacey, C. G., Frenk, C. S., et al. 2005, MNRAS, 356, 1191

Becker, G. D., Sargent, W. L. W., Rauch, M., & Simcoe, R. A. 2006, ApJ, 640, 69

Beelen, A., Cox, P., Benford, D. J., et al. 2006, ApJ, 642, 694

Benford, D. J., Cox, P., Omont, A., Phillips, T. G., & McMahon, R. G. 1999, ApJ, 518, L65

Bertoldi, F., Carilli, C. L., Cox, P., et al. 2003a, A&A, 406, L55

Bertoldi, F., Carilli, C. L., Menten, K. M., et al. 2000, A&A, 360, 92

Bertoldi, F. & Cox, P. 2002, A&A, 384, L11

Bertoldi, F., Cox, P., Neri, R., et al. 2003b, A&A, 409, L47

Bianchi, S. & Schneider, R. 2007, MNRAS, 378, 973

Blair, W. P., Ghavamian, P., Long, K. S., et al. 2007, ApJ, 662, 998

Blair, W. P., Morse, J. A., Raymond, J. C., et al. 2000, ApJ, 537, 667

Blöcker, T. & Schönberner, D. 1991, A&A, 244, L43

Bloecker, T. 1995, A&A, 297, 727

Blum, J. 2004, in Astronomical Society of the Pacific Conference Series, Vol. 309, Astrophysics of Dust, ed. A. N. Witt, G. C. Clayton, & B. T. Draine, 369–+

Bonnell, I. A., Larson, R. B., & Zinnecker, H. 2007, Protostars and Planets V, 149

Borkowski, K. J., Williams, B. J., Reynolds, S. P., et al. 2006, ApJ, 642, L141

Botticella, M. T., Pastorello, A., Smartt, S. J., et al. 2009, MNRAS, 398, 1041

Bouchet, P., De Buizer, J. M., Suntzeff, N. B., et al. 2004, ApJ, 611, 394

Bouwens, R. J., Illingworth, G. D., Labbe, I., et al. 2009, ArXiv e-prints

Bowen, G. H. & Willson, L. A. 1991, ApJ, 375, L53

Bower, R. G., Benson, A. J., Malbon, R., et al. 2006, MNRAS, 370, 645

Bower, R. G., Vernon, I., Goldstein, M., et al. 2010, MNRAS, 407, 2017

Bradley, J. P. 2003, Treatise on Geochemistry, 1, 689

Brandt, T. D., Tojeiro, R., Aubourg, É., et al. 2010, AJ, 140, 804

Bromm, V., Coppi, P. S., & Larson, R. B. 2002, ApJ, 564, 23

Bromm, V. & Larson, R. B. 2004, ARA&A, 42, 79

Bromm, V. & Loeb, A. 2003, Nature, 425, 812

Brownlee, D. 2008, Physics Today, 61, 060000

Burrows, A. 2009, in Astronomical Society of the Pacific Conference Series, Vol. 414, Astronomical Society of the Pacific Conference Series, ed. T. Henning, E. Grün, & J. Steinacker, 115–+

Calura, F., Pipino, A., & Matteucci, F. 2008, A&A, 479, 669

Carilli, C. L., Bertoldi, F., Omont, A., et al. 2001a, AJ, 122, 1679

Carilli, C. L., Bertoldi, F., Rupen, M. P., et al. 2001b, ApJ, 555, 625

Carilli, C. L., Kohno, K., Kawabe, R., et al. 2002, AJ, 123, 1838

Carilli, C. L., Neri, R., Wang, R., et al. 2007, ApJ, 666, L9

Carilli, C. L., Walter, F., Bertoldi, F., et al. 2004, AJ, 128, 997

Cernuschi, F., Marsicano, F., & Codina, S. 1967, Annales d'Astrophysique, 30, 1039

Cernuschi, F., Marsicano, F. R., & Kimel, I. 1965, Annales d'Astrophysique, 28, 860

Chabrier, G. 2003a, PASP, 115, 763

Chabrier, G. 2003b, ApJ, 586, L133

Chabrier, G. 2005, in Astrophysics and Space Science Library, Vol. 327, The Initial Mass Function 50 Years Later, ed. E. Corbelli, F. Palla, & H. Zinnecker, 41–+

Charbonnel, C., Meynet, G., Maeder, A., Schaller, G., & Schaerer, D. 1993, A&AS, 101, 415

Chary, R., Stern, D., & Eisenhardt, P. 2005, ApJ, 635, L5

Cherchneff, I. 2006, A&A, 456, 1001

Cherchneff, I. & Dwek, E. 2009, ApJ, 703, 642

Cherchneff, I. & Dwek, E. 2010, ApJ, 713, 1

Chevalier, R. A. 2005, ApJ, 619, 839

Chevalier, R. A. 2006, ArXiv Astrophysics e-prints

Chevalier, R. A. & Klein, R. I. 1978, ApJ, 219, 994

Clayton, D. D. 1979, Ap&SS, 65, 179

Clayton, D. D., Deneault, E., & Meyer, B. S. 2001, ApJ, 562, 480

Clayton, D. D., Liu, W., & Dalgarno, A. 1999, Science, 283, 1290

Cole, S., Lacey, C. G., Baugh, C. M., & Frenk, C. S. 2000, MNRAS, 319, 168

Contursi, A., Boselli, A., Gavazzi, G., et al. 2001, A&A, 365, 11

Cox, D. P. & Smith, B. W. 1976, ApJ, 203, 361

Cox, P., Omont, A., Djorgovski, S. G., et al. 2002, A&A, 387, 406

Crockett, R. M., Eldridge, J. J., Smartt, S. J., et al. 2008, MNRAS, 391, L5

Crockett, R. M., Smartt, S. J., Eldridge, J. J., et al. 2007, MNRAS, 381, 835

Crowther, P. A. 2007, ARA&A, 45, 177

da Cunha, E., Eminian, C., Charlot, S., & Blaizot, J. 2010, MNRAS, 403, 1894

Dabringhausen, J., Kroupa, P., & Baumgardt, H. 2009, MNRAS, 394, 1529

D'Antona, F. & Caloi, V. 2004, ApJ, 611, 871

D'Antona, F. & Mazzitelli, I. 1996, ApJ, 470, 1093

Danziger, I. J., Gouiffes, C., Bouchet, P., & Lucy, L. B. 1989, IAU Circ., 4746, 1

Davidson, K. 1971, MNRAS, 154, 415

De Breuck, C., Neri, R., Morganti, R., et al. 2003, A&A, 401, 911

de Jager, C., Nieuwenhuijzen, H., & van der Hucht, K. A. 1988, A&AS, 72, 259

Devereux, N., Taniguchi, Y., Sanders, D. B., Nakai, N., & Young, J. S. 1994, AJ, 107, 2006

Di Carlo, E., Corsi, C., Arkharov, A. A., et al. 2008, ApJ, 684, 471

Di Matteo, T., Croft, R. A. C., Springel, V., & Hernquist, L. 2004, ApJ, 610, 80

Dietrich, M., Hamann, F., Appenzeller, I., & Vestergaard, M. 2003, ApJ, 596, 817

Doane, J. S. & Mathews, W. G. 1993, ApJ, 419, 573

Donn, B. & Nuth, J. A. 1985, ApJ, 288, 187

Dorfi, E. A. 1998, in Saas-Fee Advanced Course 27: Computational Methods for Astrophysical Fluid Flow., ed. O. Steiner & A. Gautschy, 263–+

Dorschner, J. 1967, Astronomische Nachrichten, 290, 171

Dorschner, J. 2003, in Lecture Notes in Physics, Berlin Springer Verlag, Vol. 609, Astromineralogy, ed. T. K. Henning, 1–54

Dorschner, J., Friedemann, C., Guertler, J., & Duley, W. W. 1980, Ap&SS, 68, 159

Dorschner, J. & Henning, T. 1995, A&A Rev., 6, 271

Douvion, T., Lagage, P. O., Cesarsky, C. J., & Dwek, E. 2001a, A&A, 373, 281

Douvion, T., Lagage, P. O., & Pantin, E. 2001b, A&A, 369, 589

Downes, D. & Solomon, P. M. 1998, ApJ, 507, 615

Draine, B. T. 1979, Ap&SS, 65, 313

Draine, B. T. 1990a, in Astronomical Society of the Pacific Conference Series, Vol. 12, The Evolution of the Interstellar Medium, ed. L. Blitz, 193–205

Draine, B. T. 1990b, in Astrophysics and Space Science Library, Vol. 161, The Interstellar Medium in Galaxies, ed. H. A. Thronson Jr. & J. M. Shull, 483–492

Draine, B. T. 2009, in Astronomical Society of the Pacific Conference Series, Vol. 414, Astronomical Society of the Pacific Conference Series, ed. T. Henning, E. Grün, & J. Steinacker, 453–+

Dunne, L., Eales, S., Edmunds, M., et al. 2000, MNRAS, 315, 115

Dunne, L., Eales, S., Ivison, R., Morgan, H., & Edmunds, M. 2003, Nature, 424, 285

Dunne, L. & Eales, S. A. 2001, MNRAS, 327, 697

Dunne, L., Maddox, S. J., Ivison, R. J., et al. 2009, MNRAS, 394, 1307

Dwek, E. 1998, ApJ, 501, 643

Dwek, E., Galliano, F., & Jones, A. P. 2007, ApJ, 662, 927

Dwek, E., Moseley, S. H., Glaccum, W., et al. 1992, ApJ, 389, L21

Dwek, E. & Scalo, J. M. 1979, ApJ, 233, L81

Dwek, E. & Scalo, J. M. 1980, ApJ, 239, 193

Eales, S., Lilly, S., Gear, W., et al. 1999, ApJ, 515, 518

Edmunds, M. G. 2001, MNRAS, 328, 223

Eldridge, J. J., Izzard, R. G., & Tout, C. A. 2008, MNRAS, 384, 1109

Eldridge, J. J. & Tout, C. A. 2004, MNRAS, 353, 87

Eldridge, J. J. & Tout, C. A. 2005, in Astronomical Society of the Pacific Conference Series, Vol. 342, 1604-2004: Supernovae as Cosmological Lighthouses, ed. M. Turatto, S. Benetti, L. Zampieri, & W. Shea, 126–+

Eldridge, J. J. & Vink, J. S. 2006, A&A, 452, 295

Elmegreen, B. G. 2009, in The Evolving ISM in the Milky Way and Nearby Galaxies

Elmhamdi, A., Danziger, I. J., Cappellaro, E., et al. 2004, A&A, 426, 963

Elmhamdi, A., Danziger, I. J., Chugai, N., et al. 2003, MNRAS, 338, 939

Elvis, M., Marengo, M., & Karovska, M. 2002, ApJ, 567, L107

Ercolano, B., Barlow, M. J., & Sugerman, B. E. K. 2007, MNRAS, 375, 753

Erickson, E. F., Knacke, R. F., Tokunaga, A. T., & Haas, M. R. 1981, ApJ, 245, 148

Fan, X., Strauss, M., Richards, G., et al. 2004, in Astronomical Society of the Pacific Conference Series, Vol. 311, AGN Physics with the Sloan Digital Sky Survey, ed. G. T. Richards & P. B. Hall, 431–+

Fan, X., Strauss, M. A., Becker, R. H., et al. 2006, AJ, 132, 117

Fan, X., Strauss, M. A., Schneider, D. P., et al. 2003, AJ, 125, 1649

Feder, D. 1966, Advanced in Physics, 15, 111

Ferrarotti, A. S. & Gail, H. 2001, in Astronomische Gesellschaft Meeting Abstracts, Vol. 18, Astronomische Gesellschaft Meeting Abstracts, ed. E. R. Schielicke, 49–+

Ferrarotti, A. S. & Gail, H. 2002, A&A, 382, 256

Ferrarotti, A. S. & Gail, H. 2006, A&A, 447, 553

Filippenko, A. V. 1997, ARA&A, 35, 309

Fink, M., Hillebrandt, W., & Röpke, F. K. 2007, A&A, 476, 1133

Flower, D. R. 2001, J. Phys. B; At. Mol. Opt. Phys., 34, 2731

Foley, R. J., Berger, E., Fox, O., et al. 2010, ArXiv e-prints

Foley, R. J., Smith, N., Ganeshalingam, M., et al. 2007, ApJ, 657, L105

Fox, O., Skrutskie, M. F., Chevalier, R. A., et al. 2009, ApJ, 691, 650

Fox, O. D., Chevalier, R. A., Dwek, E., et al. 2010, ArXiv e-prints

Frayer, D. T., Ivison, R. J., Scoville, N. Z., et al. 1999, ApJ, 514, L13

Freudling, W., Corbin, M. R., & Korista, K. T. 2003, ApJ, 587, L67

Friedemann, C. 1969, Astronomische Nachrichten, 291, 177

Friedemann, C. & Schmidt, K. 1967, Astronomische Nachrichten, 290, 65

Fryer, C. L., Mazzali, P. A., Prochaska, J., et al. 2007, PASP, 119, 1211

Gail, H. 2003, in Lecture Notes in Physics, Berlin Springer Verlag, Vol. 609, Astromineralogy, ed. T. K. Henning, 55–120

Gail, H., Duschl, W. J., Ferrarotti, A. S., & Weis, K. 2005, in Astronomical Society of the Pacific Conference Series, Vol. 332, The Fate of the Most Massive Stars, ed. R. Humphreys & K. Stanek, 317–+

Gail, H., Keller, R., & Sedlmayr, E. 1984, A&A, 133, 320

Gail, H. & Sedlmayr, E. 1988, A&A, 206, 153

Gail, H. P. & Sedlmayr, E. 1987, A&A, 171, 197

Gal-Yam, A., Leonard, D. C., Fox, D. B., et al. 2007, ApJ, 656, 372

Gal-Yam, A., Mazzali, P., Ofek, E. O., et al. 2009, Nature, 462, 624

Gall, C., Andersen, A. C., & Hjorth, J. 2010, submitted to A&A

Gallagher, III, J. S., Hunter, D. A., & Tutukov, A. V. 1984, ApJ, 284, 544

Gallerani, S., Maiolino, R., Juarez, Y., et al. 2010, ArXiv e-prints

Gauger, A., Sedlmayr, E., & Gail, H. 1990, A&A, 235, 345

Gautschy-Loidl, R., Höfner, S., Jørgensen, U. G., & Hron, J. 2004, A&A, 422, 289

Gehrz, R. 1989, in IAU Symposium, Vol. 135, Interstellar Dust, ed. L. J. Allamandola & A. G. G. M. Tielens, 445–+

Georgy, C., Meynet, G., Walder, R., Folini, D., & Maeder, A. 2009, A&A, 502, 611

Gibson, B. K. & Matteucci, F. 1997, MNRAS, 291, L8

Gilra, D. P. 1971, Nature, 229, 237

Gispert, R., Lagache, G., & Puget, J. L. 2000, A&A, 360, 1

Gomez, H. L., Dunne, L., Ivison, R. J., et al. 2009, MNRAS, 397, 1621

Gomez, H. L., Vlahakis, C., Stretch, C. M., et al. 2010, MNRAS, 401, L48

Goodrich, R. W., Stringfellow, G. S., Penrod, G. D., & Filippenko, A. V. 1989, ApJ, 342, 908

Green, D. A., Tuffs, R. J., & Popescu, C. C. 2004, MNRAS, 355, 1315

Greggio, L. 2005, A&A, 441, 1055

Greggio, L. & Renzini, A. 1983, A&A, 118, 217

Greif, T. H. & Bromm, V. 2006, MNRAS, 373, 128

Greif, T. H., Glover, S. C. O., Bromm, V., & Klessen, R. S. 2010, ArXiv e-prints

Greve, T. R., Bertoldi, F., Smail, I., et al. 2005, MNRAS, 359, 1165

Groenewegen, M. A. T., Wood, P. R., Sloan, G. C., et al. 2007, MNRAS, 376, 313

Gyngard, F., Morgand, A., Nittler, L. R., Stadermann, F. J., & Zinner, E. 2009, in Lunar and Planetary Inst. Technical Report, Vol. 40, Lunar and Planetary Institute Science Conference Abstracts, 1386–+

Habergham, S. M., Anderson, J. P., & James, P. A. 2010, ArXiv e-prints

Hall, J. S. 1949, Science, 109, 166

Heger, A., Fryer, C. L., Woosley, S. E., Langer, N., & Hartmann, D. H. 2003, ApJ, 591, 288

Heger, A. & Woosley, S. E. 2002, ApJ, 567, 532

Helling, C., Dehn, M., Woitke, P., & Hauschildt, P. H. 2008, ApJ, 675, L105

Herant, M. & Benz, W. 1991, ApJ, 370, L81

Herant, M. & Woosley, S. E. 1994, ApJ, 425, 814

Herschel, W. 1785, Royal Society of London Philosophical Transactions Series I, 75, 213

Herwig, F. 2004, ApJS, 155, 651

Hildebrand, R. H. 1983, QJRAS, 24, 267

Hillebrandt, W. & Niemeyer, J. C. 2000, ARA&A, 38, 191

Hiltner, W. A. 1947, ApJ, 106, 231

Hiltner, W. A. 1949, ApJ, 109, 471

Hines, D. C., Krause, O., Rieke, G. H., et al. 2006, ApJ, 641, L85

Hines, D. C., Rieke, G. H., Gordon, K. D., et al. 2004, ApJS, 154, 290

Hirashita, H. 1999, ApJ, 510, L99

Hirashita, H. 2000, PASJ, 52, 585

Hirashita, H., Nozawa, T., Kozasa, T., Ishii, T. T., & Takeuchi, T. T. 2005, MNRAS, 357, 1077

Hirashita, H. & Yan, H. 2009, MNRAS, 394, 1061

Höfner, S. 2006, in IAU Joint Discussion, Vol. 11, IAU Joint Discussion

Höfner, S. 2008, A&A, 491, L1

Höfner, S. 2009, in Astronomical Society of the Pacific Conference Series, Vol. 414, Astronomical Society of the Pacific Conference Series, ed. T. Henning, E. Grün, & J. Steinacker, 3–+

Höfner, S. & Andersen, A. C. 2007, A&A, 465, L39

Höfner, S., Gautschy-Loidl, R., Aringer, B., & Jørgensen, U. G. 2003, A&A, 399, 589

Höfner, S., Jorgensen, U. G., Loidl, R., & Aringer, B. 1998, A&A, 340, 497

Holland, W. S., Robson, E. I., Gear, W. K., et al. 1999, MNRAS, 303, 659

Hoppe, P. 2004, in Astronomical Society of the Pacific Conference Series, Vol. 309, Astrophysics of Dust, ed. A. N. Witt, G. C. Clayton, & B. T. Draine, 265–+

Hoppe, P. 2009, in Astronomical Society of the Pacific Conference Series, Vol. 414, Astronomical Society of the Pacific Conference Series, ed. T. Henning, E. Grün, & J. Steinacker, 148–+

Hoppe, P. & Zinner, E. 2000, J. Geophys. Res., 105, 10371

Hoyle, F. & Wickramasinghe, N. C. 1962, MNRAS, 124, 417

Hoyle, F. & Wickramasinghe, N. C. 1970, Nature, 226, 62

Hughes, D. H., Dunlop, J. S., & Rawlings, S. 1997, MNRAS, 289, 766

Hughes, D. H., Serjeant, S., Dunlop, J., et al. 1998, Nature, 394, 241

Hunter, D. J., Valenti, S., Kotak, R., et al. 2009, A&A, 508, 371

Iben, Jr., I. & Renzini, A. 1981, in Astrophysics and Space Science Library, Vol. 88, Physical Processes in Red Giants, ed. I. Iben Jr. & A. Renzini

Iben, Jr., I. & Tutukov, A. V. 1984, ApJS, 54, 335

Isaak, K. G., Priddey, R. S., McMahon, R. G., et al. 2002, MNRAS, 329, 149

Ivison, R. J., Smail, I., Barger, A. J., et al. 2000, MNRAS, 315, 209

Ivison, R. J., Swinbank, A. M., Swinyard, B., et al. 2010, A&A, 518, L35+

Iwamoto, K., Nakamura, T., Nomoto, K., et al. 2000, ApJ, 534, 660

Jiang, L., Fan, X., Annis, J., et al. 2008, AJ, 135, 1057

Jiang, L., Fan, X., Brandt, W. N., et al. 2010, Nature, 464, 380

Jiang, L., Fan, X., Hines, D. C., et al. 2006, AJ, 132, 2127

Jones, A. P. 2004, in Astronomical Society of the Pacific Conference Series, Vol. 309, Astrophysics of Dust, ed. A. N. Witt, G. C. Clayton, & B. T. Draine, 347–+

Jones, A. P., Tielens, A. G. G. M., & Hollenbach, D. J. 1996, ApJ, 469, 740

Juarez, Y., Maiolino, R., Mujica, R., et al. 2009, A&A, 494, L25

Karakas, A. & Lattanzio, J. C. 2007, Publications of the Astronomical Society of Australia, 24, 103

Karakas, A. I. 2010, MNRAS, 403, 1413

Kawabata, K. S., Tanaka, M., Maeda, K., et al. 2009, ApJ, 697, 747

Kawakatu, N. & Wada, K. 2008, ApJ, 681, 73

Kawakatu, N. & Wada, K. 2009, ApJ, 706, 676

Kawara, K., Oyabu, S., Matsuoka, Y., et al. 2010, MNRAS, 402, 335

Kennicutt, Jr., R. C. 1998, ApJ, 498, 541

Kifonidis, K., Plewa, T., Janka, H., & Müller, E. 2003, A&A, 408, 621

Kitaura, F. S., Janka, H., & Hillebrandt, W. 2006, A&A, 450, 345

Komatsu, E., Smith, K. M., Dunkley, J., et al. 2010, ArXiv e-prints

Kotak, R. 2008, in IAU Symposium, Vol. 250, IAU Symposium, ed. F. Bresolin, P. A. Crowther, & J. Puls, 437–442

Kotak, R., Meikle, W. P. S., Farrah, D., et al. 2009, ApJ, 704, 306

Kotak, R. & Vink, J. S. 2006, A&A, 460, L5

Kozasa, T., Hasegawa, H., & Nomoto, K. 1989, ApJ, 344, 325

Kozasa, T., Hasegawa, H., & Nomoto, K. 1991, A&A, 249, 474

Kozasa, T., Nozawa, T., Tominaga, N., et al. 2009, ArXiv e-prints

Krause, O., Birkmann, S. M., Rieke, G. H., et al. 2004, Nature, 432, 596

Krause, O., Birkmann, S. M., Usuda, T., et al. 2008, Science, 320, 1195

Kroupa, P. 2002, Science, 295, 82

Krumholz, M. R., Cunningham, A. J., Klein, R. I., & McKee, C. F. 2010, ApJ, 713, 1120

Lagadec, E., Zijlstra, A. A., Matsuura, M., Whitelock, P. A., & van Loon, J. T. 2007a, in Astronomical Society of the Pacific Conference Series, Vol. 378, Why Galaxies Care About AGB Stars: Their Importance as Actors and Probes, ed. F. Kerschbaum, C. Charbonnel, & R. F. Wing, 268–+

Lagadec, E., Zijlstra, A. A., Sloan, G. C., et al. 2007b, MNRAS, 376, 1270

Lagadec, E., Zijlstra, A. A., Sloan, G. C., et al. 2009, MNRAS, 396, 598

Larson, R. B. 1972, Nature, 236, 21

Larson, R. B. 1998, MNRAS, 301, 569

Larson, R. B. 2006, in Revista Mexicana de Astronomia y Astrofisica, vol. 27, Vol. 26, Revista Mexicana de Astronomia y Astrofisica Conference Series, 55–59

Lattanzio, J. C. & Wood, P. 2003, in Asymptotic giant branch stars, ed. H. J. Habing & H. Olofsson, 23–104

Ledoux, C., Bergeron, J., & Petitjean, P. 2002, A&A, 385, 802

Leipski, C., Meisenheimer, K., Klaas, U., et al. 2010, ArXiv e-prints

Leitch-Devlin, M. A. & Williams, D. A. 1985, MNRAS, 213, 295

Li, Y., Hernquist, L., Robertson, B., et al. 2007, ApJ, 665, 187

Lindblad, B. 1935, Nature, 135, 133

Lisenfeld, U. & Ferrara, A. 1998, ApJ, 496, 145

Livio, M. 2000, in Type Ia Supernovae, Theory and Cosmology, ed. J. C. Niemeyer & J. W. Truran, 33–+

Lucy, L. B., Danziger, I. J., & Gouiffes, C. 1991, A&A, 243, 223

Lucy, L. B., Danziger, I. J., Gouiffes, C., & Bouchet, P. 1989, in Lecture Notes in Physics, Berlin Springer Verlag, Vol. 350, IAU Colloq. 120: Structure and Dynamics of the Interstellar Medium, ed. G. Tenorio-Tagle, M. Moles, & J. Melnick, 164–+

Maiolino, R., Cox, P., Caselli, P., et al. 2005, A&A, 440, L51

Maiolino, R., Juarez, Y., Mujica, R., Nagar, N. M., & Oliva, E. 2003, ApJ, 596, L155

Maiolino, R., Nagao, T., Marconi, A., et al. 2006, Memorie della Societa Astronomica Italiana, 77, 643

Maiolino, R., Schneider, R., Oliva, E., et al. 2004, Nature, 431, 533

Mair, G., Mueller, E., Hillebrandt, W., & Arnold, C. N. 1988, A&A, 199, 114

Maness, H., Martins, F., Trippe, S., et al. 2007, ApJ, 669, 1024

Mann, I. & Jessberger, E. K. 2003a, in Lecture Notes in Physics, Berlin Springer Verlag, Vol. 609, Astromineralogy, ed. T. K. Henning, 189–216

Mann, I. & Jessberger, E. K. 2003b, in Lecture Notes in Physics, Berlin Springer Verlag, Vol. 609, Astromineralogy, ed. T. K. Henning, 189–216

Mannucci, F., Della Valle, M., & Panagia, N. 2006, MNRAS, 370, 773

Maoz, D. 2008, MNRAS, 384, 267

Marchenko, S. V. 2006, in Astronomical Society of the Pacific Conference Series, Vol. 353, Stellar Evolution at Low Metallicity: Mass Loss, Explosions, Cosmology, ed. H. J. G. L. M. Lamers, N. Langer, T. Nugis, & K. Annuk, 299–+

Marconi, A. & Hunt, L. K. 2003, ApJ, 589, L21

Marigo, P. 2001, A&A, 370, 194

Massey, P. & Olsen, K. A. G. 2003, AJ, 126, 2867

Matsuura, M., Barlow, M. J., Zijlstra, A. A., et al. 2009, MNRAS, 396, 918

Matsuura, M., Zijlstra, A. A., Bernard-Salas, J., et al. 2007, MNRAS, 382, 1889

Matteucci, F. & Recchi, S. 2001, ApJ, 558, 351

Mattila, S., Meikle, W. P. S., Lundqvist, P., et al. 2008, MNRAS, 389, 141

Mattsson, L., Wahlin, R., Höfner, S., & Eriksson, K. 2008, A&A, 484, L5

Maund, J. R., Smartt, S. J., & Schweizer, F. 2005, ApJ, 630, L33

Mazzali, P. A., Deng, J., Hamuy, M., & Nomoto, K. 2009, ApJ, 703, 1624

McKee, C. 1989, in IAU Symposium, Vol. 135, Interstellar Dust, ed. L. J. Allamandola & A. G. G. M. Tielens, 431–+

McKee, C. F. & Tan, J. C. 2008, ApJ, 681, 771

Meikle, W. P. S., Mattila, S., Gerardy, C. L., et al. 2006, ApJ, 649, 332

Meikle, W. P. S., Mattila, S., Pastorello, A., et al. 2007, ApJ, 665, 608

Meynet, G. & Maeder, A. 2003, A&A, 404, 975

Meynet, G. & Maeder, A. 2005, A&A, 429, 581

Michałowski, M., Hjorth, J., & Watson, D. 2010a, A&A, 514, A67+

Michałowski, M. J., Murphy, E. J., Hjorth, J., et al. 2010b, ArXiv e-prints

Michałowski, M. J., Watson, D., & Hjorth, J. 2010c, ApJ, 712, 942

Miller, A. A., Smith, N., Li, W., et al. 2010, AJ, 139, 2218

Molster, F. J., Waters, L. B. F. M., & Tielens, A. G. G. M. 2002a, A&A, 382, 222

Molster, F. J., Waters, L. B. F. M., Tielens, A. G. G. M., & Barlow, M. J. 2002b, A&A, 382, 184

Molster, F. J., Waters, L. B. F. M., Tielens, A. G. G. M., Koike, C., & Chihara, H. 2002c, A&A, 382, 241

Morgan, H. L., Dunne, L., Eales, S. A., Ivison, R. J., & Edmunds, M. G. 2003, ApJ, 597, L33

Morgan, H. L. & Edmunds, M. G. 2003, MNRAS, 343, 427

Murray, S. D. & Lin, D. N. C. 1996, ApJ, 467, 728

Nagashima, M., Lacey, C. G., Baugh, C. M., Frenk, C. S., & Cole, S. 2005, MNRAS, 358, 1247

Nakano, S., Itagaki, K., Puckett, T., & Gorelli, R. 2006, Central Bureau Electronic Telegrams, 666, 1

Nath, B. B., Laskar, T., & Shull, J. M. 2008, ApJ, 682, 1055

Nittler, L. R. 2003, Earth and Planetary Science Letters, 209, 259

Nomoto, K. 1984, ApJ, 277, 791

Nomoto, K. 1987, ApJ, 322, 206

Nomoto, K., Sugimoto, D., Sparks, W. M., et al. 1982, Nature, 299, 803

Nomoto, K., Tominaga, N., Umeda, H., Kobayashi, C., & Maeda, K. 2006, Nuclear Physics A, 777, 424

Nowotny, W., Höfner, S., & Aringer, B. 2010, A&A, 514, A35+

Nowotny, W., Lebzelter, T., Hron, J., & Höfner, S. 2005, A&A, 437, 285

Nozawa, T., Kozasa, T., Habe, A., et al. 2007, ApJ, 666, 955

Nozawa, T., Kozasa, T., Tominaga, N., et al. 2010, ApJ, 713, 356

Nozawa, T., Kozasa, T., Umeda, H., Maeda, K., & Nomoto, K. 2003, ApJ, 598, 785

Nugis, T. & Lamers, H. J. G. L. M. 2000, A&A, 360, 227

Ofek, E. O., Cameron, P. B., Kasliwal, M. M., et al. 2007, ApJ, 659, L13

Omont, A., Beelen, A., Bertoldi, F., et al. 2003, A&A, 398, 857

Omont, A., Cox, P., Bertoldi, F., et al. 2001, A&A, 374, 371

Oort, J. H. & van de Hulst, H. C. 1946, Bull. Astron. Inst. Netherlands, 10, 187

Ott, U. 2003, in Lecture Notes in Physics, Berlin Springer Verlag, Vol. 609, Astromineralogy, ed. T. K. Henning, 236–265

Ott, U. & Hoppe, P. 2007, Highlights of Astronomy, 14, 341

Pakmor, R., Kromer, M., Röpke, F. K., et al. 2010, Nature, 463, 61

Papadopoulos, P., Ivison, R., Carilli, C., & Lewis, G. 2001, Nature, 409, 58

Papadopoulos, P. P., Röttgering, H. J. A., van der Werf, P. P., et al. 2000, ApJ, 528, 626

Pastorello, A., Kasliwal, M. M., Crockett, R. M., et al. 2008, MNRAS, 389, 955

Pastorello, A., Sauer, D., Taubenberger, S., et al. 2006, MNRAS, 370, 1752

Pastorello, A., Smartt, S. J., Mattila, S., et al. 2007, Nature, 447, 829

Pastorello, A., Zampieri, L., Turatto, M., et al. 2004, MNRAS, 347, 74

Pei, Y. C., Fall, S. M., & Bechtold, J. 1991, ApJ, 378, 6

Pellin, M. J., Savina, M. R., Calaway, W. F., et al. 2006, in Lunar and Planetary Inst. Technical Report, Vol. 37, 37th Annual Lunar and Planetary Science Conference, ed. S. Mackwell & E. Stansbery, 2041–+

Pettini, M., Smith, L. J., Hunstead, R. W., & King, D. L. 1994, ApJ, 426, 79

Poelarends, A. J. T., Herwig, F., Langer, N., & Heger, A. 2008, ApJ, 675, 614

Polletta, M., Courvoisier, T., Hooper, E. J., & Wilkes, B. J. 2000, A&A, 362, 75

Popescu, C. C., Tuffs, R. J., Völk, H. J., Pierini, D., & Madore, B. F. 2002, ApJ, 567, 221

Pozzo, M., Meikle, W. P. S., Fassia, A., et al. 2004, MNRAS, 352, 457

Pozzo, M., Meikle, W. P. S., Rayner, J. T., et al. 2006, MNRAS, 368, 1169

Priddey, R. S. & McMahon, R. G. 2001, MNRAS, 324, L17

Prieto, J. L., Kistler, M. D., Thompson, T. A., et al. 2008, ApJ, 681, L9

Raiteri, C. M., Villata, M., & Navarro, J. F. 1996, A&A, 315, 105

Ramstedt, S., Schöier, F. L., & Olofsson, H. 2009, A&A, 499, 515

Ramstedt, S., Schöier, F. L., Olofsson, H., & Lundgren, A. A. 2008, A&A, 487, 645

Renzini, A. & Voli, M. 1981, A&A, 94, 175

Reynolds, S. P. 1985, ApJ, 291, 152

Reynolds, S. P., Borkowski, K. J., Hwang, U., et al. 2007, ApJ, 668, L135

Rho, J., Kozasa, T., Reach, W. T., et al. 2008, ApJ, 673, 271

Rho, J., Reach, W. T., Tappe, A., et al. 2009, ApJ, 700, 579

Riechers, D. A., Walter, F., Bertoldi, F., et al. 2009, ApJ, 703, 1338

Riechers, D. A., Walter, F., Carilli, C. L., & Bertoldi, F. 2007, ApJ, 671, L13

Riechers, D. A., Walter, F., Carilli, C. L., et al. 2006, ApJ, 650, 604

Rieke, G. H., Loken, K., Rieke, M. J., & Tamblyn, P. 1993, ApJ, 412, 99

Robson, I., Priddey, R. S., Isaak, K. G., & McMahon, R. G. 2004, MNRAS, 351, L29

Sahu, D. K., Anupama, G. C., Srividya, S., & Muneer, S. 2006, MNRAS, 372, 1315

Sakon, I., Onaka, T., Wada, T., et al. 2009, ApJ, 692, 546

Salpeter, E. E. 1955, ApJ, 121, 161

Sanders, D. B. & Mirabel, I. F. 1996, ARA&A, 34, 749

Sandstrom, K., Bolatto, A., Leroy, A., et al. 2008, in Astronomical Society of the Pacific Conference Series, Vol. 381, Infrared Diagnostics of Galaxy Evolution, ed. R.-R. Chary, H. I. Teplitz, & K. Sheth, 268–+

Sankrit, R., Blair, W. P., Frattare, L. M., et al. 2008, AJ, 135, 538

Santini, P., Maiolino, R., Magnelli, B., et al. 2010, ArXiv e-prints

Scalo, J. 1998, in Astronomical Society of the Pacific Conference Series, Vol. 142, The Stellar Initial Mass Function (38th Herstmonceux Conference), ed. G. Gilmore & D. Howell, 201–+

Scalo, J. 2005, in Astrophysics and Space Science Library, Vol. 327, The Initial Mass Function 50 Years Later, ed. E. Corbelli, F. Palla, & H. Zinnecker, 23–+

Scalo, J. M. 1986, Fund. Cosmic Phys., 11, 1

Schaerer, D. & de Barros, S. 2010, ArXiv e-prints

Schaerer, D., Meynet, G., Maeder, A., & Schaller, G. 1993, A&AS, 98, 523

Schalén, C. 1929, Astronomische Nachrichten, 236, 249

Schaller, G., Schaerer, D., Meynet, G., & Maeder, A. 1992, A&AS, 96, 269

Schmidt, M. 1963, ApJ, 137, 758

Schneider, R., Ferrara, A., & Salvaterra, R. 2004, MNRAS, 351, 1379

Schneider, R., Omukai, K., Inoue, A. K., & Ferrara, A. 2006, MNRAS, 369, 1437

Schöier, F. L. & Olofsson, H. 2001, A&A, 368, 969

Schwartz, P. R. 1982, ApJ, 252, 589

Schwarzschild, M. & Spitzer, L. 1953, The Observatory, 73, 77

Scoville, N. & Young, J. S. 1983, ApJ, 265, 148

Scoville, N. Z. & Solomon, P. M. 1974, ApJ, 187, L67+

Seab, C. G. 1987, in Astrophysics and Space Science Library, Vol. 134, Interstellar Processes, ed. D. J. Hollenbach & H. A. Thronson Jr., 491–512

Sedlmayr, E. 1994, in Lecture Notes in Physics, Berlin Springer Verlag, Vol. 428, IAU Colloq. 146: Molecules in the Stellar Environment, ed. U. G. Jorgensen, 163–+

Sibthorpe, B., Ade, P. A. R., Bock, J. J., et al. 2009, ArXiv e-prints

Siess, L. 2007, A&A, 476, 893

Siess, L. 2008, in IAU Symposium, Vol. 252, IAU Symposium, ed. L. Deng & K. L. Chan, 297–307

Silvia, D. W., Smith, B. D., & Shull, J. M. 2010, ApJ, 715, 1575

Sloan, G. C., Kraemer, K. E., Wood, P. R., et al. 2008, ApJ, 686, 1056

Sloan, G. C., Matsuura, M., Zijlstra, A. A., et al. 2009, Science, 323, 353

Smail, I., Ivison, R. J., & Blain, A. W. 1997, ApJ, 490, L5+

Smartt, S. J., Eldridge, J. J., Crockett, R. M., & Maund, J. R. 2009, MNRAS, 395, 1409

Smith, N., Chornock, R., Silverman, J. M., Filippenko, A. V., & Foley, R. J. 2010a, ApJ, 709, 856

Smith, N., Foley, R. J., Bloom, J. S., et al. 2008a, ApJ, 686, 485

Smith, N., Foley, R. J., & Filippenko, A. V. 2008b, ApJ, 680, 568

Smith, N., Gehrz, R. D., Hinz, P. M., et al. 2003, AJ, 125, 1458

Smith, N., Li, W., Foley, R. J., et al. 2007, ApJ, 666, 1116

Smith, N., Miller, A., Li, W., et al. 2010b, AJ, 139, 1451

Smith, N. & Owocki, S. P. 2006, ApJ, 645, L45

Smith, N., Silverman, J. M., Chornock, R., et al. 2009, ApJ, 695, 1334

Solomon, P. M. & Barrett, J. W. 1991, in IAU Symposium, Vol. 146, Dynamics of Galaxies and Their Molecular Cloud Distributions, ed. F. Combes & F. Casoli, 235–+

Solomon, P. M., Radford, S. J. E., & Downes, D. 1992, Nature, 356, 318

Spergel, D. N., Verde, L., Peiris, H. V., et al. 2003, ApJS, 148, 175

Stanimirović, S., Bolatto, A. D., Sandstrom, K., et al. 2005, ApJ, 632, L103

Stebbins, J., Huffer, C. M., & Whitford, A. E. 1939, ApJ, 90, 209

Stecher, T. P. & Donn, B. 1965, ApJ, 142, 1681

Stickel, M., Lemke, D., Klaas, U., et al. 2000, A&A, 359, 865

Struve, F. G. W. 1847, St. Petersburg: Tip.Acad. Imper., 5, 165

Sugerman, B. E. K., Ercolano, B., Barlow, M. J., et al. 2006, Science, 313, 196

Swinbank, A. M., Lacey, C. G., Smail, I., et al. 2008, MNRAS, 391, 420

Tecza, M., Baker, A. J., Davies, R. I., et al. 2004, ApJ, 605, L109

Tegmark, M., Silk, J., Rees, M. J., et al. 1997, ApJ, 474, 1

Temim, T., Gehrz, R. D., Woodward, C. E., et al. 2006, AJ, 132, 1610

Thompson, T. A., Prieto, J. L., Stanek, K. Z., et al. 2009, ApJ, 705, 1364

Thronson, Jr., H. A. & Telesco, C. M. 1986, ApJ, 311, 98

Tielens, A. G. G. M. 1998, ApJ, 499, 267

Tinsley, B.-M. 1980, in Fundamentals of Cosmic Physics, ed. C. W. Gordon & V. Canuto, Vol. 5, 287–388

Todini, P. & Ferrara, A. 2001, MNRAS, 325, 726

Truelove, J. K. & McKee, C. F. 1999, ApJS, 120, 299

Trümpler, R. J. 1930, Lick Observatory Bulletin, 14, 154

Trundle, C., Kotak, R., Vink, J. S., & Meikle, W. P. S. 2008, A&A, 483, L47

Tumlinson, J. 2006, ApJ, 641, 1

Umana, G., Buemi, C. S., Trigilio, C., et al. 2009, ApJ, 694, 697

Umeda, H. & Nomoto, K. 2002, ApJ, 565, 385

Valiante, R., Schneider, R., Bianchi, S., & Andersen, A. C. 2009, MNRAS, 397, 1661

van Albada, G. D., van Leer, B., & Roberts, Jr., W. W. 1982, A&A, 108, 76

van den Hoek, L. B. & Groenewegen, M. A. T. 1997, A&AS, 123, 305

van Loon, J. T., Cohen, M., Oliveira, J. M., et al. 2008, A&A, 487, 1055

Vassiliadis, E. & Wood, P. R. 1993, ApJ, 413, 641

Ventura, P. & D'Antona, F. 2009, A&A, 499, 835

Vestergaard, M. 2004, ApJ, 601, 676

Vink, J. S., de Koter, A., & Lamers, H. J. G. L. M. 2001, A&A, 369, 574

Vlahakis, C., Dunne, L., & Eales, S. 2005, MNRAS, 364, 1253

Wachter, A., Winters, J. M., Schröder, K., & Sedlmayr, E. 2008, A&A, 486, 497

Wagg, J., Kanekar, N., & Carilli, C. L. 2009, ApJ, 697, L33

Walter, F., Bertoldi, F., Carilli, C., et al. 2003, Nature, 424, 406

Walter, F., Carilli, C., Bertoldi, F., et al. 2004, ApJ, 615, L17

Walter, F., Riechers, D., Cox, P., et al. 2009, Nature, 457, 699

Wanajo, S., Nomoto, K., Janka, H., Kitaura, F. S., & Müller, B. 2009, ApJ, 695, 208

Wang, R., Carilli, C. L., Neri, R., et al. 2010, ApJ, 714, 699

Wang, R., Carilli, C. L., Wagg, J., et al. 2008, ApJ, 687, 848

Webbink, R. F. 1984, ApJ, 277, 355

Weiß, A., Downes, D., Neri, R., et al. 2007, A&A, 467, 955

Weiß, A., Walter, F., & Scoville, N. Z. 2005, A&A, 438, 533

Wesson, R., Barlow, M. J., Ercolano, B., et al. 2010, MNRAS, 403, 474

Whelan, J. & Iben, Jr., I. 1973, ApJ, 186, 1007

Wickramasinghe, N. C. 1963, MNRAS, 126, 99

Williams, B. J., Borkowski, K. J., Reynolds, S. P., et al. 2008, ApJ, 687, 1054

Willott, C. J., Delorme, P., Omont, A., et al. 2007, AJ, 134, 2435

Willott, C. J., McLure, R. J., & Jarvis, M. J. 2003, ApJ, 587, L15

Willson, L. A. 2007, in Astronomical Society of the Pacific Conference Series, Vol. 378, Why Galaxies Care About AGB Stars: Their Importance as Actors and Probes, ed. F. Kerschbaum, C. Charbonnel, & R. F. Wing, 211–+

Wilson, T. L. & Batrla, W. 2005, A&A, 430, 561

Winters, J. M., Le Bertre, T., Jeong, K. S., Helling, C., & Sedlmayr, E. 2000, A&A, 361, 641

Woitke, P. 2006, A&A, 460, L9

Wolf, M. 1904, MNRAS, 64, 838

Wolf, M. 1923, Astronomische Nachrichten, 219, 109

Wooden, D. H., Rank, D. M., Bregman, J. D., et al. 1993, ApJS, 88, 477

Woosley, S. E. & Weaver, T. A. 1995, ApJS, 101, 181

Yan, L., Tacconi, L. J., Fiolet, N., et al. 2010, ApJ, 714, 100

Yoshida, N., Omukai, K., & Hernquist, L. 2008, Science, 321, 669

Yun, M. S. & Carilli, C. L. 2002, ApJ, 568, 88

Zhukovska, S., Gail, H., & Trieloff, M. 2008, A&A, 479, 453

Zijlstra, A. A., Matsuura, M., Wood, P. R., et al. 2006, MNRAS, 370, 1961

Zinner, E. 1997, in American Institute of Physics Conference Series, Vol. 402, American Institute of Physics Conference Series, ed. T. J. Bernatowicz & E. Zinner, 3–26

Zinner, E. 1998, Annual Review of Earth and Planetary Sciences, 26, 147

Co-Author statements

Declaration of co-authorship

Name:	Christa Gall	**Civ. Reg. No. (CPR No.):**	060978 4024
Department:	Niels Bohr Institute	**E-mail:**	christa@dark-cosmology.dk
Principal supervisor:	Anja C. Andersen	**Supervisor's e-mail:**	anja@dark-cosmology.dk
Position of supervisor:	Associate Professor		

Title of PhD thesis: Genesis and evolution of dust in galaxies in the early Universe

This co-authorship declaration applies to the following paper:

Genesis and evolution of dust in galaxies in the early Universe. I. Dust productivity of massive stars

The student's contribution to the paper:

Initiated and constructed the numerical code, performed the calculations, made all the plots, reached the conclusions and wrote the paper.

Signatures of co-authors:

Date	Name	Signature
5/7-2010	Anja C. Andersen	Anja Andersen
6/7-2010	Jens Hjorth	

PhD student: _____ Date: 05/07/10

Signature

A copy must be sent to the Department.

When completed, the form with signatures must be forwarded by e-mail, preferably in PDF format, to:

E-mail: PhD@science.ku.dk

PhD School at the Faculty of Science,
University of Copenhagen,
Tagensvej 16, DK-2200 Copenhagen N.

Declaration of co-authorship

Name:	Christa Gall	**Civ. Reg. No. (CPR No.):**	060978 4024
Department:	Niels Bohr Institute	**E-mail:**	christa@dark-cosmology.dk
Principal supervisor:	Anja C. Andersen	**Supervisor's e-mail:**	anja@dark-cosmology.dk
Position of supervisor:	Associate Professor		

Title of PhD thesis: Genesis and evolution of dust in galaxies in the early Universe

This co-authorship declaration applies to the following paper:

Genesis and evolution of dust in galaxies in the early Universe. II. Modeling dust evolution in starburst galaxies

The student's contribution to the paper:

Initiated and constructed the numerical code, performed the calculations, made all the plots, reached the conclusions and wrote the paper.

Signatures of co-authors:

Date	Name	Signature
5/7-2010	Anja C. Andersen	Anja Andersen
6/7-2010	Jens Hjorth	Hjorth

PhD student: _____ Date: 05/07/10

Signature

A copy must be sent to the Department.

When completed, the form with signatures must be forwarded by e-mail, preferably in PDF format, to:

E-mail: PhD@science.ku.dk

PhD School at the Faculty of Science,
University of Copenhagen,
Tagensvej 16, DK-2200 Copenhagen N.

Declaration of co-authorship

Name:	Christa Gall	**Civ. Reg. No. (CPR No.):**	060978 4024
Department:	Niels Bohr Institute	**E-mail:**	christa@dark-cosmology.dk
Principal supervisor:	Anja C. Andersen	**Supervisor's e-mail:**	anja@dark-cosmology.dk
Position of supervisor:	Associate Professor		

Title of PhD thesis: Genesis and evolution of dust in galaxies in the early Universe

This co-authorship declaration applies to the following paper:

Genesis and evolution of dust in galaxies in the early Universe. III. Rapid dust evolution in quasars at z > 6

The student's contribution to the paper:

Initiated and constructed the numerical code, performed the comparison of the calculations with observations of quasars at high redshift, made all the plots, reached the conclusions and wrote the paper.

Signatures of co-authors:

Date	Name	Signature
26/07/2010	Anja C. Andersen	Anja Andersen
26/07/2010	Jens Hjorth	Jhorth

PhD student: _____ Date: 26/07/2010

Signature

A copy must be sent to the Department.

When completed, the form with signatures must be forwarded by e-mail, preferably in PDF format, to:

E-mail: PhD@science.ku.dk

PhD School at the Faculty of Science,
University of Copenhagen,
Tagensvej 16, DK-2200 Copenhagen N.